Rheological Design of Sustainable Block Copolymers

A THESIS
SUBMITTED TO THE FACULTY OF THE GRADUATE SCHOOL
OF THE UNIVERSITY OF MINNESOTA
BY

Alexander M. Mannion

IN PARTIAL FULFILLMENT OF THE REQUIREMENTS
FOR THE DEGREE OF
Ph.D.

Frank S. Bates and Christopher W. Macosko

August, 2016

Acknowledgements

My time in graduate school has been an incredible journey, extending far beyond the results that appear in this document. As such, I have a multitude of individuals to thank for their support during these formative years.

First, I would like to thank my academic advisors, Frank Bates and Chris Macosko. Thank you so much for the numerous opportunities you have provided me during my graduate school career and for shaping me into the scientist I am today. Your diligent work behind the scenes has not gone unnoticed. Frank, I appreciate the ideas you have generated as well as your critical and constructive feedback over the years. Chris, I admire your holistic view on the education of young researchers that champions both academic and character development.

Second, I would like to thank a number of older Macosko and Bates group members who helped mentor me during my early days as a graduate student, including, but not limited to Randy Ewoldt, Luca Martinetti, Kevin Pustalka, Thanasis Touris, Carmelo Declet-Perez, Karen Haman, and Tim Gillard. A special thanks to Sangwoo Lee who taught me how to synthesize polymers during my first summer and was exceedingly patient with my numerous hiccups in the laboratory.

Third, I would like to thank all the undergraduate researchers that I have had the privilege to mentor and work with, namely Willy Voje, Max Nagarajan, Joel Updyke, McKenzie Coughlin, Jacob Wright, and Joseph Schaefer. I have grown immensely professionally because of you, and your persistent questions and ceaseless energy have pushed me to become

a better leader.

Next, I would like to thank everyone who have been instrumental in my success in the later years of graduate school – Chris Thurber, Liangliang Gu, Tuoqi Li, Rob Hickey, Ron Lewis, Dr. David Giles, and Professor Marc Hillmyer. David, your encyclopedic knowledge of rheology and the rheometers has saved me months of toil, and you have been a great sounding board for my daily practical problems. Marc, thank you for your guidance on a number of side projects and for letting me use of your laboratory's facilities.

I would also like to thank Marie Vanderlaan, Debbie Schneiderman, and Tessie Panthani (a.k.a. "Team Foam"). Entering (and winning) the BASF and Dow competitions has been an incredible experience, and I could not ask for a better set of teammates with the perfect balance of diligence, camaraderie, and humor. Beyond the foam project, Debbie, your work ethic and creativity has been an inspiring force, and I appreciate the support during those late nights in lab. Tessie, you have been an absolute pleasure to work with, but what I appreciate most is how your critical thinking, attention to detail, and insightful conversations have pushed me to become a better scientist.

To my other graduate school friends – Larry Stern, Sadie Johnson, Brittany Forkus, Neel Rangnekar, Yogesh Dhande, Chris Thurber, and Coty Jen – thank you for creating an incredibly supportive and fun work atmosphere that has allowed me to thrive. A special thanks to Sid Chanpuriya, Matt Irwin, and Jeff Ting who have been with me both inside and outside of lab since my first days of graduate school. Matt, our regular coffee breaks will be missed, as well as your hot meals. Jeff – it is hard to articulate the amount of support you have given me. Simply put, you have been my rock, and I have been extremely lucky to have you as my colleague and friend.

Finally, I would like to thank my many close friends across the globe, particularly those in Barcelona, Boston, Los Angeles, and San Francisco who have allowed me to escape the frigid Minnesota winters from time to time. And last, my family. You have been my biggest cheerleaders and steadfast supporters. Thank you so much.

Dedication

To my close friends and family

Abstract

Block copolymers are extremely versatile materials that microphase separate to give rise to a rich array of complex behavior, making them the ideal platform for the development of rheologically sophisticated soft matter. In line with growing environmental concerns of conventional plastics from petroleum feedstocks, this work focuses on the rheological design of *sustainable* block copolymers – those derived from renewable sources and are degradable – based on poly(lactide). Although commercially viable, poly(lactide) has a number of inherent deficiencies that result in a host of challenges that require both creative and practical solutions that are cost-effective and amenable to large-scale production. Specifically, this dissertation looks at applications in which both shear and extensional rheology dictate performance attributes, namely chewing gum, pressure-sensitive adhesives, and polymers for blown film extrusion. Structure-property relationships in the context of block polymer architecture, polymer composition, morphology, and branching are explored in depth. The basic principles and fundamental findings presented in this thesis are applicable to a broader range of substances that incorporate block copolymers for which rheology plays a pivotal role.

Contents

List of Tables

List of Figures

Chapter 1

Introduction

1.1 Rheology

1.1.1 Rheological design

In the 1920s, Lehigh University professor Eugene Bingham invented the term *rheology* to explain the flow behavior of new classes of synthetic materials that had begun to enter society.[1] Coming from the Greek verb $\rho\epsilon\iota\nu$ meaning "to flow," rheology is the study of deformation and flow. Typically, rheology is used to describe *viscoelastic* materials, those which have both solid-like and liquid-like characteristics. Examples of viscoelastic substances include polymer melts, polymer solutions, colloidal suspensions, particulate gels, emulsions, liquid crystals, and surfactant solutions.[2] Unlike fluid mechanists who study simple fluids under complex flows, rheologists look at such complex fluids under simple flows. Rheologists can then apply their findings to real-world situations in which more complex flows are typical.

The principles of rheology are used in the design of cosmetics,[3] construction materials,[4,5] easily processable polymers,[6,7] biological systems,[8] and even avant garde foods.[9] In many of these applications, the rheological profile of the product is intrinsically linked to its performance. A simple example is lotion that must rest on one's hand without flowing, yet

be easily spread across skin. Similarly, paint must spread well when applied to a surface to obtain a smooth, uniform coating, yet be resistant to sag which can cause defects.[10] A more complicated example is carefully engineered artificial gastropod mucus that was incorporated into robotic snail that allowed for adhesive mechanical locomotion.[11] Thus, a decent amount of attention has been given to *rheological design*; that is, the process in which one can manipulate the rheological profile of a material for a given application.

1.1.2 Fundamentals

Rheology is governed by two basic flows: shear and extension. These flows will first be explained in the context of simple *Newtonian* fluids. In shear flow, adjacent parallel fluid layers move at different speeds. This can be visualized by flow between two sliding plates separated by a distance h as shown in Figure 1.1. The top plate moves at a constant velocity V, while the bottom one remains stationary, resulting in a velocity gradient. The *viscosity* (η) of the fluid is defined as follows:

$$\eta = \frac{\sigma}{\dot{\gamma}} \tag{1.1}$$

where σ is the shear stress imposed by the fluid while $\dot{\gamma}$ is the shear strain rate imposed on the fluid. Here, $\dot{\gamma} \equiv V/h$.

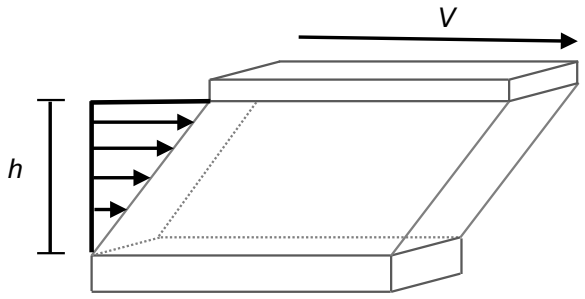

Figure 1.1: Simple shear flow between two parallel plates.

Extensional flows are flows in which the velocity profile in a given direction does not depend on the other spatial dimensions. The simplest extensional flow is *uniaxial* extension,

or extension in one direction. Like in shear flow, an *extensional viscosity* (η_E) can defined as follows:

$$\eta_E = \frac{\sigma_E}{\dot{\epsilon}} \tag{1.2}$$

in which σ_E is the extensional stress imposed by the fluid while $\dot{\epsilon}$ is the extensional strain rate imposed on the fluid. A schematic on how this could be done experimentally for a viscoelastic material is shown in Figure 1.2. The length L_0 is constant, and each set of cylinders causes the ends to move at a constant velocity V in opposing directions. Here, $\dot{\epsilon} \equiv 2V/L_0$.

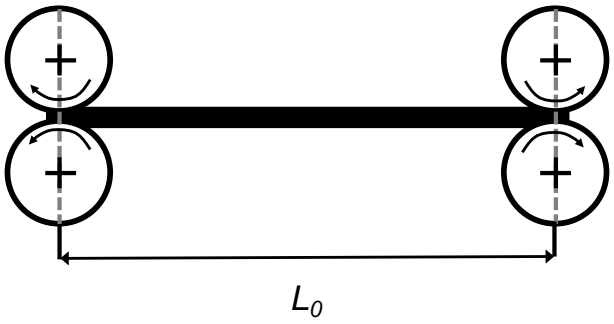

Figure 1.2: Uniaxial extensional flow.

The above scenario is very difficult to implement experimentally; in practice, often times a rectangular bar of material of initial length L_0 is set between two counter-rotating clamps and pulled to a final length L.[12] To achieve the same velocity profile as shown in Figure 1.2, the following relation must hold true:

$$\dot{\epsilon} = \frac{\partial \epsilon}{\partial t} = \frac{\partial \frac{L}{L_0}}{\partial t} \tag{1.3}$$

where ϵ is the *true* strain at any given moment in time. This ensures that the change in true strain the material feels is constant with time. In the rheological community, the extensional shear rate $\dot{\epsilon}$ is often referred to as the *Hencky strain rate* and ϵ is called the *Hencky strain*.

For simple Hookean solids, analogous equations can be written for shear and extensional deformations:

$$G = \frac{\sigma}{\gamma} \tag{1.4}$$

$$E = \frac{\sigma}{\epsilon} \tag{1.5}$$

where G is the shear modulus, γ is shear strain, and E is the elastic modulus.

Viscoelastic materials have both liquid and solid-like behavior, incorporating elements of the aforementioned equations. One of the most common ways to capture viscoelastic behavior is through small-amplitude oscillatory shear (SAOS). In SAOS, one can measure the *elastic* or *storage* modulus, G' and the *viscous* or *loss* modulus, G''. Typically, oscillatory shear is applied at a constant frequency ω and the stress response is measured and the following relation holds true:

$$\sigma(t) = \gamma_0[G' \sin(\omega t) + G'' \cos(\omega t)] \tag{1.6}$$

The G' is in phase with the strain and provides a measure of the solid-like behavior of the material; G'', in phase with the strain rate, captures the liquid-like behavior.

In the linear regime – the limit of small strains, strain rates, or stresses – $3G = E$ and $3\eta = \eta_E$. At higher strains, strain rates, or stresses, however, the *nonlinear* regime may be accessed, leading to more complicated rheological behavior. More sophisticated *constitutive* equations are needed to describe nonlinear behavior that go well beyond the basic definitions outlined here. Still, these rheology fundamentals provide a framework in which one can begin to design useful materials.

1.2 Block polymers

Instrumental in almost every man-made material today, synthetic polymers, composed of many repeating chemical subunits, can be tailored to have a wide range of thermal, mechanical, electronic, and surface properties. One interesting class of polymers are *block*

polymers that have attracted considerable attention in recent decades and are found in such applications as compatibilizers,[13] adhesives[14,15] and asphalt modifiers.[16] A block polymer is composed of two or more chemically distinct polymers that are covalently bonded. Although the simplest block polymer is composed of one "A" polymer connected to one "B" polymer to make an AB diblock, a surfeit of more complex architectures can be accessed by the addition of other polymers with alternate chemical moieties.[17]

Block polymers are attractive because they provide a marriage of disparate desirable properties into a single macromolecule. For instance, brittle polystyrene can be toughened by incorporation of a rubbery blocks like polybutadiene into its backbone.[18] The true advantage of block polymers over other copolymers, though, is that they can *microphase separate* into an array of morphologies. Well-established controlled polymerization techniques allow for these different morphologies to be easily accessed by simply adjusting the volume fraction of the blocks. Some examples are shown in Figure 1.3 depicting common spherical (BCC), cylindrical (HEX), and lamellar (LAM) morphologies that AB diblocks are known to adopt. These morphologies can have a profound impact on final material properties. For example, multiple continuous, percolating domains allow for far superior transport properties for use in filtration membranes or ion conductivity ion batteries.[19] Also, block polymer thin films for lithographic applications require lamellae or cylinders that run perpendicular the surface.[20] Generally speaking, block polymers serve as an exceedingly versatile platform for a wide range of purposes.

In many of the aforementioned applications such as membranes and adhesives, rheology can play a critical role. However, because of the rich complexities of this class of soft matter, much about their rheological behavior is unknown. The backbone architecture (e.g. linear, star, branched), block sequence, polymer composition, molecular weight, chemical species, and order-disorder transition temperature can all affect the final linear and nonlinear rheological behavior. Ronald G. Larson, a distinguished chemical engineering professor at the University of Michigan has gone to claim that the "rheological behavior of block

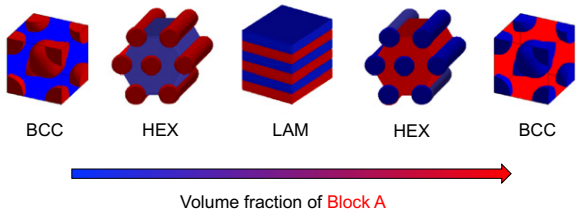

Figure 1.3: Depicted are representations of spherical (BCC), cylindrical (HEX), and lamellar (LAM) morphologies adopted by an AB diblock copolymer during self-assembly. Reprinted from *Progress in Polymer Science*, *33*, Mueller *et al.*, Polydispersity and Block Copolymer Self-Assembly, 875–893, Copyright (2008) with permission from Elsevier.[21] Format inspired from a previous adaptation.[22]

copolymers is perhaps the least understood" of the major types of complex fluids.[2] Thus, there is enormous opportunity to explore this parameter space and design unique block polymer systems tailored for specific applications.

1.3 Sustainable materials

1.3.1 Motivation

Despite the obvious advantages of polymers and plastics, they come at a significant social and environmental cost. As of 2014, approximately 310 million tonnes of plastic are produced annually, using roughly 8% of the world's oil and gas production.[23–25] These totals are expected to increase dramatically over the coming years given historical trends and the world's growing economy and population. More alarming, though, is that 50% of these materials are made for single-use items which are immediately disposed, creating a massive end-of-life management problem.[23] The majority of these plastic currently are put into landfills or leaked into the environment, much of which ends up in the ocean.[25,26] By 2050, it estimated that the weight of plastics in the ocean will be equivalent to the weight of fish,[25] leading to deleterious effects on both wildlife[27] and human health.[28]

For these reasons, there has been an immense push from both consumers and industrial

leaders to invest in the development of more sustainable polymers.[29,30] Although other aspects of green chemistry are important,[31,32] here, sustainable polymers shall be defined as those that are derived from renewable sources and are degradable or recyclable. Besides the environmental benefit, the development of such materials would protect segments of the industry from potentially volatile oil prices. Unfortunately, the relatively high current price of most sustainable polymers have prevented their widespread incorporation into commodity plastics, yet there is promise for certain polymers such as poly(lactide).[30,33]

1.3.2 Polylactide

Poly(lactide), also known as poly(lactic acid) or PLA, is a renewable, biodegradable, and compostable thermoplastic with mechanical properties similar to poly(styrene).[34] Lactic acid is made by fermentation of dextrose (derived primarily from corn) that can be polymerized via condensation to form PLA.[35] Historically, high production costs limited the use of PLA to medical applications where biocompatibility and biodegradability were required, e.g. resorbable sutures and tissue scaffolds.[36–38] As of 2013, the surcharge for PLA verses poly(ethylene terephthalate) (PET) was small enough (15-25%) to allow its use in consumer goods and as general packaging.[39–41] Unfortunately, PLA suffers from a number of deficiencies; for example, it is inherently brittle,[40] possesses poor melt strength,[42] and is prone to degradation during processing.[42] This has given rise to a new set of challenges to improve the properties of PLA so it can become competitive with conventional plastics from petroleum-based feedstocks. Much of the work highlighted in this thesis will address some of these challenges.

1.4 Outline

The focus of this thesis will be to apply the principles of rheology to design sustainable block copolymers, all with a specific application in mind. Because of the potential commercial viability of PLA, all the block polymers studied in this work incorporate PLA to some

degree. Chapters 2 and 3 focus on the application of chewing gum. Chapter 2 identifies the specific rheological fingerprint unique to chewing gum and the key rheological markers that dictate performance (in this case, sensory feel). Chapter 3 discusses how these findings were used to design blends of block polymers that are able to mimic this sensory feel. These blends, incorporating diblocks, triblocks, and multiblocks, serve as a tunable platform for next-generation chewing gum. Chapters 4 and 5 explore the synthesis and rheology of branched, multiblock polymers to create tough plastics that are amenable to processing techniques that require fast elongational flows. Chapter 4 focuses on the strategy of coupling star diblock polymers, while Chapter 5 examines an alternate coupling route that has the potential to be more versatile. Chapter 6 investigates the use of a sustainable triblock copolymer for pressure-sensitive adhesives (PSAs), correlating rheological behavior to key adhesives properties. Chapter 7 discusses efforts to create films of PLA using blown film extrusion. These films, toughened by low molecular diblocks, show promising mechanical properties. Finally, Chapter 8 provides summaries of the individual chapters.

Chapter 2

The Rheology of Chewing Gum

2.1 Introduction

Although ubiquitous in the field of food science, the term "gum" has various, and often conflicting, connotations. The Oxford dictionary defines gum as a "viscous secretion" from plants that "hardens upon drying yet is soluble in water." Examples of such exudate gums are gum arabic, guar gum, and locust bean gum. These materials are composed primarily of long chain polysaccharides and are used as food thickening or gelling agents;[44,45] however, their rheological effects vary wildly.[46] Xanthan gum is a similar thickening agent, yet it is not produced by a plant but by the bacterium Xanthomonas campestris.[47] Certain gelatin-based candies are referred to as "gums" such as gummy bears and wine gums. As opposed to the exudate gums, these substances are water insoluble, gel-like solids with smooth, bouncy textures. Modern day chewing gum is yet a different type of gum, designed as a pliable cud that releases flavorings and sweeteners in a controlled manner upon mastication. At the most general level, a gummy substance is one that is viscous or sticky. Thus, two

Part of this work was done in collaboration with Dr. Luca Martinetti, William E. Voje Jr., Renxuan Xie, and Prof. Randy H. Ewoldt from the University of Minnesota and Dr. Leslie Morgret from the Wm. Wrigley Jr. Company and is published in Martinetti et. al, *J. Rheol* **2014**, *58*, 821-838.[43] This work was sponsored by Wm. Wrigley Jr. Company.

materials both referred to as "gums" in the vernacular may host a wide range of differing rheological and physical properties, begging the question, "What is gum?"

To address this question, characterizing the mechanical properties of one subset of gum materials is focused upon - chewing gum. Chewing gum provides an excellent everyday example of nonlinear viscoelastic behavior for which most individuals have both experience and physical intuition. It flows when being chewed or pulled slowly, stresses in it persist after the deformation has ceased, and some recoil occurs when it is suddenly relieved of an externally imposed stress. The gum may also break when being blown into bubbles or pulled rapidly. Hence, understanding the rheological properties of chewing gums is important for application purposes. Examples of two common deformations are depicted in Figure 2.1. In the left inset, a piece of bubble gum undergoes biaxial extension as it is blown into a bubble, while in the right inset, a piece of bubble gum sustains stress under extension and recoils upon release of that stress.

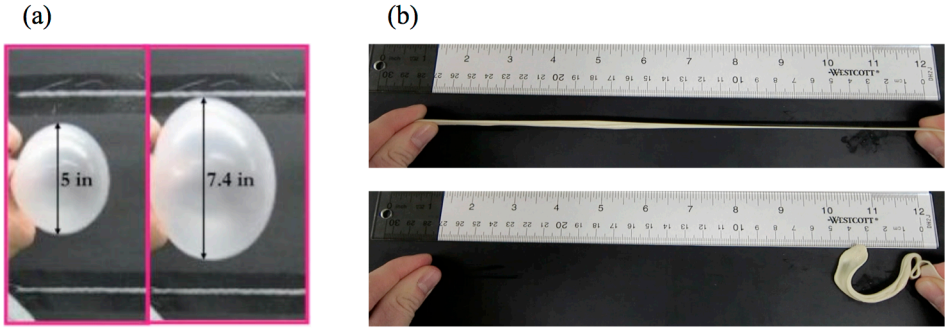

Figure 2.1: a) Bubble gum undergoes biaxial extension upon blowing. b) Bubble gum sustains large stretch under extension and recoils upon release of that stress. These are but two examples of the complex, large, and unsteady deformations that bubble gum is subjected to during use, emphasizing the importance of rheological properties on product performance

To the best knowledge of the author, no paper is found in the peer-reviewed literature regarding the rheological behavior of chewing gum. Only in a few patents is linear viscoelastic data included.[48–50] Despite the fact that chewing involves large, complex, and unsteady

deformations, no study has been published that characterizes chewing gum under these deformation regimes. The goals of this initial study are to compare the rheology of selected commercial chewing gums with bubble gums and to define the term "gum" based on its rheological properties. Henceforward, "bubble" gums, those products specially designed for producing large, stable bubbles, will be differentiated from conventional "chewing" gums, those only meant for chewing.

In this chapter, the linear and nonlinear viscoelastic behavior of selected commercial chewing and bubble gums in shear and extension will be discussed. The rheology of lab-scale gums with known formulations and a commercially available confectionary wax are included for easy comparison to similar everyday substances. Despite the heterogeneous and varied compositions of the chewing and bubble gums, all exhibit classic critical gel behavior in the linear regime. Additionally, chewing gums can be differentiated from bubble gums based on the extent of strain hardening in the start-up of steady uniaxial extension. This unique rheological fingerprint is sufficient to define gum independent of specific molecular formulation, and that similar rheological definitions are applicable to any soft material where performance is dictated by rheology.

2.2 Experimental methods

2.2.1 Materials

The composition of a typical sugar-free chewing gum is shown in Figure 2.2. Although exact formulations may vary between products, commercially successful chewing and bubble gums consist of the same basic four ingredients: a gum base, sweeteners, flavorings, and softeners.[51,52] The gum base is the most complex element, composed of elastomers, resin plasticizers, texture fillers, waxes, fats, and emulsifiers.[53] The purpose of the gum base is to provide a suitable matrix for the flavorings as well as the water-soluble sweeteners and softeners that are extracted upon mastication. Simultaneously, the gum base must provide

a pleasant chewing experience. The sweeteners and flavorings give chewing and bubble gum its taste, and softeners fine-tune the sensory feel. In this representative formulation, sweeteners represent 68 wt% of the chewing gum mass, gum base 24%, softeners 6%, and flavorings 2%. This particular gum base contains 13% by mass polyisobutylene, 10% rosin esters, 20% polyvinyl acetate, 28% waxes, 25% filler, and 4% other materials. Note that all the aforementioned ingredients are food grade. Four commercial chewing gums and four commercial bubble gums were investigated, the names of which are listed in Table 2.1.

Table 2.1: Trade names for commercial chewing and bubble gums

Sample	Trade name–flavor	Sample	Trade name–flavor
C1	Eclipse–Peppermint	B1	Hubba Bubba–Outrageous Original
C2	Winterfresh–N/A	B2	Hubba Bubba Tape–Awesome Original
C3	Trident White–Peppermint	B3	Trident–Bubble Gum
C4	Trident Soft–Peppermint	B4	BubbleYum–Original

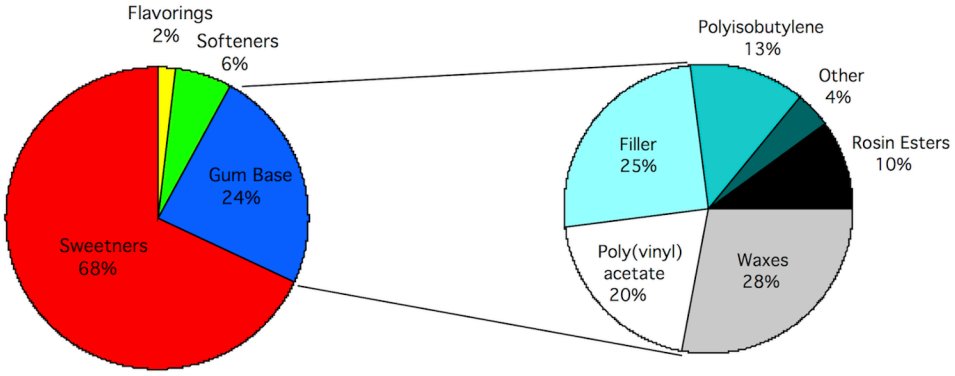

Figure 2.2: Typical sugar-free chewing gum formulation.[51,52] The four main ingredients by mass of chewing gum are sweeteners, the gum base, softeners, and flavorings. The gum base, in turn, is composed of polyisobutylene, rosin esters, poly(vinyl acetate), waxes, filler, and other ingredients.[53]

The formulations for three lab-scale gums are indicated in Table 2.2. These were created in order to directly compare the rheological fingerprint of commercial chewing and bubble

gum with materials of known compositions. Additionally, a commercially available confectionary wax, Wack-o-wax Mr. Stache (available at http://shop.tootsie.com), was utilized for certain studies and is referred to as "W1".

Table 2.2: Formulations of lab scale gums

Sample	Base	Calcium Carbonate	Sorbitol	Glycerine	Medium Chain Triglycerides	Flavorings
V1	40 wt.%	–	57 wt.%	3 wt.%	–	–
V2	30 wt.%	55 wt.%	3 wt.%	–	–	2 wt.%
V3	30 wt.%	5 wt.%	55 wt.%	3 wt.%	5 wt.%	2 wt.%

2.2.2 Material preparation

To simulate mouth chewing without the variability between human subjects, the following technique was developed. A gum sample was kneaded with hand pliers for 20 minutes in distilled water at room temperature. This hydrated the sample, removed soluble material, and allowed the gum cud mass to attain steady-state. The sample was then allowed to soak in distilled water for at least one hour at room temperature. All rheological tests were performed at 37 °C to correlate with physiological mouth temperature. A total of four bubble gums (B1-B4), four chewing gums (C1-C4), three lab-scale gums (V1-V3), and one wax (W1) were prepared in this manner.

2.2.3 Measurements

Linear viscoelasticity

In order to probe linear viscoelastic (LVE) properties, the gum samples were subjected to small strain deformations in oscillatory shear with an AR-G2 rheometer (TA Instruments, New Castle, DE). A 13 mm parallel plate was used for all LVE testing. The chewed gum cud was loaded on the bottom plate, and the top plate was lowered to make contact with the sample. A light pressure was maintained for several minutes as the gum cud was appropriately cut with a brass knife. Once the sample was properly shaped, it was

immersed in distilled water to maintain hydration and regulate temperature. Heating was controlled via a Peltier plate. To identify the range of strains that give a linear viscoelastic response, isothermal strain sweeps were conducted at the highest and lowest frequencies of the subsequent frequency sweeps. Frequency sweeps were then performed at a strain within the linear regime. To identify thermal properties, a temperature ramp from 80 °C to 20 °C at a cooling rate of 1 °C min^{-1} was conducted at a frequency of 1.0 rad s^{-1} and at a strain within the linear regime.

Nonlinear viscoelasticity: shear

Behavior during start-up of steady shear was investigated with an ARES rheometer (TA Instruments, New Castle, DE) with 8 mm parallel plates and a gap < 0.5 mm. The tests were performed at a large range of shear rates (10^{-4} to 10^{2} s^{-1}). Large amplitude oscillatory shear measurements were strain-controlled with an 8mm cone and plate on an ARES-G2 rheometer (TA Instruments, New Castle, DE). The temperature was controlled via a recirculating water bath below the bottom plate. The strain sweeps were conducted at a given frequency to strains up to 100%. The maximum strain was limited by edge failure or slip, and the data was analyzed using MITlaos.[54,55] Shear creep and recovery experiments were performed with an 8 mm, 0.1 radian cone and plate on an AR-G2 rheometer. Upon loading, the temperature was raised to 37 °C, and a particular shear stress was applied for 100 s. The strain recovery was subsequently recorded for 1 h. Edge failure limited the maximum shear stress to approximately 3000 Pa.

Nonlinear viscoelasticity: extension

Uniaxial extensional tests were conducted with an extensional viscosity fixture (EVF) (TA Instruments, New Castle, DE) on an ARES-G2 rheometer; this device operates with a counter-rotating dual drum geometry. Gum cuds were pressed at room temperature in a 1 mm thick custom metal mold containing 21 $\times$ 5 mm rectangles. Teflon sheets were

placed between the mold and exterior metal sheets to prevent adhesion and aid removal. Occasionally, dry ice was employed to lower the sample temperature in order to facilitate clean removal of the gum cud.

Samples were loaded onto the EVF and allowed to equilibrate at operational temperature for five minutes. The gum cuds were subsequently extended at a particular Hencky strain rate until failure occurred. At the lowest extension rate, 0.001 s^{-1}, sample sagging was observed. The samples displayed extensional thinning for Hencky strains ≤ 1 and necking and extensional hardening for Hencky strain rates ≥ 0.25 s^{-1}. At Hencky strains greater than about 4.3, the specimen overlaps itself, causing a slight step increase in the measured stress. Nonetheless, this produces relatively small disturbances in the measurements and tests were carried past this point to estimate strain and stresses at break. At least five fresh gum samples were tested at each Hencky strain rate.

2.3 Results and discussion

2.3.1 Thermal characterization

Thermal characterization of the chewing and bubble gums demonstrate viscoelastic transitions near 37 °C. Figure 2.3 shows temperature dependent linear elastic (G') and loss (G'') moduli for a representative chewing gum, C1, and a representative bubble gum, B1. The modulus of C1 drops more than two orders of magnitude within a ten degree window from 30 to 40 °C. For B1, the temperature dependence of the elastic modulus shifts at 37 °C. The elastic modulus of both C1 and B1 remain relatively constant between 40 and 80 °C. These thermal transitions likely correspond to either a glass-transition or crystallization of a base elastomeric component, indicating a shift from a hard, brittle material to a softer, rubbery substance.

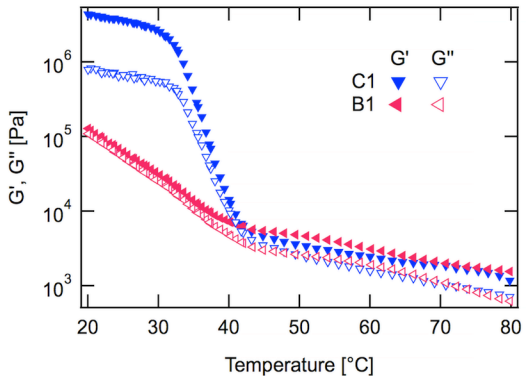

Figure 2.3: Temperature ramp for cooling at 1 °C min^{-1} at $\omega = 1$ rad s^{-1} of representative chewing gum C1 and bubble gum B1. These two and all other gums show a thermal transition near 37 °C. This transition is thought to be a glass-transition or crystallization of a gum base component. The $\tan\delta$ is less than 1 throughout the temperature range.

2.3.2 Linear viscoelasticity

Strain sweeps in small amplitude oscillatory shear (SAOS) demonstrate that the chewing gums have very low critical strains, γ_c, the strain at which the material begins to exhibit nonlinear behavior (Figure 2.4). Here, the critical strain is defined as the strain at which the modulus deviates 10% from its original value. For representative chewing gum C1, the critical shear strain is 0.37% at a frequency of 0.05 rad s^{-1} and 0.07% at a frequency of 500 rad s^{-1}. A variety of other complex materials containing micron-size filler particles such as butter,[56] reinforced polymer melts,[57] and flour-water dough[58] have critical strains on the order of 1% or lower. As opposed to polymer chains that can stretch to high strains and return to their original configuration, these filler particles cannot withstand much deformation without losing memory of prior positions. Thus, the low critical strains of chewing gum are attributed to the relatively large percentage of filler and wax in the gum base formulations.

Frequency sweeps of gums C1 and B1 show a predominantly elastic response that follows power-law behavior (Figure 4.5). Within the range of frequencies tested, the following

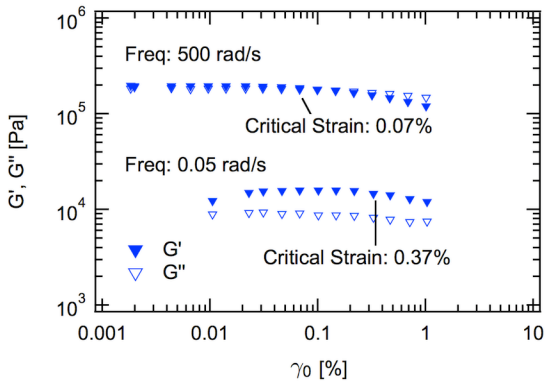

Figure 2.4: Strain sweep for chewing gum C1 at 37 °C. The critical strain is defined as the strain at which G' decreases by 10%. At both low and high frequencies, the critical strain was found to be $< 0.5\%$.

equation generally characterizes the gums:

$$G'(\omega) = G'_c \omega^n \tag{2.1}$$

where G'_c is a material constant. More specifically, the critical gel equation for oscillatory shear may be used to describe the data:[59]

$$G'_{gel}(\omega) = \frac{G''_{gel}(\omega)}{\tan n\pi/2} = \Gamma(1-n)(\cos n\pi/2) S\omega^n \tag{2.2}$$

In this equation, Γ is the gamma function, S is a material constant indicative of stiffness, and n is the power-law exponent. The critical gel fit for C1 is shown in Figure 4.5. In this analysis, the lower frequency data ($\omega < 10$ rad s^{-1}) was fit for G' and equation 2.2 was used to calculate G''. Although the critical gel model works well at these lower frequencies, both moduli deviate upwards as the crossover frequency (ω_c) is approached, where the crossover frequency ω_c is defined by $G'(\omega_c) = G''(\omega_c)$. This increase in modulus is attributed to additional Rouse-like modes, corresponding to the response of segmental building blocks of the material.[60] Such Rouse-like contributions at high frequencies (or short time scales) is well predicted by theory for entangled polymers,[61] reversible networks,[62] and cross-linked polymers[63] and they have been previously reported for a critical gel material, gluten

dough.[64,65] For oscillatory shear, the Rouse model can be reduced to the following two equations where G_R is the Rouse contribution to the modulus and λ_R is the segmental relaxation time:

$$G'_R = G_R \sum_{k=1}^{\infty} \frac{(\lambda_R \omega / k^2)^2}{1 + (\lambda_R \omega / k^2)^2} \tag{2.3}$$

$$G''_R = G_R \sum_{k=1}^{\infty} \frac{(\lambda_R \omega / k^2)}{1 + (\lambda_R \omega / k^2)^2} \tag{2.4}$$

To obtain the best combined estimate of the viscoelastic properties, the Rouse model was fit to the difference between the actual data and the critical gel fit. More specifically, the following equation was minimized:

$$\sum_i |\log(R_i) - log(D_i - G_i)| \tag{2.5}$$

where D_i is the experimental data point at a frequency i and R_i and G_i are the Rouse and critical gel model fits at this frequency, respectively. A summary of the fits for B1 and C1 are shown in Table 2.2.

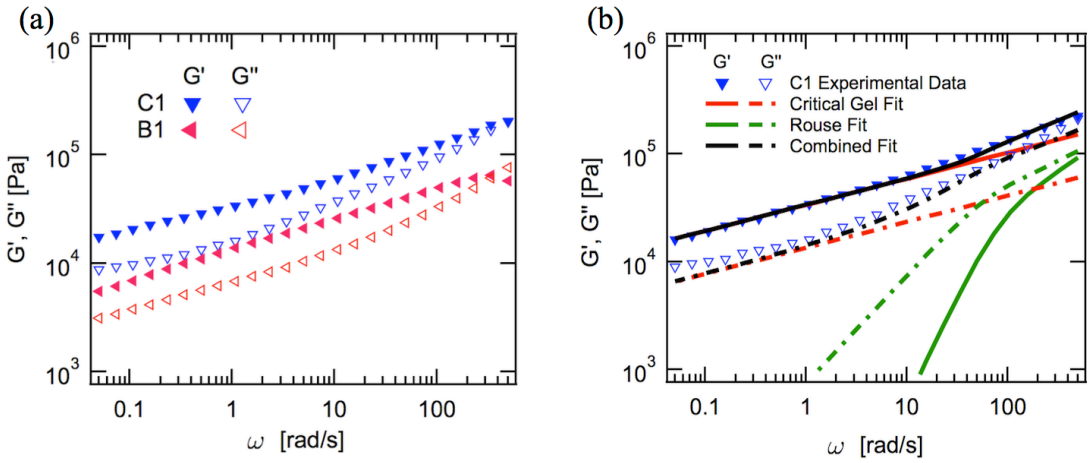

Figure 2.5: a) Frequency sweeps of C1 and B1 at a strain in the linear regime show a predominant elastic response and critical gel-like behavior. b) Critical gel, Rouse, and combined fits for frequency sweep data for C1. The combined critical gel and Rouse model fits G' and G'' well over the full range of frequencies.

Table 2.3: Critical gel and Rouse model fits for small angle oscillatory shear measurements of representative chewing and bubble gums.

Sample	S [Pa-s^n]	n [-]	G_R [Pa]	λ_R [s]
B1	30500	0.242	46400	0.01
C1	11900	0.270	501000	0.0001
B2	12800	0.251	–	–
B3	80400	0.341	–	–
B4	55000	0.352	–	–
C2	83400	0.332	–	–
C3	169000	0.226	–	–
C4	58600	0.238	–	–

B1 and C1 were fit to the full frequency sweep data with the combined fit of the critical gel and Rouse equations. Samples B2-B4, C2-C4 were only fit to the critical gel equation over the low frequency regime (0.1-10 rad s^{-1})

The relatively high values of S and low values of n for C1 and B1 are consistent with a stiff gel;[66] a soft gel has $0.5 < n < 1.0$ and an ideal gel is defined by $n = 0.5$. Although n happens to be about equal for the two samples, the discrepancy in the other fitting parameters exposes differences in their compositions. The smaller value of S for B1 means that this particular bubble gum has a lower modulus than the chewing gum. Also, the larger G_R and smaller λ_R for B1 suggest the presence of smaller components that are able to relax stress faster. Regardless of these quantitative differences, C1, B1, and all the other gums examined are qualitatively the same; that is, they behave as critical gels over a wide range of frequencies (Figure 2.6). The specific values of S and n for samples B2-B4, C2-C4 extracted from fits of the critical gel equation are also listed in Table 2.3.

2.3.3 Nonlinear viscoelasticity: start-up of steady shear

In order to characterize chewing and bubble gums under large and unsteady deformations, start-up of steady shear was employed, a relatively simple rheological test to probe nonlinear viscoelastic behavior based on established theory.[67] For C1, the transient viscosity depends greatly on shear rate, as shown in Figure 2.7. The transient viscosity at a given

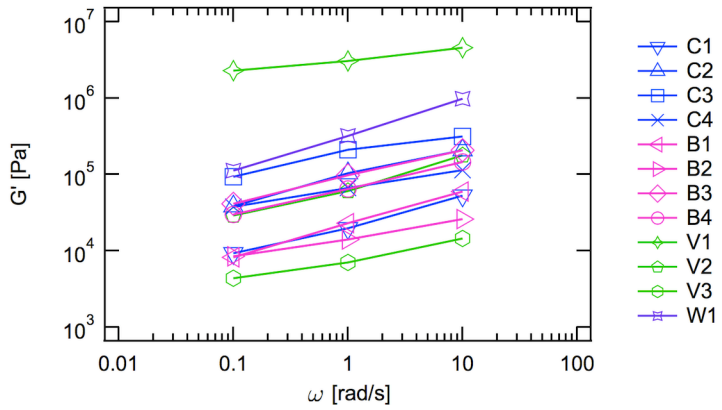

Figure 2.6: Frequency sweeps of chewing gums, bubble gums, lab-scale gums, and wax at 37 °C.

time decreases with increasing shear rate, a common phenomenon in polymeric materials. Slight stress overshoots are present at 10^2 s^{-1}, the highest shear rate employed. Note that deviations for times < 0.05 s, marked with the dashed line in Figure 2.7a, are ignored due to finite response times of the instrument, and similar designations have been made for subsequent transient tests. At a given shear rate, there were insignificant differences between chewing and bubbles gums (Figure 2.8).

Thee start-up of steady shear behavior of C1 was fit to the critical gel power-law fit extracted from the SAOS data. In the limit of linear viscoelasticity, the critical gel power-law model for start-up of steady shear can be expressed in the following manner:[64]

$$\eta^+(\dot{\gamma}_0, \gamma) = Sf(\dot{\gamma}_0)\Phi(\gamma) = \frac{S}{1-n}\dot{\gamma}_0{}^{n-1}\gamma^{1-n} \tag{2.6}$$

Factoring out the shear-rate dependence $f(\dot{\gamma}_0) = \dot{\gamma}_0{}^{n-1}$ in equation 2.6 collapses the start-up of steady shear data to a single curve dependent only on strain, $S\Phi(\gamma) = S\gamma^{1-n}/(1-n)$. The results of this analysis are shown in Figure 2.7b, using the S and n values derived from the power-law fit in SAOS. For strains < 0.1 and strain rates < 0.01 s^{-1}, the curves nearly fall onto a master curve. The critical gel power-law fit predicts the data well in this linear region, showing consistency between rheological tests. For larger strain rates and strains,

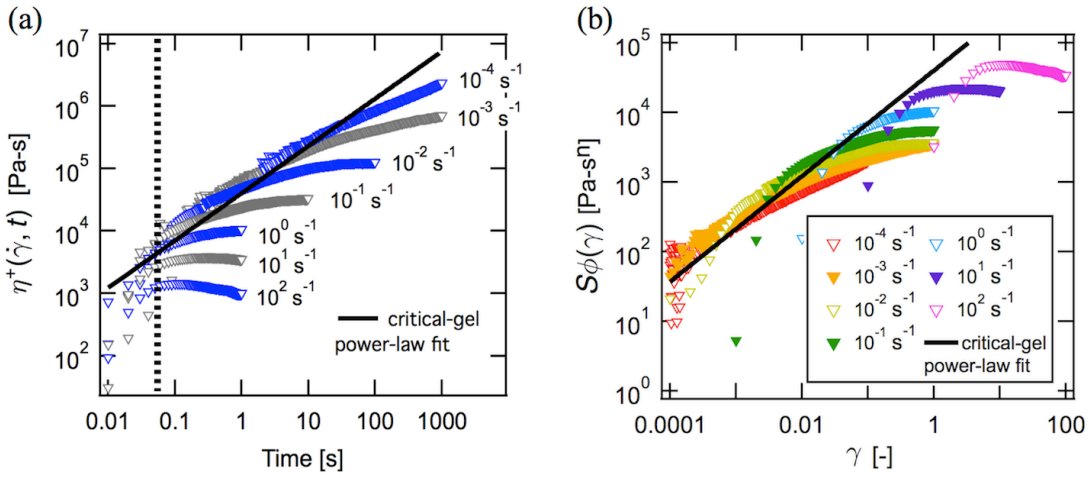

Figure 2.7: a) Start-up of steady shear results for C1. Note that a steady state could not be attained. b) $S\Phi(\gamma)$ versus total strain, where $S\Phi(\gamma)$ is equal to the transient viscosity with the critical gel shear rate dependence, $(\dot{\gamma_0}^{n-1})$, factored out. The data collapse onto a single curve for small strains, and this is accurately predicted by the critical gel power-law model.

however, large deviations occur. This demonstrates strong nonlinear behavior and network destruction with lower resistance to deformation, as all curves deviate below the critical gel power-law fit. (Network here and later is defined as a weak interconnectivity between microstructures in the gums, for example waxes and fillers or entangled polymers, which can be disrupted by shear or extension). With this start-up data, it is unclear if the network destruction corresponds to decreased elastic stored energy, viscous dissipation, or both. This can be clarified using creep recovery tests and especially nonlinear oscillatory measurements.

2.3.4 Nonlinear viscoelasticity: shear creep

Creep is a particularly useful tool for understanding relaxation phenomena at longer time scales.[68] During a more conventional step strain experiment, the long relaxation times become obscured as the measured stresses decay. In a creep experiment, the constant stress

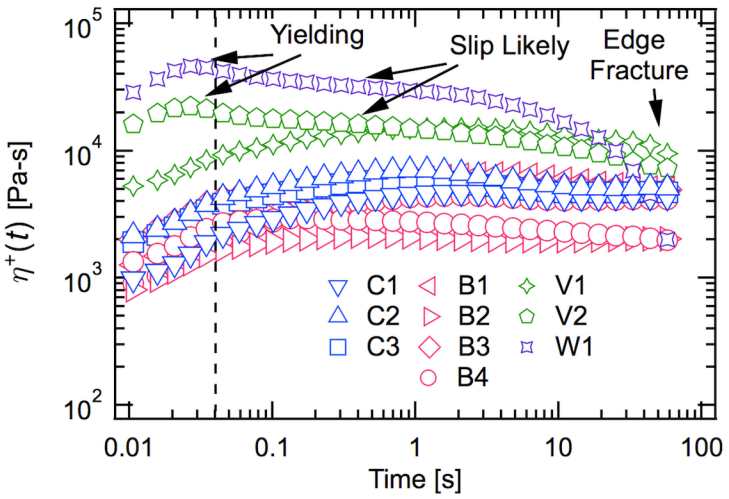

Figure 2.8: Start-up of steady shear results for chewing gums, bubble gums, lab scale gums, and wax at a strain rate of 1.732 s^{-1}. Experimental concerns included yielding, slip, and edge failure. Inconsistencies at times < 0.04 s (denoted by the dotted line) are attributed to finite start-up time of the instrument.

allows for measurable strain responses at longer times. The results obtained from a creep test on C1 are shown in Figure 4.8. At lower stresses ($100 \leq \sigma \leq 600$ Pa), the compliance is nearly independent of shear stress, although some nonlinear softening can be observed. The dependence on shear stress becomes strikingly apparent at higher stresses (> 600 Pa). At 100 s, the compliance is still increasing for all stresses in Figure 4.8, and C1 exhibits a steady state for the lower stresses ($100 \leq \sigma \leq 600$ Pa). Such behavior can be captured by a standard linear liquid model such as the 4-parameter Voigt model.[69] However, based on the previous results of SAOS and start-up of steady shear experiments, it is likely that the lower stress data is more accurately captured with the critical gel model that reduces to the following equation in shear creep:[64]

$$J(T) = \frac{1}{S\Gamma(1-n)\Gamma(1+n)} t^n \tag{2.7}$$

from which values of $n = 0.42$ and $S = 21800$ are obtained. This corresponds to a softer material (higher n, lower S) for the 100 Pa creep test compared to the small amplitude

oscillatory shear results (see Table 2.3). This is consistent with being in the nonlinear regime and softening the network. Although nonlinear, the very good fit for t $>$ 40 ms provides strong evidence that C1 behaves like a critical gel in shear creep at low stresses.

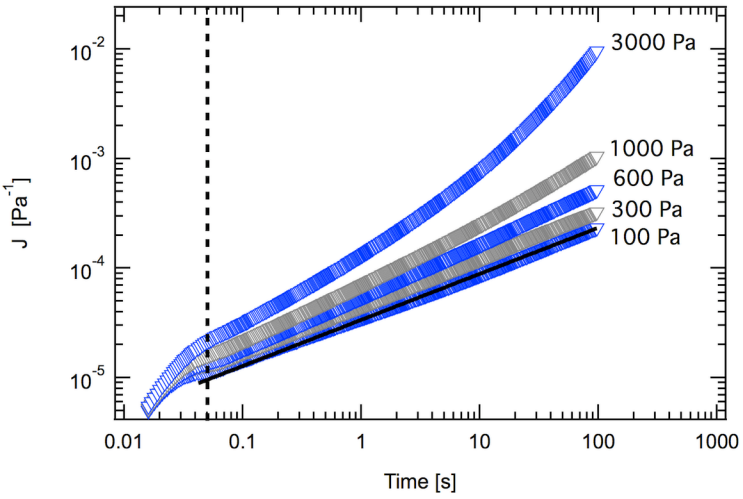

Figure 2.9: Shear creep results for C1 at various shear stresses. A power-law model was fit to the 100 Pa curve, the curve most likely to be in the linear regime. Strong non-linear behavior is readily apparent for the highest imposed stresses, 1000 and 3000 Pa. The data is ignored for times $\leq$ 40 ms due to the finite start-up time to attain the desired stress.

Close to the linear regime of stresses ($\sigma \leq$ 600 Pa), all chewing and bubble gums show similar creep responses (Figure 2.10). However, chewing and bubble gums can be distinguished by the fractional recovery upon the cessation of a large imposed shear stress as is shown in Figure 4.9. Here, fractional recovery is defined as γ_R/γ_M where γ_M is the measured strain after 100 s of deformation, marking the end of the creep test, and γ_R is the recovered strain after 100 s of zero shear stress. At low shear stresses ($\sigma \leq$ 600 Pa), all chewing and bubble gums had similar fractional recoveries. However, for an imposed shear stress of 1000 Pa (marking the onset of the more dramatically nonlinear regime), there were substantial differences in the fractional recovery between chewing and bubble gums - chewing gums recovered 25-40% of the original strain, whereas bubble gums recovered only 0-15%. With an imposed stress of 3000 Pa, none of the samples recovered more than 5%

of the original strain, masking the inherent differences in chewing and bubble gums.

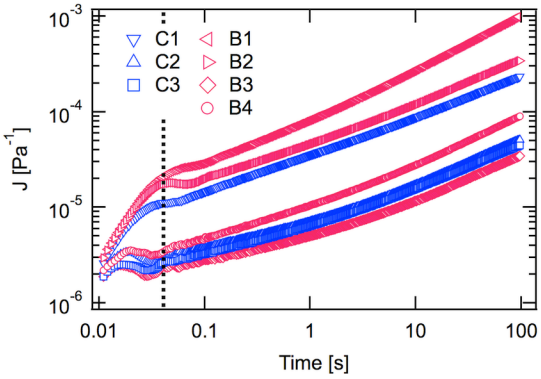

Figure 2.10: Shear creep results for chewing and bubble gums at a stress of 100 Pa showing critical gel like behavior for all samples. Inconsistencies at times < 0.04 s (denoted by the dotted line) are attributed to finite start-up time of the instrument.

This discrepancy in the fractional recovery of chewing versus bubble gums after a stress of 1000 Pa is consistent with the functionality of these commercial products. The ability for chewing or bubble gum to partially recover its original shape after being subjected to shear stresses is vital for proper sensory feel. This accounts for the relatively high fractional recoveries at smaller stresses. However, bubble gum has the additional task to form large, stable bubbles when blown at high shear stresses across the tongue. For the base of the bubble to maintain its shape and delay collapse, little to no fractional recovery is desired, such as those found at shear stresses of 1000 Pa. Chewing gum, not having this design limitation, naturally has a higher fractional recovery at this stage. At shear stresses as high as 3000 Pa all gums are strained to such a degree that even moderate fractional recoveries are impractical.

2.3.5 Nonlinear viscoelasticity: large amplitude oscillatory shear (LAOS)

Transient viscosity $\eta^+(t;\dot{\gamma}_0)$ and creep compliance $J(t;\sigma_0)$ reveal nonlinear shear network destruction of the gums studied here, but do not distinguish between decreased elastic stored energy, viscous dissipation, or both. These measures based on step inputs combine

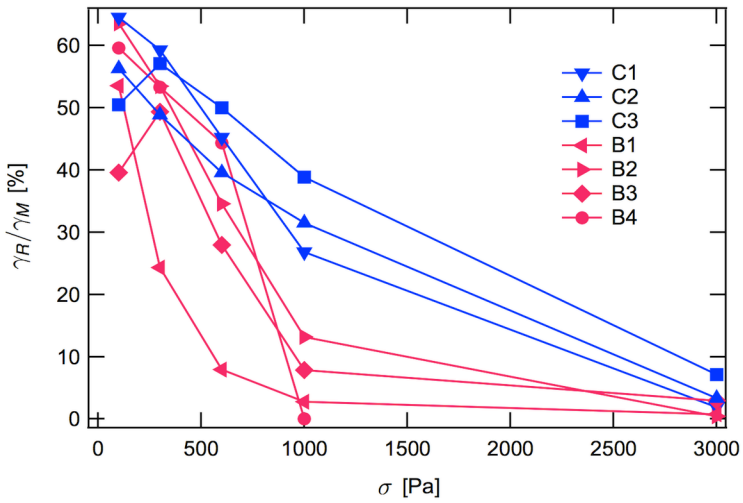

Figure 2.11: Shear creep fractional recovery at various shear stresses at 37 °C after 1 h of recovery. At $\sigma = 1000$ Pa, chewing gums show significantly greater fractional recovery than bubble gums. This stress of 1000 Pa coincides with the transition to the more dramatically nonlinear regime.

elastic and viscous effects together. In contrast, large amplitude oscillatory shear (LAOS) can decompose the effects of nonlinear elastic energy storage and viscous energy dissipation, since the oscillatory protocol imposes strain and strain-rate out of phase by exactly $\pi/2$ radians (i.e. in quadrature). Additionally, the smooth oscillatory conditions are less prone to experimental errors compared to abrupt step inputs. The resulting nonlinear oscillatory waveforms can be quantitatively described with a wide range of approaches; for a recent review on LAOS, see Hyun et al.[70] Here, the LAOS rheology of chewing and bubble gums are examined with first-harmonic moduli (cycle-averaged measures[55]), Lissajous curves, and the signs of leading order third-harmonic Chebyshev coefficients.

Figure 2.12 shows the LAOS response of chewing gum C1 at the frequency $\omega = 1$ rad s^{-1} in terms of the first-harmonic (cycle-averaged) elastic and viscous moduli, G_1' and G_1''. Sample C1 shows a nonlinear, monotonic decrease of both elasticity and dissipation as the critical gel network is disrupted by large strain amplitude. This qualitative behavior was observed all the gums listed in Table 1.1 (see Figure 2.13). A monotonic decrease of

both G_1' and G_1'' has been termed "Type I" LAOS behavior by Hyun et al.,[71] and can be found in a wide range of materials such as polymer melts, suspensions, and solutions. In the context of the linear viscoelastic critical gel network of the gums studied here, the decrease in elasticity G_1' indicates that the global (or average) network softening (e.g. due to disruption of network interactions) dominates any potential elastic stiffening (e.g. from the finitely extensible nonlinear elastic polymeric elements) which would otherwise increase G_1'.[72] The monotonic decrease in dissipation G_1'' is also noteworthy. Many yielding materials often show an initial strain-dependent increase and subsequent local maximum of G_1'', concomitant with monotonically decreasing G_1' (Type III behavior of Hyun et al.[71]). For the gum materials here, the microstructure also is yielding, but without a local maximum of G_1''.

The first-harmonic moduli G_1' and G_1'' are measures of cycle-averaged elasticity and dissipation; additional measures are required to fully characterize the nonlinear oscillatory response. The full response is shown by the raw oscillatory stress waveforms, which can be represented as a function of time, or more physically as parametric curves (Lissajous curves) as a function of the input strain or strain-rate. Representative Lissajous curves for chewing gum C1 are included in Figure 2.12 for $\omega = 1$ rad s^{-1} and $\gamma_0 = 100$, corresponding to the highest strain tested. The left Lissajous curve is normalized shear stress versus strain (the elastic perspective), with the dashed red line showing the decomposed elastic stress, a single-valued function of stress versus strain defined by Cho et al.[73] The right Lissajous curve is normalized shear stress versus strain-rate (the viscous perspective), and the dotted blue line is the decomposed viscous stress, a single-valued function of stress versus strain-rate. At this strain amplitude, the total stress curves are non-elliptical (and the decomposed stresses nonlinear), indicating that higher-harmonic nonlinearities are present. All gum materials tests showed qualitatively similar shapes to the Lissajous curves in Figure 2.12.

Higher-harmonics are interpreted to mean that local elastic energy storage and local viscous energy dissipation are changing through the deformation cycle (i.e. oscillating about

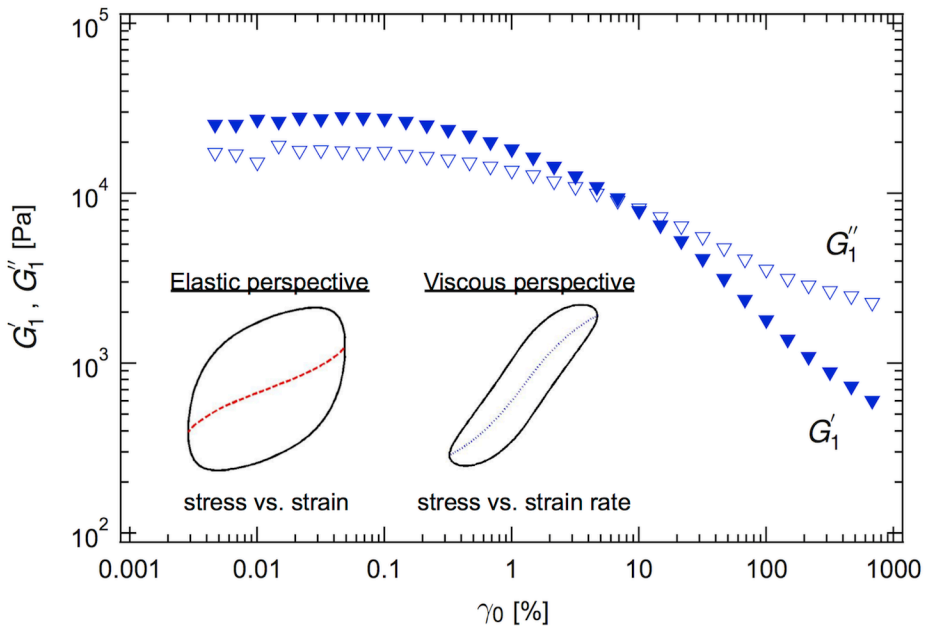

Figure 2.12: Large amplitude oscillatory shear for C1 showing the results of a strain sweep, 1st harmonic average moduli at $\omega = 1$ rad s^{-1}. The relative values of G_1' and G_1'' change in the nonlinear viscoelastic regime. The insets are of the corresponding Lissajous curves at $\omega = 1$ and $\gamma_0 = 100$; left curve depicts stress vs. strain, right curve stress vs. strain rate. Interpretations of first-harmonics, Lissajous curves, and leading-order third-harmonic nonlinearities are described in the text.

the cycle-averaged values of the first-harmonics). The concavity of the decomposed stresses, represented at leading order by the signs of third-harmonic Chebyshev coefficients,[55] indicate if these deviations are driven by locally high rates or high strains, as outlined by Ewoldt and Bharadwaj (their Fig. 7).[72] In the context of the global elastic softening of G_1', the concavity of the decomposed elastic stress curve shows that the most extreme local softening occurs at locally large values of shear-rate (which occur at zero local strain, since they are out of phase). Quantitatively, this elastic concavity corresponds to positive third-harmonic Chebyshev coefficient $e_3 > 0$, and interpreted as elastic softening driven by large strain-rate, i.e. at this frequency, large strain-rates are disrupting the elastic features of the critical gel network. Similarly, the viscous features of the critical gel network are

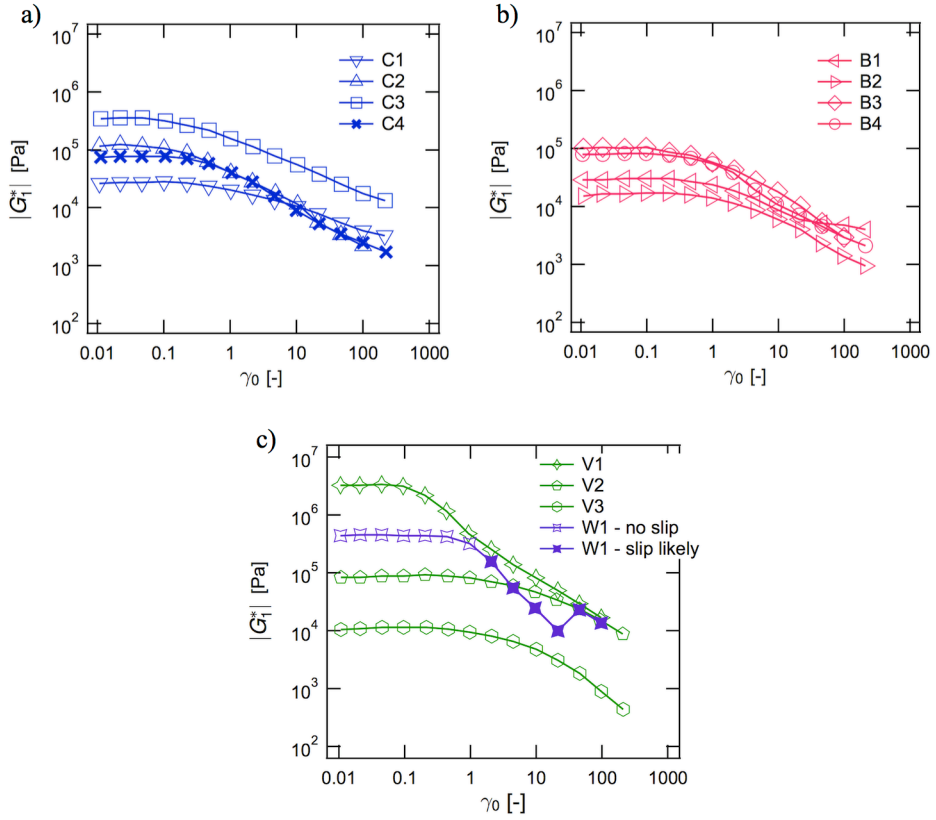

Figure 2.13: Strain sweeps showing 1st harmonic average moduli for chewing gums, bubble gums, lab-scale gums, and wax. The relative values of change in the nonlinear viscoelastic regime.

also disrupted by large strain-rates. This conclusion is supported by the observation of decreasing G_1'' along with the negative leading-order viscous third-harmonic $v_3 < 0$; this appears visually in the Lissajous curve of decomposed viscous stress as negative concavity (curve bending down) in the domain of positive instantaneous strain rate.

These LAOS results indicate that, in simple shear deformation, the critical gel network is disrupted at large shear rates, decreasing the normalized elastic stored energy and viscous dissipated energy represented by G_1' and G_1''. However, the extensional demonstrations in Figure 2.1 suggest that extensional deformations may induce elastic or viscous hardening

that dominates network disruption. This is examined in the following section with uniaxial extension tests.

2.3.6 Nonlinear viscoelasticity: start-up of steady uniaxial extension

Uniaxial extensional tests have been utilized primarily to characterize long-chain polymeric materials such as entangled homopolymer melts and solutions,[74–76] dilute and semidilute polymeric solutions,[77–79] and multiblock copolymers systems[80] in which the chain stretching mechanism, absent in most shear experiments, is of interest.[67] Due to the large elongations attainable by chewing gum, steady uniaxial extension is particularly relevant.[81] In order to apply constant rates of deformation, the gum samples were uniaxially stretched at a range of constant Hencky strain rates, $\dot{\epsilon}$, where $\dot{\epsilon}t = \epsilon = \ln(L/L_0)$. The effect of on the extensional viscosity is quite dramatic (Figure 4.17). All gum samples investigated exhibited a lack of a linear viscoelastic envelope, and macroscopic failure occurred before reaching a steady-state. At $\dot{\epsilon} \leq 0.10$ s^{-1}, the extensional viscosity plateaus before macroscopic failure occurs. In contrast, at higher $\dot{\epsilon} \geq 0.25$ s^{-1}, the samples undergo necking and significant strain hardening leading up to the point of failure. These two distinct regimes suggest that different microstructures are relevant at different time scales.

At the lower $\dot{\epsilon}$, the strain softening is indicative of the break-up of a brittle or fragile network. This network likely corresponds to the conglomeration of fillers and waxes that compose the bulk of the base. At higher $\dot{\epsilon}$, the molecular origin of strain hardening could be due to a variety of mechanisms, including non-affine deformation of flexible polymers beyond the Gaussian statistical limit,[82] strain-induced crystallization,[83] or aggregation within colloidal gels.[84]

Start-up of steady uniaxial extension was especially revealing in distinguishing commercial chewing from bubble gums as shown in Figure 4.18. Subsequent tests were run at $\dot{\epsilon} = 1$ s^{-1}, since this Hencky strain rate is indicative of the type of deformations that gum undergoes during use. The linear response (low ϵ) is rather similar between chewing and

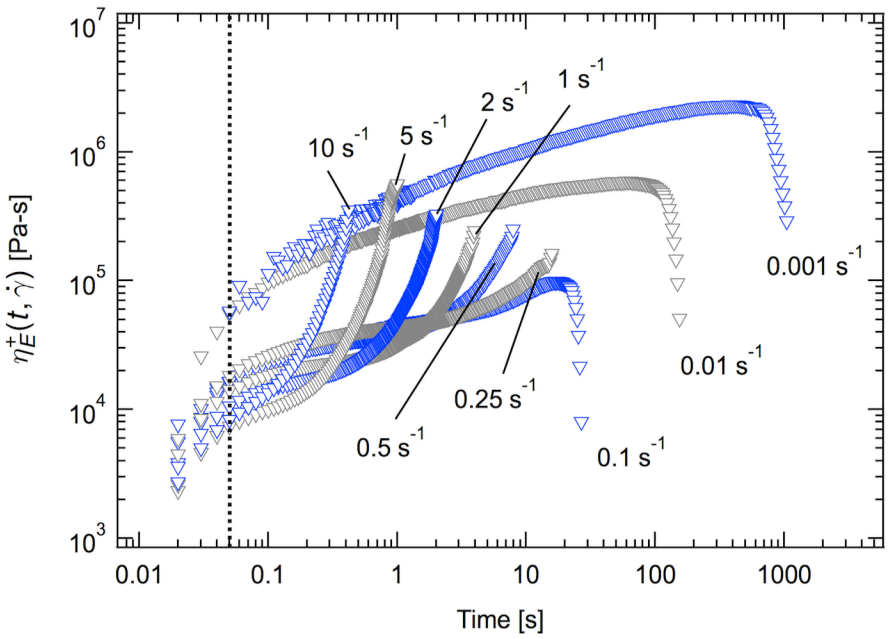

Figure 2.14: Results for start-up of steady uniaxial extension for C1 demonstrating the strong effect of strain rate on extensional behavior. The extensional viscosity plateaus before macroscopic failure at the lower strain rates ($\dot{\epsilon} \leq 0.10$ s^{-1}) while necking and strain hardening occur at larger Hencky strain rates ($\dot{\epsilon} \geq 0.25$ s^{-1}). Sagging was observed at the lowest Hencky strain rate ($\dot{\epsilon} = 0.001$ s^{-1}). The dotted line at t = 0.05 s marks the end of transient uniaxial extension due to instrument start-up.

bubble gums, but more stark differences appear at large strains ($\epsilon > 1$). Bubble gums typically sustained larger stresses and had more significant strain hardening than commercial chewing gums. To be quantitative, the peak extensional stresses of bubble gums were $> 2.0\times10^6$ Pa versus $\leq 2.0 \times 10^6$ Pa for chewing gums. The one exception was sample B2 with a maximum stress 3.0×10^5 Pa, reminiscent of a typical chewing gum. These findings are consistent with previous studies that found that extensional thickening stabilizes film blowing for polyethylene[85,86] and bubble blowing for bubble gum,[81] a trait necessary for bubble gums but not chewing gums.

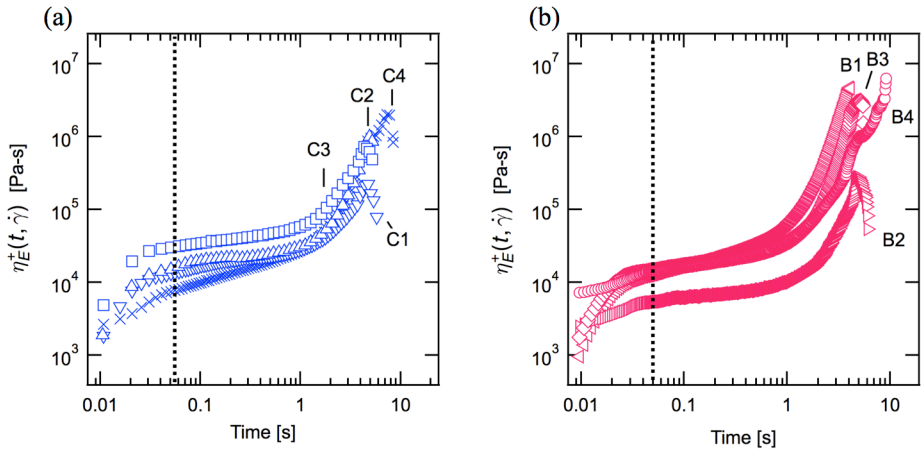

Figure 2.15: a) Chewing and b) bubble gum behavior during start-up of uniaxial extension at $\dot{\epsilon} = 1$ s^{-1}. The dotted line at t = 0.05 s marks the end of transient uniaxial extension due to instrument start-up. The bubble gums, in general, are able to withstand greater extensional stresses and have more pronounced strain hardening. A notable exception to this trend is B2, the bubble gum tape.

2.4 Conclusions

For the first time in the literature, a series of linear and nonlinear rheological tests have been conducted to characterize chewing gum at large, unsteady deformations, and chewing and bubble gum are found to share a distinct rheological profile unlike other classes of materials. To justify this claim, these findings are compared to similar materials of note. Polyisobutylene, a major polymeric component of chewing and bubble gum base, is an entangled melt with a plateau modulus.[1,63] Although chewing and bubble gum have extensional strain hardening reminiscent of that of polyisobutylene, their dynamic responses do not demonstrate terminal behavior at low frequencies. Other filled elastomers, such as highly loaded clay nanocomposities,[87] can exhibit qualitatively similar dynamic responses as chewing or bubble gum, yet there is no evidence of the Payne effect (marked by a local maximum of G_1'' in a strain sweep) in any commercial gum tested. Like chewing or bubble gum, wheat gluten[64] and poly(vinyl) chloride gels at the gel point[88] demonstrate critical

gel behavior marked by power-law fits over the gamut of linear viscoelastic tests. However, these critical gels lack the substantial strain hardening in uniaxial extension inherent in all chewing and bubble gum tested. Only in chewing and bubble gums is power-law critical gel behavior in the linear regime coupled with such dramatic large strain extensional behavior.

From the rheology, one can glean information on the microstructure of chewing and bubble gum. Shear experiments demonstrate that chewing and bubble gum behave like a *firm* critical gel at small deformations. This result suggests the presence of a percolating network of various length scales throughout the chewing gum base. However, this network is rather fragile - the linear regime only encompasses the smallest shears and shear rates, and elastic and viscous softening dominate the strain response during large amplitude oscillatory shear. Another more robust network also exists, which produces the strain-hardening behavior during uniaxial extension. With these observations and knowledge of typical chewing gum ingredients, the links between ingredients and rheology are speculated. However, in designing for *performance*, the exact material origins for the macroscopic behavior do not matter. The unique rheological fingerprint has been shown to be enough to define chewing gum, and a variety of compositions that give this rheological fingerprint will lead to the same product in terms of function. This design approach is common for complex microstructured products such as ice cream, paints, or alloys in which the structure-function framework, rather than specific materials, dictates desired properties and performance.[89,90]

Additionally, rheology was used to differentiate between chewing gum products, namely conventional "chewing" gum and "bubble" gum, and to elucidate how certain deformations correlate with product function. Shear creep recovery experiments revealed that at moderate stresses, chewing gums recover a substantially larger percentage of imposed strain than bubble gums. This was argued to be correlated with the need for bubble gum to retain strain after being spread across the tongue in order to sustain bubbles. Start-up of steady uniaxial extension showed that bubble gums withstood larger stresses before rupture. Since bubble gums are marketed to consumers for their propensity to form large bubbles, this finding is

consistent with previous reports that extensional thickening stabilizes film blowing. In the future, it would be advantageous to explore the rheological response of a stress-controlled uniaxial or biaxial extension since these deformations are more reminiscent of how chewing or bubble gums are stretched during use.

In the design of soft solids, rheology and performance are inherently linked. To ensure that these materials meet the necessary performance criteria, one must analyze the full, complex high-dimensional rheological signature including nonlinear deformations in both shear and extension. Our approach to characterizing chewing and bubble gum – correlating a unique rheological fingerprint and individual rheological responses to performance – is applicable to a wide range of materials including cosmetics, foods and adhesives. This systematic approach to product design, drawing on academic rigor and motivated by commercial viability and practical experience, forms a universal paradigm for the development of new technology.

Chapter 3

Block Copolymer Blends for Chewing Gum Applications

3.1 Introduction

Thermoplastic elastomers (TPEs) are a class of materials that have the mechanical properties of vulcanized rubber yet are thermally processable like conventional thermoplastics.[91] Typically, TPEs are microphase separated systems that contain elastomeric sections anchored by glassy or semicrystalline "hard" domains that act as physical crosslinks. Although mechanically robust at lower temperatures, above the glass transition temperature (T_g) and/or melting temperature (T_m) of the hard domains, the material becomes much softer and is often easily processable. One of the simplest architectures for a TPE is an ABA triblock copolymer in which the "A" domain is hard and the "B" domain is elastomeric, driven to microphase separate due to chemical incompatibility between the blocks.

The first patented TPE was a thermoplastic polyurethane invented by DuPont in the

Part of this work was done in collaboration with Professor Sangwoo Lee and Tao Yang from the University of Minnesota and Dr. Leslie Morgret and Niku Tseng from the Wm. Wrigley Jr. Company. Financial support came from the Wm. Wrigley Jr. Company.

1950s.[91] In the 1960s, Shell began selling anionically synthesized poly(styrene-*b*-butadiene-*b*-styrene) (SBS) and poly(styrene-*b*-isoprene-*b*-styrene) (SIS) triblock copolymers under the trade-name Kraton©.[91] Since then, a wide array of TPEs have been commercialized for applications ranging from adhesives, sealants, and coatings; bitumen modification; viscosity modifiers; blend compatibilizers; and vulcanized rubber replacements.[91] The chemical nature of TPEs are as varied as their applications, including polyolefins, polyesters, polyurethanes, polyamides, polyethers, polysiloxanes, and poly(ether-imide)s.[92]

Although the classic ABA triblock is quite versatile and widely useful, a great amount of research over the decades has been devoted to understanding ways to further modify the mechanical properties of TPEs off this basic architecture. Some have looked at more complex polymer architectures such as multigraft copolymers,[93,94] bottlebrushes,[95] and asymmetric miktoarms.[96] Others have developed TPEs that rely on other intermolecular interactions to form physical cross-links such as ionomers,[92] directed hydrogen bonding,[97] or metal-induced self-organization.[98] From "super-elastic" to self-healing materials, each class of TPEs has properties typically useful certain for applications, but no single platform serves as a panacea for the entire industry.

Here, a very simple strategy to modulate the mechanical and rheological responses of TPEs is investigated: blending in AB diblocks. A number of individuals have looked at such a strategy in the context of SIS triblocks and SI diblocks, typically for adhesives.[14,99–102] In each of these studies, the SI diblocks had identical compositions but half the molecular weights of the SIS triblocks. It was found that the addition of SI diblocks to SIS triblocks did not effect the linear viscoelastic behavior, yet they significantly altered the nonlinear extensional properties of the SIS triblocks. This occurred since the SI diblocks introduced *dangling ends* to the rubbery isoprene matrix. These entangled dangling ends were indistinguishable from entangled *bridging* domains of the SIS triblocks at small deformations; however, at large deformations, the dangling ends were free to relax, unlike the bridges

blocks whose ends are anchored within the hard domains.[101,102] The final adhesive performance properties (e.g. tack, peel strength) of the SIS triblocks, being intrinsically related to the nonlinear viscoelastic profile, changed as well.[14]

This chapter builds upon this paradigm, adopting a similar strategy to sustainable polymers based on renewable polyesters. Specifically, block polymers based on poly(D,L-lactide) (PLA or L) and poly(ϵ-decalactone) (PDL or D) were synthesized to make ternary blends of high molecular weight LDL triblocks, high molecular weight DL diblocks, and low molecular DL diblocks. First, previous work by collaborators will be discussed and the specific motivation of this study will be explained. Next, the full molecular, morphological, and rheological properties of the DL diblocks, LDL triblocks, and the blends will be discussed with particular focus on extensional behavior. These blends will then be assessed for their potential use for chewing gum bases, building off the design parameters determined in Chapter 2. Finally, preliminary results for blends of short DL diblocks with $(DL)_n$ multiblocks will be summarized along with suggestions for future work.

3.2 Background

3.2.1 Previous work

Previously, Lee et al. sought to modulate the mechanical properties of high molecular weight elastomeric LIL triblocks (L = poly(D,L-lactide), I = polyisoprene) by blending in low molecular weight, unentangled IL diblocks.[103] Representative extensional data are shown in Figure 3.1 for blends of one LIL triblock (M_n = 95.1 kg mol^{-1}, f_{PLA} = 0.36) and one IL diblock (M_n = 7.4 kg mol^{-1}, f_{PLA} = 0.41). The IL diblock was mechanically weak, strain softened, and failed at relatively low strains ($\epsilon < 1$) while the pure LIL triblock was stiff, strain hardened, and had a strain at break (ϵ_b) of 1.8. Blends of the two components had **both** the strain softening behavior of the diblock at small strains with the strain hardening behavior of the triblock at large strains. Remarkably, the ϵ_b of all the blends

tested were greater than either the LIL triblock and IL diblock, even with as little as 1 wt.% LIL triblock. From this study, it was determined the optimal blend composition that maximized both stress and strain at break was **20 wt.% triblock, 80 wt.% diblock**.

At this composition, the majority component, the diblock, dictates the small strain or *linear* viscoelastic behavior, while the minority component, the triblock, dictates the large strain or *nonlinear* viscoelastic behavior. This gives a viable route to independently tune the linear and nonlinear viscoelastic behavior with judicious choice of the starting block polymers, making it a particularly attractive platform for such applications such as chewing gum bases in which the performance is intrinsically tied to the rheological behavior and both small and large strains.

Surprisingly, this behavior held true even though the IL diblock and LIL triblock were only partially miscible and showed evidence of macrophase separation. Through small-angle X-ray scattering and transmission electron microscopy, it was determined the blends macrophase separated into distinct domains – a "diblock rich" domain and a "triblock rich" domain. Within each domain, however, there was microphase separation and the presence of both components. Although some sort of microphase separation was critical, the precise morphology did not play a major role in determining the mechanical and rheological response of these blends.

3.2.2 Purpose of this work

Based on these previous findings, it appears that blending AB diblocks and ABA triblocks is a robust and versatile platform to modulate rheological behavior to obtain a desired response. To further explore the parameter space, three additional variables were investigated in the context of modulating TPEs via blending:

1. Polymer composition

2. Diblock molecular weight

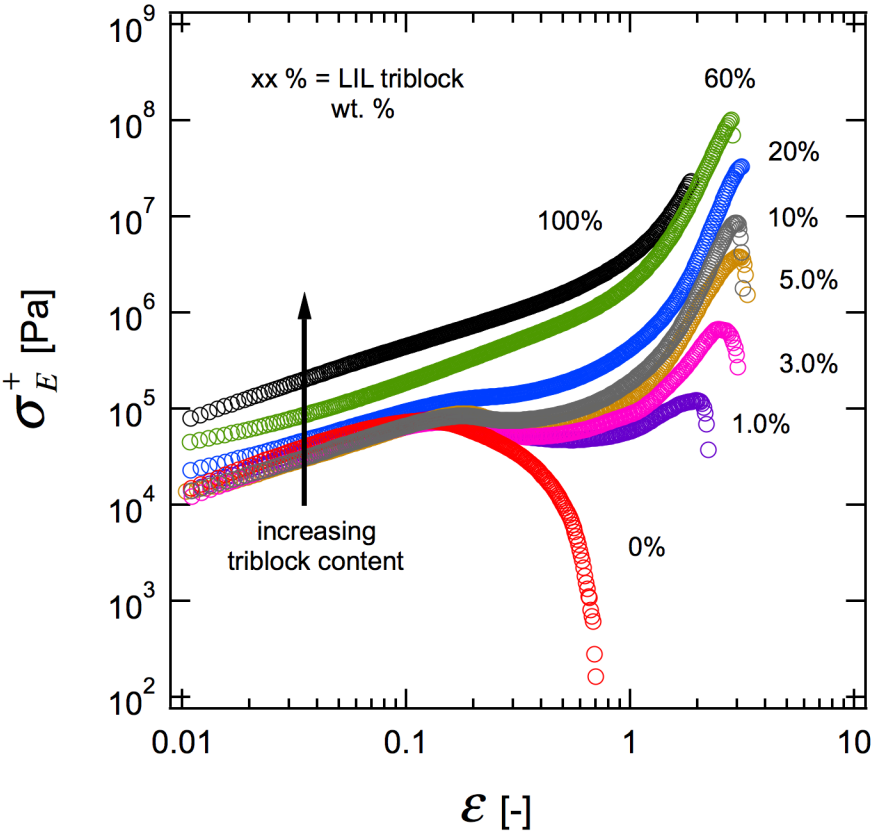

Figure 3.1: Mechanical response of blends of LIL triblocks and IL diblocks. Adopted from the literature.[103]

3. Polymer architecture

For the nonlinear behavior of ABA thermoplastic elastomers, the effect of *polymer composition* is well documented in the literature in the context of tensile testing.[104–107] Although these tensile tests are slightly different than the extensional rheological tests employed here, the same basic trends should hold true. In general, the modulus (E), yield stress (σ_y), and stress at break (σ_b) scales with the volume fraction of A (f_A), while strain at break (ϵ_b) scales with molecular weight and volume fraction of the elastomeric midblock. Also, these materials transition from *elastomeric* to *plastic* behavior at around $f_A = 0.50$.

In this chapter, only the elastomeric limit is of interest.

In terms of *diblock molecular weight*, as discussed in the introduction, others have blended high molecular weight entangled SI diblocks with elastomeric SIS triblocks and found similar general trends to Lee and coworkers.[101,108] However, no one has directly compared the effects of entangled *versus* unentangled soft blocks on the final mechanical and rheological behavior of the blends. It is hypothesized that entangled diblocks would begin to fail at higher strains than unentangled IL diblocks since the entanglements may act as temporary crosslinks, delaying the onset of failure and adding an additional relaxation time to the system. This additional relaxation time could provide another adjustable parameter to further dictate the rheological response of the blends.

The last section explores the effect of *polymer architecture* by replacing the ABA triblock with an $(AB)_n$ multiblock with a comparable molecular weight and f_A. Rather than a single, rubbery entangled midblock anchored by two hard domains like in the triblock, the multiblock is composed of many unentangled rubbery blocks held together by several shorter glassy domains. Previous work by Matsumiya and coworkers suggest remarkable extensibility for $(SIS)_n$ multiblocks,[80] yet no one has tried blending in low molecular weight diblocks or extending at relatively high Hencky strain rates ($\dot{\epsilon} \sim 1\ s^{-1}$).

3.3 Experimental methods

3.3.1 Synthesis and blend preparation

Reagents

The ϵ-decalactone (99%, Sigma-Aldrich) was distilled under reduced pressure 3× and passed through a column of activated basic alumina (Fisher Scientific) without exposure to air. Tin (II) 2-ethylhexanoate (95%, Sigma-Aldrich) was distilled before use. 1,4-benzenedimethanol (99%, Alfa Aesar) was dried under reduced pressure and room temperature for 24 h. D,L-lactide (99.5%, Purac), benzyl alcohol (99% Sigma Aldrich), and 4,4'-methylene diphenyl

diisocyanate (MDI, Sigma Aldrich) were used as received. Toluene was purified by passage through activated alumina columns (Glass Contour, Laguna Beach, CA). All the aforementioned reagents were stored and handled in a glove box filled with argon.

Poly(ϵ-decalactone) synthesis

The polymers were synthesized in a similar manner as reported in the literature.[109] For the poly(ϵ-decalactone) homopolymer, a 500 mL pressure vessel was dried in an oven at 150 °C for at least 2 h directly before transfer into the glove box. The appropriate initiator (benzyl alcohol for an alcohol and 1,4-benzene dimethanol for a linear diol) and catalyst (tin (II) 2-ethylhexanoate, also referred to as tin (II) octoate) were prepared in the glove box with a 1:1000 catalyst:monomer loading in the pressure vessel and immediately transferred outside into a silicone oil bath. The reagents were mixed at 130 °C for 18 h. The pressure vessel was brought back into the glove box and aliquots were taken for characterization. For the pure poly(ϵ-decalactone) synthesis, the resulting polymer precipitated in methanol and allowed to settle at approximately 5 °C overnight. The methanol was decanted off and the solids collected and dried.

DL diblock and LDL triblock synthesis

Either monofunctional (for the DL diblocks) or difunctional (for the LDL triblocks) poly(ϵ-decalactone) homopolymer was poured in equal parts into three clean, oven dried 500 mL pressure vessels. D,L-lactide and toluene were added to each pressure vessel at a 1:1 ratio to create the poly(D,L-lactide) (L) end blocks with the poly(ϵ-decalactone) serving as a macroinitiator. The reagents were mixed at 70 °C for 30 min to pre-dissolve the D,L-lactide and macroinitiator in the toluene. The reaction proceeded at 110 °C for 3 h. The resulting polymer, be it a DL diblock or LDL triblock, were precipitated in methanol in the same manner as the poly(ϵ-decalactone) homopolymer.

Multiblock synthesis

Multiblocks were prepared by coupling LDL triblocks. Specifically, 1× stoichiometric equivalent of MDI was added to LDL triblocks in the glovebox before precipitation, while the triblocks were still in solution. The mixture was removed from the glovebox and mixed at 100 °C for 1 h. The resulting multiblock was precipitated in methanol in the same manner as the LDL triblocks or DL diblocks. A schematic is shown in Figure 3.2.

Blend preparation

Binary and ternary blends of DL diblocks and LDL triblocks were prepared via solvent blending. Appropriate masses of polymers were co-dissolved in dichloromethane and mixed. The solvent was allowed to evaporate under vacuum for one week before use. The final blend compositions can be found in Table 3.2.

3.3.2 Molecular characterization

Proton nuclear magnetic resonance (^{1}H NMR) was used to determined the number average molecular weight (M_n) of the synthesized polymers. ^{1}H NMR spectra were obtained with a Varian Inova spectrometer operating at 500 MHz and 25 °C using a 30 s relaxation time and 8 transients. Samples were prepared by dissolving 10 mg of polymer in 0.7 mL CD_2Cl_2 (Cambridge Isotope Laboratories, Inc., 99.8 atom % D + 0.05% V/V TMS). The M_n of the poly(ϵ-decalactone) homopolymers were determined based off of the ratio of initiator peaks to those in the polymer backbone δ (ppm) = 7.34 [$\mathbf{C_6H_5}$-, BA], 7.34 [-$\mathbf{C_6H_4}$-, DMB], 5.10 [-$C_6H_4\mathbf{CH_2}$O-, initiator], 4.86 [-$CH_2\mathbf{CH}(C_4H_9)$O-, PDL]. Near quantitative agreement between initiator and end-group peaks (δ (ppm) = 3.60 [-$CH_2\mathbf{CH}(C_4H_9)$OH, end group]) was used to verify the functionality of the low molecular weight polyesters prepared using benzyl alcohol (BA) as 1.0. For the higher molecular weight species, the end group peak became too small to quantify accurately. Peak integration (δ (ppm) = 5.2 [-$\mathbf{CH}(CH_3)$O-, PLA]) was used to calculate the M_n of the final DL diblocks and LDL

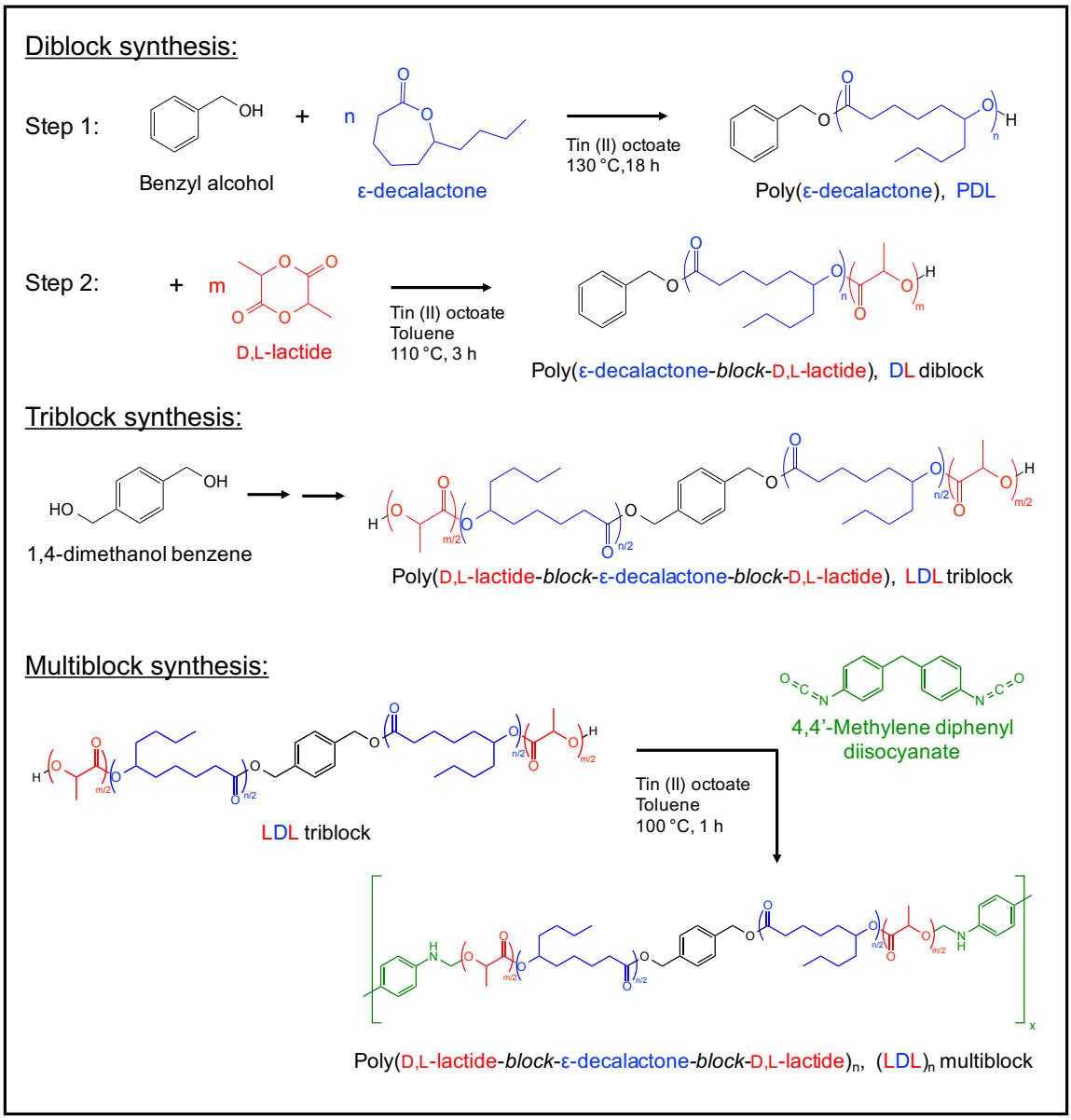

Figure 3.2: Synthesis of the DL diblocks and LDL triblocks by ring-opening polymerization, and synthesis of $(LDL)_n$ multiblocks by a combination of ring-opening and step-growth polymerizations.

triblocks. A representative ^{1}H NMR spectrum of a poly(ϵ-decalactone-*block*-D,L-lactide) diblock is shown in Figure 3.3.

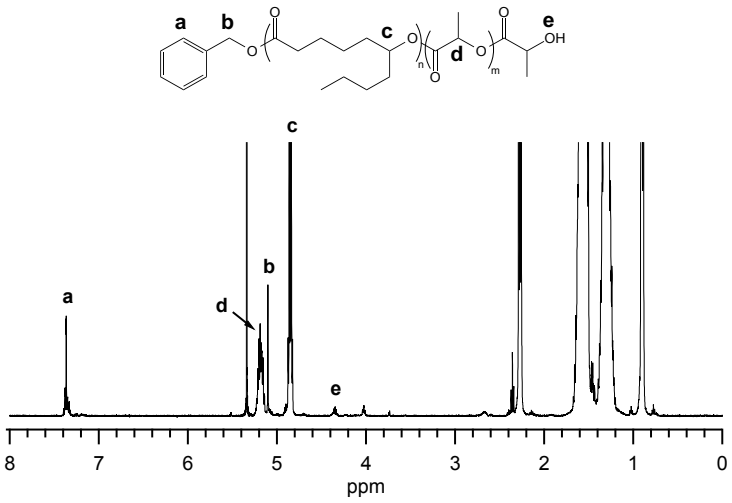

Figure 3.3: Representative ^{1}H NMR spectrum of a poly(ϵ-decalactone-*block*-D,L-lactide) diblock.

The dispersity ($Đ$) of each polymer was determined using size exclusion chromatography (SEC) performed on a Thermo Separation Products (TSP) Spectra Systems AS1000 autosampler equipped with three 5 mm Phenomenex Phenogel columns, a Waters 515 pump, and a Waters 2410 differential refractive index detector. Samples were run at room temperature in tetrahydrofuran at a flow rate of 1.0 mL min^{-1}.

3.3.3 Differential scanning calorimetry

Thermal properties of the block polymers and resulting blends were explored via differential scanning calorimetry (DSC) on a Thermal Analysis Q1000. Approximately 5 mg of sample were prepared in hermetically sealed aluminum pans. Materials were heated to 180 °C to erase thermal history, cooled to -100 °C at 10 °C min^{-1}, and heated to 180 °C at 10 °C min^{-1}. Glass transition temperatures (T_g's) are reported based upon inflection points in the second heating curve.

3.3.4 Small angle X-ray scattering

Small angle X-ray scattering (SAXS) was used to determine the morphology of the block polymers and blends. SAXS experiments were conducted at the Advanced Photon Source (APS) in Argonne National Laboratory (Argonne, IL) in sector 5-ID-D. Data were collected with an X-ray energy of 17 keV (λ = 0.729 Å) at room temperature with a detector-to-sample distance of 8.50 m. Samples were not annealed to more closely resemble the morphology that would arise during processing. The data were azimuthally integrated and are reported as intensity (I) versus the scattering wave vector (q) where $q = (4\pi/\lambda)\sin(\theta/2)$ and θ is the scattering angle.

3.3.5 Rheology

Shear rheology was investigated in small amplitude oscillatory shear (SAOS) on an ARES rheometer (TA Instruments) with 8 mm parallel plates. Samples were molded on the rheometer at temperatures above the T_g of the blocks (>60 °C) but below 180 °C to avoid degradation. Strain sweeps were conducted at a frequency (ω) of 1 s^{-1} to determine the linear viscoelastic (LVE) region. Frequency sweeps were then performed at a strain within the LVE regime. Isochronal temperature ramps were conducted at varying ramp rates and frequencies; however, in all cases, the sample was first cooled from a temperature in the disordered state to a temperature in the ordered state at a set temperature ramp rate. Then, the sample was heated at this same temperature ramp rate. The T_{ODT} is reported as the temperature in which a large drop-off in the storage modulus is observed upon heating.

Extensional rheology experiments were conducted using the extensional viscosity fixture (EVF) equipped on an ARES-G2 rheometer (TA Instruments). Samples were compression molded at room temperature to a thickness of approximately 0.5 mm. A rectangular punch was then used to create samples 25 mm × 5 mm × 0.5 mm. Samples were loaded on the EVF and annealed for at least 150 s before pulling at a constant Hencky strain rate ($\dot{\epsilon}$) of 1.0 s^{-1}.

Unless otherwise stated, all rheological experiments (both in shear and extension) were performed at 37 °C to correspond to typical mouth temperature.

3.4 Characterization of poly(ϵ-decalactone) homopolymer

For later analysis, the plateau modulus (G_N^0) and entanglement molecular weight (M_e of poly(ϵ-decalactone) must be experimentally determined as these values had not been previously documented in the literature.[2] First, a high molecular weight poly(ϵ-decalactone) was synthesized. The resulting SEC trace is shown in Figure 3.4. Due to adventitious initiation from impurities, the resulting poly(ϵ-decalactone) had a bimodal distribution with peaks corresponding to 170 kg mol^{-1} and 340 kg mol^{-1} based on polystyrene standards.

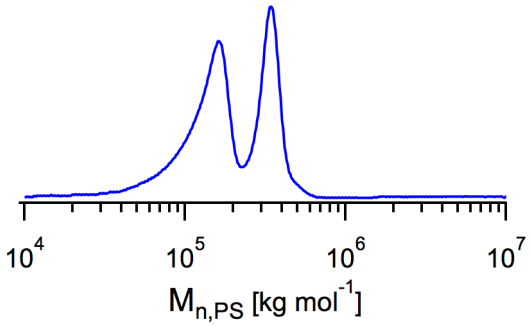

Figure 3.4: SEC plot of the high molecular weight poly(ϵ-decalactone) homopolymer.

A series of frequency sweeps were conducted at various temperatures, and the resulting data were shifted horizontally, employing the principles of time-temperature superposition (tTs) to create a linear viscoelastic master curve (Figure 3.5). The shift factors (a_T) were fit to the William Landel Ferry (WLF) equation[110] (equation 3.1) by manipulating the equation and completing a linear regression. The results of the linear regression are shown in the inset in Figure 3.5.

[2] A portion of this section appears uncredited in the literature.[109]

$$\log a_T = -\frac{C_1(T - T_r)}{C_2 + (T - T_r)} \tag{3.1}$$

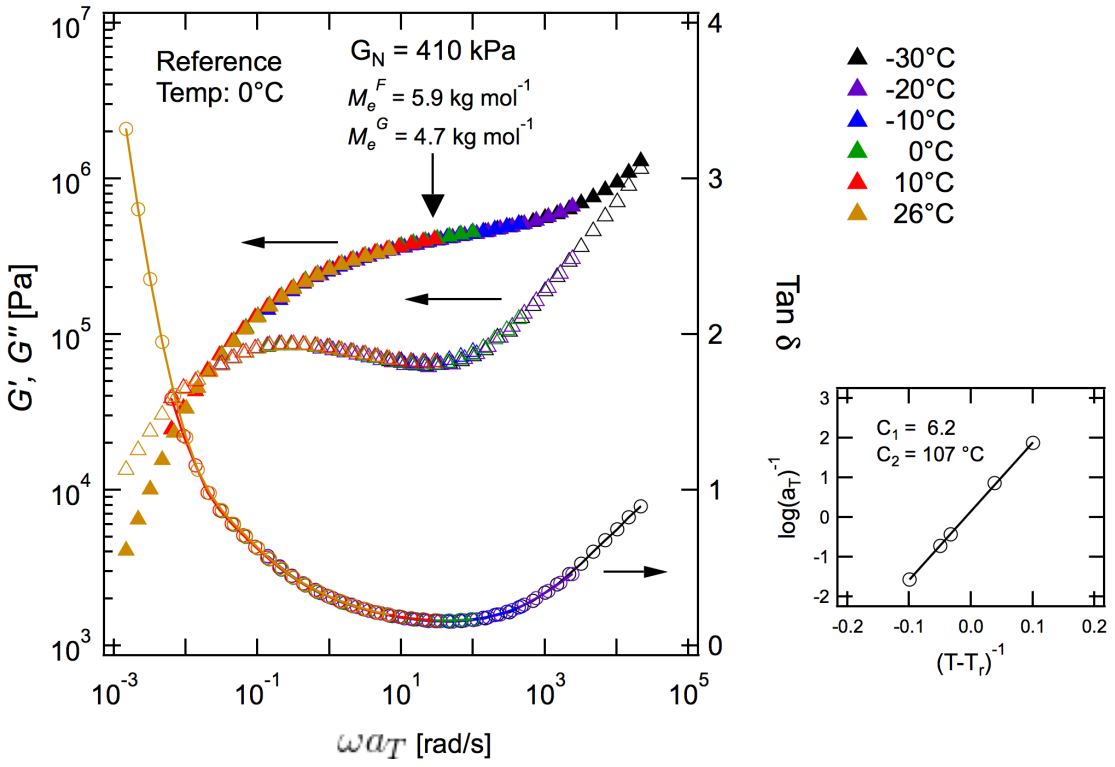

Figure 3.5: Master curves for the linear dynamic storage (G') and loss (G'') moduli of the poly(ϵ-decalactone) homopolymer with a reference temperature of 0 °C. Estimated values of M_e as well as the WLF fits are included.

From the linear viscoelastic master curve, the plateau modulus (G_N^0) was determined to be 410 kPa, taken as the value of G' at the minimum of $\tan\delta$. This approach has been shown to be a more accurate than using the value of G' at the minimum of G''.[111,112] From G_N^0, M_e can be calculated using the following relation:

$$M_e^F = \frac{\rho RT}{G_N^0} \tag{3.2}$$

where M_e^F refers to Ferry's original definition of M_e[113] which treats entanglements as

temporary rubber networks. This is contrast to the "G" definition of M_e based off the Doi-Edwards tube model that accounts for the sliding of chains along tubes; in this definition, M_e^G is defined as follows:[113]

$$M_e^G = \frac{4}{5} M_e^F \tag{3.3}$$

Using equation 3.2, M_e^F of poly(ϵ-decalactone) was determined to be **5.9** kg mol^{-1}.

In order for (G_N^0) to be accurate (within 10%) for monodisperse ($Đ$<1.1) homopolymers, the number of entanglements, Z, should be greater than 20, where $Z = \frac{M}{M_e^G}$.[112] Although the SEC trace is based off polystyrene standards, it is evident that $Z > 20$ for the poly(ϵ-decalactone) studied here. Thus, the polymer chains should be sufficiently long for the entanglement plateau to be present over a discernible frequency range. However, the bimodal distribution and larger dispersity makes it more difficult to see G_N^0 because of the faster terminal relaxation of the low molecular weight species. Based off prior studies, this measurement for G_N^0 (and the corresponding M_e^F) should be taken as estimate and accurate to roughly 20%.[112]

3.5 Behavior of the DL diblocks and LDL triblocks

3.5.1 Characterization

The DL diblock and LDL triblock polymers were synthesized using ring-opening polymerization and their molecular characteristics are summarized in Table 3.1. The M_n and composition of each polymer was calculated using ^{1}H NMR, while $Đ$ was determined from SEC. Small low molecular weight shoulders can be seen in the SEC traces for the LDL triblocks (Figure 3.6). Such shoulders are only observed in the triblocks for which a difunctional initiator is used, and thus, are attributed to adventitious initiation of monofunctional impurities.

Eight of the nine polymers showed distinct T_g's from DSC, providing evidence for microphase separation (Figure 3.7). The exception is LDL-1 in which no T_g for the L block

Table 3.1: Characterization of DL diblock and LDL triblock copolymers

Sample	[a] M_n [kg mol^{-1}]	[b] f_{PLA}	[c] $Đ$	[d] $T_{g,D}$ [°C]	[d] $T_{g,L}$ [°C]	[f] D^* [nm]	[g] T_{ODT} [°C]	[h] ϵ_b	[h] σ_b [MPa]
DL-S1	6.2	0.15	1.11	-50	12 (-5)[e]	–	< 37		
DL-S2	8.0	0.33	1.13	-49	28 (32)	15.8	132	0.56	0.016
DL-S3	9.4	0.41	1.18	-48	39 (40)	18.0	175	0.90	0.047
DL-M1	32.3	0.09	1.05	-51	19 (39)	20.0	120	1.7	0.022
DL-M2	36.6	0.21	1.06	-50	43 (48)	30.4	> 180	1.2	0.62
DL-M3	43.8	0.32	1.06	-51	52 (52)	36.3	> 180	0.49	1.9
LDL-1	102	0.05	1.07	-51	– (44)	28.5	< 110	2.8	1.0
LDL-2	111	0.11	1.09	-50	41 (52)	35.5	> 180	2.6	11
LDL-3	135	0.23	1.06	-51	51 (55)	46.5	> 180	2.3	61

[a]Calculated from ^{1}H NMR based on initiator peaks [b]Calculated from ^{1}H NMR using published densities of PLA and PDL[109] [c]Calculated from room temperature SEC in THF [d]Determined using DSC during the second heating cycle. [e]Theoretical values for T_g as predicated by the Flory-Fox equation. [f]Principal domain spacing from SAXS. [g]Measured using shear rheology. [h]From extensional rheology at $\dot{\epsilon} = 1$ s^{-1}.

was detected. It is likely that the T_g is masked by the low volume fraction of PLA (0.05). In general, the T_g of polylactide drops significantly at low molecular weights and can be quantified using the Fox-Flory equation:[114]

$$T_g = T_{g,\infty} - \frac{K}{M_n} \tag{3.4}$$

Here, $T_{g,\infty}$ is the glass transition of an infinite molecular weight polymer, M_n is the molecular weight of the polymer, and K is a constant related to the added free volume contribution from chain ends. Using the appropriate value of K of 7.40 $\times 10^2$,[115] the theoretical values of T_g were calculated and listed in Table 3.1. For most of the samples, there is good agreement between theory and experiment. The depressed values of T_g for DL-M1 and LDL-2 may be due to slight mixing of the poly(ϵ-decalactone) within the poly(lactide) domains.

3.5.2 Morphology

The morphologies of the DL diblocks and LDL triblocks were examined with SAXS, and the resulting azimuthally integrated 1-D scattering patterns are shown in Figure 3.8. Data

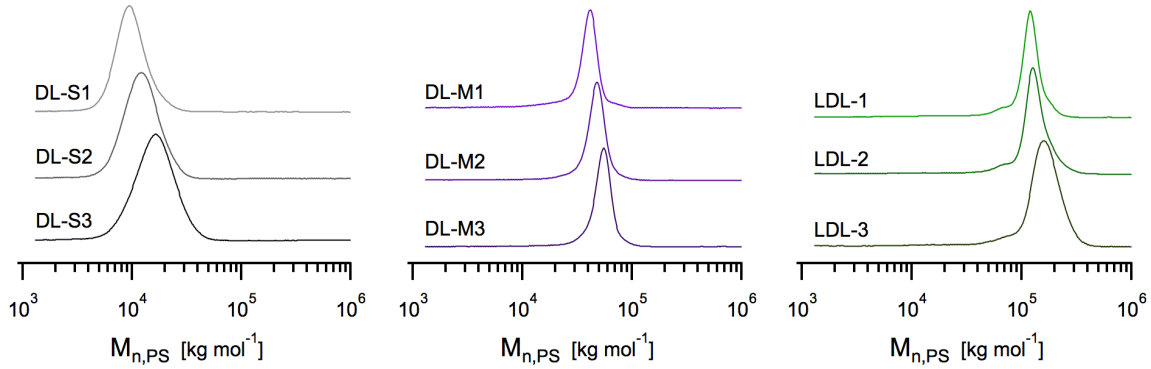

Figure 3.6: SEC results for the DL diblocks and LDL triblocks.

for sample DL-S1 could not be obtained as all of it was used to make blends before SAXS data could be collected. It is important to note that the polymers were *not* thermally annealed, and therefore, the data represent the material in a non-equilibrium state. The primary peak scattering wave vector position (q^*) was used to calculate the average domain spacing (D) of each polymer species using $D = \frac{2\pi}{q^*}$; the resulting values and are listed in Table 3.1. As anticipated, within each group of polymers, D increases with f_{PLA}.

The majority of samples have higher-order reflection peaks in the SAXS data, providing evidence for microphase separation. For most samples, indexing these higher-order peak relative to q^* does not correspond to a particular morphology. The exceptions are DL-M2 and DL-M3 for which the locations of the higher-order peaks ($q/q^* = \sqrt{3}, \sqrt{7}, \sqrt{9}, \ldots$) are consistent with hexagonally packed cylinders (Figure 3.8). It is highly likely that many of these samples would demonstrate long-range order if thermally annealed to access their equilibrium morphologies.

3.5.3 Linear rheology

A combination of isochronal temperature ramps and frequency sweeps were employed to identify the *order-disorder transition* temperature (T_{ODT}) of the samples (Table 3.1). Figure 3.9 highlights the pertinent data. The left portion of the figure shows frequency sweeps

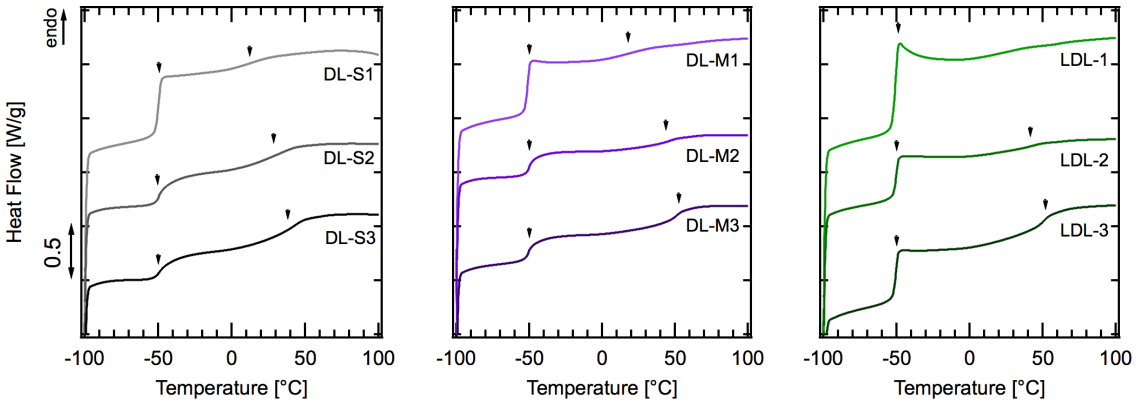

Figure 3.7: DSC traces of the DL diblocks and LDL triblocks. Shown is the the second heating trace at a ramp rate of 10 °C min^{-1}. Arrows point to inflection points corresponding to the T_g's of the D and L blocks.

of DL-S1 and LDL-1, demonstrating terminal scaling ($G' \propto \omega^{-2}, G'' \propto \omega^{-1}$) at 37 °C and 110 °C, respectively. This scaling is consistent with a disordered polymer melt and gives an upper bound for the T_{ODT}. The right portion of the figure shows isochronal temperature ramps of DL-S2, DL-S3, and DL-M1 upon heating (DL-S2: ω= 0.01 rad s^1, Δ°C min^{-1}= 0.2, DL-S3: ω= 0.1 rad s^1, Δ°C min^{-1} = 0.5, DL-M1: ω= 1.0 rad s^1, Δ°C min^{-1} = 0.5); the T_{ODT} was identified as the temperature at which the storage modulus decreases appreciably. The remainder of the samples remained solid at 180 °C, indicating microphase separation and an inaccessible T_{ODT}; above 180 °C, degradation becomes a significant concern.

When possible, frequency sweeps of the pure components were conducted at 37 °C at ω = 1.0 rad s^{-1} to correlate LVE behavior to mouth temperature; however, this was only possible for the four samples with a T_g below 37 °C; samples with a higher T_g lead to rheometer resonance. The results for DL-S2, DL-M1, and LDL-1 are shown in Figure 3.9c.

3.5.4 Extensional rheology

Extensional rheological tests were employed at 37 °C at $\dot{\epsilon}$ = 1 s^{-1} to simulate conditions relevant to mouth chewing and bubble blowing as elucidated in Chapter 2. The viscosity of

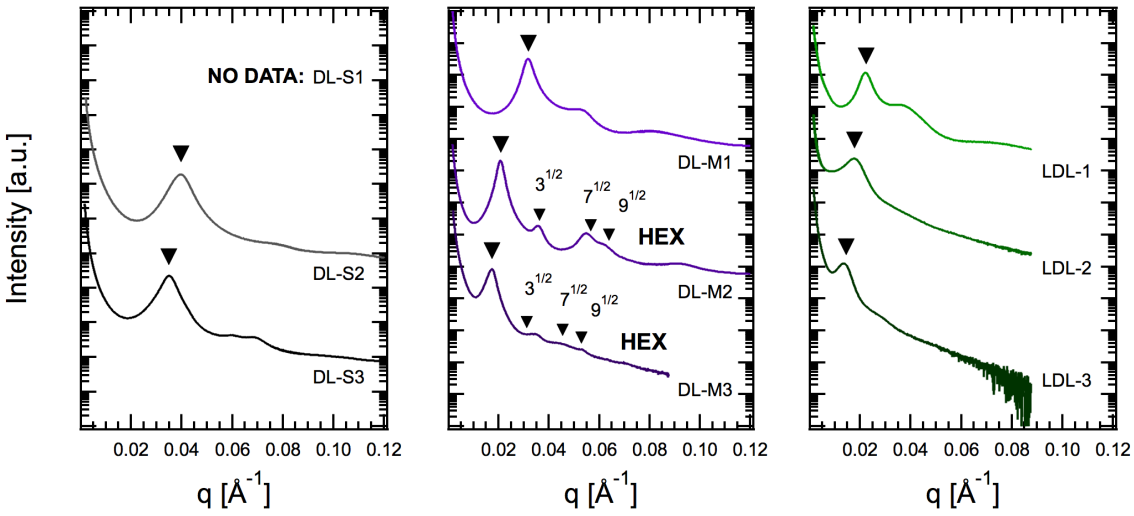

Figure 3.8: SAXS patterns of the DL diblocks and LDL triblocks.

sample DL-S1 was too low to be amenable for the EVF which requires a melt viscosity of approximately 10^4 Pa-s.[116] Representative results are shown in Figure 3.10a. Qualitatively, the extensional behavior of the three sets of polymers are quite distinct. The low molecular weight diblocks (DL-S series) begin to strain soften at very modest strains ($\epsilon < 0.6$) and remain intact until complete failure occurs at $\epsilon < 1.0$. The medium molecular weight diblocks (DL-M series) are also mechanically weak and fail at relatively low strains ($\epsilon < 1.0$); however, their failure is more abrupt, and the extensional rheological curve remains linear for a longer period of time. The high molecular weight triblocks (LDL series) all strain harden with much larger strains at break (ϵ_b) that fall between 2.0 and 3.0.

These observations are consistent with the literature for AB diblocks and ABA triblocks.[117,118] Under flow, diblocks are held together mainly by Van der Waals interactions and if applicable, chain entanglements.[117] For certain morphologies such a BCC, there may be an additional energy penalty to overcome due the thermodynamic stability of the lattice structure.[118] However, these forces are relatively weak. Alternatively, the LDL triblocks have lamellaeD blocks that can bridge and connect disparate L domains, reinforcing

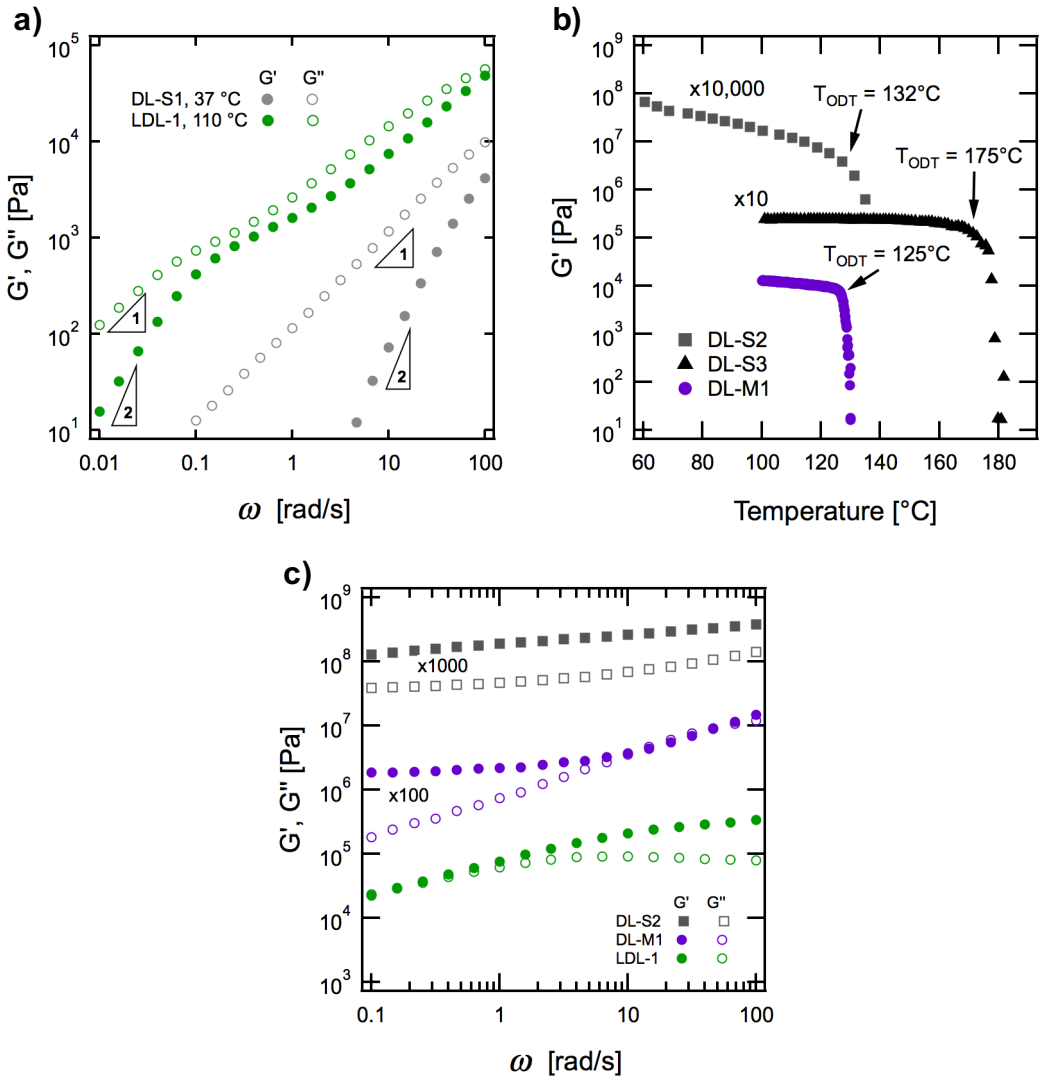

Figure 3.9: LVE behavior of select DL diblocks and LDL triblocks showing a) terminal scaling, b) T_{ODT} measurements, and c) oscillatory shear at 37 °C.

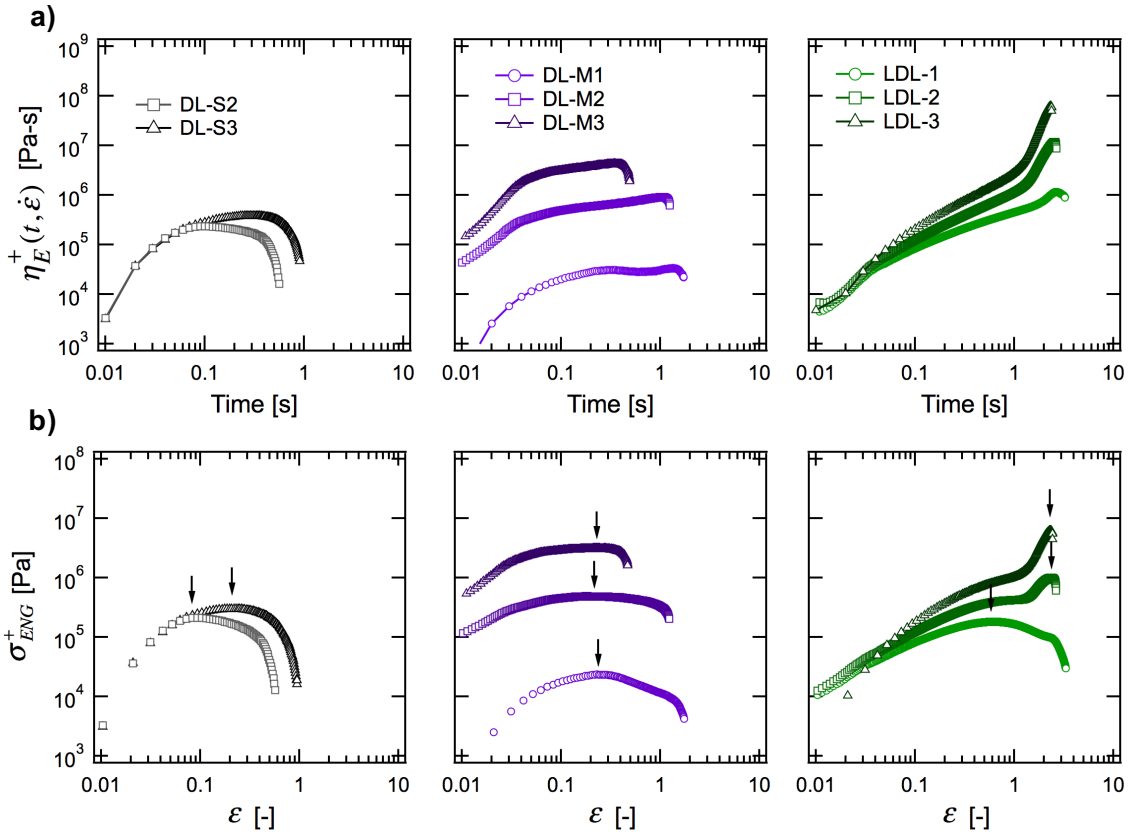

Figure 3.10: a) Extensional rheology of select DL diblocks and LDL triblocks at 37 °C, b) the same data plotted in terms of engineering stress *versus* Hencky strain.

the material during flow. Failure is attributed to *chain pullout* that involves an enthalpic penalty of mixing of the D/L domains. Strain hardening in the nonlinear regime can be attributed to this resistance to chain pullout and non-affine deformation of the rubbery midblock, similar to the behavior of vulcanized rubber with chemical crosslinks.[119] For certain morphologies such as hexagonally packed cylinders or lamellae, domain orientation may contribute to strain hardening as well.[104]

For each series of polymers, the extensional viscosity increased as f_{PLA} increased, as anticipated. Also, for the triblocks, an increase in f_{PLA} lead to more dramatic strain hardening. However, the governing factors dictating ϵ_b are not readily obvious. For example,

for the DL-S series, ϵ_b increased as f_{PLA} increased, but for the LDL series, the opposite trend held true. Recent work by a recent alumnus of the University of Minnesota found experimental evidence that the ϵ_b of ABA thermoplastic elastomers is dictated by the *ductile/fragile rupture* of the end blocks.[120] That is, ϵ_b is maximized when the "hard" end blocks are at their glassy-rubber viscoelastic transition. It is postulated that this occurs because the domains are deformable enough to dissipate energy effectively, yet are solid enough to promote cavitation and limit crack propagation, thereby delaying failure. This glassy-rubber viscoelastic transition is accessible only in the vicinity of the T_g of the end block with the exact maximum value of ϵ_b dependent on the precise extension rate and temperature. To a first approximation, ϵ_b for each series of polymers is largest when the T_g of PLA is closest to the test temperature (37 °C). Thus, it appears that ϵ_b is dependent on f_{PLA} mainly in how it manifests itself in the final T_g of the PLA domain.

An alternative way to assess the extensional rheology is by plotting the data in terms of engineering stress (σ_{ENG}) rather than the conventional extensional viscosity (Figure 3.10b). For metals, it is well established that the maximum in an engineering stress-strain curve corresponds to the *tensile strength* of the materials, after which *necking* and inhomogeneous deformation occur.[121] In the context of extensional rheology, the peak of engineering stress as been identified as the onset of *yielding* or the transition from elastic deformation to flow.[122] Because of the differing failure mechanisms of the DL diblocks and LDL triblocks, this analysis is used to help elucidate the points of failure of the individual components and the nature of the deformation (i.e. recoverable or irrecoverable).

The yield point or transition to flow occurs at relatively small strains for all the diblocks. For the low molecular weight diblocks (DL-S series), this transition appears to be sensitive to the molecular weight. DL-S1 is a disordered liquid and therefore always flows; DL-S2 has a yield point around $\epsilon = 0.1$, while DL-S3 has a yield point around $\epsilon = 0.2$. Alternatively, all the medium molecular weight diblocks (DL-M series) have a yield point at approximately $\epsilon = 0.25$ and appear to be able to sustain the bulk of their stress to larger strains. This is

attributed to the fact that the poly(ϵ-decalactone) blocks are sufficiently long to entangle, providing temporary cross-links. For the LDL triblocks, the yield points occur at higher strains, as expected. Surprisingly, though, LDL-1 shows a yield point at $\epsilon = 0.60$, much earlier than the other two triblocks and much before its ϵ_b. This may be due to the inability of the poly(lactide) end blocks to form domains that are sufficiently "hard" or glassy to as effectively resist chain-pull out. The fact that no glass transition is observed for this sample provides tangential evidence for this speculation.

3.6 Blend characterization

A total of 24 blends were created, and their compositions and thermal properties are summarized in Table 3.2. Each blend consisted of **20 wt.% triblock** and **80 wt.% diblock** since this was the optimal composition as determined from previous work (see section 3.2.1). The blend compositions were selected to probe the following effects on the shear and extensional rheological behavior:

1. Polymer composition
2. Diblock molecular weight

Careful consideration was paid to the morphology of the blends as well, which will be discussed first.

3.6.1 Morphology

The morphology of the 24 blends was assessed using SAXS, the data of which are summarized in Figure 3.6.1. The major primary peaks are denoted with a large triangle from which the principal domain spacing (D) can be obtained, highlighted in Table 3.3. Some of the blends have an additional smaller peak that arises at a q lower than q^*, an artifact attributed to the high molecular weight triblocks that have partially macrophase separated. The corresponding domain spacings for these peaks (D_2^*) can also be found in Table 3.3.

Table 3.2: Compositions of the LDL/DL blends

Sample	Composition: wt. % of each									w_{PLA}	$T_{g,L}$ [°C]
	DL-S1	DL-S2	DL-S3	DL-M1	DL-M2	DL-M3	LDL-1	LDL-2	LDL-3		
B1		80					20			0.32	26
B2		80						20		0.34	32
B3		80							20	0.37	35
B4					80		20			0.21	44
B5					80			20		0.23	45
B6					80				20	0.26	47
B7		40		40			20			0.21	25
B8		40		40				20		0.23	31
B9		40		40					20	0.26	33
B10		40			40		20			0.27	40
B11		40			40			20		0.28	41
B12		40			40				20	0.31	44
B13		40				40	20			0.32	45
B14		40				40		20		0.34	47
B15		40				40			20	0.36	48
B16	20		60				20			0.32	41
B17	20		60					20		0.34	42
B18	20		60						20	0.37	48
B19	40		40				20			0.26	18
B20	40		40					20		0.28	18
B21	40		40						20	0.30	42
B22	59		21				20			0.20	15
B23	59		21					20		0.22	16
B24	59		21						20	0.24	17

Partial macrophase separation between low molecular weight diblocks and high molecular weight triblocks is consistent with previous work discussed in section 3.2.1.[103] Although it is difficult to precisely determine the miscibility of a given set of these polymers (especially for the ternary blends), a series of papers by Hashimoto and coworkers provides some guidelines.[123–125] For lamellar forming poly(styrene-*b*-isoprene) (SI) diblocks of similar compositions, miscibility occurred when the ratio of molecular weights <5, forming a single microdomain morphology; however, when this ratio exceeded 10, a type of macrophase separation occurred.[123,124] This type of macrophase separation was designated as *macrophase separation induced by microphase separation* in which each of the distinct phases is partially swollen by the presence of the other diblock. The same general guidelines held true for cylinder and sphere forming diblocks.[125] One key difference, however, is the fact that for

the sphere forming diblocks, spheres of different sizes were *locally* macrophase separated, rather than macrophase separated at large length scales. This draws parallels to recent work on sphere-forming phases in which different sized spheres can lead to a cornucopia of more complicated morphologies.[126,127]

Table 3.3: Key properties of the LDL/DL blends

Sample	D^* [nm]	D_2^* [nm]	S [Pa-s^n]	n [-]	ϵ_y [-]	ϵ_b [-]	σ_b [MPa]
B1	17.5	–	85700	0.357	0.20	2.0	0.30
B2	18.3	59.3	99600	0.303	0.20	3.0	3.0
B3	17.6	44.2	153000	0.246	0.20	2.8	5.8
B4	31.6	–	93800	0.373	0.40	2.5	1.0
B5	31.4	–	141000	0.280	0.40	2.3	2.8
B6	33.4	–	190000	0.190	–	1.8	8.0
B7	21.7	–	16200	0.514	0.40	2.8	0.48
B8	22.2	69.8	35100	0.387	–	3.0	2.9
B9	22.4	48.3	50200	0.295	–	2.7	5.3
B10	24.4	–	72400	0.424	–	2.2	1.1
B11	24.2	–	117000	0.336	0.30	2.6	3.8
B12	24.9	60.4	154000	0.272	–	2.1	8.6
B13	27.2	–	137000	0.362	–	1.7	1.4
B14	27.4	–	209000	0.284	–	1.9	4.8
B15	29.8	–	267000	0.229	–	1.9	15
B16	21.1	–	61300	0.328	–	2.2	0.70
B17	23.0	–	133000	0.238	–	2.2	3.8
B18	23.6	49.4	156000	0.181	–	2.5	10
B19	16.3	–	15100	0.401	0.25	4.0	0.56
B20	20.8	–	32600	0.240	0.25	3.1	3.2
B21	21.8	48.5	55300	0.157	–	2.8	1
B22	19.7	–	4380	0.579	0.30	4.5	0.22
B23	19.7	–	16400	0.317	–	3.2	2.6
B24	21.2	–	31400	0.193	–	2.9	8.7

In general, these blends are consistent with these previous reports. Only the blends with largest molecular weight and compositions mismatch resulted in this macrophase separation. Interestingly, the relative domain spacings of the triblock-rich regions (D_2^*) in the macrophase separated blends are significantly larger than the pure triblocks, while the

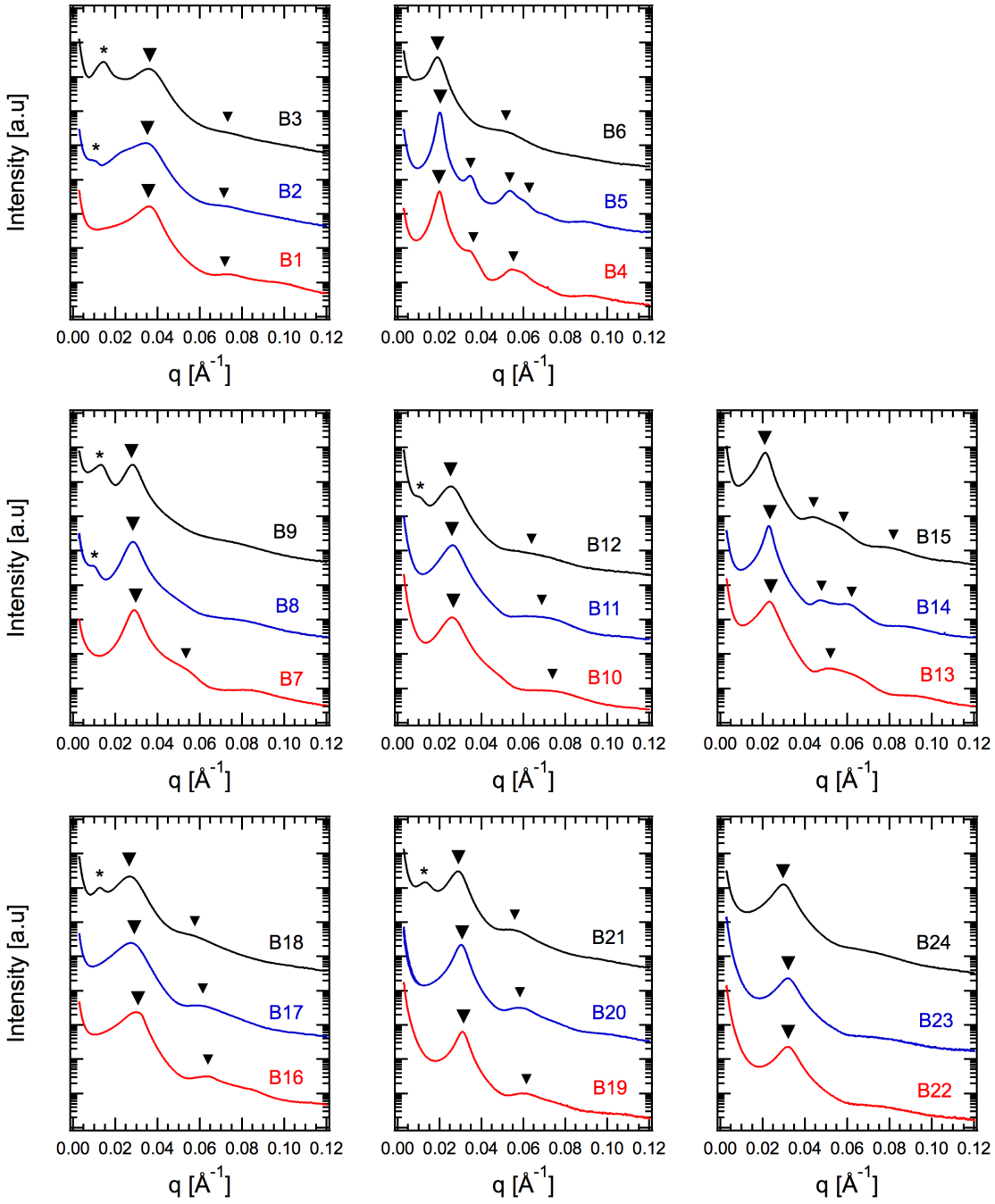

Figure 3.11: SAXS patterns for the LDL/DL blends. The large triangles designate the major primary peak, small triangles designate higher order reflection peaks, while the stars designate minority primary peaks coming from the LDL triblock.

major domain spacing (D^*, presumably corresponding to the diblock-rich region) is hardly changed. This may be explained by the ability of the triblocks to easily solubilize the lower molecular weight diblocks while the opposite is much more difficult.[125] In fact, the three blends with the largest values of D_2^* (B2, B8, B12) are the three blends in which the molecular weight mismatch between the species is the *least* pronounced, meaning a larger amount of diblock could be compatible with the triblocks and result in more dramatic swelling.

3.6.2 Linear rheology

As anticipated, the LVE behavior of each blend was primarily dictated by the majority component(s), the diblocks (Figure 3.12). Each group of blends in Figure 3.3.12 (B1-B3, B4-B6, etc.) have the same diblock composition but differ in the triblock. The moduli increase slightly as the overall w_{PLA} of each blend increases. Most of the blends have power-law like responses over the frequencies tested; the exceptions are B19, B22, and B23. These blends are approaching or have already reached the crossover frequency (w_x, defined as $G' = G''$), meaning they are transitioning to liquid-like flow within the experimental time window.

3.6.3 Extensional rheology

General trends

Extensional data for the 24 blends are shown Figures 3.13 and 3.14, displaying extensional viscosity *versus* time and engineering stress *versus* strain, respectively. From Figure 3.13, essentially all the blends display some combination of strain softening and strain hardening due to the diblocks and triblocks, respectively. The relative extent of strain softening and strain hardening correlate to the characteristics of the pure components. For example, blends B1-B3 (with DL-S2) strain soften more than B4-B6 (with DL-M2), while blends with LDL-3 strain harden more than those with LDL-1 across the board.

Somewhat surprisingly, only 10 of the 24 blends show a yield point, marked by a local

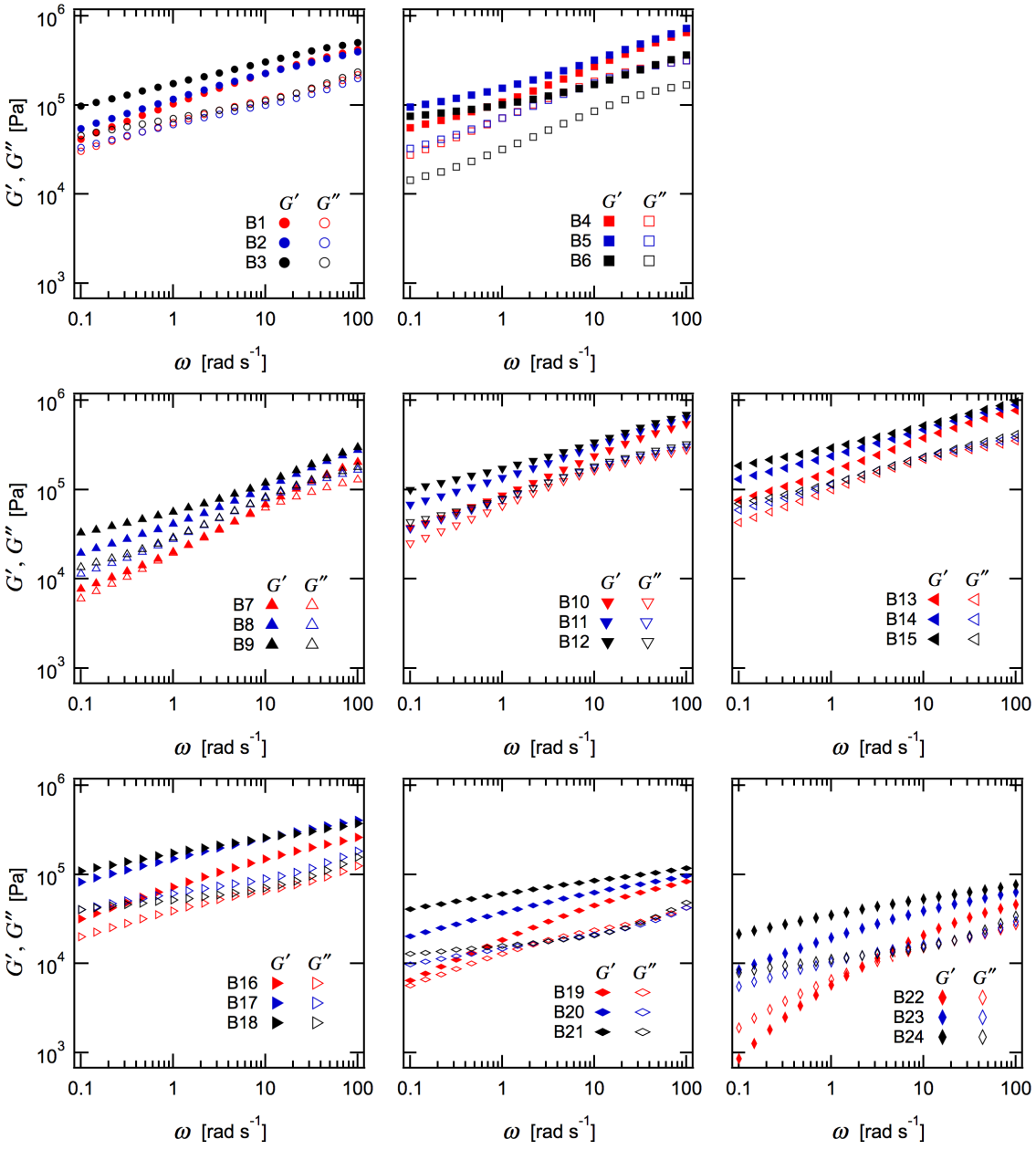

Figure 3.12: LVE behavior of the LDL/DL blends.

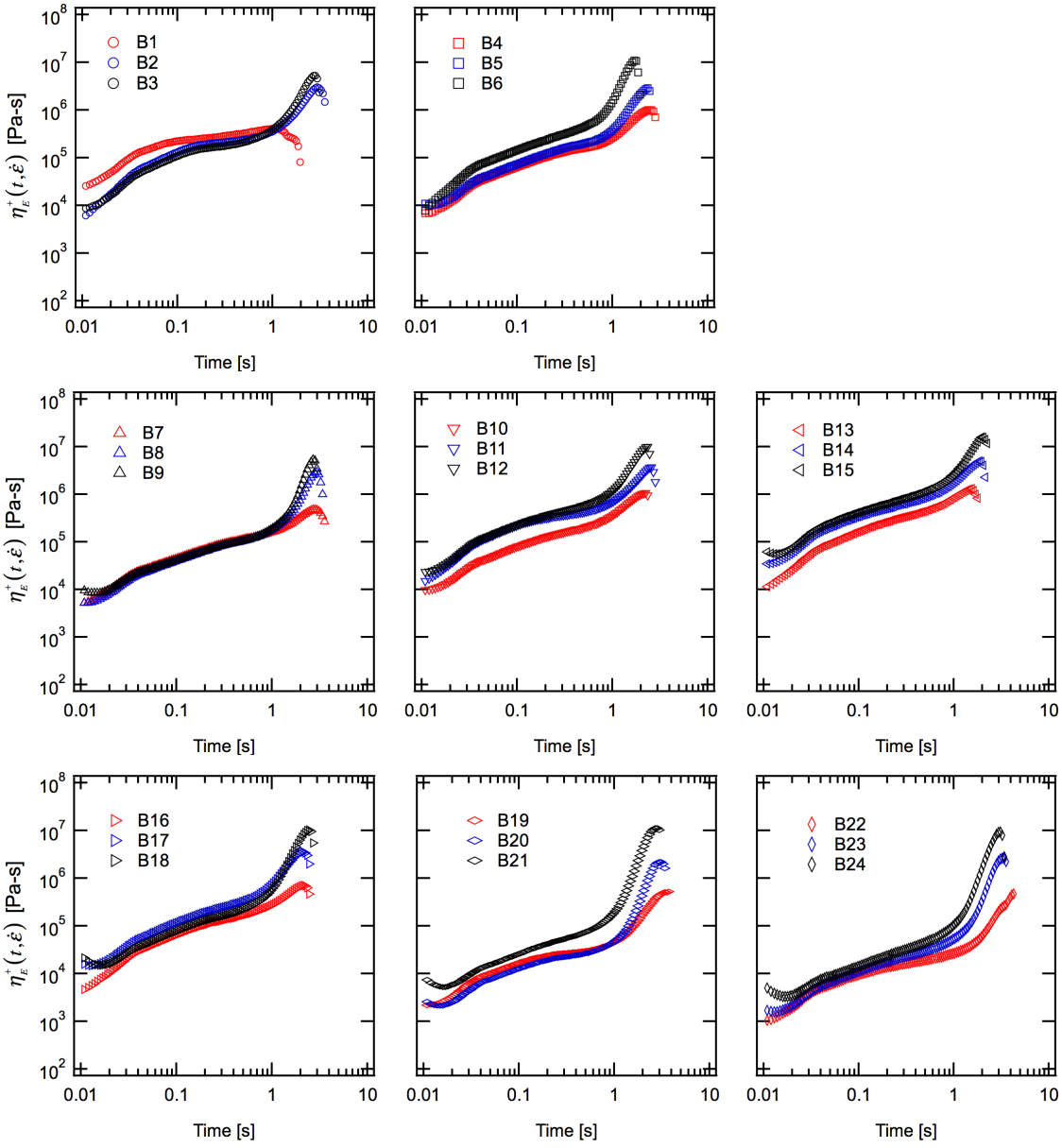

Figure 3.13: Extensional rheological response of the 24 LDL/DL blends at $\dot{\epsilon} = 1$ s^{-1}.

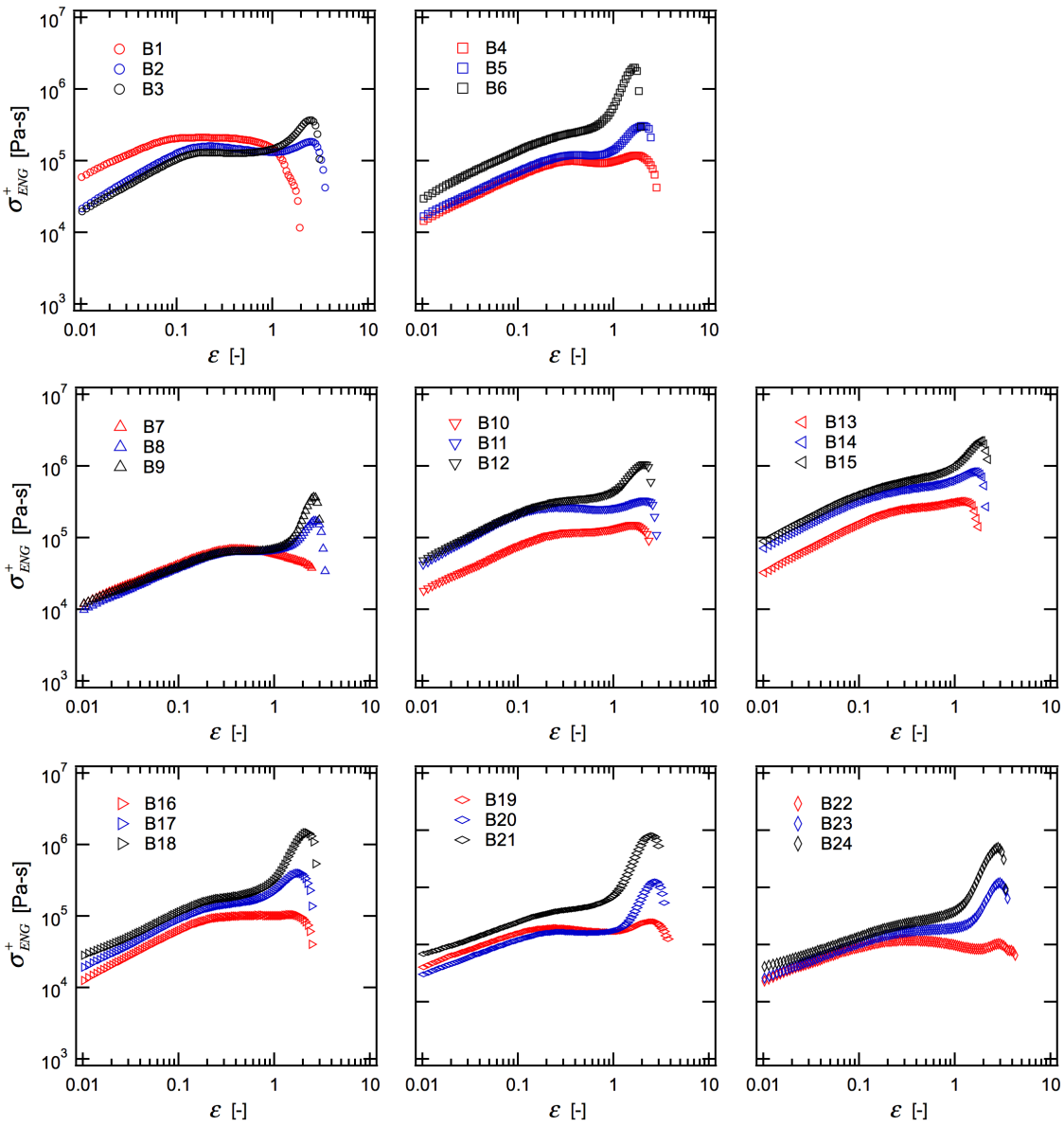

Figure 3.14: Engineering stress *versus* Hencky strain of the 24 LDL/DL blends at $\dot{\epsilon} = 1\ s^{-1}$.

maxima in the engineering stress (Figure 3.14, Table 3.3). Yield points were much more common in the binary blends (5 out of 6) rather than the ternary blends (5 out of 18). It is thought that the combination of diblocks, spanning a wider range of relaxation times and yield points, mask a distinct yield point. Finally, *none* of the 24 blends showed an increase in σ_b relative to the neat LDL triblock.

Effect of polymer composition

The effect of triblock composition is apparent from each individual plot in Figure 3.13. As the f_{PLA} of the triblock increases, the extent of strain hardening and the σ_b increases accordingly. In general, the ϵ_b is mostly unaffected by the triblock composition. The exceptions are blends B19-B24 in which the blends with LDL-1 have a much higher ϵ_b than the blends with either LDL-2 or LDL-3. This may be due to the manner in which the deformation occurs: σ_b is significantly lower than σ_y for B19 and B22, demonstrating liquid-like and irreversible flow rather than solid-like responses for B20, B21, B23, and B24.

The effect of diblock composition may most easily be seen by comparing the extensional responses of B8, B11, and B14 shown in Figure 3.15. These blends are identical except for the polymer composition of the high molecular diblock (Table 3.2). At small times or strains, the viscosity is highly dependent on diblock composition, with viscosity increasing with increased f_{PLA}. This is anticipated due to the effect of diblock composition on the LVE behavior. Surprisingly, diblock composition seems to have a large impact on the large strain behavior. Although each blend has a similar σ_b, the ϵ_b increases significantly with decreasing f_{PLA} of the diblock. It is highly possible that this effect is due to the differing T_g values of the blends (Table 3.2); as noted in section 3.5, proximity to the T_g can have a very large impact on ϵ_b.

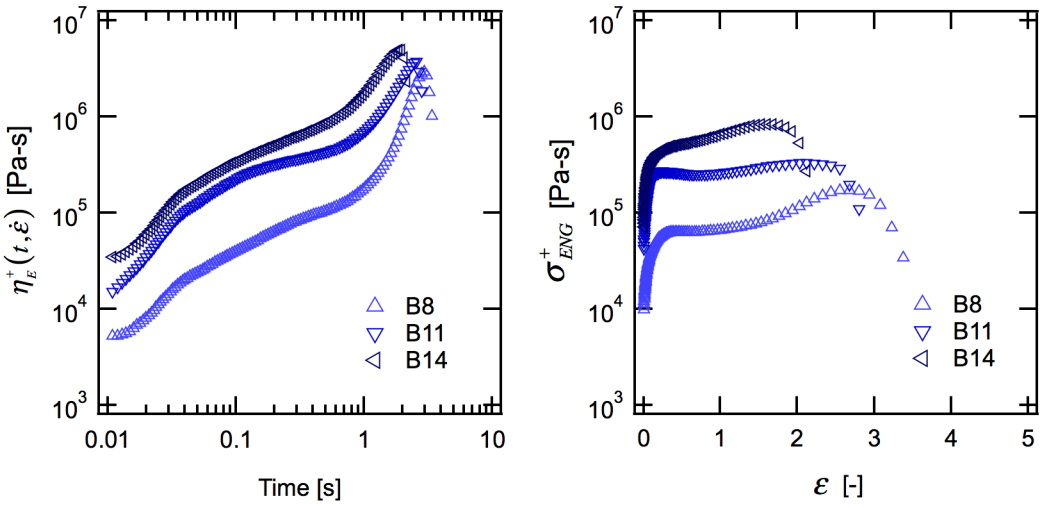

Figure 3.15: Extensional rheology of block polymer blends B8, B11, and B14 at $\dot{\epsilon} = 1$ s^{-1}. The three blends each have a high molecular diblock of differing compositions, but have the same triblock and low molecular weight diblock. The diblock compositions has a large impact on the extensional viscosity at lower strains, and surprisingly, on the strain at break. Stresses at break are independent of the diblock composition.

Effect of diblock molecular weight

The beneficial effects on the ϵ_b and σ_b observed by Lee et al. were mostly lost with the addition of the medium molecular weight diblocks. Only two blends (B8 and B9) with diblocks in the DL-M series showed increases in the ϵ_b relative to the neat LDL triblocks, and these increases were quite modest. Interestingly, both of these blends showed macrophase separation, indicating some swelling of the triblock-rich domain. For the blends without DL-M diblocks, only ones that showed macrophase separation or had a relatively large proportion of the disordered DL-S1 diblock displayed increases in ϵ_b.

Another interesting detail comes from comparing the yield strains and compositions of three blends: B2, B5, and B11. While all three blends have 20% LDL-2, B2 has 80% DL-S2, B5 is 80% DL-M2, while B11 is 40% each of DL-S2 and DL-M2. It turns out that the ϵ_y of B11 is the average of the two yield strains of B2 and B5 (Table 3.3). This fact, along

with the lack of distinct yield points for many of the ternary blends, supports the notion that the yield point and the extent of strain softening can be easily tuned by blending in diblocks of different molecular weights.

3.7 Application to chewing gum bases

Chapter 2 of this thesis provided a detailed examination of the rheological behavior of chewing and bubble gums. By applying the full gamut of rheological tests, both chewing and bubble gums were identified as **critical gel** fluids with **high extensibility**. In the *linear* viscoelastic regime, they behaved as soft critical gels. In the *nonlinear* viscoelastic regime in shear, network destruction was observed at low stresses, strains, and strain rates, while in extension, very high deformations were achieved. These observations can be quantified by the following design criteria:

- $10^4 < S < 2 \times 10^5$ [Pa-S^n]
- $0.22 < n < 0.36$
- $\epsilon_b > 4.0$
- $\sigma_b > 2 \times 10^6$ Pa for bubble gums
- $\sigma_b \leq 2 \times 10^6$ Pa for chewing gums

The parameters S and n come from equation 2.2 signifying the *stiffness* and *strength* of the critical gel, respectively.

With these design criteria in mind, the block polymer blends can be assessed for their potential use as chewing or bubble gum bases. The values of S and n are listed in Table 2.3 and were obtained by fitting the G' data from $0.1 < \omega < 10$ rad s^{-1} to equation 2.2. Roughly half the blends have values of S and n within the necessary regime, and all have values of σ_b that are appropriate for either chewing of bubble gum. However, only two

blends (B19 and B22) have $\epsilon_b > 4.0$, and both these blends have critical gel characteristics that are too soft and liquid-like (S too low, n too high) for either chewing or bubble gums.

Of the blends with appropriate linear viscoelastic behavior, the ones with the highest ϵ_b are B2, B20, and B23. Interestingly, these blends do not contain any of the medium molecular weight diblocks, only low molecular weight diblocks. The blend with the highest ϵ_b that *does* contain medium molecular weight diblocks is B9 which contains DL-M1, the one with the lowest f_{PLA}. It is also interesting to note that B2, B20, and B23 all have σ_b values at the transition between chewing and bubble gums, making them potentially viable for either application.

3.8 Multiblock polymer blends: preliminary results

As highlighted in section 2.7, one of the key design parameters dictating chewing gum performance is having a strain at break > 4.0, and none of the LDL/DL ternary blends achieved this while maintaining desirable LVE behavior. To solve this concern, some preliminary work was done to see if the LDL triblock could be replaced with a high molecular weight $(LDL)_n$ multiblock copolymer. This was inspired by a recent publication by Watanabe and coworkers that found that for sphere-forming elastomeric $(SIS)_n$ multiblock polymers, ϵ_b as high as 4.5 could be attained.[80] In their system, a plasticizer was added that preferentially solubilized the styrene blocks, thereby lowering the T_g to close to 20 °C (the test temperature). It was believed that this was a key factor in the extraordinary extensibility - the S blocks could pull out of one domain and transfer to a different S domain because of the increased mobility near the T_g. The multiblock architecture was critical in this mechanism since at least two S blocks must remain in their domains at any given moment to avoid failure, something that becomes increasingly likely with an increasing number of S blocks.

Two model multiblock polymers with T_g's close to the test temperature (37 °C) were used for this case study, their characterization listed in Table 3.4. The parameter $< n >$ is defined by the ratio of $M_{n,total}$ to $M_{n,LDL}$ and is a measure of the number of triblocks

within a multiblock, on average. The total M_n and f_{PLA} of the multiblocks are similar to LDL-3, although M_w and the individual block lengths are quite distinct. Rather than a single large midblock like in LDL-3, the multiblocks contain a large number of short poly(ϵ-decalactone) blocks that are very lightly entangled (above M_e but below M_C, the critical molecular weight for entanglement estimated as $2 \times M_e$).

Two new short DL diblocks and a poly(ϵ-decalactone) homopolymer were synthesized and blended with the multiblocks in the compositions shown in Table 3.5. Only short diblocks were synthesized because they proved to be more effective in increasing strain at break as discussed in section 3.6. The short, unentangled homopolymer was used to see if dilution of the elastomeric network could also be an effective means to positively modulate the rheological behavior.

Table 3.4: Characterization of the $(LDL)_n$ multiblock copolymers

Sample	$M_{n,LDL}$ [a] [kg mol^{-1}]	$M_{n,total}$ [b] [kg mol^{-1}]	$< n >$ [c]	$Đ$ [d]	f_{PLA} [a]	$T_{g,D}$ [°C] [e]	$T_{g,L}$ [°C] [e]	T_{ODT} [°C] [f]
$(LDL)_n$-1	13.2	121	9.2	1.5	0.28	-46	30	∼125
$(LDL)_n$-2	12.2	131	10.7	1.4	0.22	-47	21	∼50
D-1	–	4.9	–	1.13	–	-56	–	–
DL-4	–	6.3	–	1.12	0.18	-53	18	<25
DL-5	–	7.8	–	1.15	0.32	-50	25	107

[a]Calculated from ^{1}H NMR based on initiator peaks [b]Determined from multiplying M_n from NMR by the ratio of $M_{n,total}$ to $M_{n,LDL}$ from SEC. [c]The ratio of $M_{n,total}$ to $M_{n,LDL}$ [d]Determined from SEC in THF at 25 °C. [e]Determined using DSC during the second heating cycle. [f]Determined from linear rheology.

3.8.1 Linear rheology

Frequency sweep data for the two multiblocks, the two diblocks, and the poly(ϵ-decalactone) homopolymer are shown in Figure 3.16. Samples DL-4 and D-1 exhibit terminal scaling with the G'' of D-1 only detectable at the highest frequencies. The two multiblocks and DL-5 demonstrate power-law responses, similar to the ordered DL diblocks and LDL triblocks discussed in section 3.5.

Isochronal temperature ramps were employed to estimate the T_{ODT} of the multiblocks

Table 3.5: Composition of blends incorporating $(LDL)_n$ multiblock copolymers

Sample	Composition: wt. % of each				
	$(LDL)_n$-1	$(LDL)_n$-2	D-1	DL-4	DL-5
mB-1	20	–	80	–	–
mB-2	50	–	50	–	–
mB-3	20	–	–	80	–
mB-4	20	–	–	–	80
mB-5	–	20	80	–	–
mB-6	–	50	50	–	–
mB-7	–	20	–	80	–
mB-8	–	20	–	–	80

and DL-5 (Figure 3.17). Sample DL-5 has an easily identifiable T_{ODT} with a clear drop-off in G' at 107 °C. The two multiblocks, alternatively, show a more gradual transition from order to disorder, consistent with previous reports on $(LDL)_n$ multiblocks with similar T_{ODT}'s.[109] It is unclear whether the T_{ODT} would be accessible at a lower test frequency, or whether the T_{ODT} spans a wider temperature window due to the high dispersity of the multiblocks. This topic is explored more fully in Section 4.4 on a similar multiblock system.

Even if the exact values of the T_{ODT}'s are not well-defined, the fact that they are accessible for the multiblocks (well below degradation temperatures) is potentially a huge advantage from a practical standpoint. This indicates that these multiblocks are more easily **processable** in a process like melt blending, a technique much more appropriate for industrial purposes than the solvent blending used in this study. Neither LDL-2 nor LDL-3, the triblocks with the most desirable extensional properties, had accessible T_{ODT}'s, and this will generally be the case for ABA triblocks with comparable molecular weights and compositions unless the Flory-Huggins interaction parameter (χ) between the blocks is unusually low.

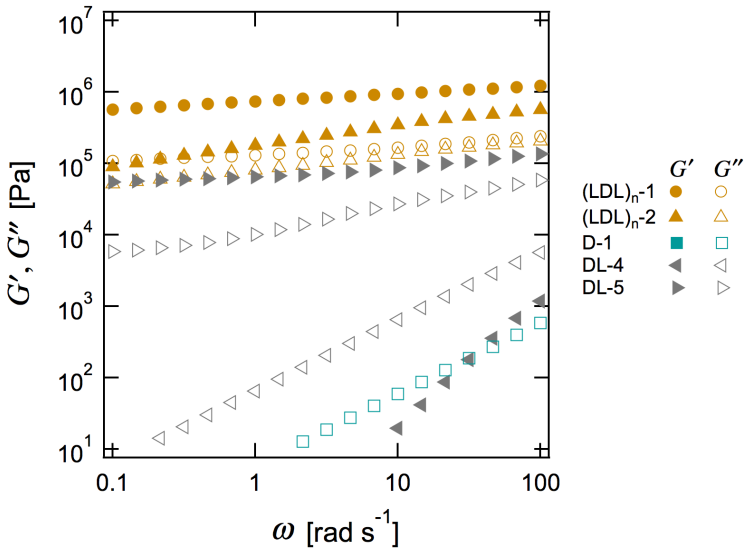

Figure 3.16: Frequency sweep data for the two $(LDL)_n$ multiblocks, the two new DL diblocks, and the poly(ϵ-decalactone) homopolymer at 37 °C.

3.8.2 Extensional rheology

The extensional responses of the pure multiblocks at $\dot{\epsilon}$ =1 s^{-1} are shown in Figure 3.18. Data are plotted both as extensional viscosity *versus* time and stress *versus* strain. At 37 °C, samples $(LDL)_n$-1 and $(LDL)_n$-2 have ϵ_b's of 2.9 and 3.3, respectively, with viscosities and σ_b that differ by about an order of magnitude. Because the overall molecular weights are similar, it is unclear whether these discrepancies are due to differences in f_{PLA}, molecular weight of the individual blocks, the T_g of the PLA domains, or a combination of the aforementioned factors. For this reason, additional extensional tests were run at temperatures approximately 30 °C below the T_g of the lactide block for each material (0 °C and -10 °C for $(LDL)_n$-1 and $(LDL)_n$-2, respectively). By normalizing the temperature relative to T_g and choosing a temperature in which the block is completely glassy, the effect of T_g is eliminated. The resulting extensional behavior of the multiblocks is remarkably similar. Both samples have almost identical values for σ_b and ϵ_b and both are much more viscous

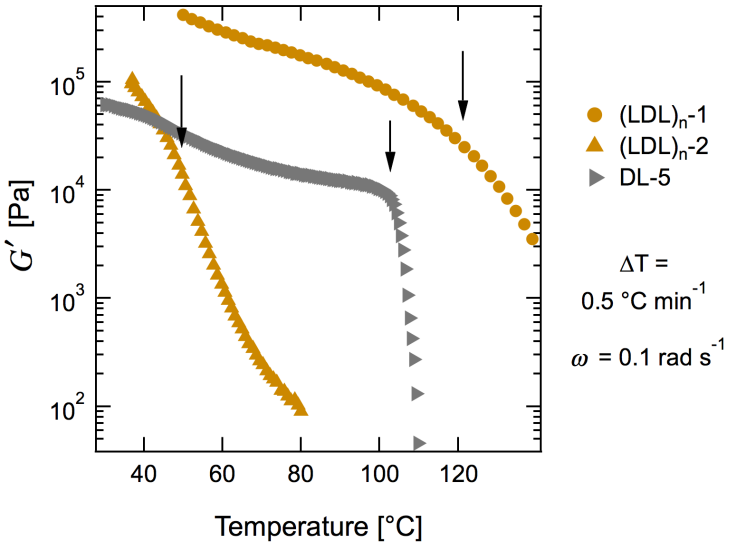

Figure 3.17: Isochronal temperature ramps for the two $(LDL)_n$ multiblocks and sample DL-5.

and less extensible than at 37 °C. This strongly suggests that the T_g of the glassy block and mobility of the hard domains is a critical parameter in dictating the final extensional behavior.

The extensional responses of the pure multiblocks and their blends at $\dot{\epsilon}$=1 s^{-1} and 37 °C is shown in Figure 3.19. Data are plotted both in terms of extensional viscosity *versus* time and stress *versus* strain. Data were not collected for blends mB-1, mB-5, and mB-7; blends mB-1 and mB-5 macrophase separated, while the viscosity of mB-7 was too low for extensional testing. Blending in DL-5 preserved much of the same behavior seen in the LDL/DL ternary blends. For blends mB-4 and mB-8, strain softening is observed at small strains, while the ϵ_b increases substantially. **Quite remarkably, blend mB-8 has a ϵ_b of 4.0**, large enough to make it a potential candidate for chewing or bubble gum bases. Although linear data has not been collected nor fit to the critical gel model, the fact that both of the individual blends components [$(LDL)_n$-2 and DL-5] display power-law responses in oscillatory shear strongly suggests that the blend would also.

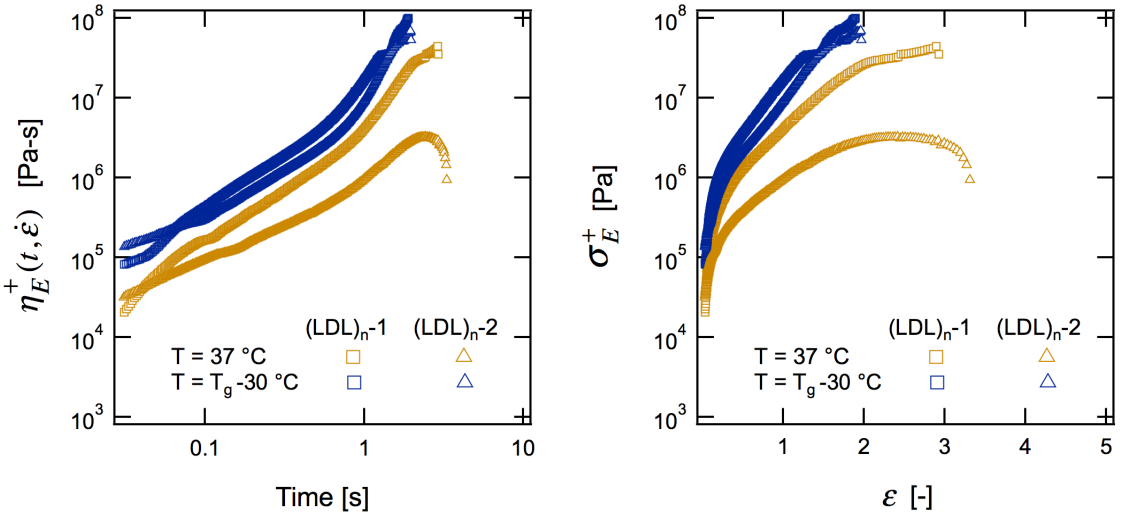

Figure 3.18: Extensional rheology of the pure $(LDL)_n$ multiblocks at $\dot{\epsilon}$=1 s^{-1} at 37 °C and a temperature 30 °C below the T_g of the PLA blocks.

Blend mB-3, containing the disordered DL-4, also exhibits a higher strain at break than neat $(LDL)_n$-1, yet it lacks the strain softening characteristics found in most of the LDL/DL ternary blends. Interestingly, adding the poly(ϵ-decalactone) homopolymer did not have any positive effect on the ϵ_b. Both mB-2 and mB-6 have similar extensional responses to the neat multiblocks except the viscosity is lower by an order of magnitude. This gives circumstantial evidence that simply diluting the rubbery matrix and increasing the effective molecular weight between entanglements is insufficient to substantially alter the strain at break.

3.9 Conclusions

This chapter examines modulating the mechanical and rheological behavior of TPEs by blending in AB diblock copolymers. In general, three parameters were investigated: *polymer composition*, *diblock molecular weight*, and *polymer architecture*.

For LDL/DL ternary blends, *polymer composition* of the diblock dictated the moduli

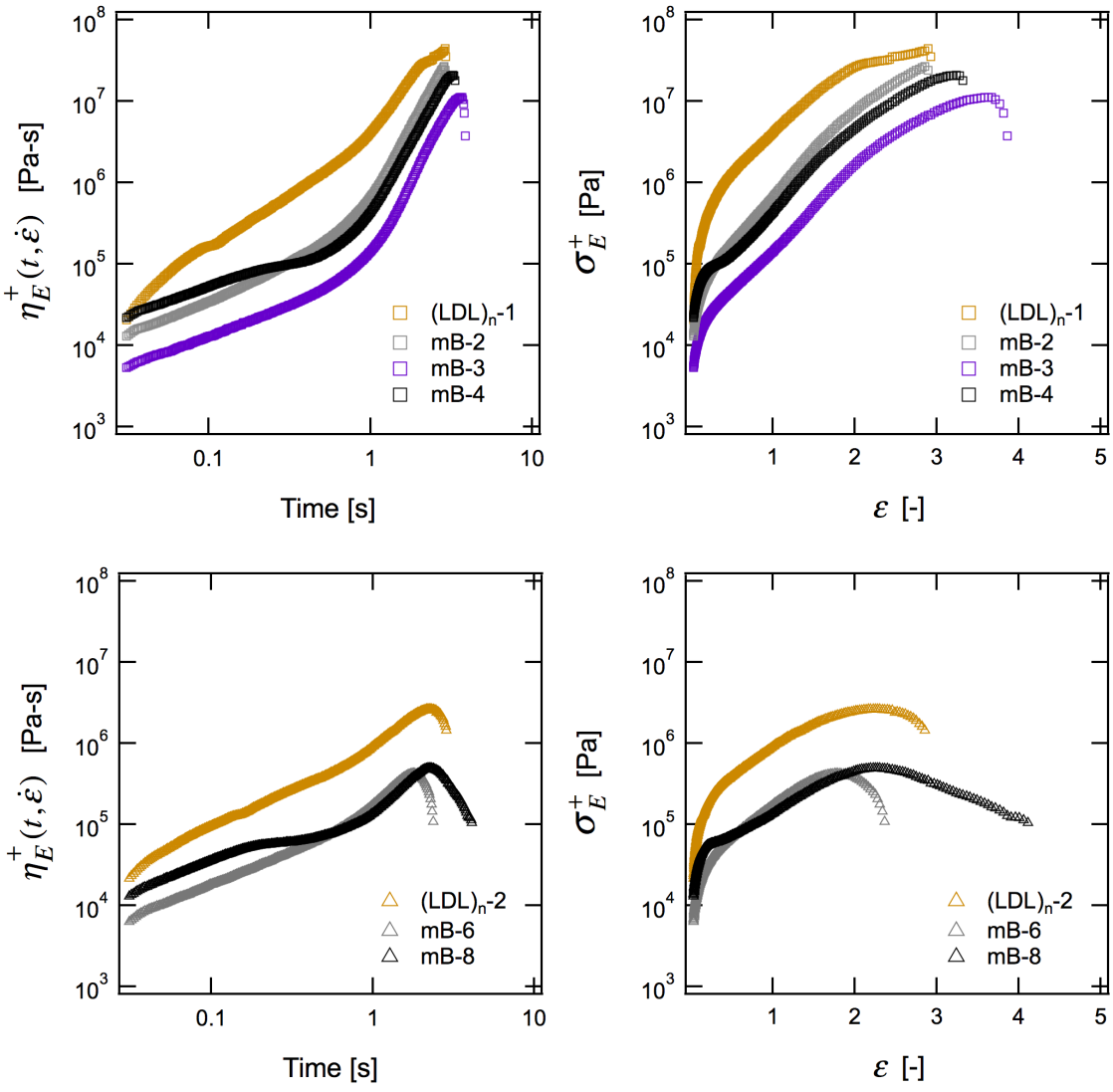

Figure 3.19: Extensional rheology of the pure $(LDL)_n$ multiblocks and their blends at a $\dot{\epsilon}$ =1 s^{-1}.

in linear viscoelasticity, while polymer composition of the triblock determined the amount of strain hardening and the σ_b in extension. The diblock composition also played a role in the strain at break (ϵ_b), but it was unclear whether this was due to the composition itself or its effect on the T_g's of the lactide blocks. With regards to *diblock molecular weight*, incorporating medium molecular weight diblocks (in which the soft block is entangled) was shown to provide additional relaxation times and mask a distinct yield point; however, the added benefit of an increased ϵ_b was mostly lost by using these diblocks. Increases in ϵ_b only appeared in systems in which some level of macrophase separation occurred and swelling of the ensuing triblock-rich domain, or in which a disordered diblock was used.

The LDL/DL ternary blends were explored as potential candidates for chewing or bubble gum bases by fitting the LVE and extensional behavior to key rheological parameters determined in Chapter 2. Although many blends had the necessary LVE behavior, very few had a high enough ϵ_b, and none of the 24 blends met both the LVE and extensional criteria necessary for chewing or bubble gums.

The effect of *polymer architecture* was examined by replacing the LDL triblock with $(\text{LDL})_\text{n}$ multiblocks of comparable f_{PLA} and M_n with the intent of increasing ϵ_b. Although only a few $(\text{LDL})_\text{n}$/DL blends were tested and the results are preliminary, some of these blends were able to attain much larger ϵ_b's than their ternary LDL/DL blend counterparts while having potentially more desirable LVE behavior. By changing the temperature during extension, it was also shown that having a T_g close to the test temperature is critical in attaining these high deformations. These promising results suggest that future work should be focused on blends of multiblock polymers with low molecular diblocks. Test temperatures should be chosen relative to the T_g of the hard domains to eliminate this confounding effect. Finally, a much more thorough characterization of the morphology should be employed to see whether macrophase separation and/or swelling of the domains plays a role in the $(\text{LDL})_\text{n}$/DL system as it did with the LDL/DL ternary blends.

Chapter 4

Branched Multiblock Polymers from Coupling 4-arm Star Diblocks

4.1 Introduction

Poly(lactic acid), also known as poly(lactide) or PLA, is a renewable, biodegradable, and compostable thermoplastic with mechanical properties similar to poly(styrene).[34] Although it is seen to be commercial competitive with conventional petroleum derived plastics such as poly(ethylene terephthalate),[41] PLA is inherently brittle[40] and possesses poor melt strength,[42] two properties which limit its potential applications.

Various strategies have been employed to toughen PLA[129] including plasticization,[130] copolymerization,[131–133] melt blending,[134] reactive blending,[135–137] modification with block copolymer micelles,[138] and orientation.[139] One versatile approach relies on covalently linking rubbery polymers to amorphous or semicrystalline poly(lactide) to form microphase separated block polymers. This strategy gives accurate control of domain size and guarantees good dispersion of the elastomeric phase within the PLA matrix, both of which are major

The work in this chapter is published in Mannion et. al, *Macromolecules* **2016**, *49*, 4587-4598.[128] It was supported by the National Science Center through the Center for Sustainable Polymers at the University of Minnesota, a Center for Chemical Innovation (CHE-1413862).

problems in melt blending. Although different block polymer architectures can toughen PLA,[40,132] multiblocks have been shown to be especially effective, increasing toughness by orders of magnitude over neat PLA.[131] In addition, a multiblock architecture allows one to decouple the accessible order-disorder transition temperature (T_{ODT}) needed for processing from the total molecular weight of the polymer that dictates desirable mechanical responses.[109,140] The major drawback of this approach is the high cost of a suitable sustainable elastomeric block, yet advances in synthetic biology leading to commercially competitive monomers may alleviate this concern in the near future.[141]

To develop a more fundamental understanding of structure-property relationships of these sustainable multiblock polymers, controlled polymerization techniques are of interest. Specifically, sequential ring opening transesterfication polymerization (ROTEP) can be used to synthesize reactive polyester triblocks that can be coupled using difunctional small molecules (e.g. diisocyanates, diacids, or epoxides). This strategy represents a robust, scalable synthetic method to produce multiblocks with precisely controlled block size, molecular weight, architecture, and morphology, giving unparalleled ability to target specific thermal, mechanical, and rheological properties. The synthesis can be done in a one-pot approach without extensive purification steps and often without solvent, making it potentially tractable on a commercial scale. Also, the versatile nature of ROTEP allows for the use of many lactones such as ϵ-caprolactone,[142] β-methyl-δ-valerolactone,[141] or trimethyl carbonate,[143] giving flexibility in monomer choice.

The poor melt strength of PLA leads to processing challenges for techniques that involve fast elongational flows such as blow molding, foaming, blown film extrusion, or sheet extrusion.[42] To make PLA more amenable to such processing methods, some investigators have looked at increasing strain induced crystallization[144] and introducing stereocomplexes,[145] but the majority of studies have sought to incorporate long chain branching (LCB) into the polymer architecture.[145–153] Typically, LCB is marked by the presence of branches that exceed the critical molecular weight (M_C) of entanglement and at least one interior section

of entangled polymer bordered by two branching points (i.e. an entangled section with no free dangling ends).[67] Polymers with LCB tend to exhibit shear thinning behavior and extensional strain hardening; the magnitude of each effect is dependent on the exact architecture. Previous literature has shown that copolymerization of lactide with cyclic esters with an available hydroxyl group,[145–147] reactive extrusion of linear PLA,[148,149] and cross-linking linear with star prepolymers in solution[154] can all be used to produce long chain branched PLA. Most of these strategies lack control of the final branched architecture, and none incorporate rubbery blocks for toughening.

In this study, the advantages of the multiblock architecture are combined with branching to simultaneously improve the mechanical properties and processability of PLA. Previously, hyperbranched block polyesters have been synthesized from click chemistry of "A_2" and "B_3" macromonomers[155] or polycondensation of "AB_2" macromonomers.[156] However, these strategies involve several synthetic steps and are not amenable to large-scale synthesis. Very recently, Liu et al. coupled 3-arm ϵ-caprolactone stars with monofunctional poly(L-lactide) to prepare branched block materials, but like most other studies, this synthesis was not well controlled; moreover, the authors focused on the crystallization behavior with only a cursory look at the rheological response.[157] Here, a similar coupling approach is utilized that is both simple and scalable to create PLA-based branched multiblock copolymers with precise control over the composition. These materials exhibit increased toughness and processability relative to pristine PLA.

Amorphous poly(D,L-lactide) was chosen rather than semicrystalline poly(L-lactide) (PLLA) to avoid the effects of crystallization, focusing on the morphological and rheological behavior. First, a well-defined telechelic four-arm star poly(ϵ-decalactone)-*b*-poly(D,L-lactide) diblock polymer was synthesized using a one–pot two-step ROTEP approach. These star diblocks were subsequently coupled to make a branched multiblock copolymer (Figure 4.1). The monomer ϵ-decalactone was chosen to build the elastomeric block because it is renewable and can reach near full conversion at room temperature.[109,158,159] Linear

triblock and multiblock analogs were also synthesized to serve as controls. The thermal, morphological, rheological, and mechanical properties of the four polymers were thoroughly investigated in the context of processability and practicality.

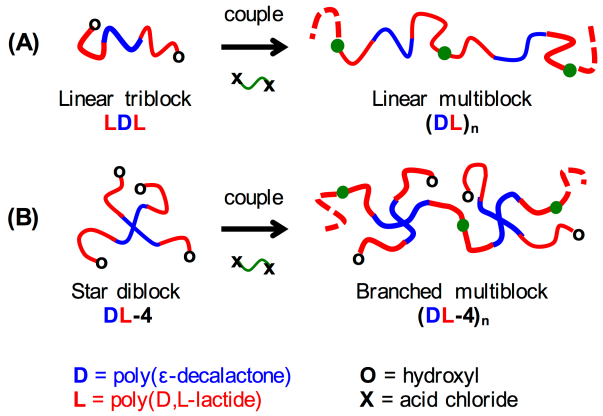

Figure 4.1: Schematic representation of the strategy to synthesize (A) linear and (B) branched multiblocks. A linear triblock and corresponding star diblock were synthesized, and each was coupled with itself to form linear and branched multiblocks, respectively. The coupling strategy utilizes a diacid chloride that reacts with the hydroxyl end groups of the block polymers.

4.2 Experimental methods

Reagents

The ϵ-decalactone (99%, Sigma-Aldrich) was distilled under reduced pressure and passed through a column of activated basic alumina (Fisher Scientific) without exposure to air. Tin (II) 2-ethylhexanoate (∼95%, Sigma-Aldrich) was distilled before use. 1,4-benzenedimethanol (99%, Alfa Aesar) and pentaerythritol (99%, Sigma-Aldrich) were dried under reduced pressure and room temperature for 24 h. D,L-lactide (99.5%, Purac) was used as received. Toluene was purified by passage through activated alumina columns (Glass Contour, Laguna Beach, CA). Pyridine (>99%, Acros Organics) was dried over sodium hydroxide for

2 weeks in a light-free environment. Sebacoyl chloride (99%, Sigma-Aldrich) was used as received. All the aforementioned reagents were stored and handled in a glove box filled with argon.

Linear triblock and star diblock synthesis

A 250 mL pressure vessel was dried in an oven at 150 °C for at least 2 h directly before transfer into the glove box. The poly(ϵ-decalactone) (D) block was prepared first. The appropriate initiator (1,4-benzenedimenthanol for the linear diol and pentaerythritol for the 4-arm star tetrol) and catalyst (tin (II) 2-ethylhexanoate) were prepared in the glove box with a 1:1000 catalyst:monomer loading in the pressure vessel and immediately transferred outside into a silicone oil bath. The reagents were mixed at 110 °C for ∼12 h. The pressure vessel was brought back into the glove box and aliquots were taken for characterization. After the polymerization of ϵ-decalactone reached near complete conversion, D,L-lactide and toluene were added to the pressure vessel at roughly a 1:1 ratio to create the poly(D,L-lactide) (L) end blocks with the telechelic poly(ϵ-decalactone) serving as a macroinitiator. The reagents were mixed at 70 °C for 30 min to pre-dissolve the D,L-lactide and macroinitiator in the toluene. The reaction proceeded at 110 °C for ∼3 h. The resulting linear LDL triblock and star DL-4 diblock were precipitated in methanol and allowed to settle at ∼5 °C overnight. The methanol was decanted off and the solids collected and dried.

Multiblock synthesis

Linear $(DL)_n$ multiblock polymers were synthesized as follows. Linear LDL triblocks were dried and dissolved in a 4:1 mixture of toluene and pyridine to make a 30 wt. % solution. A stoichiometric amount of sebacoyl chloride was slowly titrated into the solution in an argon-filled glove box while mixing at room temperature. After all the sebacoyl chloride was added, the solution was mixed at room temperature for 1 h. The solution was passed through filter paper (P5 medium porosity, Fisherbrand) to remove salts and precipitated

in methanol.

Branched $(DL\text{-}4)_n$ multiblock polymers were synthesized in a similar manner but by coupling star DL-4 diblocks with a substoichiometric quantity of sebacoyl chloride. The ratio of crosslinking agent to prepolymer was determined using titration experiments; when higher amounts of sebacoyl chloride were added, a residual gel fraction was observed in the filtration step. However, at < 0.7 eq., there was no evidence of gelation. Full dissolution in tetrahydrofuran (THF) and no resistance during filtration prior to SEC analysis reaffirmed this assessment.

Characterization

^{1}H NMR spectra were obtained with a Varian Inova spectrometer operating at 500 MHz and 25 °C using a 30 s relaxation time and 8 transients. Samples were prepared by dissolving 10 mg of polymer in 0.7 mL $CDCl_3$ (Cambridge Isotope Laboratories, Inc., 99.8 atom % D + 0.05% V/V TMS). End-group analysis was used to calculate the M_n of the linear and star homopolymers. δ (ppm) = 5.10 [-C6H4**CH2**O- BDM], 4.86 [-CH2**CH**(C4H9)O-], 4.16 [-C**(CH2)**4- PERYT], 3.60 [-CH2**CH**(C4H9)OH end group]. Near quantitative agreement between initiator and end-group peaks was used to verify the functionality of the polyesters prepared using 1,4-benzene dimethanol and pentaerythritol as 2.0 and 4.2 respectively. Molecular weight of the full polymer was calculated by comparing peaks of the poly(ϵ-decalactone) backbone to the poly(D,L-lactide) backbone with knowledge of the homopolymer molecular weight. δ (ppm) = 5.2 [-**CH**(CH3)O-]. Using established densities of 1.25 g cm^{-3} for amorphous PLA[160,161] and 0.97 g cm^{-3} for poly(ϵ-decalactone),[109] the volume fraction of PLA, f_{PLA}, for each polymer was calculated.

Size-exclusion chromatography (SEC) analysis was performed using an Agilent 1260 Infinity LC system equipped with three Waters Styragel columns in series, a Wyatt DAWN Heleos II 18-angle laser light scattering (MALS) detector, and a Wyatt OPTILAB T-rEX refractive index (RI) detector. SEC samples were analyzed at 25 °C in a THF mobile

phase at a flow rate of 1.0 mL min^{-1}. From the RI detector, we report the dispersity ($Đ = M_w/M_n$) relative to 12 linear polystyrene standards (5800 - 2 × 10^6 g mol^{-1}, Agilent Technologies). Absolute molar mass was determined with the MALS detector using (dn/dc) = 0.0530, as measured by the instrument for both linear and branched polymers assuming 100% mass elution. This (dn/dc) value was verified by consistent measurements between repeated samples and allowed us to use $(DL)_n$ as a suitable linear standard to calculate the branching index (g) for $(DL\text{-}4)_n$.

Differential scanning calorimetry

Thermal properties were explored via differential scanning calorimetry on a Thermal Analysis Q1000. Approximately 5 mg of sample were prepared in hermetically sealed aluminum pans. Materials were heated to 180 °C to erase thermal history, cooled to -100 °C at 10 °C min^{-1}, and heated to 180 °C at 10 °C min^{-1}. Glass transition temperatures are reported upon the second heating curve.

Small angle X-ray scattering

Small angle X-ray scattering (SAXS) experiments were conducted at the Advanced Photon Source (APS) in Argonne National Laboratory (Argonne, IL) in sector 5-ID-D. A wavelength of 0.729 Å was used at a detector-to-sample distance of 8.50 m. Samples were prepared in aluminum pans and annealed at temperatures above the glass transition of the amorphous poly(lactide) block but below the order-disorder transition temperature of the material. This was done to try to ensure the morphologies of the samples were at equilibrium. Specifically, the LDL and DL-4 polymers were annealed at 50 °C for approximately 4 days, and the $(DL)_n$ and $(DL\text{-}4)_n$ polymers were annealed at 80 °C for 3 h. For variable temperature experiments (VT-SAXS), samples were annealed at the indicated temperature for 2 min, and the data were then collected using 1 s exposure times. The scattering patterns of LDL and DL-4 were examined at 5 °C intervals from 40 °C to 75 °C, while those

of $(DL)_n$ and $(DL\text{-}4)_n$ were examined at 10 °C intervals from 50 °C until the sample was clearly disordered.

Transmission electron microscopy (TEM)

The branched and linear multiblocks were compression molded at 140 °C to access the disordered state and annealed at 80 °C for 3 h. Samples were trimmed using a LEICA EM UC6 Ultramicrotome to form a sharp tip, then stained with RuO_4 vapors for 4 h. Thin samples for TEM analysis were then cut using a Reichert UltraCut S Ultramicrotome with a diamond knife blade. Images were acquired using a Tecnai G2 Spirit BioTWIN, a 20-120 kV / LaB6 Transmission Electron Microscope.

Rheology

Shear rheology was investigated in small amplitude oscillatory shear with an ARES rheometer (TA Instruments) with 8 mm parallel plates. Samples were molded on the rheometer at approximately 160 °C. Extensional rheological tests were conducted with the extensional viscosity fixture (EVF) on an ARES-G2 rheometer. The polymers were compression molded at temperatures between 100 °C and 160 °C for 5 min to form a sheet of thickness ∼0.3 mm. A rectangular punch was then used to prepare samples 25 mm × 5 mm × 0.3 mm for extensional testing. Each sample was annealed on the EVF at the experimental temperature for 150 s, and the sample was observed with a camera to ensure sagging did not occur. For all rheological tests, experiments were conducted under nitrogen gas in an enclosed oven.

Tensile testing

A RSA-G2 solids analyzer (TA Instruments) was used for uniaxial tensile tests. Polymers were compression molded at temperatures between 100 °C and 160 °C for 5 min to form sheets of thickness 0.2 mm. A punch was used to prepare dog-bone samples with a total

length of 25 mm, a gauge length of 6 mm, a width of 3.2 mm, and a thickness of approximately 0.2 mm. The dog-bone specimens were aged at room temperature under vacuum to remove residual moisture for 48 h before testing. Samples were pulled at a rate of 0.1 mm s^{-1} until failure. The engineering stress ($\sigma = F/A_0$) was calculated from the measured force (F) and the initial cross-section area (A_0). Strain ($\epsilon = (\Delta l)/l_0$) was obtained from the change in grip-to-grip distance (l) and initial gauge length (l_0). Young's modulus ($E = \sigma/\epsilon$) was determined from the linear portion of the stress-strain curve. Toughness was taken as the area under the stress-strain curve. For each sample, the data reported are the average and standard deviation of at least five specimens.

4.3 Characterization

4.3.1 Synthesis

The characteristics of the polymers prepared in this work are listed in Table 4.1. In the nomenclature here, "D" signifies the poly(ϵ-decalactone) block, "L" signifies the poly(D,L-lactide) block, "4" signifies a 4-arm star, while $(A)_n$ signifies a multiblock composed of chemical subunits "A". The M_n of the star DL-4 diblock polymer is roughly double that of the linear LDL triblock with nearly identical f_{PLA} and $Đ$. Thus, the star DL-4 diblock can be thought of as two linear LDL triblocks connected at their midpoints. This was done intentionally so that their thermal and morphological properties would be as similar as possible. Two additional values are highlighted in Table 4.1 that will be useful in the discussion of mechanical properties. The first value, $< n >$, is a measure of the connectivity of the multiblock. The parameter $< n >$ is defined as the ratio of the M_n of the multiblock to the M_n of its parent polymer. For example, a $< n >$ of 4.6 for $(DL)_n$ indicates that, on average, there are 4.6 triblocks in each multiblock. For these calculations, the M_n of the multiblock was estimated by taking M_w from SEC-MALS and dividing by $Đ$. There is inherent imprecision in this calculation given that $Đ$ is based on linear polystyrene standards,

and thus, $< n >$ should be taken as a crude approximation. The second value, $< L >$, is the average number of L blocks per chain.

Table 4.1: Characterization of samples LDL, DL-4, $(DL)_n$, and $(DL\text{-}4)_n$

Sample	[a] M_n [kg mol^{-1}]	[b] M_w [kg mol^{-1}]	[c] f_{PLA}	[d] $Đ$	$< n >$	[e] $< L >$	[f] $T_{g,D}$ [°C]	[f] $T_{g,L}$ [°C]
LDL	14.7	18.4	0.72	1.14	–	2	42 (44)	-39 (-52)
DL-4	33.3	39.7	0.73	1.10	–	4	37 (45)	-40 (-52)
$(DL)_n$	–	159	0.72	1.92	4.6	5.6	42 (48)	-39 (-52)
$(DL\text{-}4)_n$	–	151	0.73	2.00	2.3	7.9	44 (46)	-37 (-52)

[a]Calculated from ^{1}H NMR based on initiator peaks. [b]Determined using SEC-MALS in THF. [c]Calculated from ^{1}H NMR using published densities of PLA and PDL.[109] [d]Calculated with SEC with an RI detector in THF at room temperature. [e]The parameter $< L >$ was calculated by the equation $(L-1) < n > +1$ where L is the number of L blocks per subunit. [f]Determined using DSC during the second heating cycle. The values in parentheses are the glass transition temperatures expected for a homopolymer of the same molar mass, calculated using the Flory-Fox equation.

The SEC traces from the RI detector of the four polymers are shown in Figure 4.2. Typical of controlled ROTEP, the LDL and DL-4 block polymers have relatively low dispersities (near 1.10). The molecular weight distributions of the linear multiblock is broader (close to 2.0), characteristic of step growth polymerizations such as the coupling approach employed.[110] The small shoulder present in the SEC trace for the linear multiblock is likely due to the presence of a minor amount of residual triblock. From normalized areas of these traces, it is estimated that this triblock fraction comprises approximately 9 wt.% of the sample. Because the synthesis of the branched multiblock was conducted using a substoichiometric amount (0.63 eq.) of sebacoyl chloride, there is a significant fraction of residual DL-4 (roughly 40 wt.%) in the $(DL\text{-}4)_n$ sample. At higher amounts of coupling agent (>0.70 eq.), gelation occurred, a common problem in the synthesis of branched polyesters such as PET[162] and in reactive extrusion strategies used to add branching to PLA.[149,162]

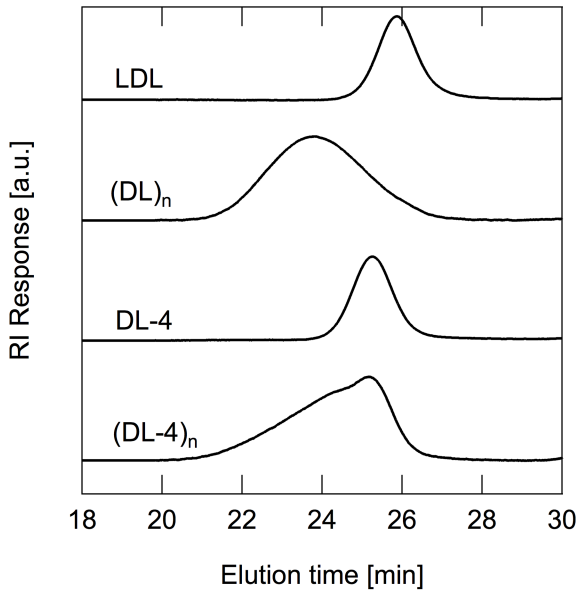

Figure 4.2: SEC traces from a RI detector for linear polymers LDL and $(DL)_n$ and branched polymers DL-4 and $(DL\text{-}4)_n$. The narrow dispersities of LDL and DL-4 demonstrate controlled polymerization. The dispersity of $(DL)_n$ approaches 2, characteristic of coupling difunctional macromolecules. Polymer $(DL\text{-}4)_n$ has a large peak corresponding to DL-4 (its parent polymer) because a substoichiometric amount of coupling agent was used to avoid gelation.

4.3.2 SEC-MALS

The branched nature of the polymers was assessed using SEC with a multi-angle light scattering detector (SEC-MALS). SEC-MALS provides a direct measure of the molecular weight (M_w) and radius of gyration (R_g) of a polymer sample. The radius of gyration of a branched polymer can be compared to a linear control of the same molar mass to find the branching index (g).[162] The lower the value of g, the higher the branching content.

$$g = \left.\frac{R_{g,branched}}{R_{g,linear}}\right|_{MW} \tag{4.1}$$

In Figure 4.3, R_g and g are shown as a function of M_w for $(DL)_n$ and $(DL\text{-}4)_n$. Data points at molecular weights below 130 kg mol^{-1} and higher than 700 kg mol^{-1} are cut off

due to significant noise in the R_g measurements, although polymers chains with M_w values of approximately 10^3 kg mol^{-1} were detected for both samples (Figure 4.4). The value of g increases from 0.76 at 130 kg mol^{-1} to 0.89 at 700 kg mol^{-1}, indicating that as more and more DL-4 chains couple, the polymer becomes increasingly linear in nature. From these data, it is believed that the high molecular weight species of $(DL\text{-}4)_n$ are more similar to comb polymers with a long linear backbone and short side chains (Figure 4.5c) than to densely packed hyperbranched materials (Figure 4.5b).

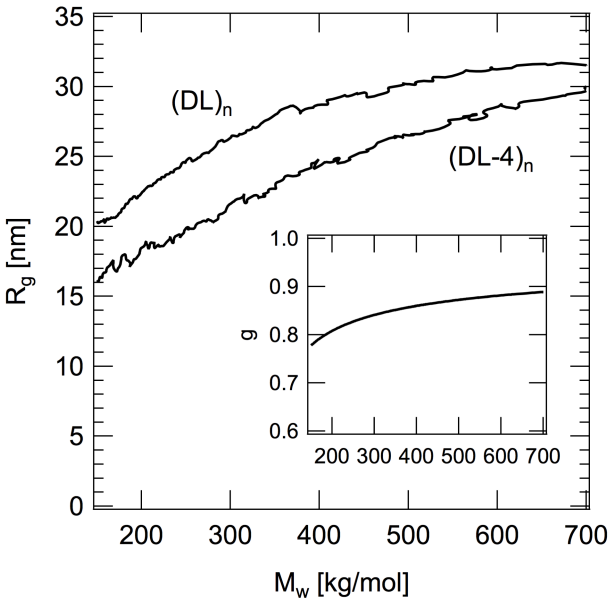

Figure 4.3: SEC-MALS results for $(DL)_n$ and $(DL\text{-}4)_n$. The branching coefficient, g, is determined by the ratio of the radii of gyration (R_g) at equivalent M_w. The value of g increases with M_w, indicating that the highly coupled star polymers are more similar to linear-like comb polymers than densely packed hyperbranched chains.

4.3.3 Thermal properties

As shown in the DSC curves in Figure 5, all of the block polymer samples have two distinct glass transition temperatures (T_g's) near -40 and 45 °C. These glass transitions are assigned to the poly(ϵ-decalactone) and poly(lactide) blocks, respectively, and experimental values

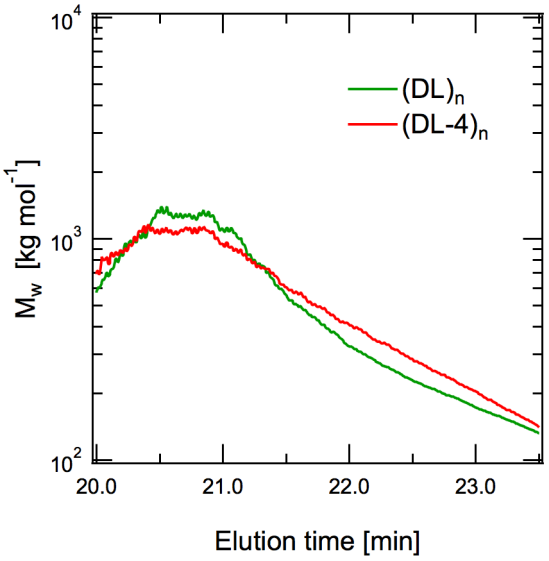

Figure 4.4: SEC-MALS results showing absolute molar mass as a function of elution time for the two multiblocks. Chains with molar masses as high as 10^3 kg mol^{-1} were detected (well below the instrument detection limit of 10^6 kg mol^{-1}), but none with higher molecular weights. The increase in M_w from 20 to 21 minutes of elution time is attributed to very low polymer concentrations and inherent scatter in signal.

are listed in Table 4.1. The reported glass transition temperatures (T_g's) of L are lower than the literature value of 57.0 °C.[115] Most of this discrepancy is attributed to the fact the blocks are relatively short and can be quantified using equation 3.4 the Flory-Fox equation.[114] Inserting M_n into the Flory-Fox equation and using the appropriate value of K (7.40×10^4),[115] the theoretical values for T_g of L are calculated and listed in Table 4.1. In the same manner, the theoretical values for T_g are calculated for the D blocks using -51.4 °C and 3.4×10^3 for $T_{g,\infty}$ and M_n, respectively.[109]

Even taking the molecular weight dependence into consideration, the observed glass transition values of L are slightly lower than expected, and the D blocks are slightly high. These observations suggest that the block polymers are microphase separated with partial mixing of the two domains.

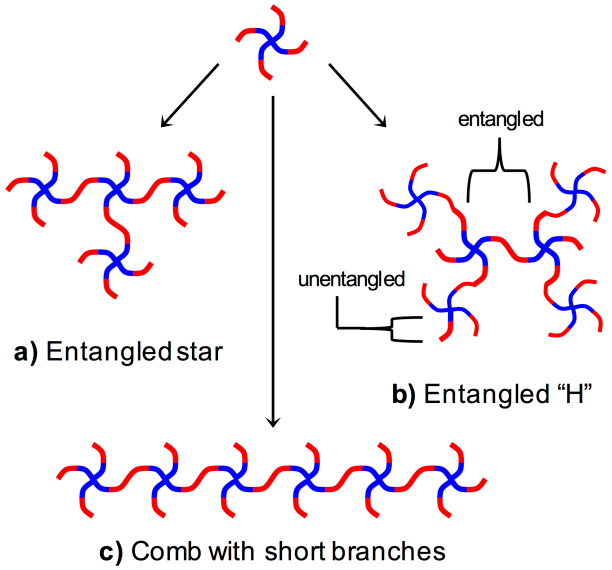

Figure 4.5: Possible architectures that result from coupling the star diblocks: a) entangled three-arm star polymer, b) entangled "H" polymer, or c) comb polymer with short branches.

4.4 Morphology

The morphology and order-disorder transition temperatures (T_{ODT}'s) of the block polymers were investigated using variable temperature small angle X-ray scattering (VT-SAXS). The scattering data for the four samples are plotted as the Lorentz-corrected intensity, Iq^2, versus the wave vector, q, in Figure 4.7 and Figure 4.8. At 40 °C, samples LDL and DL-4 both have a broad primary peak (denoted as q^*) at about $q = 0.5$ nm^{-1} and exhibit a slight shoulder near $q = 1.0$ nm^{-1} (Figure 4.7). The specific values for q^* and corresponding domain spacing ($D = 2\pi/q^*$) are listed in Table 4.2. These data suggest the materials are not well ordered yet may still be microphase separated. It is unclear whether a structure with long-range order could form after longer annealing, or whether the T_{ODT} is prohibitively close to T_g of the L block. Another confounding factor is weak electron density contrast between the D and L blocks which broadens the scattering peaks for this system regardless of whether the architecture is well-defined.[109]

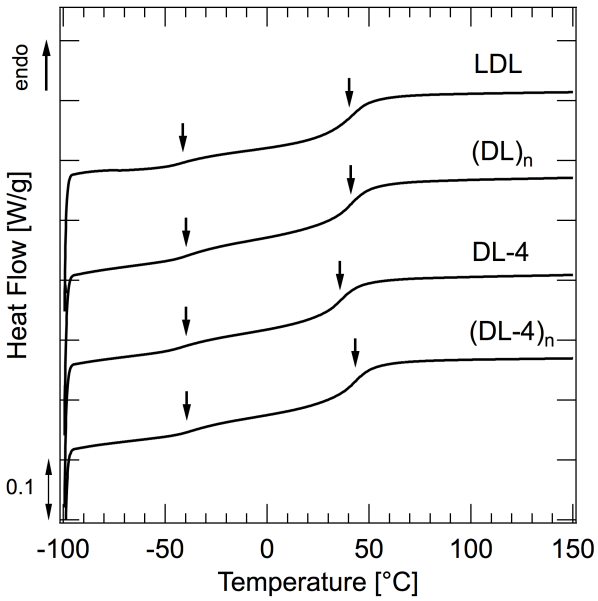

Figure 4.6: Differential scanning calorimetry (DSC) second heating curves for the four samples. Each curve shows two distinct inflection points near -40 °C and 45 °C (arrows), attributed to glass transitions of the D and L blocks, respectively. This provides evidence for microphase separation, yet quantitative disagreement from literature suggests partial mixing of the domains.

As the temperature increases, the peak intensity drops, the primary peak broadens, and the small shoulder near $2q^*$ disappears, consistent with the polymers passing through a transition to a disordered and homogeneous state. Because neither material exhibits long-range order, the transition temperature is more correctly classified as a microphase separation transition temperature (T_{MST}) rather than an order-disorder transition temperature (T_{ODT}). The T_{ODT} and T_{MST} are the same for monodisperse diblock polymers in the limit of infinite molecular weight; however, the two transitions are distinct at finite molecular weight and low segregation strength where fluctuations come into play.[163] Mean-field theory predicts that in the disordered state, the inverse intensity (I^{-1}) of q^* should scale linearly with the inverse temperature (T^{-1}). In this work, the T_{MST} is identified as the temperature at which I^{-1} deviates from such linear behavior.[164–166] For both LDL and

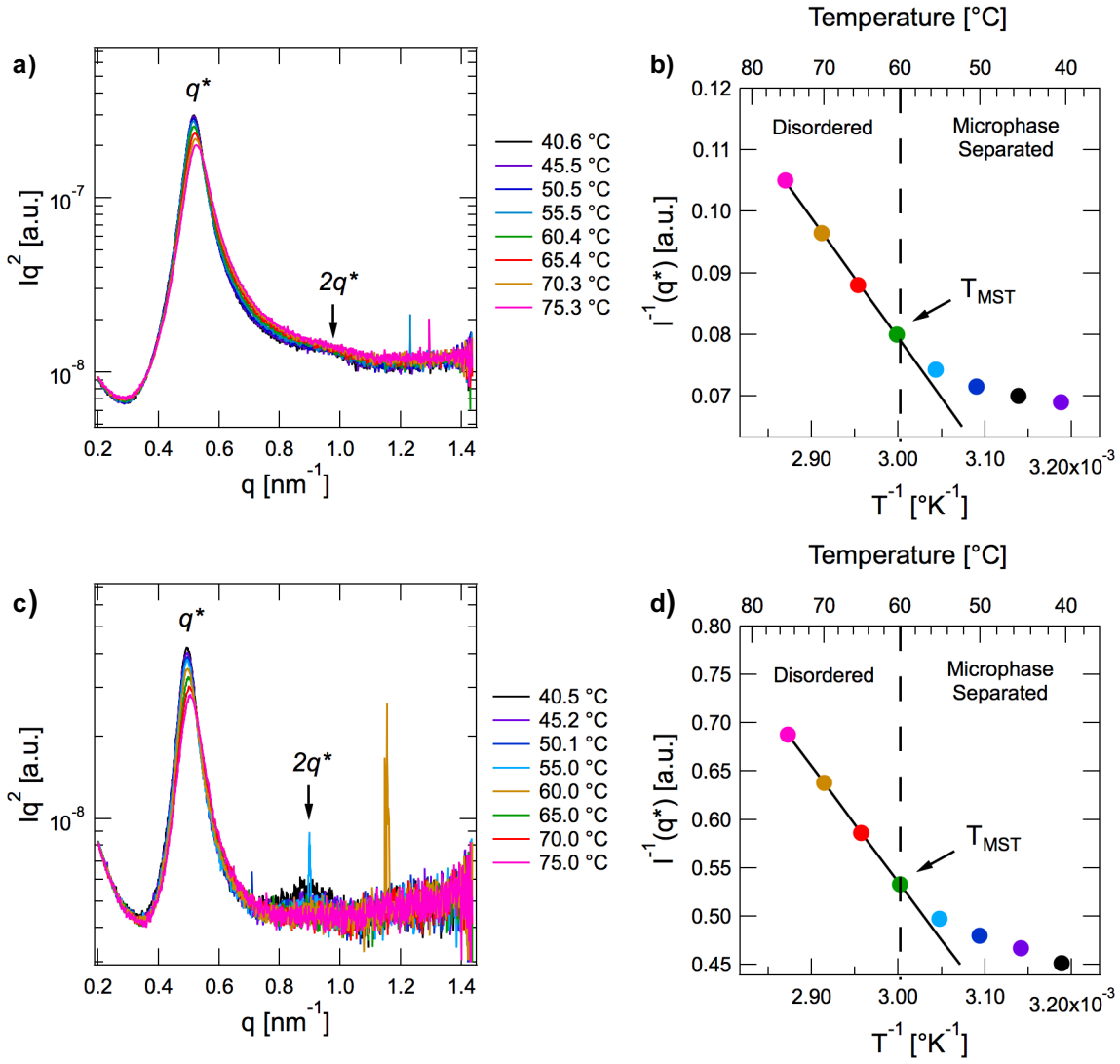

Figure 4.7: Variable temperature small angle X-ray scattering (VT-SAXS) results for a) LDL and c) DL-4. Lorentz-corrected scattering intensities, Iq^2, are plotted against the wavevector, q. A weak shoulder around $2q^*$ at lower temperatures provides evidence for microphase separation. As the temperature increases, q^* drops and the shoulder disappears, indicating a transition into a disordered state. Plotting $I(q^*)^{-1}$ vs. T^{-1}, the T_{MST} is estimated to be 60 °C for both LDL and DL-4.

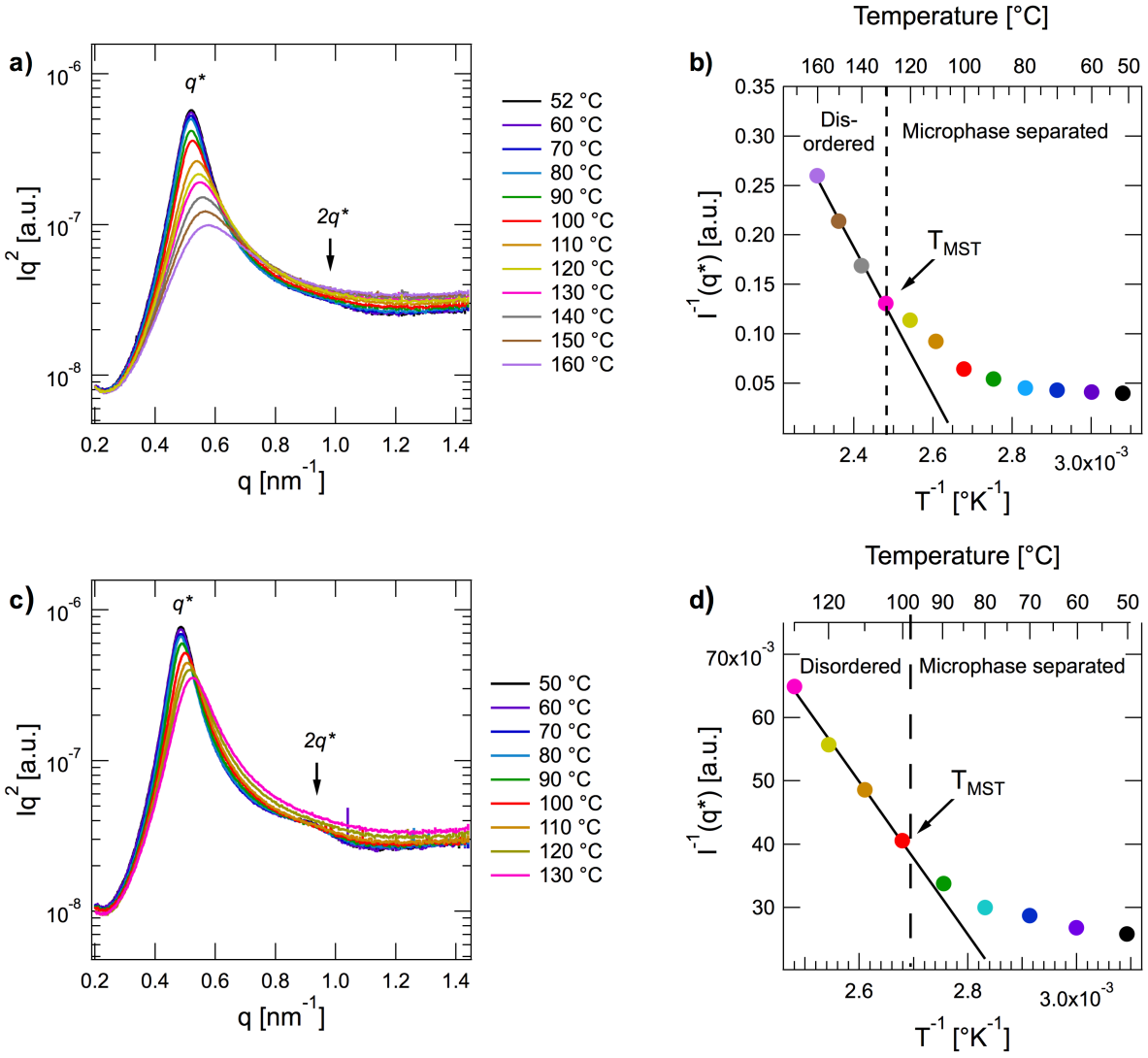

Figure 4.8: Variable temperature small angle x-ray scattering (VT-SAXS) results for a) $(DL)_n$ and c) $(DL\text{-}4)_n$. Lorentz-corrected scattering intensities (Iq^2) are plotted against the wave vector (q). A weak shoulder around $2q^*$ at lower temperatures provides evidence for microphase separation. As the temperature increases, q^* drops, the primary peak broadens, and the shoulder disappears, indicating a transition into a disordered state. Plotting $I(q^*)^{-1}$ vs. T^{-1}, T_{MST} is estimated to be 130 °C for $(DL)_n$ and 100 °C for $(DL\text{-}4)_n$.

DL-4, the T_{MST} is approximately 60 °C (Figure 4.7, Table 4.2). This finding is consistent with a T_{ODT} calculated from published values of χ_{D-L}[109] - for LDL, T_{ODT} is estimated as 56 °C; DL-4 should have a similar T_{ODT}.

The same T_{MST} analysis was conducted for $(DL)_n$ and $(DL\text{-}4)_n$ (Figure 4.8). Again, a broad primary peak with a shoulder at $2q^*$ indicates microphase separation but without long-range order. For these multiblock materials, the T_{MST} is higher, estimated at 130 °C and 100 °C for $(DL)_n$ and $(DL\text{-}4)_n$, respectively (Figure 4.8, Table 4.2). The nonlinear dependence of $I^{-1}(q^*)$ on T^{-1} at temperatures below T_{MST} resembles the scattering behavior of strongly fluctuating diblock copolymers in the disordered state near T_{ODT}.[167–169] Because the materials studied are multiblocks with relatively high dispersities ($Đ \sim 2$), however, the theory that describes fluctuation effects in monodisperse diblocks may not be strictly applicable here.[167] Rather, both the kinetic limitations of ordering[170] and the range of molecular weights and block sizes can smear out the microphase separation regime in which ordered and disordered phases exist simultaneously over a wide temperature window.[171] Studies of model polyurethanes[172] have previously brought to light difficulties that can arise when attempting to differentiate a homogeneous melt with strong local fluctuations from a weakly segregated material with no long-range order. In short, the SAXS data suggests the multiblocks possess a segregated structure over a relatively broad temperature range that is neither well-ordered nor homogeneous.

Representative TEM images of $(DL)_n$ and $(DL\text{-}4)_n$ are shown in Figure 4.9. These images corroborate the interpretation of the SAXS and DSC data - the block polymers are microphase separated yet lack long-range order, adopting a fluctuating, bicontinuous-like structure. Although the distinctive dark and light areas (corresponding to the poly(ϵ-decalactone) and poly(D,L-lactide) blocks, respectively) suggest microphase separation, the boundaries are hazy and the domains are not well defined. Because of this, it is difficult to assess a precise value for the average domain spacing from these images.

It is interesting to compare these findings to the morphologies of other complex block

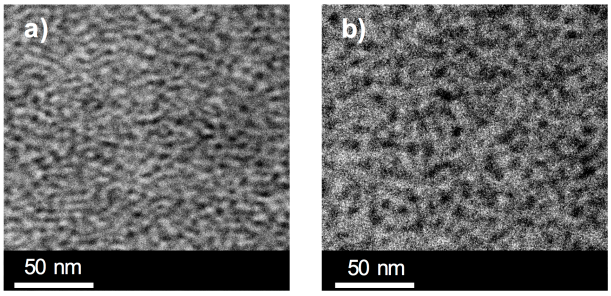

Figure 4.9: Representative TEM images of a) $(DL)_n$ and b) $(DL\text{-}4)_n$. The samples were annealed at 80 °C for three hours and stained with RuO_4 for four hours. Dark domains corresponding to the poly(ϵ-decalactone) domains while the light domains are poly(D,L-lactide). Both materials show microphase separation with hazy boundaries and no long-range order.

Table 4.2: SAXS and shear rheology results for samples LDL, DL-4, $(DL)_n$, and $(DL\text{-}4)_n$

Sample	[a]q^* [nm^{-1}]	[a]D [nm]	[b]T_{MST} [°C]	[c]T_{MST} [°C]
LDL	0.488	12.9	60	≤ 70
DL-4	0.466	13.5	60	≤ 75
$(DL)_n$	0.513	12.2	1300	≤ 130
$(DL\text{-}4)_n$	0.513	12.2	1300	≤ 130

[a]Acquired at 50 °C. [b]Determined using VT-SAXS. [c]Determined using linear rheology.

polymer architectures reminiscent to $(DL\text{-}4)_n$. Mays et al. have investigated tetrafunctional multigraft block copolymers with polystyrene arms attached to a linear polyisoprene backbone.[94,173,174] They found that an increased number of branched points along the backbone effectively inhibited the formation of long-range order, although for certain samples, long-range order was preserved for a modest number of branch points (< 5). Similarly, Hutchings et al. reported the complete loss of long-range order for hyperbranched block copolymers made by coupling ordered poly(styrene-*b*-isoprene-*b*-styrene) triblock copolymers.[175,176] Although observations of $(DL\text{-}4)_n$ are consistent with these previous reports, it is difficult to make a fair comparison since the star diblock precursor, DL-4, also lacked

long-range order. The final morphology of a branched multiblock polymer made by coupling a well-ordered star diblock polymer would be a suitable question for future inquiry.

4.5 Shear rheology

To verify the estimates of T_{MST} from the VT-SAXS experiments, small amplitude oscillatory shear rheology was used to probe the linear viscoelastic (LVE) behavior. Typically, well ordered block polymers exhibit a sharp decrease in the shear moduli upon heating through the order-disorder transition, indicative of the change from an ordered soft solid to a disordered liquid. Initial temperature ramp experiments, however, were inconclusive as no discernible drop-offs in the moduli were observed for any of the polymers (Figures 4.10, 4.11, and 4.12). When LDL was heated at a moderate rate (ΔT = 1 °C min^{-1}) at ω = 1 rad s^{-1}, thee T_{MST} was first estimated to be 75 °C based on a slight shoulder in G' and $\tan\delta$ (Figure S3a). However, at a lower heating rate and angular frequency (ΔT= 0.3 °C min^{-1} and = 0.3 rad s^{-1}) the T_{MST} is estimated as 70 °C (Figure 4.10b). This discrepancy is attributed to the fact that the T_{MST} is only visible at relatively low frequencies because of the slow dynamics close to the T_g of the L blocks - the longest relaxation time of the polymer chain must be traversed in order to see liquid-like behavior. Even at low oscillatory shear rates, DL-4 exhibits similarly inconclusive behavior, though a slight shoulder in G' may indicate a T_{MST} at 75 °C (Figure 4.11). Unlike their parent polymers, $(DL)_n$ and $(DL\text{-}4)_n$ did not exhibit any discernible T_{MST} on heating (Figure 4.12).

Thus, frequency sweeps were conducted and time-Temperature superposition (tTs) was employed to identify T_{MST} by noting the lowest temperature that showed terminal scaling ($G' \sim \omega^2, G'' \sim \omega$). It is well documented that thermorheological complexity and failure of tTs can arise in systems with more than one fundamental time constant such as in block polymers with two or more distinct T_g's[177] and branched polymers.[178,179] Still, tTs worked well for all four polymers as the horizontal shift factors obeyed the Williams-Landel-Ferry (WLF) equation (Figure 4.13).

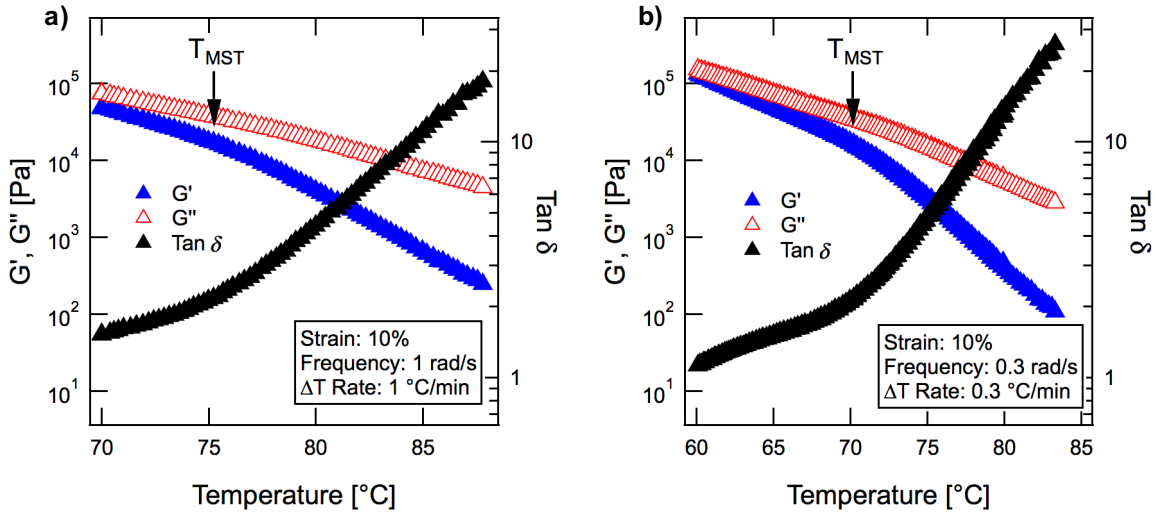

Figure 4.10: Isochronal temperature ramp for LDL. Depending on the frequency probed, the apparent T_{MST} deviates as much as 5 °C. Thus, the value for the T_{MST} is unclear.

The linear rheology master curves for the four polymers show a relatively smooth superposition until terminal scaling occurs at the lowest reduced frequencies, lacking an obvious T_{MST} (Figure 8). For LDL and DL-4, this is attributed to the inability to access the low frequency regime necessary to identify the T_{MST}; for example, from the WLF fits, terminal scaling is estimated to begin below 0.01 rad s^{-1} for LDL at 60 °C, the T_{MST} elucidated from SAXS. For $(DL)_n$ and $(DL\text{-}4)_n$, the T_{MST} is believed to be masked by both this inability to access the low frequency regime. Thus, the final T_{MST} estimates (Table 4.2) from shear rheology are likely overestimates since this method depends on mechanical relaxation of segments of the polymer chain that may not be accessible within experimentally relevant time scales. SAXS proves to be more dependable for these particular materials as it relies on fundamentally different physical phenomena that are not hampered by slow kinetics.

The results from tTs were also used to glean information on the architecture of the four polymers. Both LDL and DL-4 show similar LVE behavior with a small plateau region that extends roughly two decades. Because this plateau region lies at temperatures above the T_{MST}, its existence is attributed to lightly entangled chains. For star polymers,

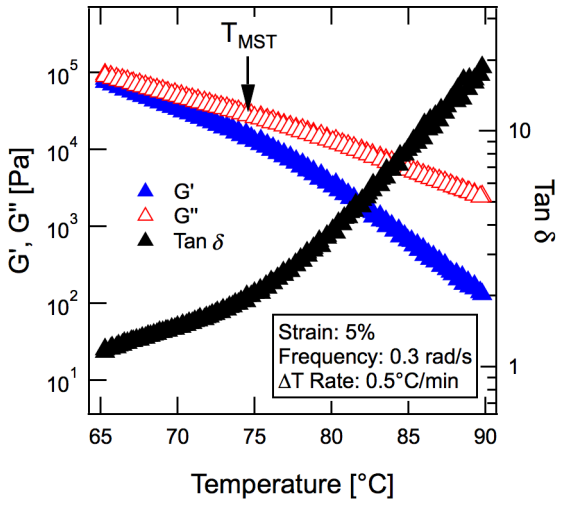

Figure 4.11: Isochronal temperature ramp of DL-4 showing the apparent T_{MST} at 75 °C. However, the drop-off in G' is small, so it unclear whether this is a true T_{MST}.

entanglement of the individual arms results in significantly longer relaxation times and an intermediate scaling of moduli.[180] The fact that these characteristics for DL-4 are not observed strongly suggests that the individual arms are unentangled; rather, the plateau comes from slight entanglements from the star polymer as a whole. To confirm this assessment, M_c, the critical molecular weight for entanglements, is estimated for a DL block polymer (M_c = 9.8 kg mol^{-1} at f_{PLA} = 0.72) by taking a weighted average of M_n of the individual blocks.[181] Given this approximation, the linear chain of LDL (M_n = 14.7 kg mol^{-1}) is expected to be lightly entangled whereas the individual arms of DL-4 (M_n = 8.3 kg mol^{-1}) to be unentangled.

In contrast to the parent polymers, which are rheologically identical, the two multiblocks have dramatically different LVE responses. Multiblock $(DL)_n$ has a relatively flat plateau while $(DL\text{-}4)_n$ exhibits intermediate scaling marked by a change in the slope from $\omega_x < \omega <$ 10 rad s^{-1}, where 10 rad s^{-1} is the terminal relaxation time of the individual star diblocks at the reference temperature of 80 °C. Because the star diblocks have relaxed, the viscoelastic response in this regime is dominated by the higher molecular weight species. This type of

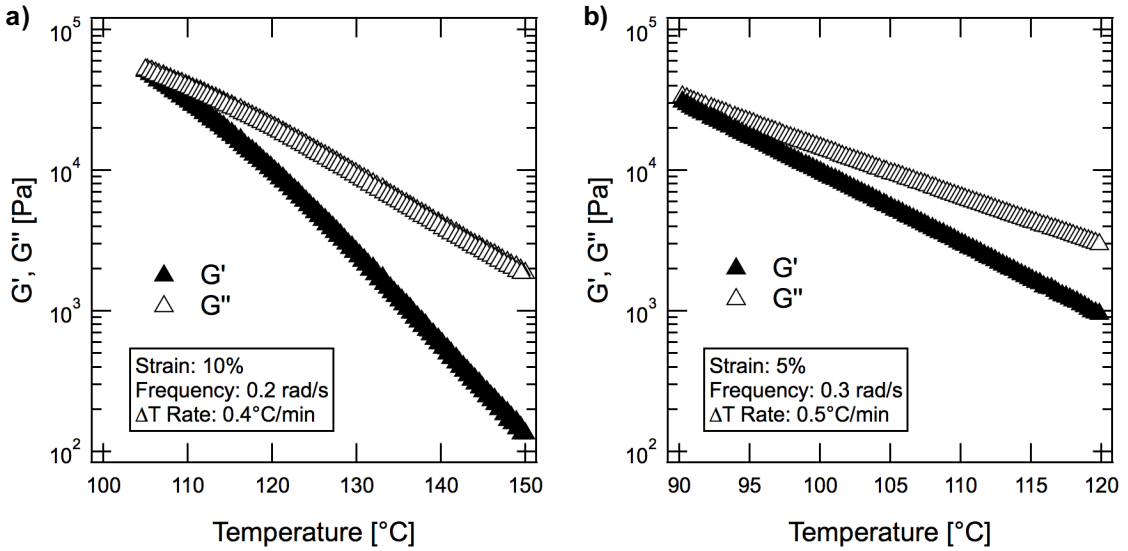

Figure 4.12: Isochronal temperature ramps of a) $(DL)_n$ and b) $(DL\text{-}4)_n$. No discernible T_{MST} can be found, despite the fact that low frequencies and slow heating rates were employed.

intermediate scaling has been observed for a variety of branched systems and is attributed to arm retraction mechanisms that effectively freeze the backbone in place.[180,182,183] The arm retraction is perhaps more easily seen in the response of $\tan\delta$ and is marked by a distinct inflection point for $(DL\text{-}4)_n$ that is not present in linear $(DL)_n$ (Figure S7). Also, despite similar molecular weights, the ω_x for the multiblocks differ significantly – this is attributed to the presence of unentangled or lightly entangled arms in $(DL\text{-}4)_n$ that contribute to the molecular weight but should not increase the longest relaxation time.

At low frequencies ($\omega < \omega_x$), both multiblocks achieve terminal scaling at approximately the same frequency (10^{-4} rad s^{-1}), yet the region of non-terminal liquid-like flow for $(DL\text{-}4)_n$ spans a much larger range of frequencies. Similar broad transitions to terminal scaling have been previously observed in lightly branched polybutadiene,[184] but other architectures such as entangled stars[179] or bottlebrushes[185] could also lead to such an effect, making it nearly impossible to surmise the cause of this subtle yet distinct feature. Although the intermediate

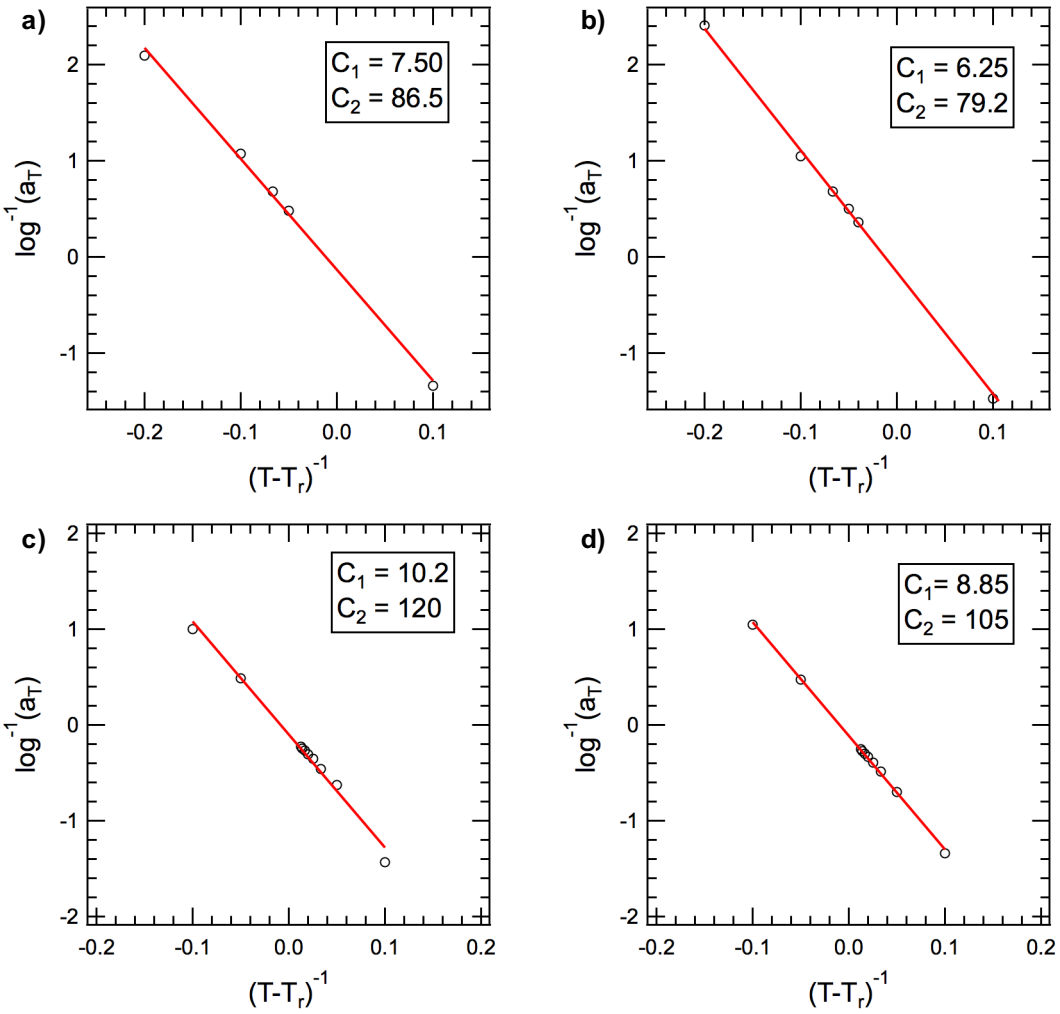

Figure 4.13: WLF fits for a) LDL, b) DL-4, c) $(DL)_n$, and d) $(DL\text{-}4)_n$.

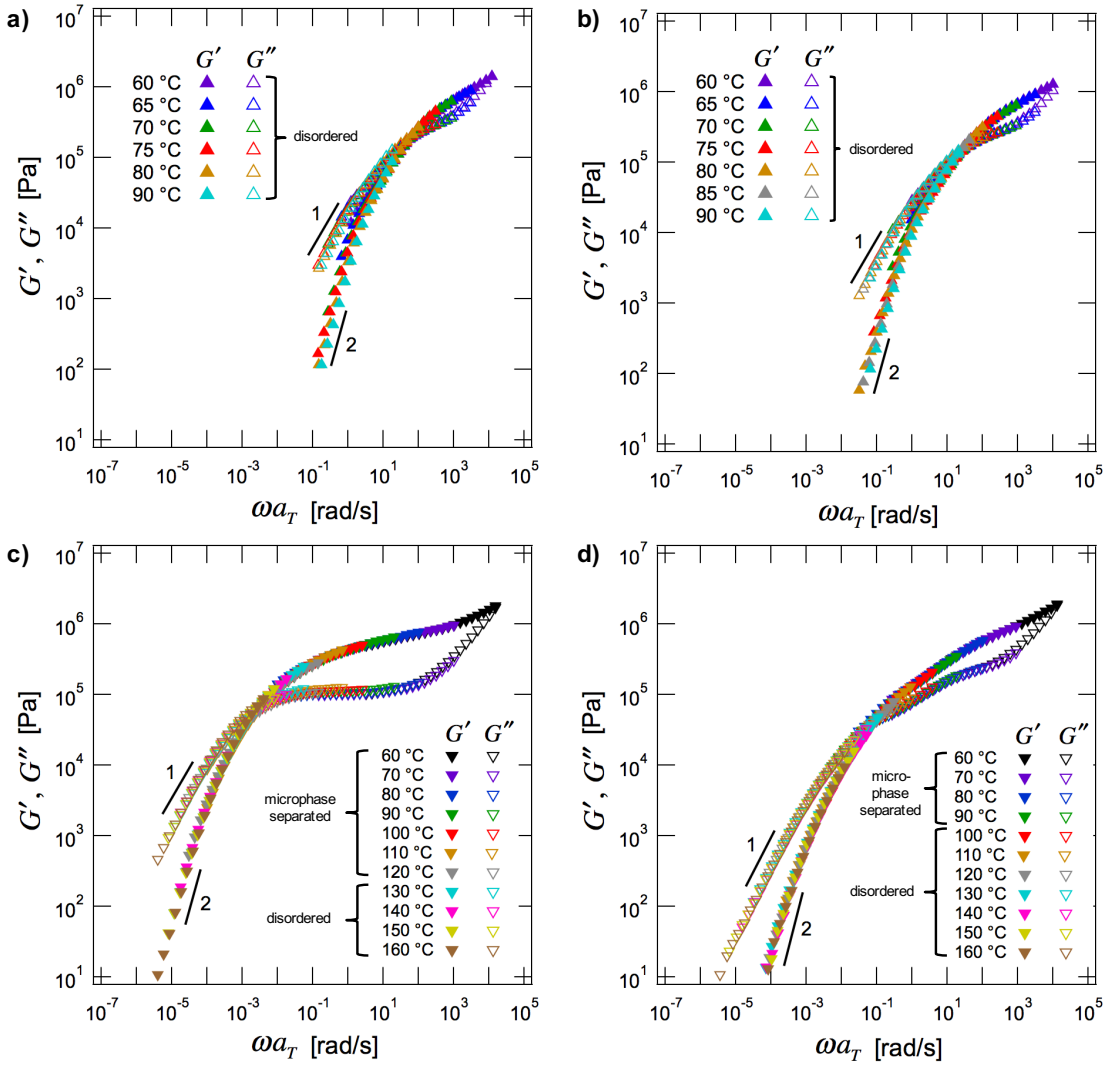

Figure 4.14: Master curves for the linear dynamic storage (G') and loss (G'') moduli of a) LDL b) DL-4 c) $(DL)_n$ and d) $(DL\text{-}4)_n$ at a reference temperature of 80 °C. The legends indicate the temperatures corresponding to microphase separation or disorder according to VT-SAXS. The T_{MST} is masked due to the inability to reach low enough frequencies at relevant temperatures. The LVE responses of LDL and DL-4 are remarkably similar while the two multiblocks are quite distinct. The $(DL)_n$ multiblock has a broad plateau and terminal scaling at 130 °C, while $(DL\text{-}4)_n$ shows an alternate response at intermediate frequencies characteristic of branched materials.

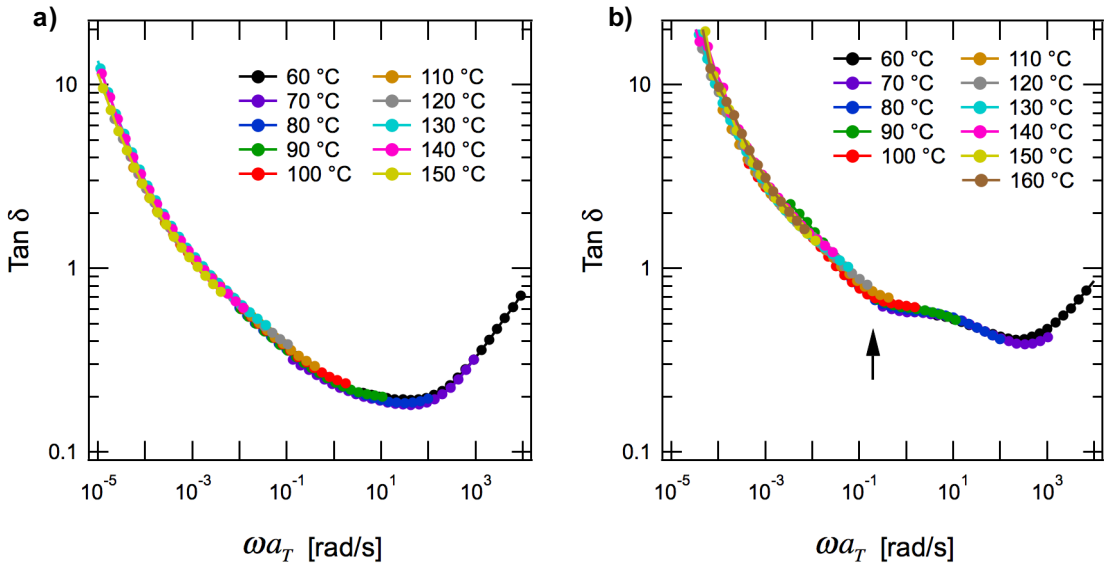

Figure 4.15: Plots of tan δ *versus* reduced frequency for a) $(DL)_n$ and for b) $(DL\text{-}4)_n$. The latter shows an inflection point at intermediate reduced frequencies due to the additional relaxation mechanism from the branched architecture.

scaling and more gradual transition to terminal scaling are not direct signatures of LCB, they are indicators that the high molecular weight chains with a more complex branched architecture are playing a prominent role in the rheological response of $(DL\text{-}4)_n$.

The complex viscosities of the multiblocks were also compared to the steady shear viscosity (Figure 4.16), determined with parallel plates and adjusted using the single-point correction.[186] Good agreements between oscillatory and steady shear measurements at temperatures above the T_{MST} indicate that these materials follow the Cox-Merz rule. The flow activation energies (E_A) were estimated by fitting the zero-shear viscosities at high temperatures (140 to 180 °C) to the following Arrhenius relationship which is typically accurate at temperatures $\geq T_g + 80$ °C:[162]

$$\eta_0(T) = A_0 \exp\left(\frac{E_A}{RT}\right) \tag{4.2}$$

The resulting values for E_A were 1.10 × 10^5 J mol^{-1} and 1.02 ×10^5 J mol^{-1} for $(DL)_n$

and $(DL\text{-}4)_n$, respectively. From this, it is concluded that the branched structure of $(DL\text{-}4)_n$ does not give rise to an elevation in activation energy as is sometimes observed for polyethylene and other branched systems,[178,179] consistent with previous studies on long chain branching in PLA.[149,187]

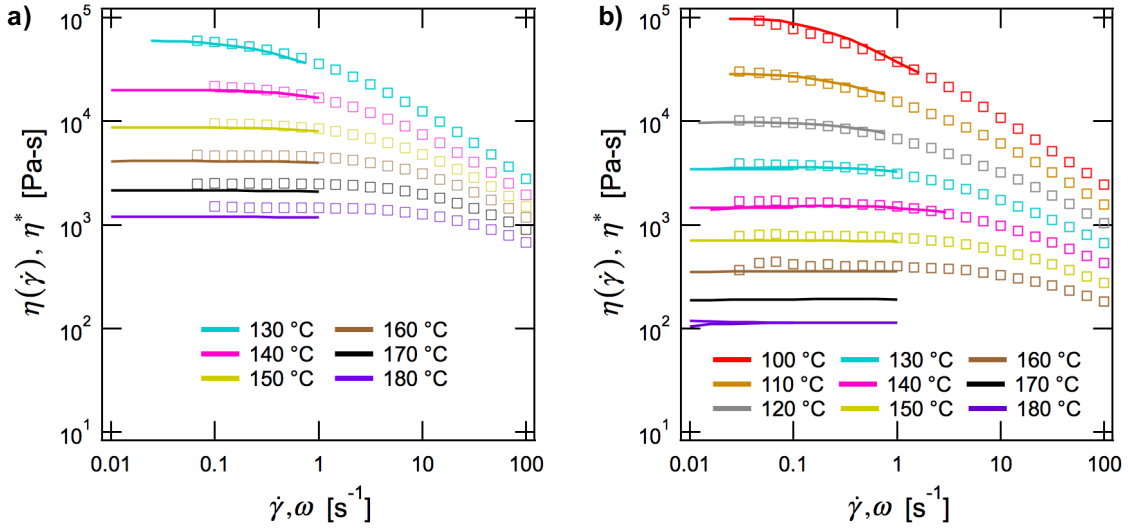

Figure 4.16: Steady shear viscosity (solid lines) and complex viscosity (markers) versus shear rate or frequency for a) $(DL)_n$ and b) $(DL\text{-}4)_n$. Overall, the data is in decent agreement and obeys the Cox-Merz rule, but degradation of the materials prevented a more quantitative assessment.

4.6 Extensional rheology

Extensional rheology is widely used to characterize LCB in polymer melts since it is known to cause strain hardening, a phenomenon marked by a sharp increase in extensional viscosity above the linear viscoelastic prediction.[116] Although quantitative information about the molecular architecture cannot be surmised *a priori*, extensional rheology is most relevant for practical purposes and provides a wealth of qualitative information. For example, more dramatic strain hardening correlates with more long chain branches, more entanglements

per branch, and more entanglements between branch points.[188] Extensional rheology is often preferable to other characterization methods since it is relatively insensitive to molecular weight distribution, does not require linear standards, and is highly sensitive to low levels of LCB.

Uniaxial extension tests were conducted at temperatures at the T_{MST} for $(DL)_n$ and $(DL\text{-}4)_n$ (130 °C and 100 °C, respectively) to eliminate the potentially confounding effects of microphase separation.[80,189–191] Samples were pulled at three different Hencky strain rates, and the results are shown in Figure 4.17. A curve showing the expected linear viscoelastic response is also included, equal to three times the transient viscosity as measured in shear at 0.1 s^{-1}. The good agreement between the linear viscoelastic predictions and the extensional measurements at small strains and times gives us confidence in the accuracy of the data.

An important parameter to consider is the Weissenberg number (Wi), a dimensionless quantity that when greater than unity, predicts the onset of nonlinearity for flows in which stresses are independent of time.[67] For steady uniaxial extension, Wi can be defined as the product of a characteristic relaxation time, $< \tau >$ with the Hencky strain rate, $\dot{\epsilon}$. According to the Doi-Edwards model, strain hardening would occur in entangled melts only at rates faster than the inverse Rouse time, τ_R^{-1}, due to friction of the chain retracting within its tube.[61] However, Bach et al. reported strain hardening at Hencky strain rates as slow as τ_d^{-1}, the inverse tube disengagement time.[74] At rates close to τ_d^{-1} , this strain hardening effect is small. With this in mind, $< \tau >$ is defined as $2\tau_d$, roughly twice the longest relaxation time of the system (estimated from the low-frequency crossover frequency). At the experimental temperatures, $Wi > 1$ at $\dot{\epsilon} > 1$ s^{-1} for $(DL)_n$ and $\dot{\epsilon} > 0.9$ s^{-1} for $(DL\text{-}4)_n$. Thus, at these conditions, deviations from linearity with or without branching may be observed, and the extent of these deviations will increase with larger Hencky strain rates.

As anticipated, $(DL)_n$ closely follows the linear viscoelastic envelope at $\dot{\epsilon} = 0.1$ s^{-1} and $\dot{\epsilon} = 1$ s^{-1} and demonstrates slight strain hardening at $\dot{\epsilon} = 10$ s^{-1} until the point of rupture. In contrast, $(DL\text{-}4)_n$ shows significant strain hardening at all three Hencky strain rates tested,

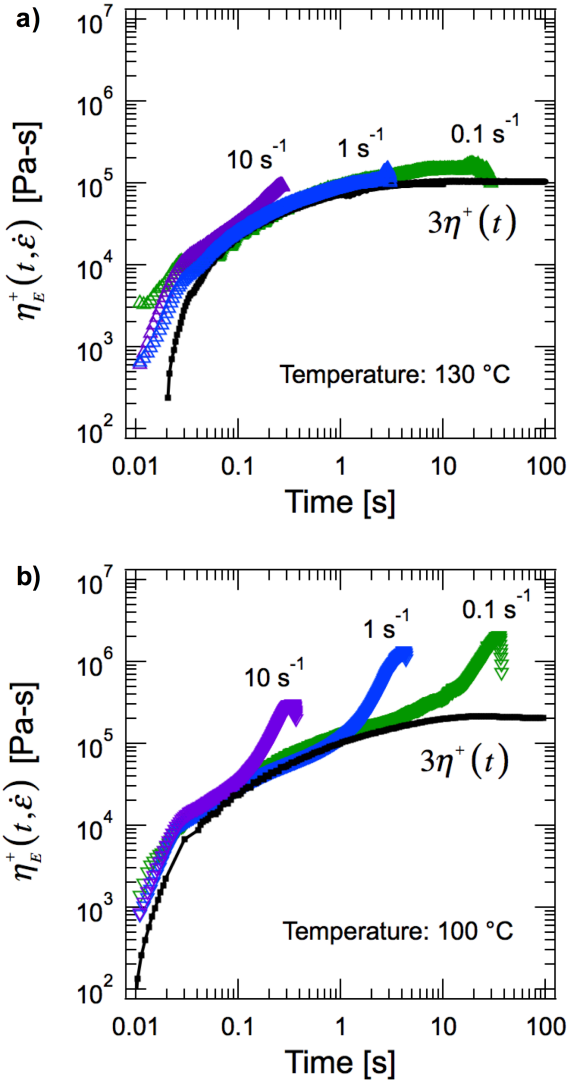

Figure 4.17: Results from uniaxial extension showing transient extensional viscosity for the a) $(DL)_n$ and b) $(DL\text{-}4)_n$ at three different Hencky strain rates. The solid line represents the linear viscoelastic envelope and is three times the start-up of steady shear. The significant extensional hardening for the $(DL\text{-}4)_n$ (not present in $(DL)_n$) is attributed to the branched architecture.

something which cannot be accounted for by the Wi. The possibility is ruled out that this strain hardening comes exclusively from a high molecular weight tail as has previously been observed in bimodal distributions.[192,193] The SEC traces (Figure 4.2) and a detailed look at the highest molecular weight species (Figure 4.4) clearly demonstrate that $(DL)_n$ and $(DL\text{-}4)_n$ have similarly broad distributions with no measurable chains above 10^6 kg mol^{-1}. Rather, the strain hardening of $(DL\text{-}4)_n$ is believe to come from the branched architecture. Some of the possible types of branched architectures resulting from coupling star diblocks are shown in Figure 4.5. Previously, from the SEC-MALS data, it was argued that the high molecular weight species most closely resembles that in Figure 4c, comb polymers with "short" branches. Indeed, structures similar to entangled stars (Figure 4.5a) or entangled "H" pom-poms (Figure 4.5b) are possible, but simple stars are not expected to show strain hardening, while the latter is likely to have formed in negligible concentrations from a statistical standpoint.

The word "short" used here must be qualified. Although these branches (8.3 kg mol^{-1}) are below the estimated value of M_c (9.8 kg mol^{-1}), they are well above M_e (estimated at 4.3 kg mol^{-1}). Model comb polystyrenes with similar "short" side chains in linear and nonlinear shear and extensional flow have been investigated.[194,195] Hepperle et al. reported significant extensional hardening in comb polystyrenes with side chain molecular weights as low as M_e and as few as four grafts per linear chain. Kempf et al. observed the same effect with side chains slightly below M_e of polystyrene, even at Hencky strain rates less than τ_d^{-1}. These previous observations for graft polystyrene are remarkably consistent with these PLA-based materials, allowing one to attribute the considerable extensional hardening of $(DL\text{-}4)_n$ to the high molecular weight species that resemble comb polymers with short side chains.

4.7 Tensile testing

Representative curves from tensile testing for the four polymers are shown in Figure 4.18. LDL is brittle with mechanical properties comparable to poly(D,L-lactide), while DL-4, $(DL)_n$, and $(DL\text{-}4)_n$ are all ductile, showing a clear yield point, necking, and significantly greater toughnesses. Both multiblocks demonstrate strain hardening which can be described as a plastic-to-ductile transition,[131] while DL-4 does not. Average values for key mechanical properties, namely tensile modulus (E), strain at break (ϵ_b), stress at break (σ_b), yield stress (σ_y), and toughness are highlighted in Table 4.3 and are reported as the average and standard deviation of at least five specimens.

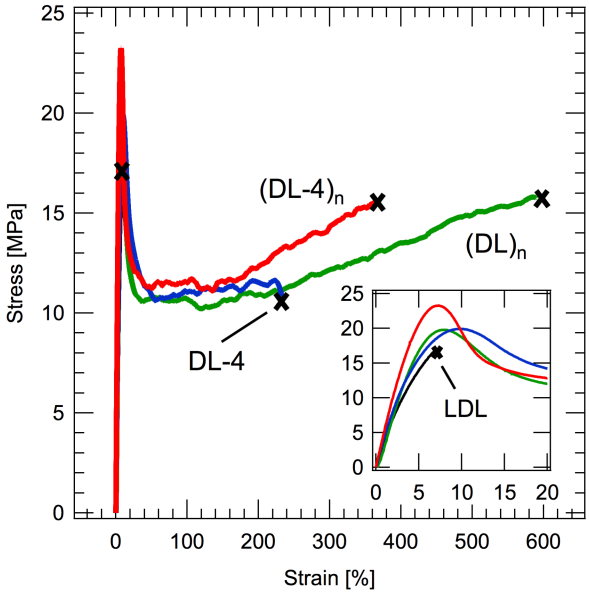

Figure 4.18: Representative curves of tensile testing results of the four polymers. At least five specimens of each polymer were pulled at a rate of 0.1 mm s^{-1} on a RSA rheometer at room temperature. The mechanical properties are summarized in Table 3. The superior toughness of the multiblocks over their parent polymers is attributed to the increased connectivity from the multiblock architecture.

The brittle behavior of LDL is consistent with previous findings for short poly(D,L-lactide-*b*-butadiene-*b*-D,L-lactide) triblocks.[131] The low molecular weight is believed to be a key factor leading to brittleness - reports of higher molecular weight PLA-*b*-rubbery-*b*-PLA triblocks of similar compositions have demonstrated ductile behavior.[196,197] For example, PLA-b-TMC-co–CL-b-PLA triblock polymers (TMC = trimethylene carbonate, ϵ-CL = ϵ-caprolactone, M_n = 20 - 65 kg mol^{-1}, w_{PLA} = 0.80) had elongations at break of 50 - 280% in tensile testing.[196] Also, for a series of LFL triblock polymers (L = poly(L-lactide), F = perfluoropolyether, $M_{n,F}$ = 500 g mol^{-1}), as the polylactide composition increased from 5 to 20 wt.%, the mechanical response transitioned from ductile to brittle; the authors claimed this occurred because the overall molecular weight of the polymer decreased.[198] Thus, it appears that a ductile response of PLA-*b*-rubbery-*b*-PLA triblocks relies on the combined effect of rubber toughening from the midblock with entangled lactide chains that provide additional reinforcement in the bulk phase.

However, the large increase in toughness for $(DL\text{-}4)_n$ over LDL is surprising, given similar block sizes and only slightly different architectures. Enhanced toughness of graft polymers such as $(DL\text{-}4)_n$ typically comes from the increased number of points within a given molecule to transfer stress, and this stress transfer occurs between entanglements in the matrix phase.[132] Yet the molar mass of each L block within DL-4 is only 6.5 kg mol^{-1} (above M_e but below M_c) meaning these segments are only very lightly entangled, if at all.

In general, linear plastic $(AB)_n$ multiblock polymers are tougher than corresponding ABA triblocks with equivalent block sizes[18,131,199] and the toughness increases with a larger number of blocks.[199] This effect is attributed to interior L blocks that can act as bridges connecting neighboring rubbery domains, inhibiting crack propagation that leads to macroscopic failure. The greater the number of total blocks, the more bridging domains there are per polymer chain, leading to greater connectivity and tougher materials. It is observed that $(DL\text{-}4)_n$ and $(DL)_n$ demonstrate tensile behavior consistent with these previous findings. Both have larger strains at break and toughnesses than the parent materials (Figure

4.18, Table 4.3). Additionally, $(DL)_n$ is considerably tougher than $(DL\text{-}4)_n$, as anticipated from the larger <n> and increased connectivity. This effect persists despite having a lower value of <L> than $(DL\text{-}4)_n$, supporting the notion that the interior bridging L blocks play the predominant role in the toughening mechanism. Dangling ends which make up the bulk of the L blocks in $(DL\text{-}4)_n$, seem to have a much smaller effect on toughness.

Table 4.3: Summary of mechanical properties from tensile testing of samples LDL, DL-4, $(DL)_n$, and $(DL\text{-}4)_n$

Sample	E [MPa]	ϵ_b [%]	σ_b [MPa]	σ_{yield} [MPa]	Toughness [MJ m^{-3}]
[a]PLA control	1360 ± 120	8.2 ± 2.8	29.6 ± 11.5	36.3 ± 3.9	2.2 ± 0.8
LDL	428 ± 42	6.3 ± 1.4	16.4 ± 2.0	–	0.65 ± 0.23
$(DL)_n$	345 ± 153	622 ± 165	16.0 ± 2.7	20.2 ± 0.7	81.9 ± 25.5
DL-4	465 ± 42	229 ± 14	7.7 ± 1.8	20.4 ± 1.3	26.4 ± 2.2
$(DL\text{-}4)_n$	360 ± 118	367 ± 43	14.5 ± 1.9	23.0 ± 0.7	50.5 ± 6.0

All measurements represent the average with standard deviations of at least five runs. [a]PLA homopolymer, $M_w \sim 90$ kg mol^{-1}.

The tensile moduli are lower than neat amorphous PLA due to the incorporation of a rubbery component. The decrease in E by a factor of 3 - 4 is quite significant as compared to PLA blends with other common elastomeric materials. For example, blends of 20 wt.% poly(ethylene) or poly(ϵ-caprolactone) in PLLA show a modest 30 - 50% reduction in E over neat PLA.[200,201] However, the observed reduction in E is consistent with blended materials that have molecular weights and thermal properties comparable to the poly(ϵ-decalactone) blocks used in this work. Meng et al. used poly(butyl acrylate) (PBA), a low T_g elastomer, to toughen PLLA and found a 3-fold reduction in E at 15 wt.% PBA.[202] Numerous others have blended oligomeric plasticizers that have decreased E between 30-99%, the extent of which depending on the plasticizer molecular weight and solubility in PLA.[40,203,204]As previously noted, for the $(DL)_n$ and $(DL\text{-}4)_n$ multiblocks, the poly(ϵ-decalactone) blocks are slightly mixed into the PLA matrix, indicating some level of plasticization. It is suspected that this further decreases E as compared to block polymers that are strongly segregated such as the poly(D,L-lactide-*b*-butadiene-*b*-D,L-lactide) system investigated previously.[131]

4.8 Conclusions

A robust and versatile platform has been proposed and investigated to address multiple deficiencies of PLA using a single material with a complex macromolecular architecture. By coupling together star diblocks that have a rubbery core of poly(ϵ-decalactone), it has been unequivocally demonstrated that one can simultaneously modulate the rheological and mechanical responses of PLA to improve its processability and expand its profile of potential applications. The coupling strategy resulted in branched structures similar to comb polymers. Even though the comb side chains were quite short – molecular weights just under M_c – this was sufficient to lead to significant extensional hardening in the homogeneous disordered state. Interestingly, the multiblocks studied are not completely microphase separated and have a broad microphase separation transition regime. This may have led to the marked decrease in the moduli by 3-4×, yet the materials are still over an order of magnitude tougher than neat PLA. These findings suggest that targeting a low but accessible T_{MST} to avoid degradation during processing conditions is an appropriate approach in the design of poly(D,L-lactide)-based multiblock polymers. Future research will focus on optimizing the coupling chemistry to further enhance mechanical and rheological properties while avoiding gelation. The results of this work provide a framework to develop practical sustainable materials with applicability to polymer processes techniques such as blown film extrusion or foaming where extensional rheology plays a critical role.

Chapter 5

Branched Polyesters from Coupling Diols

5.1 Introduction

The previous chapter highlighted a viable route to create branched multiblock polymers. These materials, made from linking star diblocks, exhibited extensional hardening in the disordered melt state while having remarkable tensile toughness. Despite these properties, this approach suffered from one main deficiency – the onset of gelation limited the amount of coupling and the total number of diblock subunits in the final multiblock.

This chapter builds upon these earlier efforts, exploring an alternative and potentially more versatile method to synthesize branched multiblock polymers. Rather than linking four arm stars with difunctional coupling agents, linear diols will be linked with mixtures of di- and tri-functional coupling agents. First, the theory behind this strategy is explored, showing how the extent of coupling and quantity of long-chain branched structures can be predicted. Next, both "short" and "long" PLA diols are coupled with varying amounts

Financial support for this work came from the National Science Center through the Center for Sustainable Polymers at the University of Minnesota, a Center for Chemical Innovation (CHE-1413862).

of "B_2" and "B_3" moieties to gain a fundamental understanding on how various synthetic parameters (e.g. composition of coupling agents, extent of coupling, etc.) effect the final rheological behavior. Neat PLA was chosen for this detailed study to decouple the rheological manifestations of morphology/microphase separation from polymer architecture. Finally, sustainable triblock copolymers amenable to this strategy were synthesized and characterized and shown to be potential candidates as precursors for tunable branched multiblock polymers.

5.2 Theory

As alluded to in the introduction, one of the main deficiencies of coupling A_4 molecules with a substoichiometric amount of B_2 species is that $< n >$, the total number of A_4 subunits in the average resulting polymer, is limited by the onset of gelation. In chapter 4, it was shown experimentally that linking 4-arm star poly(ϵ-decalactone-*b*-D,L-lactide) diblocks with difunctional sebacoyl chloride lead to a multiblock in which $< n > = 2.3$ (when close to the gel point). Relatively simple theory can be utilized to predict the maximum value of $< n >$ for a generic A_f/B_g coupling reaction without the need of experiments. First tackled in 1940s by the legendary Paul Flory,[205–207] the process of predicting molecular weights of nonlinear polymers was simplified by Macosko and Miller in the late 1970s.[208] In this theory, the following assumptions are made:

1. all functional groups of the same type have the same reactivity,
2. all functional groups act independently from one another, and
3. there are no intramolecular interactions.

From these assumptions, it has been shown that the gel point occurs when the following condition holds true:

$$p_A p_B = \frac{1}{(f_e - 1)(g_e - 1)} \tag{5.1}$$

where p_A is the probability that an A type group has reacted, p_B if the probability that a B type group has reacted, f_e is the average functionality of the A_f molecules, and g_e is the average functionality of the B_g molecules. To calculate these parameters, the following relations can be used:

$$a_{fi} = \frac{f_i A_{fi}}{\sum_i f_i A_{fi}} \tag{5.2}$$

$$b_{gj} = \frac{g_j B_{gj}}{\sum_j g_j B_{gj}} \tag{5.3}$$

$$f_e = \sum_i f_i a_{fi} \tag{5.4}$$

$$g_e = \sum_j g_j b_{gj} \tag{5.5}$$

$$p_B = \frac{\sum_i f_i A_{fi}}{\sum_j g_j B_{gj}} p_A = rp \tag{5.6}$$

where a_{fi} is the mole fraction of all A's on A_{fi} molecules, b_{gj} is the mole fraction of all B's on B_{gj} molecules, and r is ratio of total functional groups A to total functional groups B. For the purposes of this chapter, the A molecules are always **polymers** being linked by **small** B molecules.

By definition, $< n >$ is equal to the final polymer molecular weight, $M_{n,f}$, divided by the molecular weight of the starting A polymer, $M_{n,A}$. $M_{n,A}$ is equal to total mass of A, $m_{t,A}$, divided by the initial number of molecules present, A_{fi}. The final $M_{n,f}$ is equal to the final total mass, $m_{t,f}$, divided by the final number of molecules present, N_f. In turn, N_f is equal to the initial number of molecules present, N_0, minus the number of new bonds formed, N_b. For the general case here,

$$N_0 = \sum_i A_{fi} + \sum_j B_{gj} \tag{5.7}$$

$$N_b = p_A \sum_i f_i A_{fi} \tag{5.8}$$

Using these relations, and assuming the mass of the additional B molecules are negligible ($m_{t,A}$=$m_{t,f}$), the equation for $< n >$ reduces to the following:

$$< n >= \frac{\sum_i A_{fi}}{\sum_i A_{fi} + \sum_j B_{gj} - p_A \sum_i f_i A_{fi}} \tag{5.9}$$

With these equations, the maximum value of $< n >$ is calculated for the following basic scenarios in which all the A polymers are identical (same functionality), all B coupling agents are identical (same functionality), and in which A is always in excess:

Table 5.1: Values of $< n >$ for different A_f/B_g coupling reactions

f_e \ g_e	2	3	4	5	6
2	∞	3.0	2.0	1.7	1.5
3	4.0	2.0	1.6	1.4	1.3
4	3.0	1.8	1.5	1.4	1.3
5	2.7	1.7	1.4	1.3	1.3
6	2.5	1.7	1.3	1.3	1.3

.

As listed in Table 5.1, the maximum theoretical value of $< n >$ for the A_4/B_2 reaction employed in chapter 4 is 3.0. Situations in which both f_e and g_e are close to 2, though, would result in higher values of $< n >$.

From these calculations, the most robust strategy appears to be linking A_2 polymers with a *mixture* of B_2 and B_3 coupling agents. A mixture of B_2 and B_3 gives a value of g_e between 2 and 3, meaning $< n >$ should exceed 3.0. This strategy was chosen over coupling a mixture of A_2 and A_3 polymers with B_2 molecules for practical reasons – it is much easier to synthesize a single A_2 polymer than a mixture of A_2 and A_3 polymers. This is especially true if the polymers are block polymers in which a particular morphology is being targeted.

Under the conditions of coupling A_2 polymers with a substoichiometric *mixture* of B_2 and B_3 molecules, the aforementioned equations can be solved to find $< n >$ at the gel point for any given ratio of B_2:B_3 molecules. Defining p as the fraction of B_2 molecules

relative to all B_j molecules, equation 5.9 reduces to the following:

$$< n >= \frac{3-2p}{1-p} \tag{5.10}$$

where $0 \leq p \leq 1$. This equation can be viewed visually in Figure 5.1.

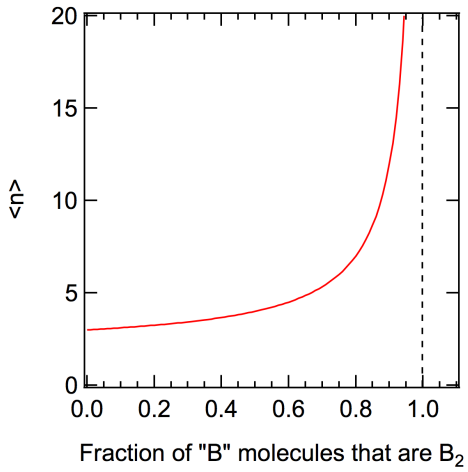

Figure 5.1: Theoretical maximum values of $< n >$ for different A_2/B_g reactions where $2 \leq g \leq 3$.

However, $< n >$ is not the only important parameter – the other goal is to have sufficient long chain branching to lead to extensional hardening. The simplest molecule that typically exhibits long chain branching is an "H" polymer with two branching points; simple star polymers, with only one branch point, generally do not.[67] To calculate the probability that a given molecule in the A_2/B_g reaction has at least two branch points, it is easiest to calculate the probability that this does *not* happen. Here, x is defined as the ratio of moles of B coupling agents to moles of A polymers, and p is defined the same as before. Start with a "B_3" molecule. Each g functional end will be linked to a f functional end from an "A" polymer with an additional free f end group. To not react with another "B_3" molecule, this free f functional end can either react with nothing (probability: $1-x$) or react with a B_2 molecule (probability: px). If it reacts with a B_2 molecule, this cycle continues, creating

this infinite series:

$$(1-x)[1+px+(px)^2+(px)^3+...] = (1-x)[1+\sum_{k=0}^{\infty}(px)^k] = (1-x)[1+\frac{px}{1-px}] = \frac{1-x}{1-px} \tag{5.11}$$

Equation 5.11 captures the probability that a given g functional end of the starting B_3 molecule does *not* link to another B_3 molecule. Equation 5.11 is cubed (because there are three arms), and this expression is subtracted from 1 to obtain the probability that *at least one* g functional end links to another B_3 molecule. Multiplying this expression by the probability of choosing a B_3 molecule to start, $(1-p)x$, gives the final expression for the probability that a given polymer has two branch points, i.e. is an "H" polymer (p_H):

$$p_H = ((1-p)x)\Big[1-(\frac{1-x}{1-px})^3\Big] \tag{5.12}$$

At the gel point, p_H can be solved explicitly and plotted in Figure 5.2. It should be emphasized that this is the *highest* theoretical percentage of branched polymers. In practice, the gel point may not be reached or the coupling efficiency may be $< 100\%$, resulting in a lower percentage of "H" polymers.

5.3 Experimental methods

Reagents

The ϵ-decalactone (99%, Sigma-Aldrich) was distilled under reduced pressure and passed through a column of activated basic alumina (Fisher Scientific) without exposure to air. The β-methyl-δ-valerolactone (MVL) monomer was synthesized and purified in the same manner as reported previously.[209] Tin (II) 2-ethylhexanoate (tin octoate, ~95%, Sigma-Aldrich) was distilled before use. Diphenyl phosphate (DPP, Sigma Aldrich) and 1,4-benzene dimethanol (99%, Alfa Aesar) were dried under reduced pressure and room temperature for 24 h. D,L-lactide (99.5%, Purac) was used as received. Toluene was purified by passage through activated alumina columns (Glass Contour, Laguna Beach, CA). Pyridine (>99%, Acros

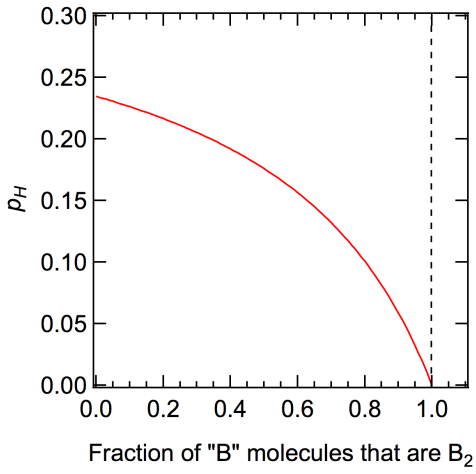

Figure 5.2: Percent of polymers that are "H" polymers for different A_2/B_g reactions at the gel point where $2 \leq g \leq 3$.

Organics) was dried over sodium hydroxide for 2 weeks in a light-free environment. Sebacoyl chloride (99%, Sigma-Aldrich) and trimesoyl chloride (98%, Sigma-Aldrich) were used as received. All the aforementioned reagents were stored and handled in a glove box filled with argon.

Poly(D,L-lactide) synthesis

A 500 mL pressure vessel was dried in an oven at 150 °C for at least 2 h directly before transfer into the glove box. Appropriate amounts of 1,4-benzene dimethanol, D,L-lactide, and catalyst (tin (II) 2-ethylhexanoate) were added to the pressure vessel with approximately a 1:20,000 catalyst:monomer loading. Toluene was then added to make a 40 wt.% solution. The pressure vessel was transferred outside into a silicone oil bath and reacted at 100 °C for several hours. Frequently, the pressure vessel was brought back into the glove box for characterization to see if the target M_n had been achieved. Rather than letting the reaction go close to 100% conversion, the reaction was stopped at roughly 65% conversion to avoid transesterfication and maintain a low dispersity. Once the desired M_n was attained,

the polymer was diluted in dichloromethane and slowly precipitated in cold methanol. The methanol was decanted off and the solids collected and dried.

Triblock synthesis

Poly(D,L-lactide-*b*-ϵ-decalactone-*b*-D,L-lactide) (LDL) triblocks were synthesized in the same manner as described in chapter 4.2.

Poly(D,L-lactide-*b*-β-methyl-δ-valerolactone-*b*-D,L-lactide) (LVL) triblocks were synthesized in the same manner as reported previously.[209] In a glove box with a nitrogen atmosphere, 1,4-benzene dimethanol and MVL monomer were added to a pressure vessel. The vessel was stirred for approximately 15 minutes. When the initiator had fully dissolved, DPP was added and the pressure was capped, then removed from the glove box. After 6 h (observed conversion 90% by NMR), the catalyst was deactivated by the addition of triethyl amine. The polymer was then dissolved in chloroform and precipitated in hexanes (2×). The sample thus obtained was dried under reduced pressure at room temperature to obtain poly(β-methyl-δ-valerolactone) (PMVL).

A portion of the PMVL sample was transferred to a pressure vessel. To the same pressure vessel in a glove box, D,L-lactide was added. Dry toluene was used to dissolve the PMVL, although some residual lactide remained insoluble. To this mixture, tin octoate was added at about a 1:1500 catalyst:monomer molar ratio. The pressure vessel was then capped, removed from the glove box, and stirred in an oil bath at 110 °C for 5 h (observed conversion by NMR 95%). This solution was then cooled, diluted with chloroform, and precipitated in methanol. The precipitate was allowed to settle in a -20 °C freezer overnight, then the methanol was removed by filtration and the solids dried under reduced pressure at room temperature yielding the PLA-PMVL-PLA triblock polymer. A schematic is shown in Figure 5.3.

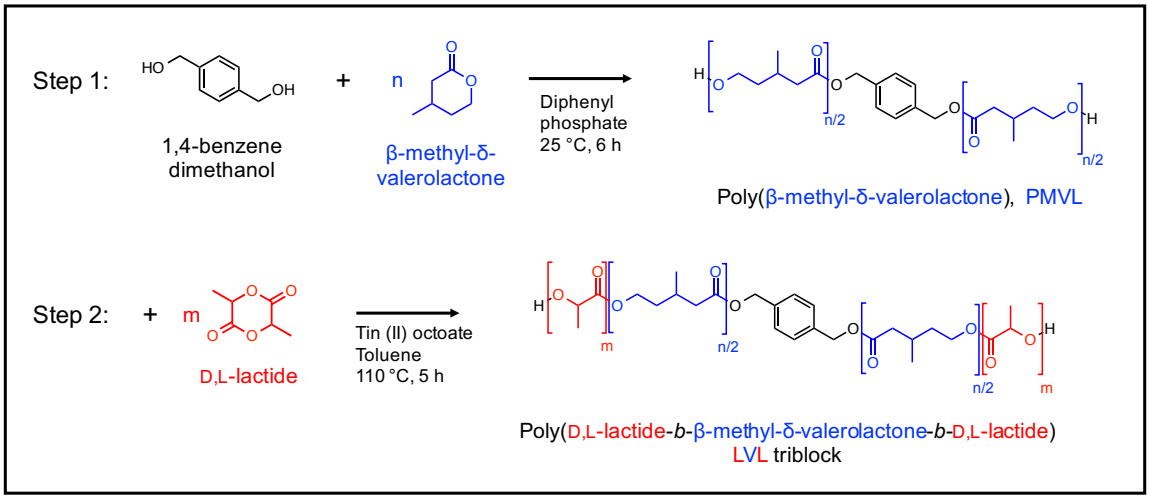

Figure 5.3: Synthetic scheme for the PLA-PMVL-PLA (LVL) triblock copolymer.

Branched polymer synthesis

To remove residual methanol that would interfere with the coupling reaction, samples were freeze dried with benzene. For each sample, a 250 mL pressure vessel was dried in an oven at 150 °C for at least 2 h. About 5 g of freeze-dried polymer were quickly added to the vessel and dried on a vacuum line overnight ($>$ 12 h) to remove residual moisture. While sealed from the atmosphere, the vessels were transferred into a glove box. Toluene was added to make a 30 wt.% solution and allowed to dissolve the polymer for several hours. Roughly 2 mL of pyridine was added to act as a hydrogen chloride acceptor and prevent side reactions. Meanwhile, solutions of pure sebacoyl chloride, pure trimseoyl chloride, or mixtures of both were created.

For samples made from the low molecular weight PLA (PLA-19k), trimesoyl chloride solution was added to the pressure vessel first while stirring. The reaction was allowed to proceed for 1 h. Aliquots were taken for characterization. Sebacoyl chloride solution was then added and allowed to react at room temp for 1 h. Once removed from the glove box, some samples were then allowed to react at 70 °C for 2 h (while sealed), while others were not.

For samples made from the high molecular weight PLA (PLA-52k), solutions that contained both sebacoyl chloride and trimesoyl chloride in the appropriate amounts were titrated into the pressure vessels. At various times, the pressure vessels were taken out of the glove box and allowed to react at 70 °C for 2 h. They were then brought back into the glove box so an aliquot could be taken for SEC. From SEC, the extent of reaction could be monitored. Once samples became difficult to pass through a filter during SEC preparation, the reactions were deemed finished.

Outside of the glove box, a large excess of toluene (not dry) was then added to each sample, and the solutions were stirred at around 50 °C for $\sim$ 1 h to fully dissolve the polymer. The solutions were passed through filter paper (P5 medium porosity, Fisherbrand) to remove salts and precipitated in methanol.

Characterization

^{1}H NMR spectra were obtained with a Varian Inova spectrometer operating at 500 MHz and 25 °C using a 25 s relaxation time and 8 transients. Samples were prepared by dissolving 10 mg of polymer in 0.7 mL $CDCl_3$ (Cambridge Isotope Laboratories, Inc., 99.8 atom % D + 0.05% V/V TMS). End-group analysis was used to calculate the M_n of the linear poly(D,L-lactide), poly(D,L-lactide-*b*-ϵ-decalactone-*b*-D,L-lactide), and poly(D,L-lactide-*b*-β-methyl-δ-valerolactone-*b*-D,L-lactide) diols. δ (ppm) = 5.2 [bm, -C=O-**CH**(CH_3)-O-, PLA], 5.10 [-C_6H_4**CH_2**-O-, BDM], 4.86 [-CH_2**CH**(C_4H_9)-O-, PDL], 4.35 [-C=O-**CH**(CH_3)-OH, PLA end group], 4.15 [-C=O-CH_2CH(CH_3)CH_2**CH_2**-O-, PMVL], 3.65 [-**CH_2**-OH, PMVL end group], 3.60 [-CH_2**CH**(C_4H_9)-OH, PDL end group]. Near quantitative agreement between initiator and end-group peaks was used to verify the functionality of the polyesters prepared as 2.0.

Using established densities of 1.25 g cm^{-3} for amorphous PLA,[160,161] 0.97 g cm^{-3} for poly(ϵ-decalactone),[109] and 1.10 g cm^{-3} for PMVL,[141] the volume fraction of PLA (f_{PLA}) for each polymer was calculated.

To determine M_w, size-exclusion chromatography (SEC) analysis was performed using an Agilent 1260 Infinity LC system equipped with three Waters Styragel columns in series, a Wyatt DAWN Heleos II 18-angle laser light scattering (MALS) detector, and a Wyatt OPTILAB T-rEX refractive index (RI) detector. SEC samples were analyzed at 25 °C in a THF mobile phase at a flow rate of 1.0 mL min^{-1}. For the branched materials, absolute molar mass (M_w) was determined with the MALS detector using $(dn/dc) = 0.0490$ for PLA homopolymer.[210–212]

The dispersity ($Đ$) of each polymer was determined using (SEC) performed on a Thermo Separation Products (TSP) Spectra Systems AS1000 autosampler equipped with three 5 mm Phenomenex Phenogel columns, a Waters 515 pump, and a Waters 2410 differential refractive index detector. Samples were run at room temperature in tetrahydrofuran at a flow rate of 1.0 mL min^{-1}.

Differential Scanning Calorimetry

Thermal properties were explored via differential scanning calorimetry on a Thermal Analysis Q1000. Approximately 5 mg of sample were prepared in hermetically sealed aluminum pans. Materials were heated to 180 °C to erase thermal history, cooled to -100 °C at 10 °C min^{-1}, and heated to 180 °C at 10 °C min^{-1}. Glass transition temperatures are reported upon the second heating curve.

Small Angle X-ray Scattering

Small angle X-ray scattering (SAXS) experiments were conducted at the Advanced Photon Source (APS) in Argonne National Laboratory (Argonne, IL) in sector 5-ID-D. A wavelength of 0.729 Å was used at a detector-to-sample distance of 8.50 m. Samples were prepared in aluminum pans and annealed for 1 h at temperatures above the glass transition of the amorphous poly(lactide) block and approximately 20 °C below the order-disorder transition temperature of the material. This was done to try to ensure the morphologies of

the samples were at equilibrium.

Rheology

Shear rheology was investigated in small amplitude oscillatory shear with an ARES rheometer (TA Instruments) with 8 mm and 25 mm parallel plates. Samples were compression molded at approximately 130 °C. Strain sweeps were conducted a frequency (ω) of 1 s^{-1} to determine the linear viscoelastic (LVE) region. Frequency sweeps were then performed at a strain within the LVE regime. Temperature ramps were conducted at varying ramp rates and frequencies; however, in all cases, the sample was first cooled from a temperature in the disordered state to a temperature in the ordered state at a set temperature ramp rate. Then, the sample was heated at this same temperature ramp rate. The T_{ODT} is reported as the temperature in which a large drop-off in the storage modulus is observed upon heating.

Extensional rheological tests were conducted with the extensional viscosity fixture (EVF) on an ARES-G2 rheometer. The polymers were compression molded at temperatures between 100 °C and 160 °C. Some samples were pressed to form a sheet of thickness ∼0.3 mm. A rectangular punch was then used to prepare samples 25 mm × 5 mm × 0.3 mm for extensional testing. Other samples were prepared from a mold to the final dimensions of 25 mm × 5 mm × 0.5 mm. Each sample was annealed on the EVF at the experimental temperature for 150 s, and the sample was observed with a camera to ensure sagging did not occur. For all rheological tests, experiments were conducted under nitrogen gas in an enclosed oven.

5.4 Branched PLA from a 19k diol

5.4.1 Synthesis

A monodisperse, "low" molecular weight ($Đ$ = 1.06, M_n = 19 kg mol^{-1}) PLA diol was synthesized as described in section 5.3. This same diol was used to produce a series of

branched PLA polymers with different amounts of branching by changing the ratio of "B_3" trimesoyl chloride and "B_2" sebacoyl chloride used. The coupling agents were then added to the PLA diol at this ratio in quantities that would get as close to the gel point as possible. In the nomenclature here, "bPLA" refers to branched poly(lactide), "19k" refers to the molecular weight of the starting diol, and the final number indicates the percentage of "B" molecules that are B_2 (the rest are B_3). The polymers synthesized are listed in Tables 5.2 and 5.3.

As mentioned in the experimental methods section, the B_3 trimesoyl chloride was added to the reaction vessel first. This was to ensure that this reaction proceeded and to understand the necessary reaction conditions. SEC traces were taken after this first step (Figure 5.4a). The presence of a shoulder for all four branched samples indicated that coupling did occur in each case. As anticipated, as the percentage of B_3 increased, the amount of coupling increased as well. Interestingly, samples bPLA-19k-80 and bPLA-19k-50 have shoulders that are quite broad, distinct from what is typically observed when coupling with difunctional molecules. The final SEC traces (Figure 5.4b) reveal other trends worthy of note. Each branched PLA has a small peak corresponding to the original PLA diol. The presence of this peak is a consequence of the substoichiometric coupling necessary to avoid gelation. As the amount of B_2 decreases and B_3 increases, the relative size of this peak increases, corresponding to smaller values of $< n >$ (see Table 5.3) as predicted by the theory outlined in section 5.2.

A summary of the synthesis results are highlighted in Table 5.2, showing the total amount of coupling agent added (in terms of stoichiometric equivalents), the theoretical amount of coupling agent needed to reach the gel point at the given B_2/B_3 ratio, and the efficiency of each step. The efficiency of each reaction was monitored by ^{1}H NMR by noting the actual disappearance of the hydroxyl end group (δ (ppm) = 4.35 [-C=O-**CH**(CH_3)-OH]) relative to the theoretical disappearance assuming that each acid chloride moiety reacts with one hydroxyl end group.

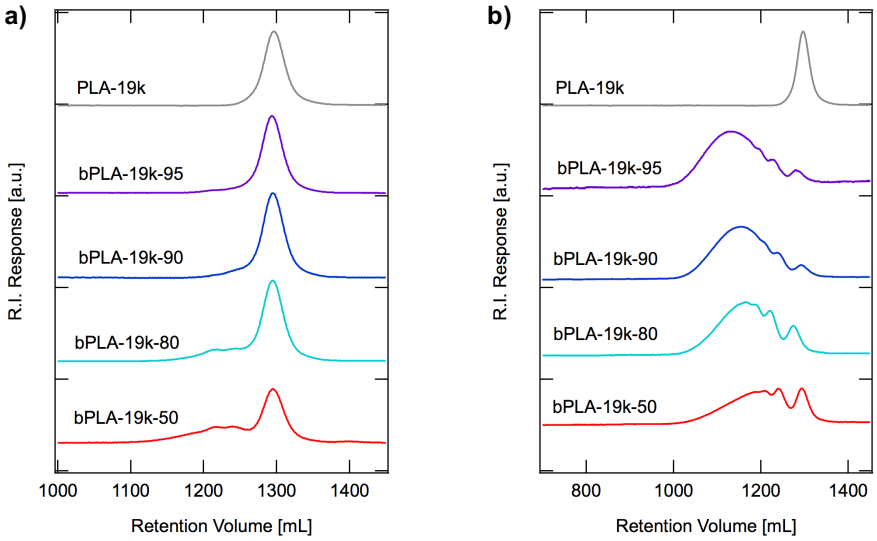

Figure 5.4: SEC traces for PLA-19k and the resulting branched polymers a) after step 1, addition of the B_3 trimesoyl chloride and b) after step 2, addition of the B_2 sebacoyl chloride.

The efficiency for step 1 ranged from 45 - 80%, lower than initially anticipated. This could have occurred because either the reaction had not reached completion, or some of the trimesoyl chloride reacted with impurities (e.g. water). Interestingly, for samples bPLA-19k-90 and bPLA-19k-50, the efficiencies for step 2 were *greater* than 100%. These two samples underwent an extra step in which they were reacted at 70 °C for an additional hour. This gives credence to the speculation that the trimesoyl chloride had not finished reacting in step 1 and continued to react in step 2, after the addition of the sebacoyl chloride. The elevated temperature of 70 °C may have increased the reaction kinetics are contributed to this effect. These observations were initially surprising because it had been qualitatively observed (from the work in chapter 4) that the sebacoyl chloride reached completion within minutes at room temperature; however, there is precedence in the literature that states the aliphatic acid chlorides react faster than homologous aromatic acid chlorides.[213] For these reasons, it is impossible to determine the precise number of B_2 molecules that reacted *versus* B_3 molecules, although the relatively high final efficiencies (69%-96%) demonstrate

the actual ratio of reacted B_2:B_3 is relatively close to that which was targeted.

A couple of final points should be noted regarding the synthesis. A very small amount of gelation ($\approx$ 1 wt.%) was observed for sample bPLA-19k-50 as indicated by residual solids stuck to the side of the pressure vessel. Between sticking to the vessel and the filtration step, though, none of the gel fraction should be in the final characterized polymer. Also, any residual unreacted acid chlorides were likely quenched upon addition of toluene during the pre-filtration step or removed during precipitation.

Table 5.2: Key parameters during the synthesis of branched PLA from a "short" diol

Sample	[a]B_2 %	B:A_2 added	[b]B:A_2, gel point	[c]Step 1 Efficiency	Step 2 Efficiency	Overall Efficiency
bPLA-19k-95	95	0.897	0.909	78.2%	84.6%	84.1%
bPLA-19k-90*	90	0.865	0.833	45.4%	104%	95.7%
bPLA-19k-80	80	0.732	0.714	58.3%	91.4%	69.2%
bPLA-19k-50*	50	0.533	0.500	60.9%	131%	88.9%

[a]Percent of B molecules that are B_2 [b]Theoretical molar ratio of B molecules to A_2 molecules at the gel point at the given percent B_2 [c]Efficiency is calculated by the disappearance of the hydroxyl end group relative to the theoretical maximum *Allowed to react at 70 °C for an additional 1 h in the second reaction step.

5.4.2 Characterization

The full characterization of the final branched PLA polymers based on PLA-19k are highlighted in Table 5.3. The M_n based off linear polystyrene (PS) standards is listed, but because these materials are branched, this is not the most accurate assessment of molecular weight. Rather, M_w determined from SEC-MALS (listed next in the table) is more reliable as it is a direct rather than indirect measurement. In general, as the amount of B_3 used in the synthesis increases, M_w decreases due to the larger presence the starting PLA diol. The exception is between bPLA-19k-80 and bPLA-19k-50, attributed to the much higher coupling reaction efficiency of the latter. Next, the dispersities ($Đ$) are reported as measured by both the RI detector and LS detector. The value of $Đ$ is consistently lower according to the LS detector – this is explained by the inability of the LS detector to accurately measure

the low molecular weight species due to the low (dn/dc), a known instrument limitation.[211] For this reason, the $Đ$ from the RI detector is taken to be more accurate, despite the fact that it is based on PS standards. From these data, the value of M_n is estimated by dividing M_w from LS and by $Đ_{RI}$. The parameter $< n >$ is then calculated by dividing this estimated M_n ($M_{n,est}$) by M_n of the diol as determined from ^{1}H NMR.

Table 5.3: Characterization of the bPLA-19k samples

Sample	[a]B_2 %	[b]$M_{n,PS}$ [kg mol^{-1}]	[c]M_w [kg mol^{-1}]	[b]$Đ_{RI}$	[c]$Đ_{LS}$	[d]$M_{n,est}$ [kg mol^{-1}]	[e]$< n >$	[f]$< n >_{gel}$
PLA-19k	–	28.7	25.7	1.06	1.01	[g]18.7	–	–
bPLA-19k-95	95	114	189	1.98	1.59	95.5	5.1	22
bPLA-19k-90	90	108	156	1.92	1.70	81.2	4.3	12
bPLA-19k-80	80	73.8	120	1.84	1.40	65.2	3.5	7.0
bPLA-19k-50*	50	62.8	128	2.21	1.96	57.9	3.1	4.0

[a]Percent of B molecules that are B_2 [b]Measured with SEC with an RI detector in THF at room temperature. [c]Measured with SEC with a MALS detector in THF at room temperature [d]Estimated by dividing M_w by $Đ_{RI}$ [e]Calculated by dividing $M_{n,est}$ by M_n of PLA-19k [f]Theoretical value of $< n >$ from Equation 5.10 [g]Calculated from ^{1}H NMR based on initiator peaks. *Minor gelation (≈1 wt.%) was observed.

5.4.3 SEC-MALS

In addition to determining M_w, the SEC MALS is able to obtain the radius of gyration (R_g) of the polymer at a given molecular weight. As discussed in section 4.3.2, the branched nature of the material can be assessed by noting how R_g scales with M_w; the more branched a material, the smaller the R_g for a given molecular weight (equation 4.1). The resulting data are shown in Figure 5.5a along with a linear standard. Data for molecular weight species less than 150 kg mol^{-1} are cut off due to significant noise. The data in Figure 5.5a was fit to the following power-law relation:

$$R_g = KM_w^{\alpha} \tag{5.13}$$

where K and α are constants. Since the data are plotted log-log, the slope of the lines shown correspond to α. The value of α for the linear control is 0.59, similar to what has

been reported in the literature.[214] From these fits, the values of g can be calculated using equation 4.1, and the results are shown in Figure 5.5b. Unlike sample $(DL\text{-}4)_n$ in chapter 4, the values of g decrease with increased molecular weight, typical of polymers with long-chain branching like low density polyethylene.[215,216] Sample bPLA-19k-50 has the lowest values of g, indicating the most branching which is attributed to the greater fraction of B_3 used during its synthesis. Samples bPLA-19k-95 and 90 are virtually indistinguishable, probably due to similar percentages of B_2 used during their syntheses; still, both demonstrate low values of g (~0.6) for the highest molecular weight species detected. Interestingly, the value of g is close to unity at M_w around 150 kg mol^{-1} for samples bPLA-19k-95 and 90. This may because most of the lower molecular weight species are linear due to the high amount of B_2 added. Meanwhile, the higher molecular weight species have a very high degree of coupling and, therefore, are more likely to have incorporated a B_3 during synthesis, leading to smaller values of g.

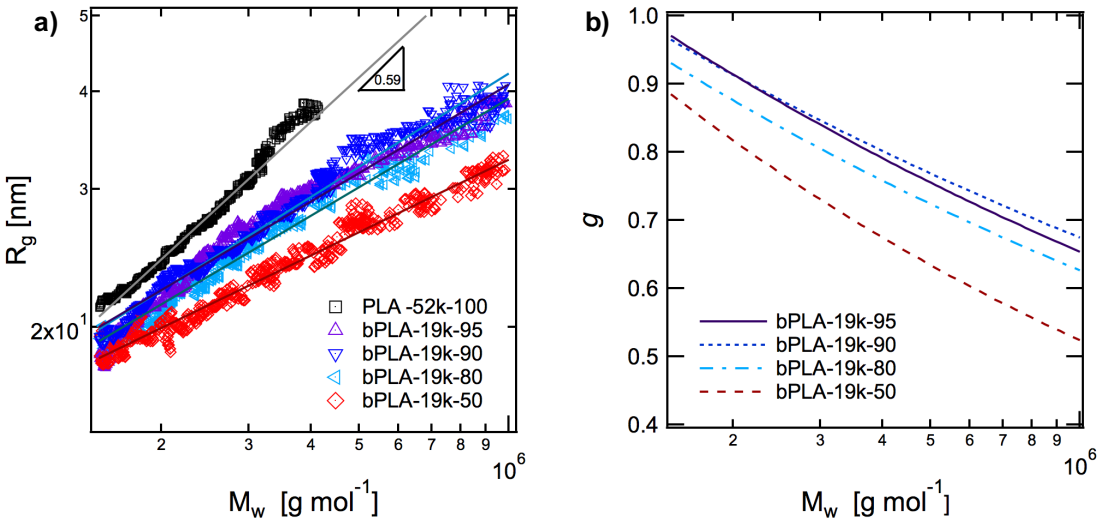

Figure 5.5: a) Radius of gyration (R_g) *versus* molecular weight (M_w) for the branched PLA-19k polymers, along with a linear control, PLA-52k-100. Fits of the data to Equation 5.13 are included. b) The values of g for the samples bPLA-19k-50, 80, 90, and 95 calculated from the fits to 5.13.

5.4.4 Linear rheology

Master curves for the linear dynamic storage (G') and loss (G'') moduli (Figure 5.6) were constructed by employing the principles of time-temperature superposition (tTs). Specifically, oscillatory shear data was taken at various temperatures and the $\tan\delta$ data was shifted horizontally to a reference temperature of 120 °C (Figure 5.7) to obtain the appropriate shift factors (a_T). The shift factors were then used to horizontally shift G' and G'' with no vertical shift. Most of the data look similar, with slightly different values of the crossover frequency (ω_x, defined as G'=G'' before the onset of terminal scaling) due to differences in molecular weights. The longest relaxation time (τ_d) is estimated from ω_x and included on each plot. The one distinct sample is bPLA-19k-50, which has a very broad transition from ω_x to terminal scaling. A similar feature was observed for sample $(DL\text{-}4)_n$ in chapter 4 (Figure 4.14) and has been observed for other branched polymers such as lightly branched butadiene,[184] entangled stars,[179] and bottlebrushes.[185] These subtle features are perhaps more easily seen in the $\tan\delta$ data (Figure 5.7) in which an inflection point is an indication of arm retraction of a branched unit that effectively freezes the backbone in place.[183] Samples bPLA-19k-80 and bPLA-19k-50 show this inflection point while the other two samples do not.

5.4.5 Extensional rheology

Extensional rheological testing was completed at three Hencky strain rates ($\dot{\epsilon}$) for each sample. The $\dot{\epsilon}$ were chosen so that the corresponding Weissenberg numbers (Wi, defined as $\dot{\epsilon}\tau_d$) would be <1, thereby eliminating the deformation rate as a potential origin for any observed strain hardening.[74] The final data are shown in Figure 5.8.

Only sample bPLA-19k-95 does not demonstrate extensional hardening. For samples bPLA-19k-90, 80, and 50, the amount of extensional hardening increases with the amount of B_3 used in the synthesis. This is consistent with Equation 5.12 that predicts a larger proportion of "H" polymers with more B_3 units (on average) in the polymer backbone.

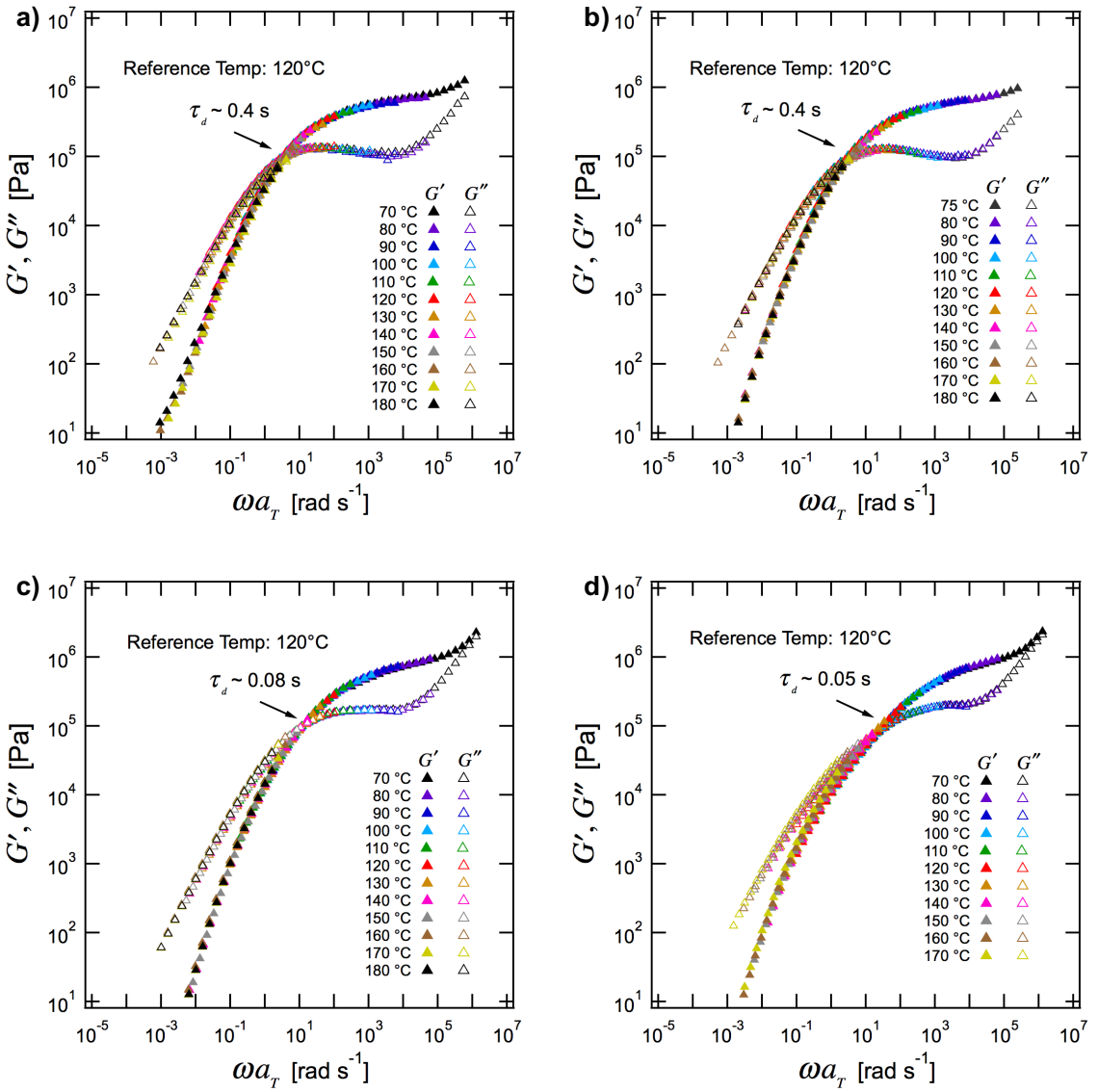

Figure 5.6: Master curves for the linear dynamic storage (G') and loss (G'') moduli of a) bPLA-19k-95 b) bPLA-19k-90 c) bPLA-19k-80 and d) bPLA-19k-50 at a reference temperature of 120 °C. Included are estimates of the longest relaxation time (τ_d) based on ω_x.

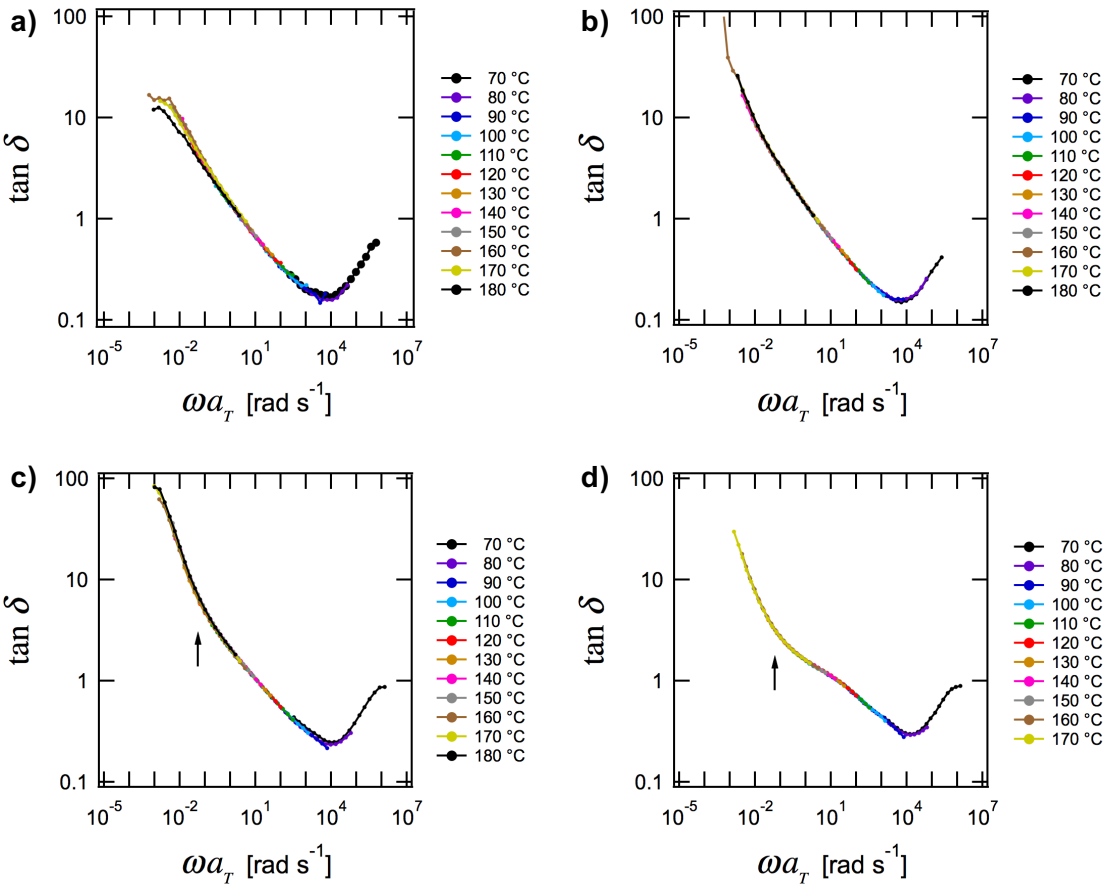

Figure 5.7: Tan δ *versus* reduced frequency (ωa_T) for a) bPLA-19k-95 b) bPLA-19k-90 c) bPLA-19k-80 and d) bPLA-19k-50 at a reference temperature of 120 °C. Arrows designate inflection points characteristic of arm retraction in branched polymers.

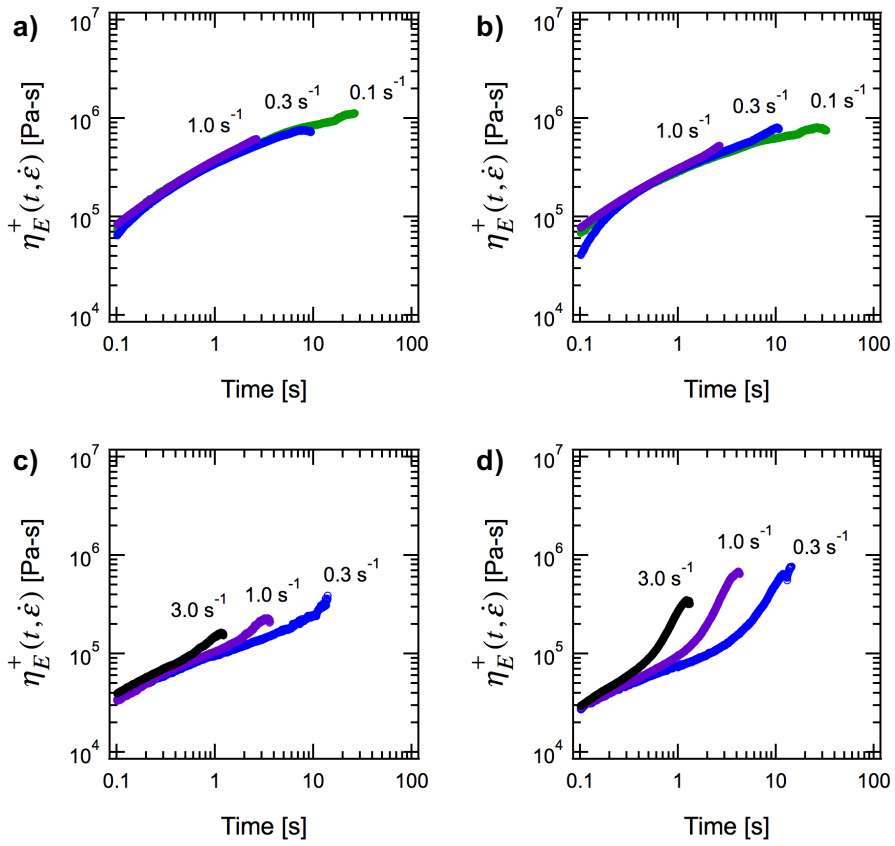

Figure 5.8: Extensional rheology for a) bPLA-19k-95 b) bPLA-19k-90 c) bPLA-19k-80 and d) bPLA-19k-50 at 120 °C. Each sample was pulled at three different Hencky strain rates ($\dot{\epsilon}$) so that Wi=$\dot{\epsilon}\tau_d$<1.

However, as noted in Table 5.4.2, the resulting values of $< n >$ are indirectly proportional to the amount of B_3 used in the synthesis. This trade-off between extensional hardening and $< n >$ is important to keep in mind in the context of multiblock polymers in which high values of $< n >$ are required for toughness.

5.5 Branched PLA from a 52k diol

5.5.1 Motivation

The results of branching PLA from the 19k diol suggest that the coupling A_2 diols with a mixture B_2 and B_3 in substoichiometric quantities is a viable approach to create polymers with both high coupling and long chain branching. For the PLA diol of 19 kg mol^{-1}, the number of entanglements Z per diol can be calculated using the following relation:[112]

$$Z = \frac{M}{M_e^G} \tag{5.14}$$

where M is molecular weight and M_e^G is defined by Equation 3.3. For sample PLA-19k, M_e^G = 3170 g mol^{-1},[120] resulting in Z = 5.9. In order explore the effect of Z, a larger molecular weight PLA diol was synthesized with M_n = 52 kg mol^{-1}, listed in Table 5.4 as "PLA-52k." The corresponding value of Z is 16.5, meaning there are roughly 2.8× as many entanglements per chain.

5.5.2 Synthesis

Attempts were made to synthesize branched polymers from PLA-52k in the same manner as the bPLA-19k polymer series. However, initial trials proved difficult. Adding the designated amount of coupling agents resulted in no coupling, and coupling occurred only after a large stoichiometric excess of coupling agent was added. An example is shown in terms of SEC data (Figure 5.9) for sample bPLA-52k-100, a linear control made by coupling PLA-52k with only B_2 molecules. Aliquots at different points in the reaction are shown relative to

the amount of stoichiometric equivalents of coupling agent added, where one stoichiometric equivalent corresponds to the amount of B_2 needed to make an infinite polymer chain assuming 100% efficiency. The data are normalized to the height of the peak corresponding to PLA-52k.

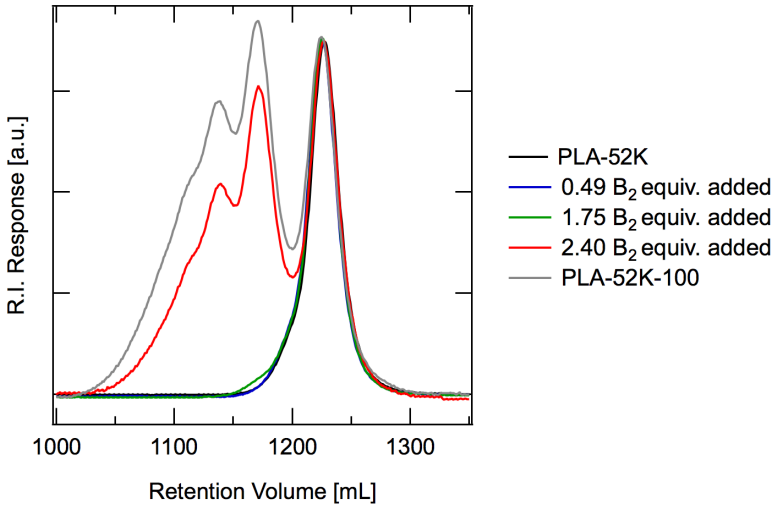

Figure 5.9: SEC traces taken during the synthesis of PLA-52k-100.

At 0.49 stoichiometric equivalents, no change is observed relative to the starting diol. At 1.75 stoichiometric equivalents, a very small shoulder at lower retention volumes is observed. At 2.40 stoichiometric equivalents, there is a dramatic increase in molecular weight. The final polymer was made by slowly titrating more B_2 into the reaction vessel until >4 stoichiometric equivalents were added and all end groups disappeared as deduced from ^{1}H NMR.

This abrupt change from 1.75 to 2.40 stoichiometric equivalents is attributed to the presence of residual water or primary alcohols (e.g. methanol) that should react with the acid chlorides much faster than the PLA end group which is a secondary alcohol.[217] Only after the water and/or primary alcohols have been consumed do the PLA end groups react. This effect is exacerbated with the 52k PLA diol because the concentration of end groups

is so low due to its high molecular weight.

Because of the difficulty in targeting a specific conversion, a different coupling approach was utilized. Instead of adding the B_3 and B_2 species in distinct steps, a master solution of *both* at the desired ratio was created. This solution was subsequently *titrated* into the solution in batches containing ~ 0.5 stoichiometric equivalents until coupling was observed via SEC (here, one stoichiometric equivalent is the theoretical amount of the mixture solution needed to reach the gel point assuming 100% efficiency). Then, batches of $\sim$0.2 stoichiometric equivalents were added, Periodically, the sample would be taken out of the glove box and allowed to react at 70 °C for 2 h to ensure complete conversion. By titrating, the acid chlorides would "kill" the water or primary alcohol impurities before reacting with the PLA end groups. The pre-made mixture helped ensure that the final product contained the correct ratio of B_2 to B_3 molecules.

5.5.3 Characterization

The full characterization of the final branched PLA polymers made from PLA-52k are highlighted in Table 5.4. In this nomenclature, "bPLA" signifies the samples are branched PLA, "52k" designates the molecular weight of the starting diol, and the last number refers to the percentage of B_2 molecules used relative to the total number of "B" molecules. Sample "PLA-52k-100" has no "b" since it serves as a linear control. As with the bPLA-19k series, listed is M_n based on PS standards, M_w as measured from SEC-MALS, dispersities from both RI and LS detectors, an estimated M_n taken by dividing M_w by $Đ_{RI}$, the calculated value of $< n >$, and the theoretical value of $< n >$ at the gel point. SEC traces of the bPLA-52k samples are shown in Figure with relatively high concentrations of the starting PLA-52k diol as evidenced by prominent peaks at higher retention volumes.

Overall, the molecular weights of the bPLA-52k polymers are slightly higher than the bPLA-19k ones; however, the final value of $< n >$ is much smaller. This is due to 1) the higher concentration of water or primary alcohol impurities relative to end group that

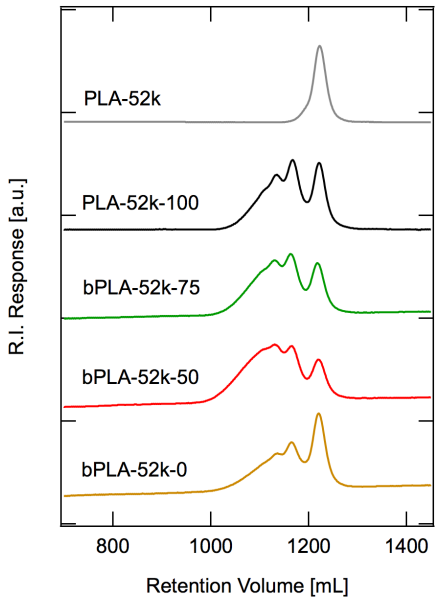

Figure 5.10: SEC traces (RI detector) of the branched polymers synthesized from PLA-52k.

compete with coupling and 2) relatively low amounts of coupling agents added because of difficulties in filtering the samples for SEC analysis. Interestingly, both samples bPLA-52k-75 and bPLA-52k-50 have values of $< n >$ greater than bPLA-52k-100, despite being stopped well before the gel point. Sample bPLA-52k-100, meanwhile, was slowly titrated with B_2 in an attempt to maximize the value of $< n >$. This suggests for high molecular weight diols, adding a small amount of multifunctional coupling agent could be a viable approach to produce multiblocks with higher values of $< n >$ given the practical limitations of these materials.

5.5.4 SEC-MALS

The data from SEC MALS are shown in Figure 5.11 plotting R_g *versus* M_w and the corresponding values of g. As with the bPLA-19k series, the values of g for samples bPLA-52k polymers decrease as the amount of B_3 coupling agent increased. However, overall, the values of g are closer to 1; for instance, at 10^6 kg mol^{-1}, bPLA-52k-50 has a value of

Table 5.4: Characterization of the bPLA-52k samples

Sample	[a]B_2 %	[b]$M_{n,PS}$ [kg mol^{-1}]	[c]M_w [kg mol^{-1}]	[b]$Đ_{RI}$	[c]$Đ_{LS}$	[d]$M_{n,est}$ [kg mol^{-1}]	[e]$< n >$	[f]$< n >_{gel}$
PLA-52k	–	63.9	55.3	1.07	1.01	[g]52.4	–	–
PLA-52k-100	100	128	147	1.55	1.33	94.8	1.8	∞
bPLA-52k-75	75	148	175	1.66	1.42	105	2.0	6
bPLA-52k-50	50	160	216	1.92	1.54	113	2.1	4
bPLA-52k-0	0	106	154	1.69	1.60	91.1	1.7	3

[a]Percent of B molecules that are B_2 [b]Measured with SEC with an RI detector in THF at room temperature. [c]Measured with SEC with a MALS detector in THF at room temperature [d]Estimated by dividing M_w by $Đ_{RI}$ [e]Calculated by dividing $M_{n,est}$ by M_n of PLA-19k [f]Theoretical value of $< n >$ from equation 5.10. [g]Calculated from ^{1}H NMR based on initiator peaks.

g of ≈ 0.8 while for bPLA-19k-50, g ≈ 0.5. This is attributed to the differing molecular weights of the starting diols. At a given molecular weight and $B_2 : B_3$ ratio, a branched polylactide based on a 19 kg mol^{-1} diol has more branched points, on average, than a branched polylactide based on a 52 kg mol^{-1}, resulting in lower values of g.

Somewhat surprisingly, the R_g *versus* M_w curves are nearly identical for samples bPLA-52k-75 and bPLA-52k-50. This could be explained by the differing reactivities of the sebacoyl chloride and trimesoyl chloride, mentioned in Section of 5.4.1. During titration, there will be a particular batch of coupling agent solution added that will consume all the adventitious water or primary alcohol impurities and begin to couple the polylactide. Sebacoyl chloride, being more reactive, may preferentially react with the impurities during this step. This would result in a higher than anticipated concentration of B_3 coupling agents incorporated into the polymer backbone. It is speculated that titrating the coupling agents into the polymer diol solution in a gradual manner would have resulted in a more controlled synthesis.

5.5.5 Linear rheology

Master curves of the linear dynamic storage (G') and loss (G'') moduli and $\tan\delta$ for the bPLA-52K polymers are shown to a reference temperature of 120 °C (Figures 5.12 and

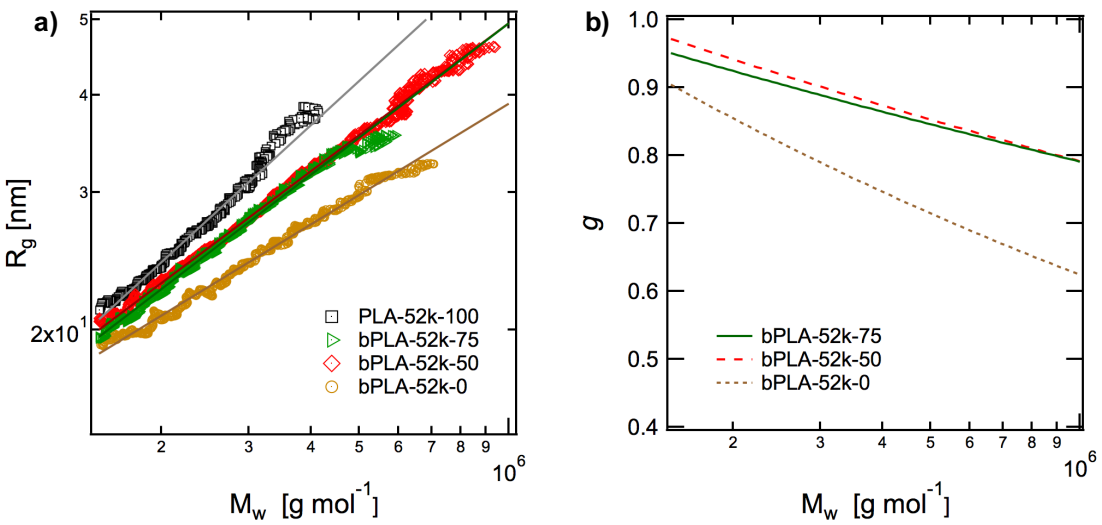

Figure 5.11: a) Radius of gyration (R_g) *versus* molecular weight (M_w) for the bPLA-52k polymers, along with a linear control, PLA-52k-100. Fits of the data to equation 5.13 are included. b) The values of g for the samples bPLA-52k-0, 50, and 75 calculated from the fits to 5.13.

Figure 5.13). Aside for varying longest relaxation times (listed in Figure 5.12), the LVE master curves look nearly identical between the four polymers. Assessing the $\tan\delta$ data in Figure 5.13, an inflection point is only observed for sample bPLA-52k-0 in which only B_3 coupling agent was used. The lack of an inflection point for samples bPLA-52k-50 and 75 is attributed to the low concentration of branch points as known by the low values of $< n >$.

5.5.6 Extensional rheology

As with the bPLA-19k polymers, extensional rheological testing was completed at three Hencky strain rates ($\dot{\epsilon}$) for each sample in which $\dot{\epsilon}$ were chosen so that the corresponding Wi would be <1. The data are shown in Figure 5.14. Somewhat surprisingly, the three branched samples exhibit very little extensional hardening. Even sample bPLA-52k-0, for which *only* B_3 coupling agents were used, has substantially less hardening than sample bPLA-19k-50. From the SEC and SEC-MALS data, it is conclusive that the B_3 and B_2

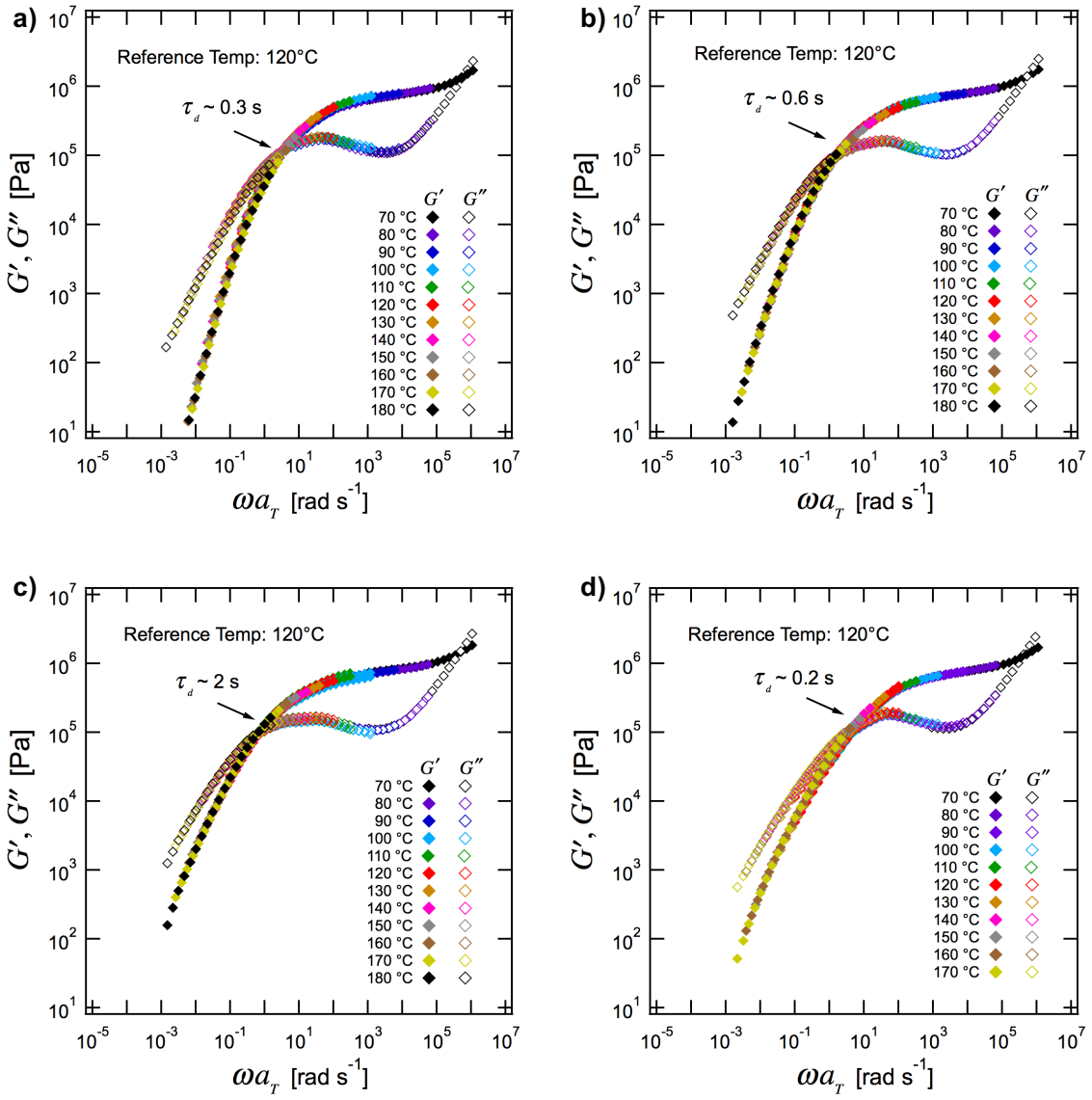

Figure 5.12: Master curves for the linear dynamic storage (G') and loss (G'') moduli of a) bPLA-52k-100 b) bPLA-52k-75 c) bPLA-52k-50 and d) bPLA-52k-0 at a reference temperature of 120 °C.

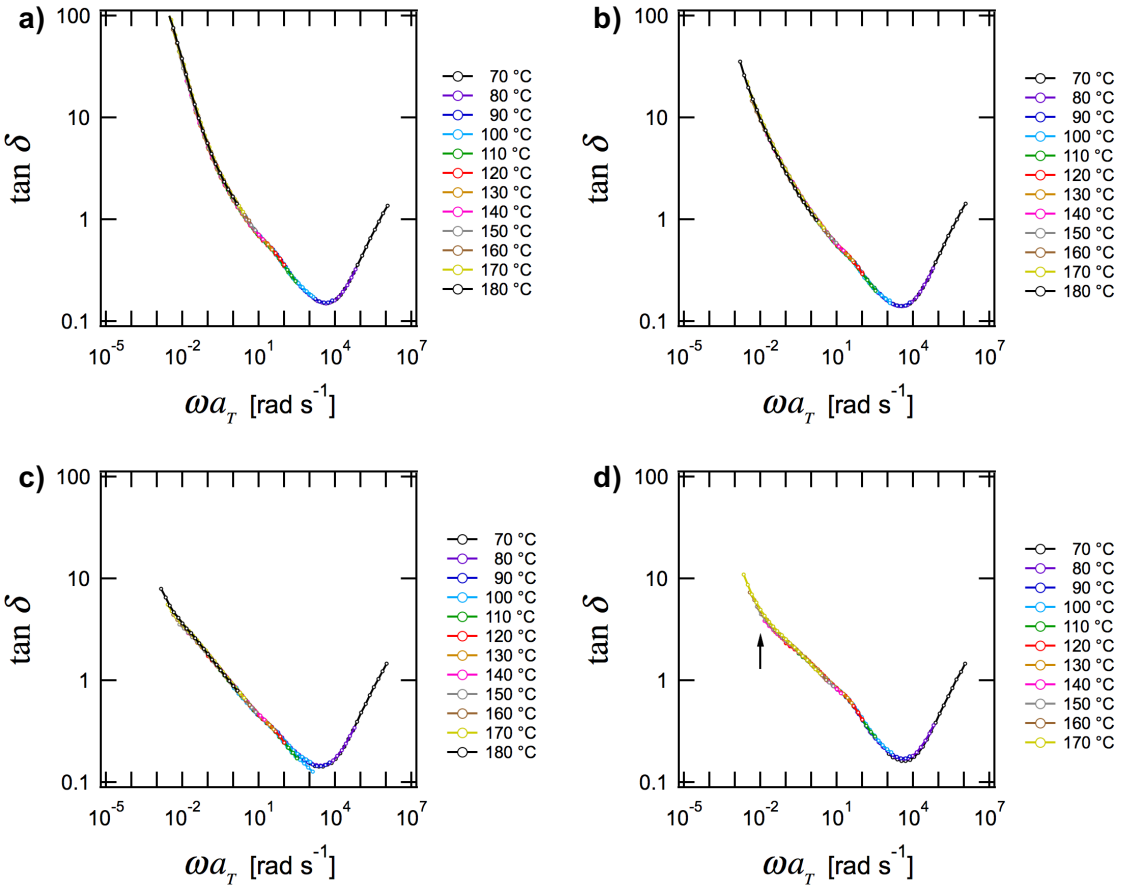

Figure 5.13: Tan δ *versus* reduced frequency (ωa_T) for a) bPLA-52k-100 b) bPLA-52k-75 c) bPLA-52k-50 and d) bPLA-52k-0 at a reference temperature of 120 °C. Arrows designate inflection points characteristic of arm retraction in branched polymers.

coupling agents reacted with the PLA diol to create a branched structure. Thus, the small amount of hardening is attributed to the low values of $< n >$ and low probability of "H" polymers forming. As noted in previous sections, any three-arm star polymers formed would *not* lead to strain hardening. The almost non-existent strain hardening for bPLA-52k-50 and 75 is consistent with the lack of infection points observed in the tan δ data.

These qualitative observations are consistent with the literature for model polystyrene comb polymers. Hepperle et al. observed that it is the *number* of branch points, not the length of branches, that dictates the amount of strain hardening (assuming the branches are entangled).[194] Further work by others support this claim, but only at high Hencky strain rates.[188,195] These authors found that as the number of entanglements per arm increases, the onset of strain hardening shifted to lower $\dot{\epsilon}$, making strain hardening much more prominent in the regime of low $\dot{\epsilon}$. Thus, it appears that the potential additional benefit of longer diols with more entanglements is offset by the difficulty in achieving high coupling efficiencies and a high number of branch points.

5.6 Application to block copolymers: preliminary results

5.6.1 Design of LDL and LVL triblocks

In the previous sections, the appropriate coupling conditions to create branched PLA with the desired rheological behavior have been established. With this knowledge, fully sustainable LDL and LVL triblock copolymers were designed and synthesized. Characterization of the synthesized diols (triblocks and PLA diols) is listed in Table 5.5. The triblocks met the following criteria:

1. Molecular weight comparable to the PLA diols
2. $0.6 \leq f_{PLA} \leq 0.8$
3. Accessible T_{ODT}

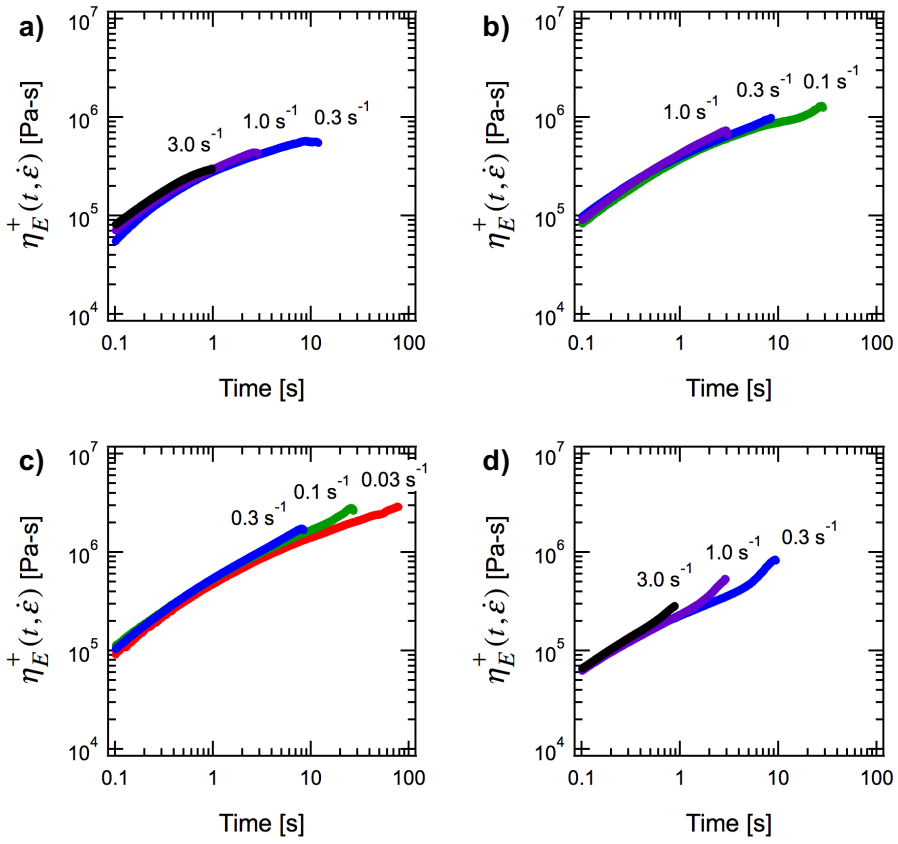

Figure 5.14: Extensional rheology for a) bPLA-52k-100 b) bPLA-52k-75 c) bPLA-52k-50 and d) bPLA-52k-0 at 120 °C. Each sample was pulled at three different Hencky strain rates ($\dot{\epsilon}$) so that $Wi{=}\dot{\epsilon}\tau_d{<}1$.

The molecular weights were similar to that of the PLA diols so that the branched PLA samples could be used as suitable rheological controls for potential branched multiblocks. The polymer composition was chosen judiciously so the resulting multiblock would have desirable mechanical properties. For example, as f_{PLA} decreases, E drops, and eventually the material will become elastic.[107] If the f_{PLA} is too high, the advantages of a multiblock architectures are lost due to morphology.[131] Previous work has shown that the rubbery phases must span at least one dimension (e.g. lamellae or hexagonally packed cylinders) for the multiblock to have very high toughness; when the rubbery domains are discontinuous (e.g. disordered spheres) at high f_{PLA}, the material behaves like a triblock and breaks at relatively low strains. Finally, the T_{ODT} must be accessible to make these materials processable.

Following these design criteria, the polymer compositions and molecular weights for a given block polymer system are somewhat constricted. This was the primary reason why two different midblocks with varying χ interaction parameters with PLA were chosen. At 150 °C, $\chi_{PDL-PLA} = 0.091$, while $\chi_{PMVL-PLA} = 0.029$, meaning PLA-PMVL-PLA triblocks care roughly 3× the molecular weight as PLA-PDL-PLA triblocks at a given T_{ODT}.

5.6.2 Characterization

The full characterization of the LDL triblocks, LVL triblock, and PLA diols is shown in Table 5.5. As desired, the final M_n and $Đ$ of the LDL triblocks are quite similar to that of the PLA-19k diol. The $Đ$ for the LVL triblock is slightly high. It is speculated that the PMVL midblock degraded slightly before subsequent addition of the lactide end blocks – PMVL is known to be especially prone to depolymerization due to its low ceiling temperature.[209] The values of M_e^G for PDL and PMVL are similar to PLA (PDL = 5.9 kg mol^{-1} [section 3.4], PMVL = 4.3 kg mol^{-1},[218] and PLA = 4.0 g mol^{-1}.[181]), meaning the final value of Z for the triblocks should be similar to their corresponding PLA diols. Slight depression of the T_g of the lactide blocks for the LDL triblocks is attributed to the low molecular weight

of the lactide blocks and be accounted for by equation 3.4.

Table 5.5: Characterization of the LDL and LVL triblocks

Sample	[a] M_n [kg mol^{-1}]	[b] f_{PLA}	[c] $Đ$	[d] $T_{g,L}$ [°C]	[d] $T_{g,D/V}$[°C]	[e] T_{ODT} [°C]
PLA-19k	18.7	–	1.06	49	–	–
LDL-20k-75	20.4	0.75	1.06	42	-45	114
LDL-20k-76	19.7	0.76	1.11	41	-44	97
LDL-20k-78	20.3	0.78	1.09	44	-42	96
PLA-52k	52.4	–	1.06	52	–	–
[f]LVL-50k-73	50.3	0.73	1.17	49	-47	126

[a]Calculated from ^{1}H NMR based on initiator peaks. [b]Calculated from ^{1}H NMR using published densities of PLA, PDL, and PMVL. [c]Calculated with SEC with an RI detector in THF at room temperature. [d]Determined using DSC during the second heating cycle. [e]Determined from isochronal temperature ramps. [f]Synthesized by Debbie Schneiderman

5.6.3 Linear rheology: T_{ODT}

Each of the four triblocks synthesized have an accessible T_{ODT}'s that are easily visible from isochronal temperature ramps. The T_{ODT}'s range from 95 °C to 130 °C, well below degradation temperature but sufficiently above the T_g of the lactide blocks, allowing equilibrium morphologies to form on experimentally accessible time scales.

5.6.4 Morphology

The morphology of the triblocks was probed via SAXS, the patterns of which shown in Figure 5.16. All three LDL triblocks have very similar values for q^*, indicating similar domain spacings, with well-defined higher-order peaks whose locations ($q/q^* = \sqrt{3}, \sqrt{7}, \sqrt{9}, \ldots$) are consistent with hexagonally packed cylinders (HEX). Alternatively, the primary peak of LVL triblock has two bumps and the pattern has no clear higher order reflection peaks. This may be due to the very high molecular weight that slows the kinetics of ordering, or the slightly elevated dispersity ($Đ$=1.17). It is believed that the material is microphase separated, though, by the relative sharpness of the primary peak, the existence of two distinct

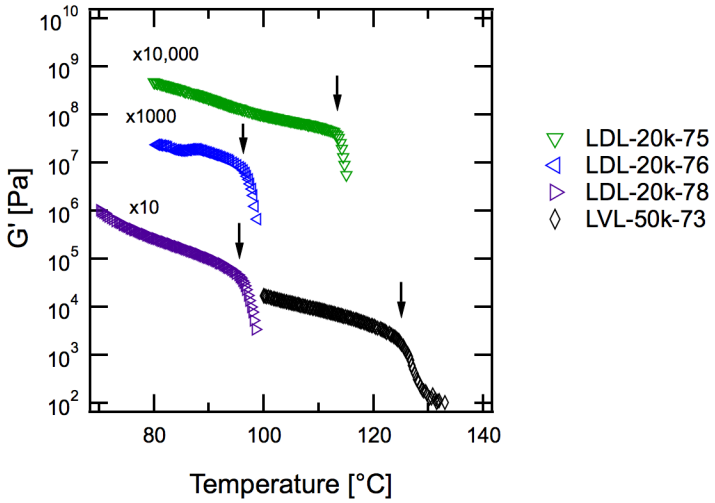

Figure 5.15: Isochronal temperature ramps of select triblock copolymers. The T_{ODT} is identified by the large drop-off in the storage modulus upon heating.

T_g's (Table 5.5), and a clear T_{ODT} (Figure 5.15).

5.7 Conclusions and future work

This chapter examines a method to synthesize branched polyesters by coupling diols. Theoretical calculations demonstrate the linking A_2 polymers with a mixture of B_2 and B_3 coupling agents provides the most attractive route to create materials with high coupling with suitable long chain branching. To this end, PLA diols of two different molecular weights (19 kg mol^{-1} and 52 kg mol^{-1}) were coupled with acid chlorides with varying ratios of di- and tri-functional moieties. From SEC-MALS, it was determined that the synthesized polymers achieved high molecular weights with values of R_g that were smaller than a linear analog, indicating branching. Due to impurities, the coupling efficiencies for the longer diols was much lower than for the short diols. This proved to be the most important factor in dictating the amount of extensional hardening. Although both the number of entanglements per branch and the number of branched points are known to influence extensional

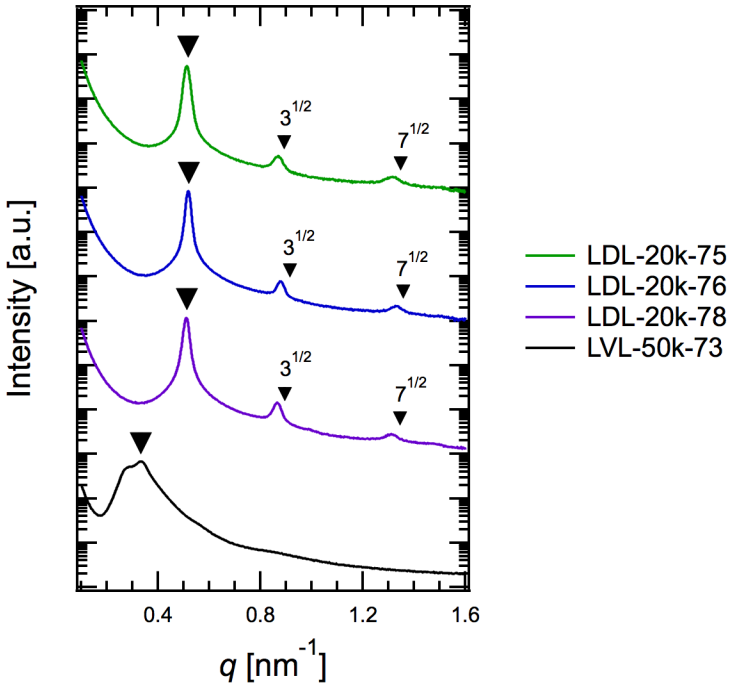

Figure 5.16: Azimuthally integrated small angle X-ray scattering patterns of select triblock copolymers. Primary peaks are designated with a large triangle. Higher order reflection peaks corresponding to a HEX morphology are shown by small triangles.

hardening, because the concentration of branch points is low in these samples, the latter appears to be the dominating effect for this particular system. Finally, triblock analogs to the PLA diols were synthesized with comparable M_n's and accessible T_{ODT}'s. Future work should focus on adopting this coupling strategy for the triblocks to create branched multiblocks. The resulting morphology and its effect on the kinetics of ordering could be of particular interest for these materials. Additionally, one could examine the effect of microphase separation on strain hardening by looking at the extensional rheological response in the ordered melt state.

Chapter 6

Pressure-Sensitive Adhesives Based on a Poly(lactide-*b*-β-methyl-δ-valerolactone-*b*-lactide) Triblock Copolymer

6.1 Introduction

Pressure sensitive adhesives (PSAs) are an important class of materials that can stick to almost any surface under light pressure. They can be found in a range of applications including tapes, labels, and materials for skin contact. PSAs are required to easily deform and quickly form a physical bond upon application onto the substrate of interest; however,

Portions of this work was done in collaboration with Dr. Tessie R. Panthani and McKenzie Coughlin and have been published previously.[219] Financial support for this work came from the National Science Center through the Center for Sustainable Polymers at the University of Minnesota, a Center for Chemical Innovation (CHE-1413862).

they simultaneously must display solid-like behavior and resist deformation once adhered. The three main classes of PSAs are based on natural rubber, poly(acrylates), and styrenic block copolymers.[220] The latter is usually mixed with a tackifying agent and is often used due to the ability to finely control physical properties while remaining inexpensive.[221]

The most basic and common architecture for these styrenic block polymers is an ABA triblock copolymer. The "A" poly(styrene) blocks constitute the minority component with a high T_g (well above use temperature) while the "B" blocks make up the rubbery majority component with a low T_g (well below use temperature). The blocks microphase separate due to chemical incompatibility to form distinct hard "A" domains and soft "B" domains, creating a thermoplastic elastomer with mechanical properties of vulcanized rubber yet thermally processable. In order for these triblocks to possess properties required of a PSA, they are often blended with a high T_g tackifier at 30-70 wt.%. This tackifier selectively swells the rubbery midblock and serves two purposes: 1) lowers the elastic modulus and 2) raises the T_g. This softens the material, allowing it to flow upon pressure, while helping provide cohesive strength at high pull-off speeds.

Here, a fully sustainable PSA has been created using the ABA triblock paradigm, using recent literature as inspiration.[15,222,223] Rather than being petroleum-derived like conventional styrenic block polymers, all the materials here are made from renewable sources and are degradable. The base component is a high molecular weight poly((lactide-*b*-β-methyl-δ-valerolactone-*b*-lactide) (LVL) triblock copolymer that possess comparable mechanical properties to styrenic block polymers. The poly(β-methyl-δ-valerolactone) (PMVL) midblock is a promising, low T_g renewable polymer made from a precursor which can be produced by a scalable and economical fermentation process.[141] The PSAs described here are formulated with a rosin ester tackifier, a renewable component made by isolating the non-volatile component of pine tree resin.[224] In addition to being renewable, a further benefit of utilizing rosin ester is that they have demonstrated biocompatibility comparable to PLA,

making the formulated PSAs promising candidates for adhesives used in biomedical applications.[225] This chapter first describes the synthesis and characterization of the triblock copolymer. Blends of the triblock and tackifier were formulated and the miscibility of the components and resulting morphology were characterized. Oscillatory shear, shear creep, and uniaxial extensional experiments were performed to characterize the linear and nonlinear viscoelastic properties of the triblock copolymers and formulated PSAs. These results are compared to standard tests utilized in adhesive testing including probe tack, 180° peel, and shear resistance tests. Finally, a discussion of the possible applications of the PSAs are outlined.

6.2 Experimental methods

6.2.1 Synthesis and characterization

Synthesis of β-methyl-δ-valerolactone from 1,5-pentanediol

Synthesis of β-methyl-δ-valerolactone monomer from a sustainable route involves a multistep process which includes using an engineering E. coli capable of producing mevalonate at high titer, collecting the fermentation broth, refluxing the broth with concentrated sulfuric acid at high temperature to produce anhydromevalonatelactone, solvent extracting the product (anhydromevalonatelactone), catalytically hydrogenating anhydromevalonatelactone, and isolating the product by distillation.[141] This process is laborious and tedious, at least on the bench scale. Thus, an alternative route to MVL synthesis was employed.[226] To this end, one liter of 3-methyl-1,5-pentanediol was added to a 3 liter round bottom flask with a 10 wt.% loading of copper chromite (catalyst). A heating mantle was utilized to heat the flask to about 200 °C and the reaction mixture was refluxed overnight while stirring. The flask was allowed to cool to ambient temperature and the MVL product was recovered by distillation.

Synthesis of the poly(D,L-lactide-*b*-β-methyl-δ-valerolactone*b*-D,L-lactide) (LVL) triblock copolymer

The poly(D,L-lactide-*b*-β-methyl-δ-valerolactone-*b*-D,L-lactide) (LVL) triblock copolymer was synthesized by a two step process similar to that employed in section 5.3. First, a dried pressure flask equipped with a stir bar was brought inside a dry box. MVL (monomer), 1,4-benzene dimethanol (BDM, initiator), and triazobicyclodecene (catalyst) were added to the flask. The flask was capped and the contents of the flask were stirred at room temperature inside the dry box. After 30 minutes, the flask was removed from the glove box and excess 2M hydrochloric acid in diethyl ether was added to quench the reaction. Chloroform was added to reduce the viscosity of the polymer and the contents of the flask were precipitated in cold methanol. The sample was recovered by decanting the methanol and the resulting PMVL polymer was dried under vacuum until reaching baseline. The dihydroxy-terminated PMVL polymer was utilized as the macroinitiator for the ring-opening polymerization of D,L-lactide to synthesize the LVL triblock copolymer. PMVL and a stir bar were added to a pressure flask and the contents of the flask were dried under dynamic vacuum overnight. The flask was brought into the dry box and D,L-lactide, tin(II) octoate (0.01 wt.% relative to monomer), and toluene were added. The flask was removed from the dry box and placed in an oil bath heated to 70 °C. After 30 minutes, the temperature of the oil bath was increased to 105 °C. After 2.5 hours, the reaction was quenched by placing the flask in ice water followed by precipitating in cold methanol. The methanol was decanted and the recovered polymer was dried under dynamic vacuum for several days until the vacuum line reached baseline pressure.

Triblock/tackifier blend preparation

Blends of LVL triblock copolymer and rosin ester tackifier (SYLVALITE^{TM} RE 10L, Arizona Chemical) were formulated by co-dissolving the two components in dichloromethane to make an approximately 10 wt.% solution in a sample jar. The solutions were left uncapped in a

fume hood overnight to remove the solvent. The sample jars were placed under dynamic vacuum for approximately two days in order to remove the remaining residual solvent.

Nuclear Magnetic Resonance (NMR)

^{1}H NMR spectra were obtained with a Varian Inova spectrometer operating at 500 MHz and 25 °C using a 25 s relaxation time and 8 transients. Samples were prepared by dissolving 10 mg of polymer in 0.7 mL $CDCl_3$ (Cambridge Isotope Laboratories, Inc., 99.8 atom % D + 0.05% V/V TMS). The M_n of PMVL was determined based off of the ratio of initiator peaks to those in the polymer backbone with near quantitative agreement with the end group: δ (ppm) = 7.34 [-$\mathbf{C_6H_4}$-, BDM], 4.15 [-C=O-CH_2CH(CH_3)$CH_2$$\mathbf{CH_2}$-O-, PMVL backbone], 3.65 [-C=O-CH_2CH(CH_3)$CH_2$$\mathbf{CH_2}$OH, PMVL end group]. The M_n of the LVL triblock was determined by the ratio of PLA backbone peaks to PMVL backbone peaks with knowledge of the PMVL molecular weight: δ (ppm) = 5.2 [-C=O-$\mathbf{CH}$(CH_3)-O-, PLA backbone]. Using published densities of 1.25 g cm^{-3} for amorphous PLA[160,161] and 1.10 g cm^{-3} for PMVL,[141] the volume fraction of PLA (f_{PLA}) was calculated.

Size-exclusion chromatography (SEC)

Size-exclusion chromatography (SEC) analysis was performed using an Agilent 1260 Infinity LC system equipped with three Waters Styragel columns in series, a Wyatt DAWN Heleos II 18-angle laser light scattering (MALS) detector, and a Wyatt OPTILAB T-rEX refractive index (RI) detector. SEC samples were analyzed at 25 °C in a THF mobile phase at a flow rate of 1.0 mL min^{-1}. Absolute molar mass (M_w) was determined with the MALS detector using dn/dc as measured by the instrument assuming 100% mass elution.

Differential Scanning Calorimetry

Thermal properties were explored via differential scanning calorimetry on a Thermal Analysis Q1000. Approximately 5 mg of sample were prepared in hermetically sealed aluminum

pans. Materials were heated to 180 °C to erase thermal history, cooled to -100 °C at 10 °C min^{-1}, and heated to 180 °C at 10 °C min^{-1}. Glass transition temperatures are reported upon the second heating curve.

Small Angle X-ray Scattering

Small angle X-ray scattering (SAXS) experiments were conducted at the Advanced Photon Source (APS) in Argonne National Laboratory (Argonne, IL) in sector 5-ID-D. A wavelength of 0.729 Å was used at a detector-to-sample distance of 8.50 m. Samples were prepared in aluminum pans and annealed for 3 h at 110 °C. The data were azimuthally integrated and are presented as intensity (I) versus scattering wave vector q, where $q = (4\pi/\lambda)\sin(\theta/2)$ and θ is the scattering angle.

6.2.2 Rheology

Linear viscoelasticity: oscillatory shear

Shear rheology was investigated in small amplitude oscillatory shear (SAOS) on an ARES rheometer (TA Instruments) with 8 mm parallel plates. Samples were molded on the rheometer at temperatures above the T_g of the blocks (>60 °C) but below 180 °C to avoid degradation. Strain sweeps were conducted at a frequency (ω) of 1 s^{-1} to determine the linear viscoelastic (LVE) region. Frequency sweeps were then performed at a strain within the LVE regime.

Shear creep

Shear creep experiments were conducted on a DHR-3 rheometer (TA Instruments) with a cone and plate geometry (diameter = 8 mm, cone angle = 5.73° truncation gap = 0.044 mm). Temperature was maintained at 25 °C using a Peltier Plate. Samples were molded on the rheometer and allowed to rest until the normal force stabilized before testing. Creep compliance was measured for one hour at low stresses to measure the linear viscoelastic

response, and directly after, the recovery compliance was measured for one hour. Once the linear viscoelastic response was determined, the creep compliance was measured for one hour at 30 kPa to correlate to shear resistance experiments. Though the stresses of 30 kPa were found to be in the non-linear regime for all the samples, no edge fracture was observed.

Uniaxial extension

Uniaxial elongation measurements were made using a ARES G2 rheometer (TA instruments) equipped with an extensional viscosity fixture (EVF). Samples were compression molded between layers of teflon. The samples were pressed between 60 and 90 °C. The temperature was varied in order to obtain approximately the same film thickness for all samples. Samples were made with a metal rectangular punch and resulted in specimens with dimensions of 5 mm × 25 mm × 0.3 mm. Samples were cooled using dry ice in order to minimize stretching when removing each specimen. Measurements were conducted at room temperature at a rate of 1 s^{-1}.

6.2.3 Adhesion testing

Sample preparation: wire coating

Samples for adhesion testing were prepared by solution coating. First, 100 milligrams of sample were dissolved in 0.5 milliliters of chloroform. The solution was cast on a flexible PET sheet (0.002 inch thickness) with a wire wound rod. Both the wire wound rod and PET substrate were washed with acetone and dried with compressed air prior to casting the solution. This resulted in a film with thickness on the order of 10 μm. The films were dried overnight at ambient conditions prior to testing.

Probe Tack

Probe tack measurements were performed using a DHR-3 rheometer, and the procedure was adopted from ASTM D2979. Samples were attached to the bottom plate using double

sided tape. Probe tack measurements were conducted using a stainless steel (diameter = 5 mm, root mean square (rms) roughness = 0.42 μm) cylindrical probe. A Tencor P-10 Profilometer (University of Minnesota Characterization Facility) was used to measure the surface roughness. The probe approached the sample at a rate of 0.003 mm s^{-1} until the pressure reached 1 MPa after which the probe dwelled for one second. The probe was pulled off of the substrate at a rate of 0.5 mm s^{-1} and the force was recorded as a function of the probe displacement distance.

180° Peel

The experimental procedure was adopted from the Pressure Sensitive Tape Council (PSTC) 101 Peel Adhesion test method. Samples for peel tests were prepared by the same wire wound rod coating procedure described previously. For each test, a 1 inch wide strip was cut and adhered to a polished stainless steel substrate (ChemInstruments, Fairfield, OH) using a 1 kg roller. Samples with noticeable air bubbles were discarded. Peel force measurements were performed on a Shimadzu Autograph AGSS17 X Series 115 tensile tester (Columbia, MD). The stainless steel substrate was held by the top grip while the unadhered end of the PET strip was held in the bottom grip (see Figure 6.1). All samples were pulled at a velocity of 5 mm s^{-1}. Average values of the peak force normalized by the width are reported for at least five specimens for each sample.

Shear resistance

The experimental procedure was adopted from the Pressure Sensitive Tape Council (PSTC) 107 Shear Adhesion test method. The PET film was cut into strips with a width of 0.5 inches and a length of approximately 6 inches. The adhesive was placed on a polished stainless steel and rolled on with a 500 gram roller. The adhesive was placed on the plate such that it formed a 0.5 inch by 0.5 inch contact area. Double-sided tape was applied to the uncoated length of the PET film and rolled up and a binder clip was attached to the

Figure 6.1: Set-up for the 180° peel test.

film (see Figure 6.2). The aluminum plate was suspended using clamps and a level was used to ensure the plate was parallel to the ground. 500 gram weights were hung on the binder clips using copper wire. A motion sensitive camera was placed in proximity to the set-up in order to record the falling of any adhesives. The time it took for the PET films to pull away from the aluminum substrate was recorded. Three samples were tested for each adhesive.

6.3 Characterization

6.3.1 Summary of samples

A summary of the molecular characterization of the PMVL homopolymer and final LVL triblock copolymer utilized in the PSA formulations is given in Table 6.1. Molecular weight (M_n) was estimated by two methods: ^{1}H NMR analysis and SEC with a multi-angle light scattering (MALS) detector. Determination of M_n with ^{1}H NMR analysis was determined by using the benzylic methylene protons as an internal standard. The discrepancy in the

Figure 6.2: Set-up for the shear resistance test.

measured M_n of PMVL by ^{1}H NMR and SEC is likely due to the inherent inaccuracy of ^{1}H NMR for polymers of high molecular weight. ^{1}H NMR analysis was also used to determine the volume fraction of PLA in the LVL triblock copolymer (f_{PLA}) of 0.23.

SEC provides further evidence of the successful growth of the PLA block as evidence by the shift of LVL SEC trace to lower retention times relative to the starting PMVL homopolymer (Figure 6.3). Interestingly, the estimated M_n by SEC of the PMVL homopolymer is greater than that of the LVL triblock copolymer. This is likely due to some a small amount of depolymerization of the PMVL polymer during the polymerization of the PLA block.

6.3.2 Miscibility of tackifier and triblock copolymer

PSAs with modulated rheological properties were formulated by blending the LVL triblock copolymers with the rosin ester tackifier. Five blends were made, each containing between 30 wt.% and 70 wt.% rosin tackifier. The miscibility of the rosin tackifier with the

Table 6.1: Characterization of the PMVL midblock and LVL triblock

Sample	M_n (NMR) [kg mol^{-1}]	[d] M_n (SEC) [kg mol^{-1}]	[e] f_{PLA}	[f] Đ	[g] $T_{g,L}$ [°C]	[g] $T_{g,V}$ [°C]
PMVL[a]	[b]102	137.8	–	1.02	-50	–
LVL	[c]130	105.8	0.23	1.12	-50	50

[a]Synthesized by Debbie Schneiderman. [b]Calculated from ^{1}H NMR based on initiator peaks. [c]Calculated from ^{1}H NMR based on the M_n of PMVL and polymer composition. [d]Determined from SEC with a multi-angle light scattering (MALS) detector in THF at room temperature. [e]Volume fraction of PLA in sample, determined from ^{1}H NMR. [f]Dispersity from SEC. [g]Determined using DSC during the second heating cycle.

poly(β-methyl-δ-valerolactone) midblock was determined by DSC. Compatibility between the midblock and tackifier has been shown to be necessary to improve adhesive properties in block copolymer-based PSAs.[227] Figure 6.4 shows the second heating traces taken at a rate of 10 °C min^{-1} for the pure LVL triblock copolymer, the pure rosin ester (tackifier), and the five LVL/tackifier blends. The T_g of the pure tackifier is around -26 °C. The pure triblock copolymer has two $T_g's$ of -50 °C and 49.5 °C, attributed to the PMVL and PLA domains, respectively. At 30 wt.% tackifier content, the T_g associated with the tackifier is no longer observed, suggesting that it is mixing with either the PLA or PMVL domains. To determine which component (PLA or PMVL) the Fox equation was employed:[228]

$$\frac{1}{T_{g,mixed-domain}} = \sum_i \frac{w_i}{T_{g,i}} \tag{6.1}$$

where $T_{g,mixed-domain}$ is the glass transition temperature of the mixed domain, $T_{g,i}$ is the glass transition temperature of component i, and w_i is the weight fraction of component i. Given negligible mixing between the PLA and PMVL domains, the expected $T_{g,PMVL-domain}$ and $T_{g,PLA-domain}$ can be calculated assuming that all tackifier preferentially mixes with either the PLA domain or PMVL domain. Assuming that all the tackifier mixes with the PLA domain, it is estimated that the 30 wt.% tackifier blend would have a

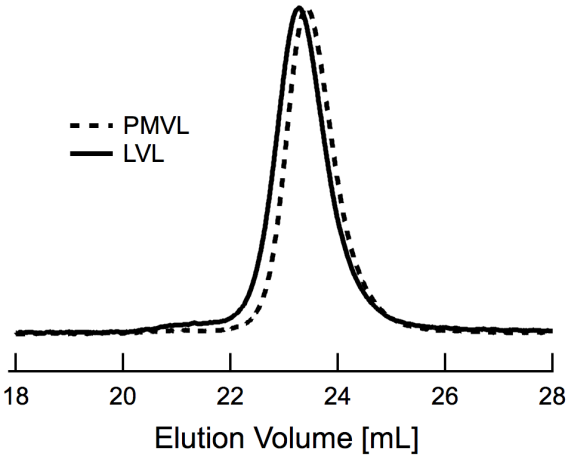

Figure 6.3: Size-exclusion chromatography (SEC) traces of the PMVL homopolymer and LVL triblock. The shift to lower retention volumes for the LVL triblock provides evidence for successful growth of the lactide blocks off the PMVL midblock.

T_g of 0.3 °C, significantly lower than the observed $T_{g,PLA-domain}$ of 43.4 °C. In contrast, the estimated $T_{g,PMVL-domain}$ for complete mixing of PMVL and tackifier is -43.9 °C which is in agreement with the measured value of -44.5 °C. These observations and calculations are consistent with the tackifier preferentially mixing with the PMVL block. The slight depression of $T_{g,PLA-domain}$ is most likely due to either a small amount of mixing between the PLA/PMVL interface or a slight plasticization of the PLA by the rosin tackifier. The additional glass transition temperature around 10 °C which is attributed to interfacial mixing of PLA and the tackifier.

Increasing the tackifier content to 40 or 50 wt.% leads to further elevation and depression of $T_{g,PMVL-domain}$ and $T_{g,PLA-domain}$, respectively. Interestingly, at 60 and 70 wt.% tackifier content, three T_g's are observed, suggesting that the tackifier is beginning to macrophase separate, forming a separate domain. In addition, these samples appeared somewhat hazy, supporting the notion that macrophase-separation occurs in this system. As such, further experiments focused on the 30, 40, and 50 wt.% PSA samples which will

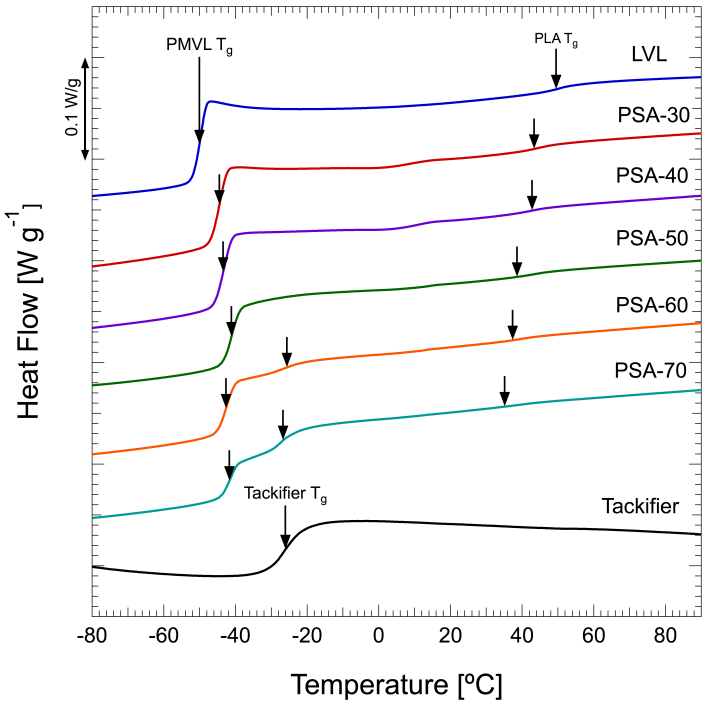

Figure 6.4: Differential scanning calorimetry (DSC) traces for the LVL triblock, tackifier, and their blends. Inflection points are marked with arrows and attributed to glass transitions.

be referred to as PSA-30, PSA-40, and PSA-50 henceforth.

6.3.3 Morphology

The morphology of LVL, PSA-30, PSA-40, and PSA-50 was probed by small angle X-ray scattering (SAXS) measurements. The room temperature SAXS patterns acquired on these samples is shown in Figure 6.5. The SAXS measurements indicate that all the samples are microphase-separated, though the peaks are rather broad and could not be definitively indexed as being associated with either hexagonal symmetry or a body-centered cubic (BCC) structures that are usually observed at asymmetric volume fractions in ABA triblock copolymers. Based upon the scattering patterns, it can be inferred that the samples lack long-range order. The principle domain spacing ($D = \frac{2\pi}{q^*}$) is estimated to be 45.9 nm

for LVL. For PSA-30, D increases to 58.0 nm which is in agreement with what would be expected if the tackifier swelled the PMVL matrix. Further increases in tackifier content to 40 wt.% leads to an increase of D to 60.0 nm. The scattering pattern from PSA-50 is rather ambiguous which may be due to low electron density contrast between the PMVL/tackifier and PLA domain. The peak position, therefore, is difficult to ascertain, and it is roughly estimated that $D = 57$ nm for this sample.

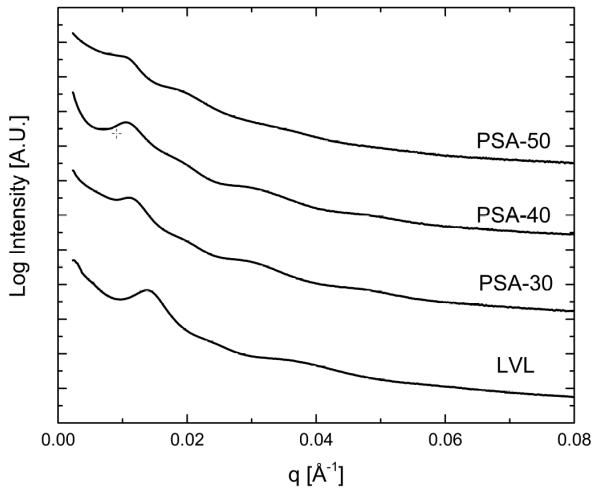

Figure 6.5: Small angle X-ray scattering (SAXS) patterns of the LVL triblock and resulting PSAs.

6.4 Rheology

6.4.1 Linear viscoelasticity: oscillatory shear

The linear viscoelastic (LVE) properties were probed with small angle oscillatory shear (SAOS. Data were acquired between -20–140 °C, and the data were horizontally shifted in order to construct a master curve with a reference temperature of 20 °C (roughly corresponding to room temperature) as shown in Figure 6.6. The horizontal shift factors (a_T)

were fitted with the Williams-Landel-Ferry (WLF) equation and the resulting fit parameters are included in the inset. Understanding the LVE behavior of a PSA is of critical importance since it will determine the bonding and debonding character of the adhesive. It is well known that a PSA must be able to wet a substrate upon application of very light pressure. An empirical rule developed by Carl Dahlquist of 3M Corporation requires the measured dynamic elastic shear modulus G' to be less than 3×10^5 Pa at a frequency (ω) of 1 rad s^{-1} in order to have adequate wetting of the substrate during a one second bonding process.[229] This so-called Dahlquist criterion is highlighted by the dashed lines in Figure 6.6.

Clearly, the LVL triblock copolymer has a G' well above the Dahlquist criteria value at 1 rad s^{-1}. Increasing the tackifier content leads to an apparent decrease in G' at 1 rad s^{-1}. Generally speaking, the plateau modulus (G_N) decreases with increasing tackifier content as highlighted in Figure 6.7 (here, G_N is estimated as the value of G' at which G'' is at a minimum).[112] As such, PSA-30, PSA-40, and PSA-50 all appear to satisfy the Dahlquist criteria. Assuming all of the tackifier resides within the rubbery phase, G_N is expected to decrease with an increase in tackifier content as follows:

$$G_N = \frac{\rho RT}{M_e} V_p^2 (1 + 2.5c + 14.1c^2) \tag{6.2}$$

where M_e is the entanglement molecular weight, V_p is the volume fraction of the polymer in the polymer/tackifier blend, ρ is the density of the rubbery phase, and c is the filler volume fraction (in this case f_{PLA}).[227,230] In physical terms, Equation 6.2 translates to the dilution of entanglements of the rubbery PMVL matrix with an increase in tackifier content. Using published values of ρ and M_e for PMVL,[231] and ρ for the tackifier,[232] the calculated values of G_N are plotted against the data in Figure 6.7. Good agreement between theory and experiment gives validity to this model and can help one predict the minimum amount of tackifier need to satisfy the Dahlquist criterion.

In addition to predicting the ability of an adhesive to wet a substrate during the bonding step, the LVE behavior can also be used to forecast the efficacy of the adhesive during

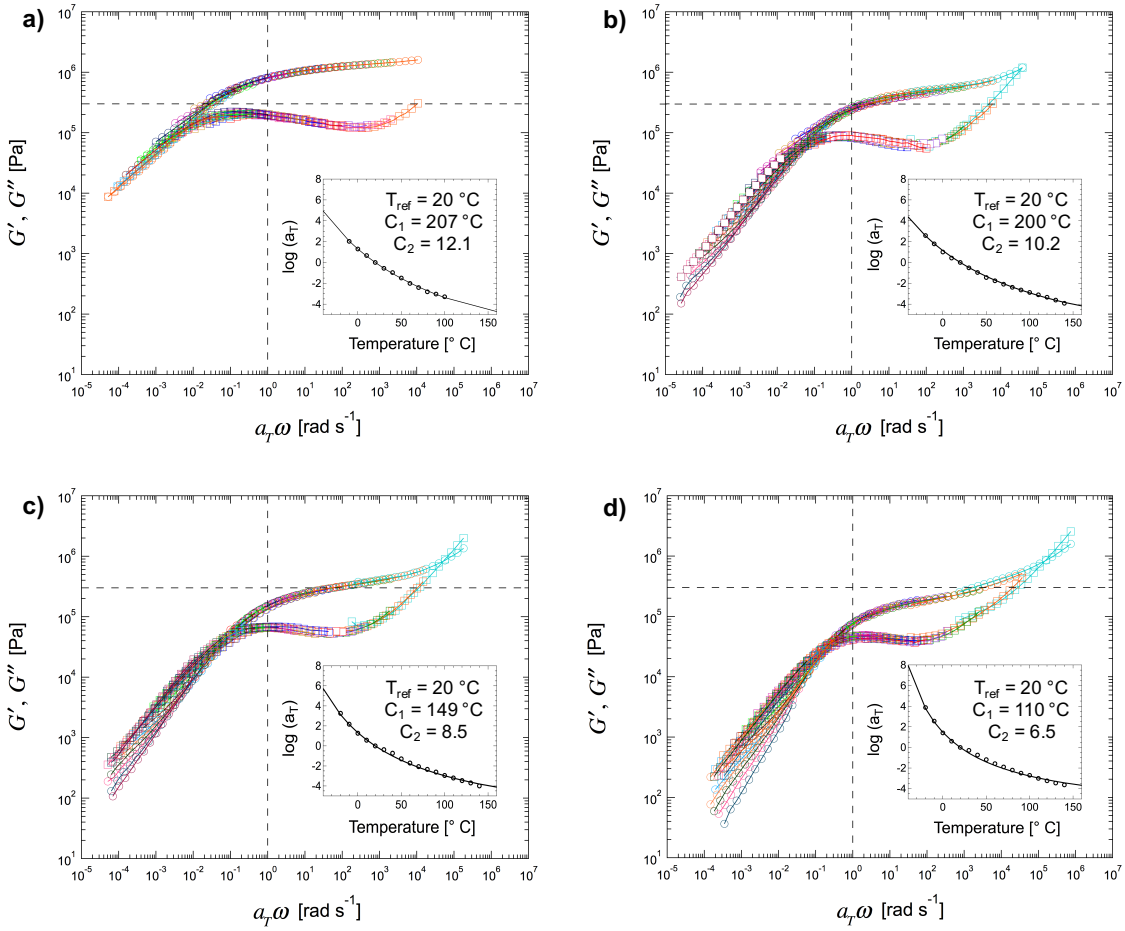

Figure 6.6: Master curves for the linear dynamic storage (G') and loss (G'') moduli of a) LVL b) PSA-30 c) PSA-40, and d) PSA-50.

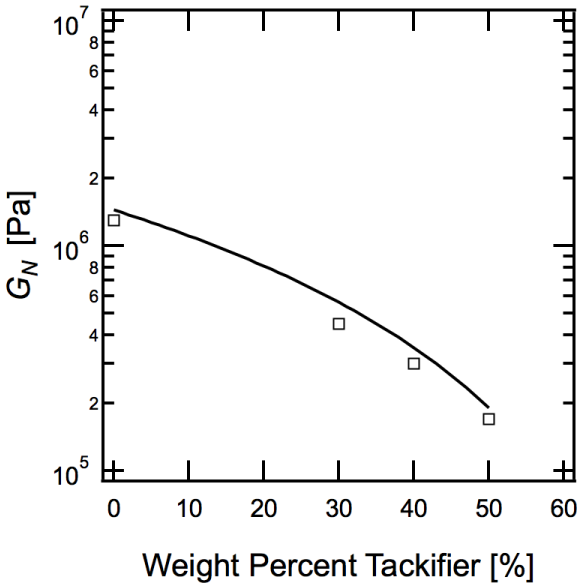

Figure 6.7: The plateau modulus G_N as a function of tackifier content.

debonding. The relevant frequency corresponding to a particular application can be related to the debonding velocity (V_{deb}) associated with a particular application or experiment:

$$\omega = \frac{2\pi V_{deb}}{h_0} \tag{6.3}$$

where h_0 is the thickness of the layer.[233] While the characteristic time for the bonding step is ∼1 second, debonding processes typically happen on much quicker time scales corresponding to 100–1000 rad s^{-1}.[234] Equation 6.3 will be used in later sections to help qualitatively explain the different observed in the probe tack, shear resistance, and 180° peel experiments.

Figure 6.8 shows the measured G' and G'' taken during an isochronal temperature ramp at a frequency of 1 rad s^{-1} and a heating rate of 2 °C min^{-1} for the LVL triblock copolymer. The data lacks a sharp drop in G', making it difficult to precisely determine a T_{ODT}. Instead, a gradual drop in the G' is observed from 170-190 °C. To discern whether the material was disordered at 190 °C, a frequency sweep was employed. Because the scaling does not match with that of a disordered liquid ($G' \sim \omega^2$, $G'' \sim \omega$), the triblock is deemed

to be ordered, and the T_{ODT} is inaccessible.

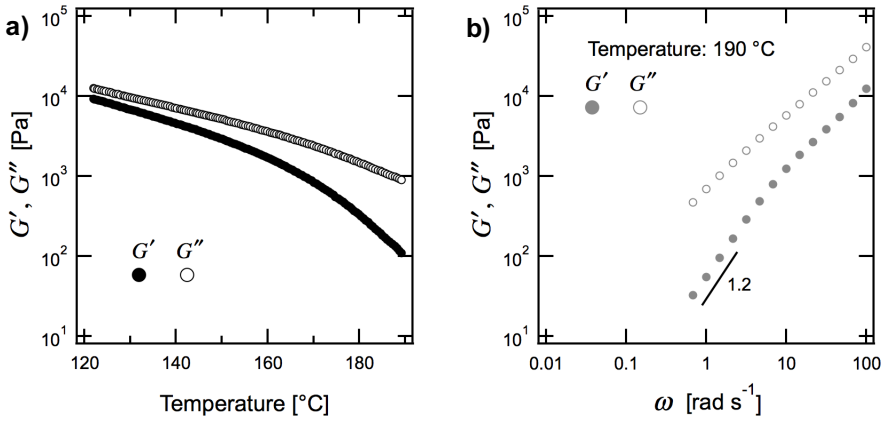

Figure 6.8: Oscillatory shear rheology of LVL showing a) isochronal temperature ramp at a frequency of 1 rad s^{-1} and a heating rate of 2 °C min^{-1} and b) frequency sweep at 190 °C.

6.4.2 Nonlinear viscoelasticity: uniaxial extension

Nonlinear extensional properties are imperative to adhesive performance, since it can dictate the large strain behavior experienced by fibrils formed when debonding an adhesive.[102] The mechanical properties of different adhesives were compared by testing LVL, PSA-30, PSA-40, and PSA-50 under uniaxial extension at room temperature using an extensional viscosity fixture (EVF). Figure 6.9 shows the true (Hencky) strain (ϵ) as a function of true stress (σ_E) for the samples, taken at a Hencky strain rate ($\dot{\epsilon}$) of 1 s^{-1}. Additionally, the predicted elastic modulus (E) based upon SAOS shear measurements ($E = 3G_N$, Figure 6.9) is indicated by the dotted lines. Qualitatively, the behavior of the four samples is very similar. All samples show strain hardening at similar values and ultimately fail around $\epsilon \approx 3 - 4$. Also, the samples show a decrease in E with an increase in the tackifier content.

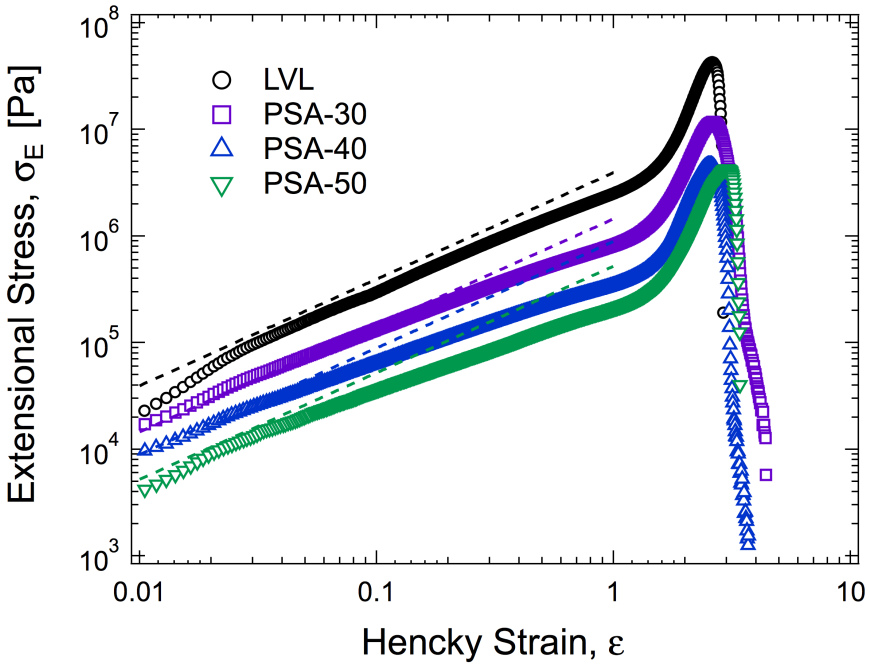

Figure 6.9: Extensional stress (σ_E) versus true (Hencky) strain (ϵ) for the pure LVL triblock and PSA-30, PSA-40, and PSA-50. Dashed lines correspond to the linear elastic behavior predicted based upon measured values of G_N.

6.4.3 Nonlinear viscoelasticity: shear creep

Shear strength is an important property when designing PSAs and is characterized by the ability to resist deformation under an applied stress. Creep measurements were taken on the samples in order to gain a more fundamental understanding of the stiffness of the PSA and behavior under an imposed stress. Figure 6.10 shows the measured creep compliance $J(t)$ versus time for LVL, PSA-30, PSA-40, and PSA-50 taken while imposing a stress of 30 kPa taken at 25 °C. The stress was chosen to roughly correspond to the stress in the shear resistance experiment in which a weight of 500 grams is hung from 0.5 by 0.5 inch adhesive adhered to a stainless steel plate (6.2.3). Increasing the tackifier content results in a greater creep compliance, while the pure triblock copolymer (LVL), with the lowest creep

compliance, has the greatest resistance to creep.

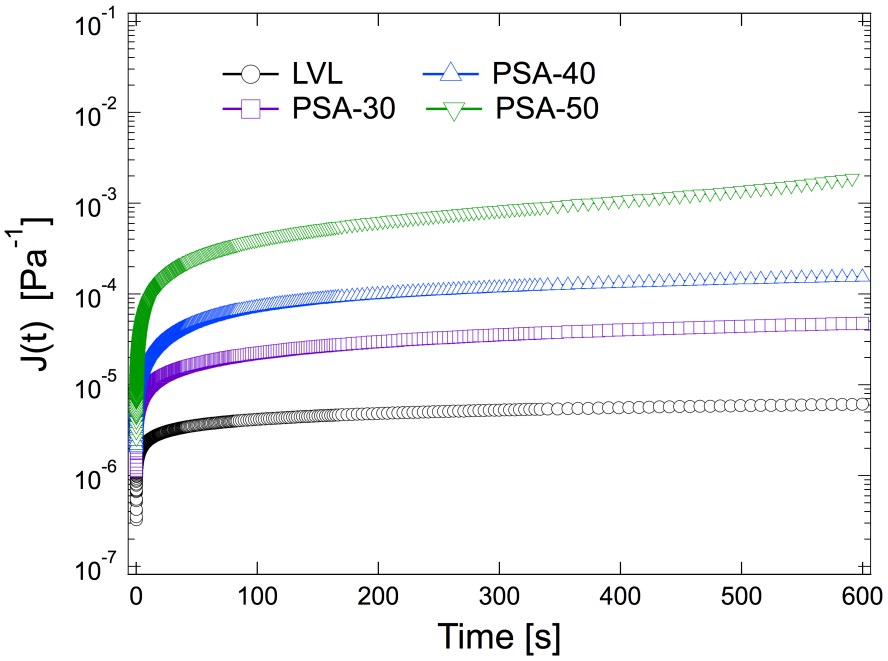

Figure 6.10: Shear creep compliance *versus* time for LVL, PSA-30, PSA-40, PSA-50 measured while imposing a stress of 30 kPa. Data was acquired at 25 °C.

6.5 Adhesive behavior

6.5.1 Tack

Probe tack experiments were conducted to elucidate the bonding and debonding characteristics of the PSAs. A steel probe was brought into contact with the PSA and dwelled for one second. The probe was removed from the PSA at a rate of 0.5 mm s^{-1} and the force was measured as a function of the probe displacement. The engineering strain was calculated based upon the thickness of the PSA film. A representative data set acquired during a probe tack experiment is shown in Figure 6.11. The peak stress corresponds to the formation of cavities within the adhesive[235] while the stress plateau observed after the

peak stress is typically attributed to fibrillation.[236] Debonding is thought to occur when cracks on the adhesive substrate interface propagate and coalesce.[237]

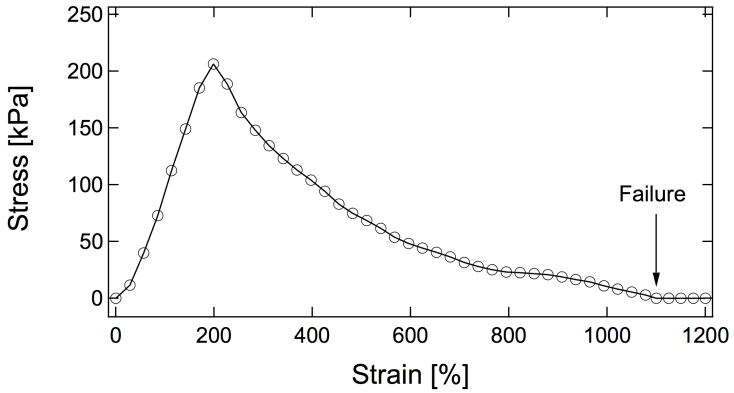

Figure 6.11: Representative data for a probe tack adhesion experiment plotting engineering stress *versus* strain (sample is PSA-40).

The tackiness of the adhesive can be deciphered by examining the peak stress in the experiment and the amount of energy dissipated during the experiment is related to the total work of adhesion (W_{adh}). The latter can be calculated by the area under the stress versus strain curve using the following equation:

$$W_{adh} = h_o \int_0^{\epsilon_{max}} \sigma(\epsilon) d\epsilon \tag{6.4}$$

where h_o is the thickness of the adhesive, ϵ_{max} is the maximum strain, and $\sigma(\epsilon)$ is the stress at a particular strain.

The average peak stress observed during the debonding for each formulated PSA and for select commercial adhesives is shown in Figure 6.12. Measurements were taken with a stainless steel and aluminum probe which had a root-mean squared (RMS) roughness of 0.42 μm. The data show that the peak stress value is relatively insensitive to the tackifier content for the formulated PSAs but are comparable to the two commercial adhesives tested. The adhesive work of the probe tack measurement was calculated using Equation 6.4 and the average values for each adhesive is shown in Figure 6.13. The adhesive work

for PSA-40 is slightly higher than the other formulations, but again, the effect of tackifier content is minimal. When compared to the commercial adhesives, the measured adhesive work values of PSA-30, PSA-40, and PSA-50 are roughly equal to a Post-it note but less than double-sided tape.

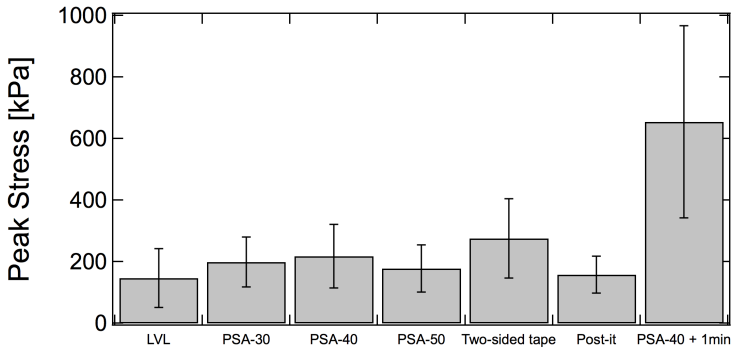

Figure 6.12: Average peak stress during the probe tack adhesion test for the PSA samples. Error bars represent standard deviations of at least five specimens.

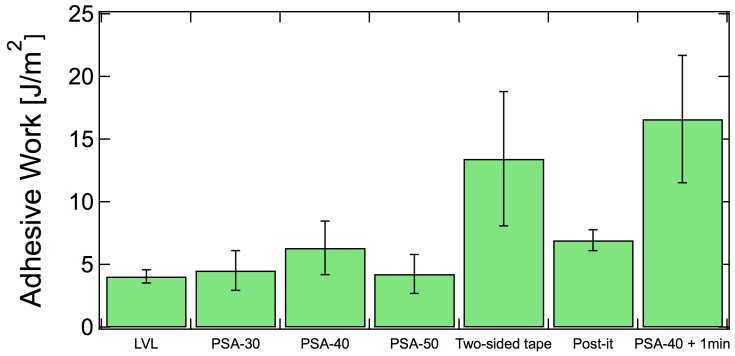

Figure 6.13: Average work of adhesion during the probe tack adhesion test for the PSA samples. Error bars represent standard deviations of at least five specimens.

Correlating the test bonding and debonding conditions to the viscoelastic behavior at these test frequencies can give insight into the origin of the different adhesive behavior of the PSAs. The debonding velocity (V_{deb}) in this experiment was 0.5 mm s^{-1}. Using Equation

6.3 and a sample thickness of 10 microns, this corresponds to a frequency of approximately 300 rad s^{-1}. The contact time of one second corresponds to a frequency of 1 rad s^{-1}. It has been proposed that the adhesive strength is related to the G' and G'' as follows:

$$Adhesive\ strength \propto \frac{G''(\omega_{debond})}{G'(\omega_{bond})} \tag{6.5}$$

where $G''(\omega_{debond})$ is the dynamic loss modulus at the debonding frequency and $G'(\omega_{bond})$ is the dynamic storage modulus at the bonding frequency.[234,238] Others have also correlated the resistance to debonding (tack) with the loss modulus measured at the corresponding debonding rate when the adhesive fulfilled the Dahlquist criterion.[239] Examining the G' and G'' master curves in Figure 6.6 reveals that the debonding frequency is fairly close to the minimum value of G''. Interestingly, applying the data in Figure 6.6 to Equation 6.5 reveals that the adhesive strength should be roughly the same for all four adhesives. (Adhesive strength is characterized by the peak stress values in Figure 6.12). The experimental debonding rate is relatively low compared to the suggested debonding rate of 10 mm s^{-1} specified in the ASTM standard test method for measuring tack of adhesives with an inverted probe.[234,240] Therefore, it is likely that the measured peak stress would be higher at faster debonding rates which correspond to higher frequencies with relatively higher values G''.

An additional experiment was conducted for PSA-40 in which the probe was held in contact for 1 minute (60 seconds) rather than 1 second. This corresponds to $\omega = 0.017$ rad s^{-1} (rather than 1 rad s^{-1} in the standard protocol), smaller than the crossover frequency of approximately 0.1 s^{-1}. This indicates that the longest relaxation time (τ_d) of the system has likely been traversed, and therefore, there is potentially better contact between the PSA and probe. Indeed, the corresponding peak stress and adhesive work are roughly 3× greater for this longer dwell time than for the standard.

6.5.2 Peel adhesion

Peel adhesion, or the amount of force necessary to remove an adhesive from a substrate, is an important parameter to consider when designing a pressure sensitive adhesive. A summary of the peel strength measured in a 180° peel test is shown in Figure 6.14. The data show that the peel strength is greatest for PSA-30 and PSA-40. When the tackifier content is increased to 50 wt.%, the peel adhesion drops significantly and has only a slightly higher average value than that of the pure LVL triblock copolymer. It has been found that the peel adhesion is related the behavior under uniaxial extension.[241] The extensional rate ($\dot{\epsilon}$) associated with a peel experiment can be calculated by

$$\dot{\epsilon} = \frac{v}{h_0} \tag{6.6}$$

where h_0 is the adhesive thickness and v is the peel velocity.[242] Therefore, it is possible that the lower peel strength is due to break up of fibrils. If this type of cohesive failure could be avoided, samples should fail adhesively by crack propagating at the surface and ultimate peel strengths are expected to be higher.[233] The observation of PSA residue on the stainless steel plate after conducting peel tests on PSA-50 supports the hypothesis that this adhesive failed cohesively.

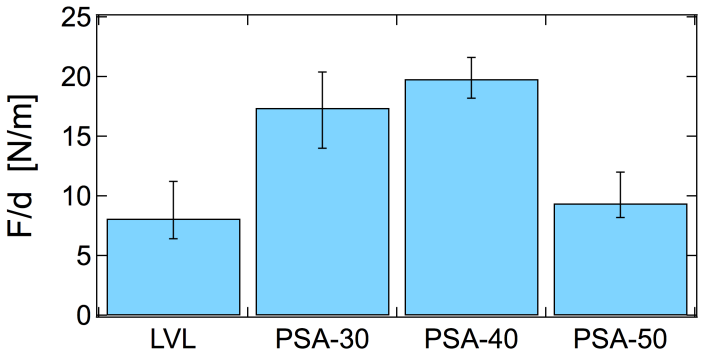

Figure 6.14: Average peel strength for the PSA samples. Error bars represent standard deviations of at least five specimens.

It has been found that the maximum peel force is highly dependent on time and temperature. Kaeble was able to construct a peel adhesion "master curve" based upon shift factors obtained from dynamic rheological measurements.[243] From these master curves, it was found that peel force was maximized at peel rates or temperatures corresponding to the rubber-to-glass transition. From Equation 6.6, the peel velocity of this experiment corresponds to a frequency of roughly 3000 rad s^{-1}. Examining the master curves in Figure 6.6 reveals that the experimental time scale corresponds to a frequency within the rubbery plateau. As such, enhanced peel strength is expected at either faster peel rates or lower temperatures.

6.5.3 Shear resistance

Shear resistance was examined by examining the holding power of the adhesive under a constant load. Samples were coated on a PET strip with a width of 0.5 inches and a length of approximately 6 inches. The adhesive was placed on an aluminum plate with a contact area of 0.5 by 0.5 inches. A 500 gram weight was attached to the unadhered PET strip. The time it took for the strip to pull the adhesive away from the stainless steel plate was recorded for three samples. Figure 6.15 shows a summary of the results. The various adhesives show dramatically different shear strength as demonstrated by the orders of magnitude difference in the ability to hold the hanging weight. The high shear strength of the pure LVL triblock copolymer is more than likely an underestimate since the experiment was terminated after 8 days at which time two out of three samples had not yet fallen. In contrast, PSA-50 showed very low strength and fell within seconds of hanging the weight.

The results of the shear resistance experiment are not surprising, considering the creep results in Figure 6.10. In the creep experiment, a stress of 30 kPa was applied to adhesives. The LVL triblock copolymer showed the highest resistance to creep while PSA-50 showed the lowest resistance to creep. After the shear resistance test, a small amount of residue was found on the stainless steel plate, indicating that the adhesives failed cohesively. One

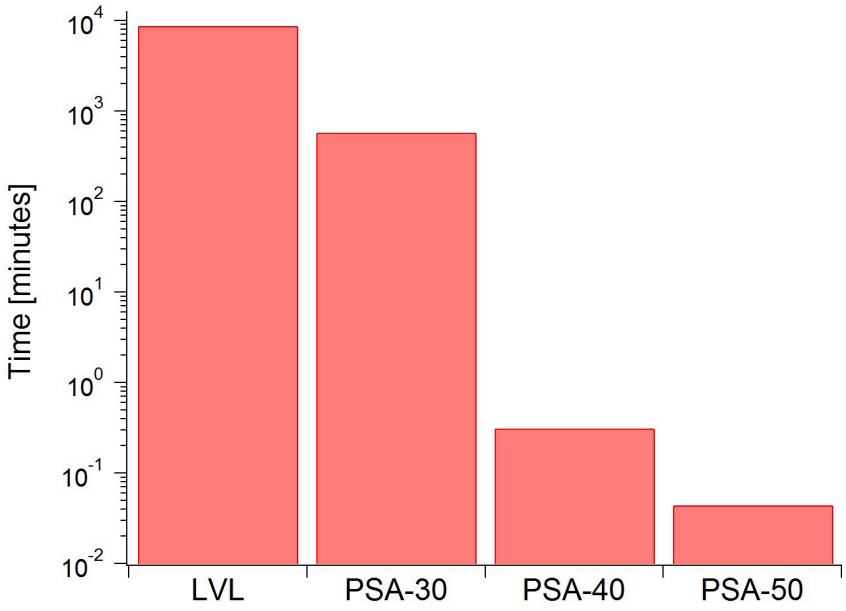

Figure 6.15: Shear resistance measured by average time adhesive held 500 gram weight before falling.

could assume that LVL, PSA- 30, PSA-40, and PSA-50 would fail at similar strains based upon the similar uniaxial extension data in Figure 6.9. Then, one can evaluate the time it takes to reach the same strain in the shear creep measurements to gain insight into how the compliance of these materials should influence the time scales of failure under shear load. Based upon the measured compliance in Figure 6.10, it would take 5.4 days, 7.6 hours, 43 minutes, and ≈1 second for LVL, PSA-30, PSA-40, and PSA-50 to reach a strain of 10%. While the strain at failure of the adhesive in the shear resistance experiment is unknown, this at least qualitatively explains the orders of magnitude difference in the shear holding ability of the four samples.

6.6 Potential applications

The behavior of PSAs is highly dependent on temperature and the bonding and debonding rates. Tack, peel strength, and shear resistance are important properties, but the tests utilized to measure these properties represent only a specific set of test conditions. Chang developed the concept of "viscoelastic windows" in order to develop guidelines for designing PSAs based upon the measured G' and G'' at the application frequencies and temperature.[234,244] The concept of viscoelastic windows is based upon the observation that G' and G'' usually fall between a certain range at the bonding frequency and debonding frequency of 10^{-2} and 10^{2} rad s^{-1}. The specific value of G' and G'' depends on the application, but typically ranges from 10^{3} to 10^{6} Pa. By plotting four different coordinates (G' at 10^{-2} rad s^{-1}, G'' at 10^{-2} rad s^{-1}; G' at 10^{2} rad s^{-1}, G'' at 10^{2} rad s^{-1}; G' at 10^{-2} rad s^{-1}, G'' at 10^{2} rad s^{-1}; G' at 10^{2} rad s^{-1}, G'' at 10^{-2} rad s^{-1}) on a cross-plot of G' and G'', one can identify which quadrant of the viscoelastic window a PSA lies in and identify a potential application. Such a plot is shown in Figure 6.16.

The adhesive behavior and possible application of an adhesive can be related to where a specific viscoelastic window of a PSA resides. Consistent with the analysis by Chang and Yang, four quadrants are defined in Figure 6.16.[234] Quadrant 1 represents the high G' and low G'', which is typically ineffective for PSA applications due to the high elasticity of the samples. Quadrant 2 is the high G' and high G''. This region is ideal for PSAs that require high cohesive strength, which translates to high shear strength. Quadrant 3 is the low G' and low G'' region which is related to adhesives with relatively low peel strengths; this region is often associated with removable adhesives and medical tape. Finally, Quadrant 4 is the region in which the PSA exhibits low G' and high G''. The ability of the PSA to flow with a short contact time makes this quadrant ideal for quick-stick or Cold-stick PSAs. Figure 6.16 gives insight into potential applications of the four samples. The LVL triblock copolymer clearly falls within Quadrant 2, which is consistent with its remarkably high shear strength and resistance to creep discussed previously. However, the high value of G' makes LVL less

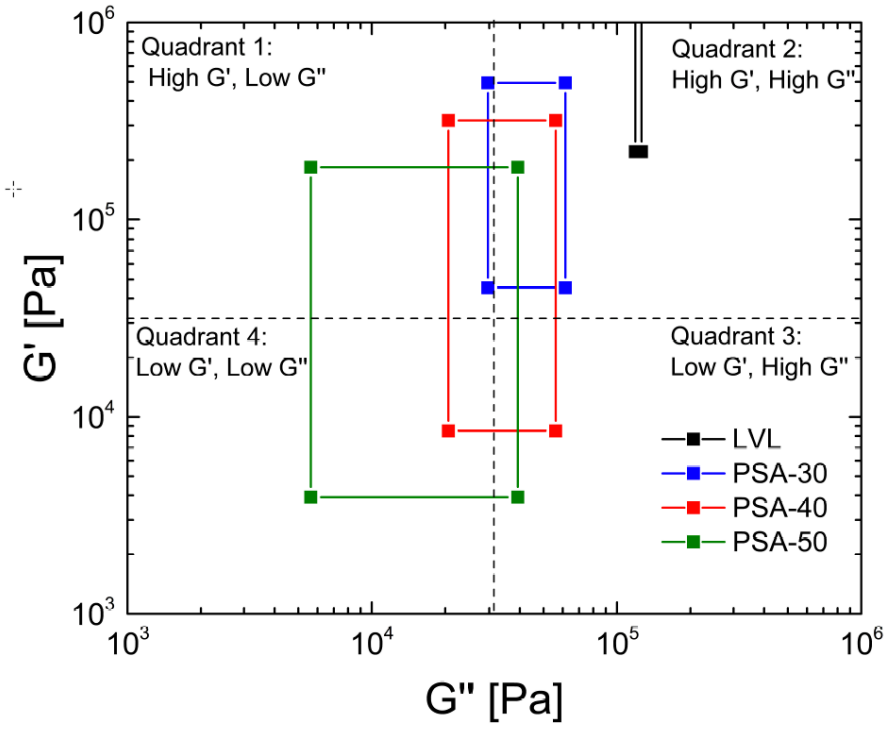

Figure 6.16: Viscoelastic window for LVL, PSA-30, PSA-40, and PSA-50.

than ideal since it requires longer contact times in order to wet the substrate. PSA-30 is also within Quadrant 2, making it also suitable for similar applications. Even though the shear strength of PSA-30 was not as high as that of the LVL polymer, this sample may be more practical since it can form a bond with a substrate much quicker. PSA-40 fall within the central region of the viscoelastic window. Yang and Chang discuss how this region is generally for general use PSAs. Unsurprisingly, PSA-40 was characterized by intermediate tack and shear strength and high peel strength in previous experiments. Finally, PSA-50 lies in the central region and mainly falls in Quadrant 3. The low peel strength of PSA-50 demonstrates its ability to easily debond from a substrate and highlights its potential use as a removable adhesive.

6.7 Conclusions

The work here gives insight into the potential application of a LVL triblock copolymer towards the development of PSAs made from completely renewable content. A LVL triblock copolymer was synthesized by ring-opening polymerization of MVL monomer. The PMVL polymer was used as a macroinitiator for the ring-opening polymerization of D,L-lactide which resulted in the LVL triblock copolymer. The LVL polymer was characterized by ^{1}H NMR and SEC. A series of PSAs were formulated by blending the triblock copolymer with a rosin ester. Miscibility of the triblock copolymer and the rosin ester was examined for five different blends using DSC. The three blends which showed miscibility of the rosin ester in the PMVL midblock were subjected to further testing. The PSA performance was evaluated using industrial relevant tests and the behavior was correlated with rheological measurements. Potential applications of the adhesive varied but included potential general purpose applications as well as applications requiring high shear resistance or easy removability. Future work could include using a tackifier with a higher T_g. Using a higher T_g tackifier would move the transition region between rubbery to glassy behavior to low frequencies, which could improve the peel strength of the adhesive.[242,243] Still, the adhesives developed here show promise and could be potentially used as a low-cost replacement for petroleum-derived PSAs currently on the market.

Chapter 7

Blown Film Extrusion of PLA-based Materials

7.1 Introduction

As of 2016, the plastic sheet, film, and bag industry in the US is valued at over $45 billion (by revenue) and is expected to grow to over $55 billion by 2021 due to robust and increasing consumer demand.[245] Approximately 30% of the market is for packaging, 25% for bags, and the rest are for sheets and films for non-packaging purposes. Major players include food and beverage manufacturers and retailers, construction industries, agricultural industries, and pharmaceuticals and medical manufacturers.

The two most commonly used processes for making plastic sheets (thickness $>$ 25 microns) and films (thickness $<$ 25 microns) are cast film extrusion and blown film extrusion.[246] Cast film extrusion involves the horizontal extrusion of molten polymer through a flat die in which the melt undergoes biaxial or planar extension, resulting in highly oriented films in the machine direction (the direction of flow). Blown film extrusion, in contrast,

Part of this work was done in collaboration with Tuoqi Li, Liangliang Gu, Jacob Wright, and Joseph Schaefer. Financial support for this work came from the National Science Center through the Center for Sustainable Polymers at the University of Minnesota, a Center for Chemical Innovation (CHE-1413862).

produces films by extruding molten polymer vertically through an annual die in which the melt undergoes biaxial extension. Typically, cast film extrusion results in better thickness homogeneity, yet blown film extrusion is cheaper and has more uniform properties (due to less anisotropy).

The vast majority of plastic sheets, films, and bags are from non-renewable resources and are not degradable, many of which are composed of polyethylene due to its low cost, versatility, and processability. Recently, there have been several economic drivers to develop materials from renewable sources that are degradable. Lawmakers and environmental regulators have become increasing sensitive to the disposal of single-use plastic bags, and there exists legislation regarding plastic bag bans in 14 states.[245] In Minnesota, yard waste must be disposed of in biodegradable bags.[247] In the agricultural sector, farmers need plastic films to protect cultivation and desire those than can be plowed underground and degrade; conventional plastics are often burned or left on the field.[248,249]

Despite these demands, there are no commercial plastic film produced from blown films extrusion that are composed primarily of polylactide (PLA), one of the most ubiquitous and cheapest sustainable resins on the market today.[250] Degradable films that incorporate PLA do exist; for example, Natur-Tec (a subsidiary of Northern Technologies IC) sells a compostable bag, Natur-bag. The main component of these bags, though, is poly(butyrate adipate terephthalate) (PBAT), a petroleum-derived polymer that is significantly more expensive than PLA. The addition of PBAT is necessary to both increase the melt strength and to improve the mechanical properties of PLA.

A recent discovery at the University of Minnesota has found that remarkably low loadings (≤ 5 wt.%) of low molecular poly(ethylene oxide)-based diblocks can effectively toughen amorphous PLA.[138] Because poly(ethylene oxide) is degradable and cheap, this technology could have immediate commercial viability. Thus far, this concept had only been demonstrated on the lab-bench. The goal of this work is to transform this discovery into a useful

product, utilizing polymer processing techniques that would be found in industry. Specifically, blown film extrusion was explored as a way to produce tough PLA-based films. This chapter will begin by giving background on this technology and blown film extrusion. Next, the specific methodologies for melt mixing and blowing films will be explained along with a full molecular and rheological characterization of the blends. Finally, the mechanical performance of the films will be assessed with recommendations for future work.

7.2 Background

7.2.1 Micelle toughening

Researchers at the University of Minnesota melt blended short poly(ethylene oxide)-*b*-poly(butylene oxide) (PEO-PBO) diblocks into commercial PLLA.[138] Adding as little as 1.25 wt.% diblock increased the tensile toughness and Izod impact strength, and adding 5 wt.% resulted in an order of magnitude increase for both properties. Remarkably, neither the elastic modulus nor transparency decreased appreciably. The authors observed that the PEO-PBO diblocks formed well-dispersed micelles within the PLLA matrix due to favorable mixing of the corona PEO block with the PLLA, a feature encapsulated by a negative Flory-Huggins interaction parameter (χ) between PEO and PLLA.

7.2.2 Blown film extrusion process

A schematic of a blown film extrusion is shown in Figure 7.1. Polymer resin is fed into a single screw extruder which heats the material to the desired temperature and pressure to force it through an annual die. An air supply from underneath blows the molten polymer biaxially to form a bubble. Cooling air from the sides solidifies the polymer and helps dictate the final bubble dimensions. The bubble is often stabilized with rollers or cages until it is passed into a collapsing frame that pre-flattens the polymer before it hits the nip rolls. Once through the nip rolls, the cooled polymer films are wrapped into its final form

via winders.

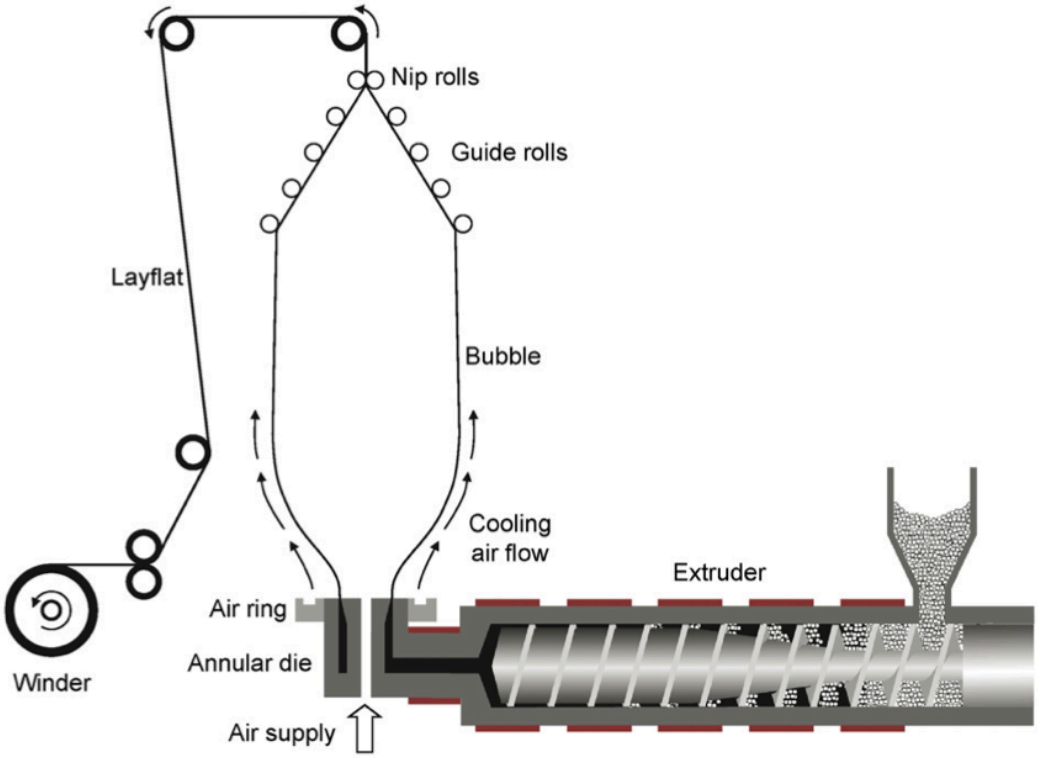

Figure 7.1: Schematic of a blown film extrusion line. Reprinted from *Progress in Polymer Science*, *33*, Lim *et al.*, Processing Technologies for Poly(lactic acid), 820–852, Copyright (2008), with permission from Elsevier.[42]

Relevant processing parameters include screw temperatures, screw speed, cooling rate, nip speed, and bubble volume. The screw temperature must be high enough to sufficiently lower the polymer viscosity so it can be easily extruded through the die, but low enough to avoid degradation. Degradation is a particular problem with processing PLA due to chain scission that occurs at relatively modest processing temperatures.[251] The screw speed dictates the mass flow rate, limited by the power output of the extruder. The cooling rate helps stabilize the bubble and dictate the final dimensions. Often, materials will exhibit a *frost line*, a horizontal demarcation indicating the moment in which the molten polymer

has solidified. This frost line may be anywhere from 2-10 times the die diameter, depending on the material and the desired bubble diameter.[252] The final bubble volume is typically defined by the term "blow-up ratio" (BUR):

$$BUR = \frac{D_{bubble}}{D_{die}} \tag{7.1}$$

where D refers to the diameter. Another important parameter is often referred to as the take-up ratio (TUR):

$$TUR = \frac{v_{nip}}{v_{die}} \tag{7.2}$$

where v is the velocity. Assuming a constant mass flow rate, equation 7.2 can be reduced to the following:

$$TUR = \frac{A_{die}\rho_{die}}{A_{nip}\rho_{nip}} \tag{7.3}$$

in which A is the cross-sectional area at the nip rollers or die and ρ refers to the density at these locations. The BUR and TUR together help determine the final thickness of the film. Finally, the level of anisotropy can be measured by the *forming ratio* (FR) defined as the ratio of the TUR to BUR:

$$FR = \frac{TUR}{BUR} \tag{7.4}$$

In general, one wishes to produce film as fast as possible to maximize profit; this is especially important given the high capital costs of equipment and high volume, low-profit margin nature of products made via blown film extrusion.

7.2.3 Importance of extensional rheology

Bubble stability is critical during blown film extrusion for final film homogeneity and robust processing. Variations in sample thickness can result in product failure, wasted material, and reduced profits. Given the high velocities attained in blown film extrusion, the bubble is particularly susceptible to a number of instabilities such as draw resonance, helical instability, frost line oscillation, bubble sag, bubble tears, and breathing.[252] Although adjustment

of processing parameters can help limit these instabilities, an ideal way to ameliorate these concerns is by tuning the **extensional rheology** of the material.

Due to the fast elongation flows used in blown film extrusion, it is no surprise that there is a strong correlation between the extensional rheology of the material and bubble stability. A number of individuals have investigated the correlation between the extensional rheological profile of materials (mostly polyethylenes) with bubble stability, processability, and film homogeneity.[253–255] Although blown film extrusion utilizes biaxial extension, behavior in uniaxial extension has been shown the be a viable way to assess performance and is much easier to do experimentally.[256] Münstedt and coworkers focused on a variety of polyethylenes with varying degrees of long-chain branching and extensional viscosities.[255] They found that bubble stability increased as the take-up force increased, a parameter directly correlated with the extensional viscosity. This increase in extensional viscosity could come from either higher molecular weight materials or from the introduction of long-chain branching. However, for the best thickness homogeneity, some degree of strain hardening was necessary at higher Hencky strain rates (> 0.5 s^{-1}), no matter the maximum value of the extensional viscosity ($\eta_{E,max}$).

This trend was verified through modeling; Kolarik et al. showed that for optimal processing conditions (maximum bubble stability and minimum film thickness), one must increase both the melt strength and amount of strain hardening (quantified by the ratio $\frac{\eta_{E,max}}{3\eta^+}$). Interestingly, they found that for a given $\frac{\eta_{E,max}}{3\eta^+}$, there was a *minimum* extensional viscosity that maximized the processing conditions. In other words, if the polymer had too much strain hardening, processability decreased. This was explained by the fact that for high $\frac{\eta_{E,max}}{3\eta^+}$, the melt strength could no longer accommodate the much larger stresses being imposed due to the long-chain branching and would break prematurely. Although the exact relationship between extensional viscosity (η_E) and the amount of strain hardening ($\frac{\eta_{E,max}}{3\eta^+}$) depends on the numerical values of each, in many cases, a relatively small amount of strain hardening ($\frac{\eta_{E,max}}{3\eta^+}<3$) is sufficient.

7.2.4 Design parameters

To summarize section 7.2.3, a set of rheological design parameters can be identified for good processability in blown film extrusion:

- $\eta < 5{,}000$ Pa-s at $\dot{\gamma} > 10$ s^{-1}, T = T_{die}
- $\eta_E > 5{\times}10^4$ Pa-s at $\dot{\epsilon} \geq 0.5$ s^{-1}, $\epsilon_H \geq 3.0$, $T_{\text{die}} <$ T $< T_m$ or T_g
- $1 < \frac{\eta_{E,max}}{3\eta^+} < 10$ at $T_{\text{die}} <$ T $< T_m$ or T_g

These conditions were qualitatively confirmed by blown film extrusion of a commercial LLDPE (Exxon Mobil LL 3003) that was observed to have decent processability (BUR $\approx$ 2.5, TUR $\approx$ 10, stable bubbles) on the blown film extrusion line. Figure 7.2 highlights the pertinent rheological data. At the die temperature of 160 °C, this LLDPE has a $\eta < 5{,}000$ Pa-s across all shear rates. In extension, the viscosity was slightly below the recommended value (10^4 Pa-s rather than $5{\times}10^4$ Pa-s); however, as the material crystallized around 120 °C, the extensional viscosity rose dramatically and showed very high strain hardening. The portion that was semicrystalline was apparent by the location of the frostline was only about 4 inches (4× die diameter) above the die. Thus, the region in which the bubble was in its melt state was quite small, allowing the stiffer bubble above to accommodate the slightly lower than recommended extensional viscosity.

7.3 Experimental methods

Characterization

Proton nuclear magnetic resonance (^{1}H NMR) was used to determined the number average molecular weight (M_n) of commercial PDLLA 4060D (Natureworks). ^{1}H NMR spectra were obtained with a Bruker Avance III HD spectrometer operating at 500 MHz and 25 °C using a 30 s relaxation time and 16 transients. Samples were prepared by dissolving

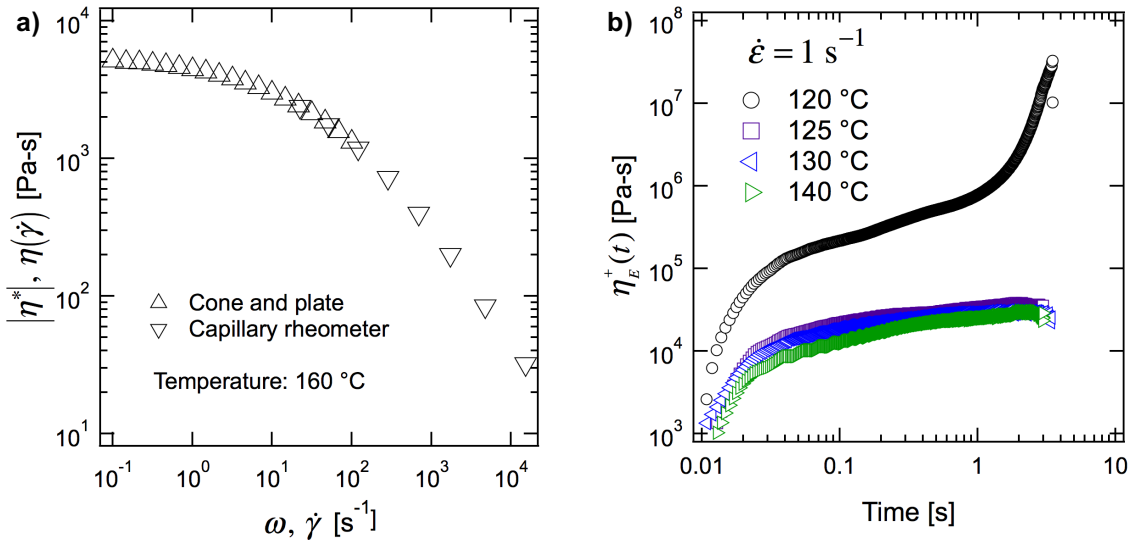

Figure 7.2: Results from a) shear and b) extensional rheology of a commercial LLDPE that exhibited good processability on the lab-scale blown film extrusion line.

10 mg of polymer in 0.7 mL $CDCl_3$ (Cambridge Isotope Laboratories, Inc., 99.8 atom % D + 0.05% V/V TMS). The M_n was determined based off of the ratio of backbone to hydroxyl end group peak, assuming one hydroxyl end group per polymer chain δ (ppm) = 5.2 [C=O-**CH**(CH_3)O-, backbone], 4.35 [-C=O-**CH**(CH_3)-OH, end group].

The dispersity ($Đ$) of each polymer was determined using size exclusion chromatography (SEC) performed on a Thermo Separation Products (TSP) Spectra Systems AS1000 autosampler equipped with three 5 mm Phenomenex Phenogel columns, a Waters 515 pump, and a Waters 2410 differential refractive index detector. Samples were run at room temperature in tetrahydrofuran at a flow rate of 1.0 mL min^{-1}.

Thermal properties of the block polymers, neat PDLLA, and resulting blends were explored via differential scanning calorimetry (DSC) on a Thermal Analysis Q1000. Approximately 5 mg of sample were prepared in hermetically sealed aluminum pans. Materials were heated to 180 °C to erase thermal history, cooled to -100 °C at 10 °C min^{-1}, and heated to 180 °C at 10 °C min^{-1}. Glass transition temperatures (T_g's) are reported based upon

inflection points in the second heating curve.

Melt blending

Melt blending was performed with a Prism TSE 16 TC twin screw extruder (Prism Engineering) equipped with 16 mm diameter screws with a 25:1 L:D ratio equipped with two mixing zones each 5 cm in length. Polylactide (PLA Natureworks 4060D) pellets were added through an automatic feeder. PEO-PBO diblock was dissolved in acetone and dripped into the feed section with a syringe pump. The volumetric flow rate of the syringe pump was specified so that the mass flow rate of diblock entering the blend is of the desired quantity. Clumping of PLA pellets in the feed was prevented by diligent breakage of conglomerates by hand. The PLA / diblock mixture was subsequently heated, compressed, and mixed through the twin screws before exiting through a circular die. The mixing speed was approximately 100 rpm and the temperature was set to 180 °C. The final blend was cooled in a water bath, pelletized, and dried under vacuum for at least 48 h before use. Residence time, measured by the insertion of colored polystyrene pellets, was approximately 2 min at these conditions.

Rheology

Shear rheology was investigated in small amplitude oscillatory shear (SAOS) on an ARES rheometer (TA Instruments) with 25 mm parallel plates. Samples were pressed at elevated temperature and pressure to form suitable 1 mm thick disks with no air bubbles. Strain sweeps were conducted at a frequency (ω) of 1 s^{-1} to determine the linear viscoelastic (LVE) region. Frequency sweeps were then performed at a strain within the LVE regime.

Extensional rheology experiments were conducted using the extensional viscosity fixture (EVF) equipped on an ARES-G2 rheometer (TA Instruments). Samples were compression molded at room temperature to a thickness of approximately 0.3 mm. A rectangular punch was then used to create samples 25 mm $\times$ 5 mm $\times$ 0.3 mm. Samples were loaded on the

EVF and annealed for at least 150 s before pulling at a constant Hencky strain rate ($\dot{\epsilon}$). Tests were run in triplicate at each testing condition (temperature and $\dot{\epsilon}$).

Blown Film Extrusion

Films were created with a lab-scale blown film extrusion line. The single screw extruder diameter is 1 inch and a length of 25:1, L:D. The metering zone is 10:1, L:D and has a square pitch (L_{pitch}=D_b) with a depth H of 0.065 inch, a flight thickness e of 0.14 inch and a helix angle of 17.7 degrees. The annular die has an outer diameter of 1 inch, and the geometry can be approximated by the dimensions in Figure 7.3. Pressure is measured in two locations – inside the die and in the inlet tube that connects the extruder to the die. The extruder pressure is rated at 1200 psi. The air flow is set for both the air ring and the internal bubble pressure. The air for the cooling ring is controlled by a pressure regulator and is measured in terms of inch water. The puller speed ranges from 0 to 0.2 m s^{-1}.

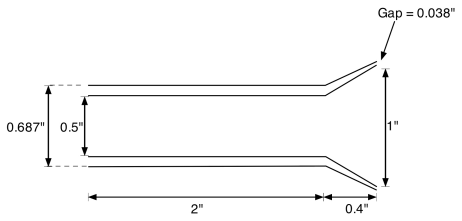

Figure 7.3: Approximate dimensions of a blown film extrusion die. Reproduced from a class handout.[257]

The extruder temperature was set at 180 °C, the die temperature at 160 °C, the RPM at 5.0, and the roller velocity at 0.06 m s^{-1}. A photo of the blown film extrusion process is shown in Figure 7.4 for the neat PDLLA 4060D. Marked are the machine direction (MD) and transverse direction (TD). For all samples, the BUR was maximized, but typically ranged from 1.0-1.5. The BUR was limited due to the propensity of the PLA to tear in the melt state. The most common point of tear was the location 180° away from the single screw entrance to the die. This problem became more prevalent as the diblock content

increased, to the point that Blend 5.0 could not be blown into films. The thickness of the final films ranged from 0.025 - 0.10 mm, as measured by a micrometer (resolution = 0.001 mm). Thickness variation is mainly attributed to inhomogeneous mass flow rate while exiting the die – the side closer to the single screw entrance to the die were consistently thicker than the side 180° away.

Using equation 7.3, the density of PLA at room temperature[160,161] and 170 °C,[258] and the final film measurements, the TUR was calculated to be 6.5-8.5. From this, v_{die} can be calculated (equation 7.2) to estimate the relevant shear rates ($\dot{\gamma}$ ~10-20 s^{-1}) with knowledge of the die dimensions. Because of the heterogeneous nature of the biaxial extension in which temperatures and velocities are changing, precise extensional rates are hard to predict; however, using basic dimensional arguments, relevant extensional rates range from 0.1 s^{-1} to 0.5 s^{-1} under these processing conditions. Both these shear and extensional rates are close to what may occur on a larger scale industrial blown film extrusion line, but fall on the low end of the spectrum.

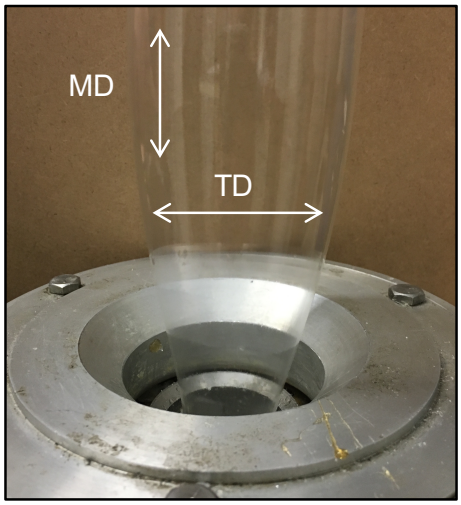

Figure 7.4: Photo of blown film extrusion of PDLLA 4060D. Marked are the machine direction (MD) and transverse direction (TD). No frost line was observed.

Transmission electron microscopy (TEM)

TEM was employed to characterize the block copolymer morphology in blown films. The free-standing films were first embedded in medium grade LR White Resin (Ted Pella) to create block specimens. Then, specimens were cryo-sectioned at -100 °C using a Reichert UltraCut S ultramicrotome (Model FC-S cryo-attachments) fitted with a Micro Star diamond knife, producing ultrathin frozen sections (ca. 70 – 90 nm) that were collected onto copper grids. TEM grids were then vapor stained for 15 min with 0.5 wt.% RuO_4 aqueous solution, before being imaged using an FEI Tecnai T12 transmission electron microscope with a 120 kV accelerating voltage.

Mechanical testing

Uniaxial tensile tests were performed on a Schimadzu Autograph AGSS17 X series tensile tester with a cross-head moving velocity of 5 mm min^{-1} according to ASTM Standard D882-12: Standard Test Method for Tensile Properties of Thin Plastic Sheeting. Dog-bone samples were prepared with a total length of 38 mm, a gauge length of 12 mm, and width of 5.0 mm in the both the machine direction (MD) and transverse direction (TD) to look at the effect of anisotropy. The engineering stress ($\sigma = F/A_0$) was calculated from the measured force (F) and the initial cross-section area (A_0). Strain ($\epsilon = \Delta(l)/l_0$) was obtained from the change in grip-to-grip distance (l) and initial gauge length (l_0). Young's modulus ($E = \sigma/\epsilon$) was determined from the linear portion of the stress-strain curve. Toughness was taken as the area under the stress-strain curve. For each sample, the data reported are the average and standard deviation of at least six specimens.

Trouser tests were conducted on a Schimadzu Autograph AGSS17 X series tensile tester with a cross-head moving velocity of 10 mm min^{-1} according to ASTM Standard D1938-14: Tear-Propagation Resistance (Trouser Tear) of Plastic Film and Thin Sheeting by a Single-Tear Method. Force *versus* time was plotted, and the force was taken as the average value in the plateau region of the curve. For each sample, the data reported are the average

and standard deviation of at least five specimens. Outside of the crack zone, the final dimensions were the same as at the start of test; thus, deformation of the material did not contribute to the tear strength, a potential problem for ductile materials.[259]

7.4 Blend characterization

Characterization of the neat PLA 4060D, PEO-PBO diblock, and the blends are shown in Table 7.1. In the nomenclature used here, the blend samples are designated "Blend" followed by the wt.% of diblock in the blend (e.g. Blend-1.25 has 1.25 wt.% of the PEO-PBO diblock). This commercial grade of PLA is amorphous, so there is no crystallization or melting temperature. To emphasis this fact, it will henceforth be referred to as "PDLLA." This grade without crystallization was chosen intentionally; the toughening effect of the block copolymer micelles was only observed when semicrystalline PLLA was quenched fast enough to avoid crystallization.[138] Using amorphous PDLLA will avoid the potential confounding effects of crystallization on processability, rheological characterization, and final film mechanical properties.

Table 7.1: Characterization of neat commercial PDLLA 4060D, the PEO-PBO diblocks, extruded PDLLA 4060D, and PDLLA/diblock blends

Sample	[a] M_n [kg mol^{-1}]	[b] $M_{n,PS}$ [kg mol^{-1}]	[b] $Đ$	[c] f_{PEO}	[d] T_g [°C]
Neat PDLLA	63.6	106	2.0	–	57
PEO-PBO	7.0	8.2	1.10	0.32	-71[e]
Extruded PDLLA	–	105	2.1	–	–
Blend-1.25	–	79.6	2.7	–	56
Blend-2.5	–	68.2	3.1	–	57
Blend-5.0	–	53.2	3.6	–	53

[a]Determined from ^{1}H NMR end-group analysis. [b]Determined from room temperature SEC in THF. [c]Calculated from ^{1}H NMR and published densities ρ_{PEO} = 1.07 g cm^{-3}, ρ_{PBO} = 0.92 g cm^{-3}.[138] [d]Determined using DSC during the second heating cycle. [e]Only one T_g is observed; this value is known to be close to the T_g of both PEO and PBO homopolymers.

No appreciable change in M_n was observed between the neat PDLLA and the extruded

PDLLA control. This suggests that very little or no degradation occurs during melt mixing at the specified conditions (180 °C for 2 min). The decrease in M_n for the blends, therefore, is due to the presence of the low molecular weight diblocks. This notion is supported by the fact that the M_w of the blends (taken by multiplying M_n by $Đ$) is nearly identical across all samples. Glass transitions or melting peaks from the PBO-PEO diblocks in the blends were not observed; this suggests good dispersion, although the low concentration of diblock may mask these features.

7.5 Rheology of blends

7.5.1 Shear rheology

Master curves for the linear dynamic storage (G') and loss (G'') moduli were constructed by employing the principles of time-Temperature superposition (tTs) (Figure 7.5a). Specifically, oscillatory shear data were taken at various temperatures and the $\tan\delta$ data were shifted horizontally to a reference temperature of 120 °C to obtain the appropriate shift factors (a_T). The shift factors were then used to horizontally shift G' and G'' with no vertical shift. The PDLLA 4060D has linear viscoelastic behavior typical of an entangled polymer melt with a longest relaxation time (τ_d) estimated as 0.3 s.

The LVE behavior of the three blends is nearly identical to the neat PLA with very similar longest relaxation times. Minor differences are observed for Blend 5.0 which has a slightly lower viscosity, as shown in Figure 7.5b. This origin could be two-fold. Very small amounts of degradation impossible to detect in SEC may have occurred during melt mixing. Because zero-shear viscosity is extremely sensitive to molecular weight for entangled polymers ($\eta_0 \sim M_w^{3.4}$), this small amount of degradation could have a large impact on the final rheology. Another potential cause for this lower viscosity may arise from wetting of the polymer brush on the micelle surface as observed by Jones et al. for small quantities of poly(ethylene-*b*-ethylethylene) diblocks added to polypropylene.[260]

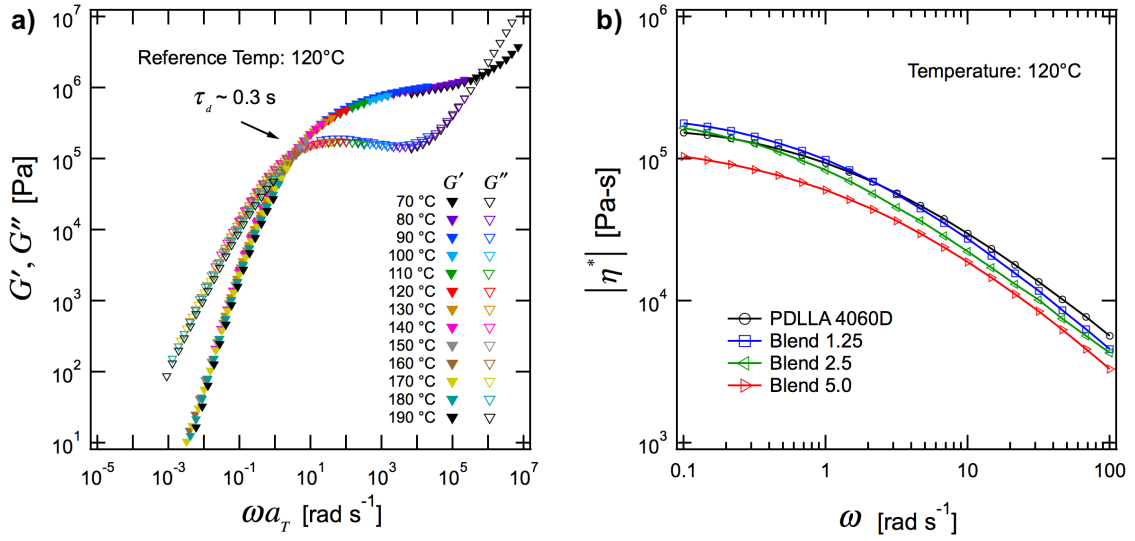

Figure 7.5: a) Master curves for the linear dynamic storage (G') and loss (G'') moduli of PDLLA 4060D, and b) Complex viscosity of neat and modified PLA at 120 °C.

7.5.2 Extensional rheology

The extensional rheological behavior of the neat PDLLA and the three blends was investigated at $\dot{\epsilon} = 1$ s^{-1} and a temperatures ranging from 100 °C to 180 °C. These temperatures correspond to actual processing conditions during the blown film extrusion process. The Hencky strain rate used is slightly higher than the predicted values for the production of the films studied here; however, it serves as a more relevant rate for blown film extrusion in general. As expected for a linear polymer at modest extension rates, no strain hardening is observed for PDLLA 4060D (Figure 7.6a). At 160 and 180 °C, the extensional viscosity is below the recommended range highlighted in section 7.4.3. In addition, the Hencky strains at break range from 2.5 - 2.8, less than ideal values of 3.0 or more. For these three reasons (no strain hardening, low viscosity at high temperatures, and low strain at break), it is no surprise that PLA 4060D is a difficult material from which to blow films.

Virtually no differences in the extensional behavior was observed for the three blends compared to the neat PLA; example data at 120 °C is shown in Figure 7.6b. Like with the

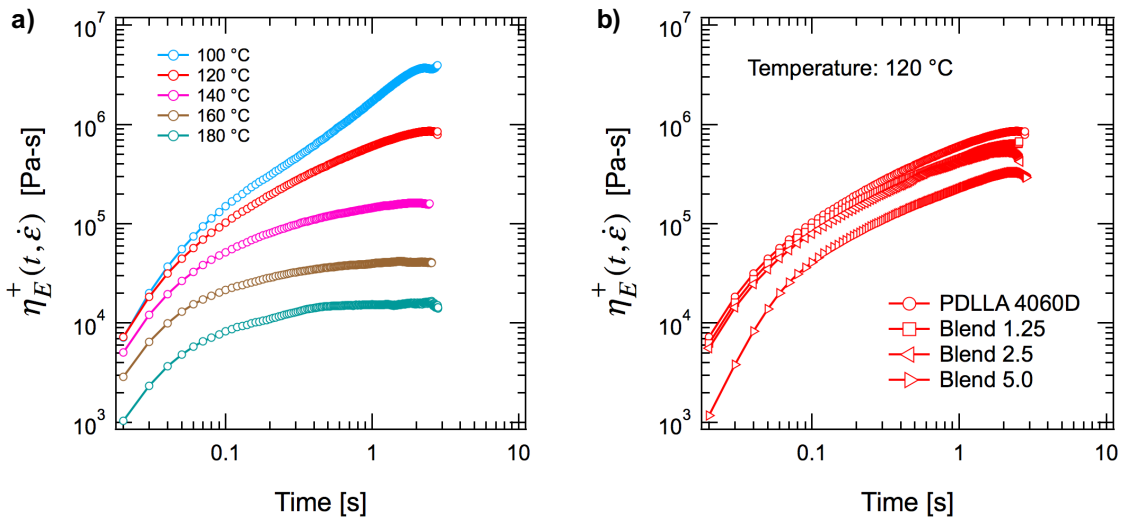

Figure 7.6: a) Extensional rheology of PDLLA 4060D at $\dot{\epsilon} = 1$ s^{-1} at a variety of temperatures, and b) extensional rheology of PDLLA 4060D and the three blends at at $\dot{\epsilon} = 1$ s^{-1} and 120 °C.

shear data, the viscosity of blend 5.0 is slightly lower than the other samples. Again, it is unclear if this is an effect of degradation or the higher percentage of the diblock.

7.6 Mechanical properties of the blends

7.6.1 Tensile testing: compression molded samples

Before blends were blown into films, Blend-2.5 was compression molded into dog-bones for tensile testing. This was to verify that under the same processing conditions, the block polymer micelles toughened amorphous PDLLA 4060D in qualitatively the same manner as the semicrystalline PLLA 2003D used in the literature. The results are shown in Figure 7.7 in which the blend with PLLA 2003D is labelled "PLLA Blend-2.5." The two blends show qualitatively the same behavior. The difference in σ_y is attributed to the different dog-bone dimensions and testing conditions used: Blend 2.5 was done in the same manner as designated in chapter 4.2, while the data for "PLLA Blend-2.5" followed ASTM Standard

D1708.

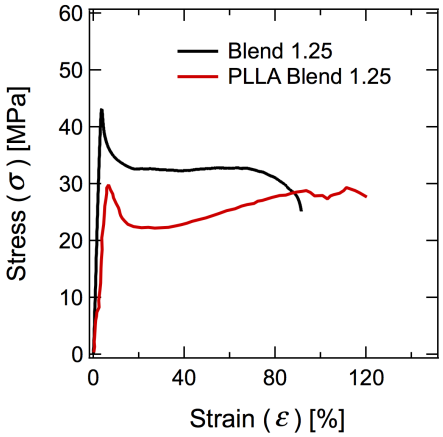

Figure 7.7: Tensile test data from compression molding. The red curve for "PLLA Blend-2.5" is reproduced from the literature.[138]

7.6.2 Tensile testing: blown film samples

The mechanical properties of films blown from the neat PDLLA, Blend 1.25, and Blend 2.5 were probed via tensile testing in both the machine direction (MD) and transverse direction (TD). The final data can be found in Figure 7.8, and the relevant properties are summarized in Table 7.2. Significant anisotropy occurred for all three samples affecting almost all their mechanical properties. The strain at break (ϵ_b), stress at break (σ_b), and yield stress (σ_{yield}) were consistently greater in the MD than the TD by a factor of 2, and toughness was higher by a factor of 3-4. This is attributed to significant orientation in the MD, due to the the relatively high FR ($\geq$ 5.0) used during processing and is a commonly known phenomenon.[252] TEM images show that the micelles are also oriented in the MD (Figure 7.9) and that these changes are not due solely to orientation of the polylactide chains.

Interestingly, the neat PDLLA sample have values for E and σ_b much lower than the reported values for amorphous PLA of 3.90 GPa and 44 MPa, respectively.[129] This is a

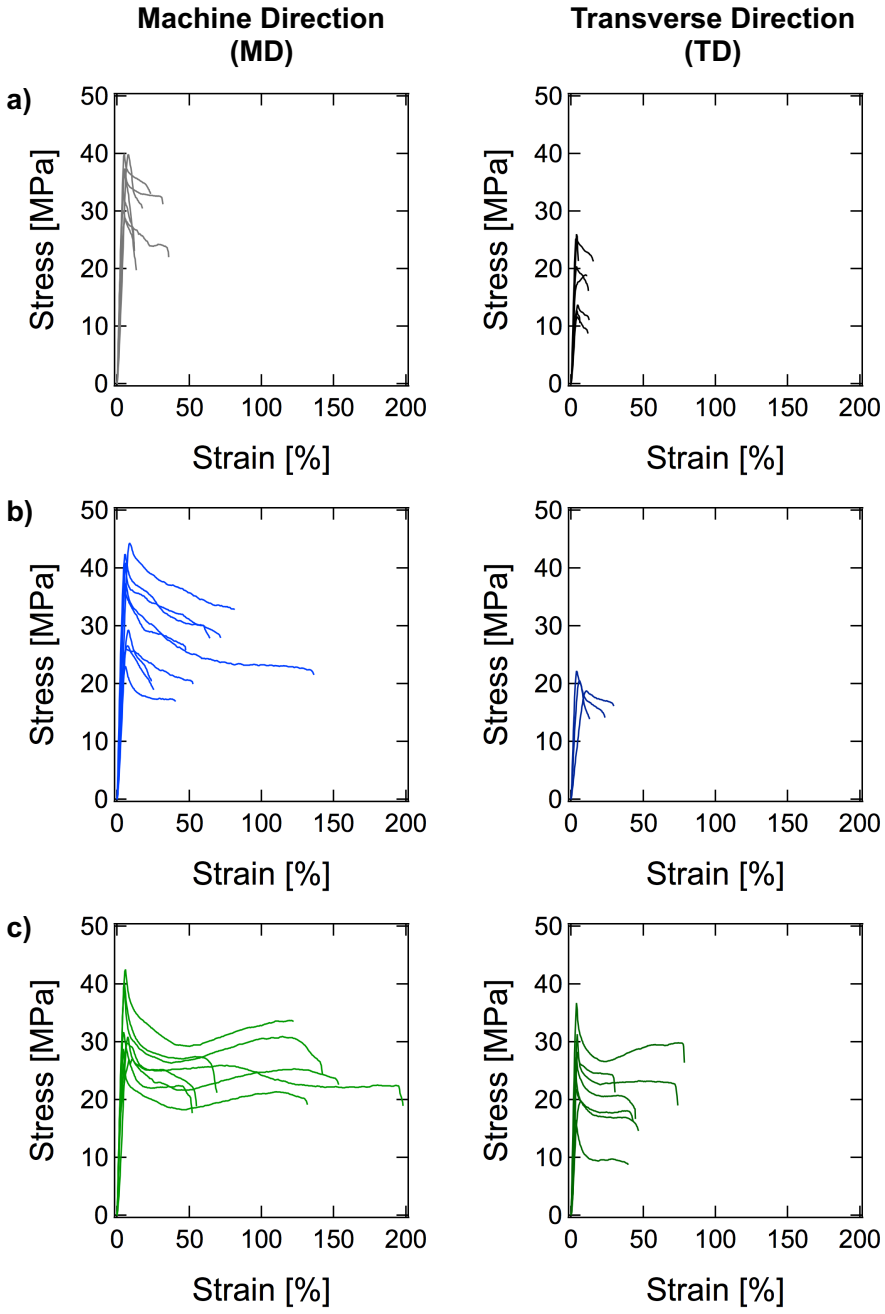

Figure 7.8: Tensile testing of blown films of a) Neat PDLLA, b) Blend-1.25, and c) Blend-2.5.

Table 7.2: Summary of the mechanical properties obtained from tensile testing on blown films of the neat and modified PDLLA 4060D

Sample	Direction	E [MPa]	ϵ_b [%]	σ_b [MPa]	σ_{yield} [MPa]	Toughness [MJ m^{-3}]
Neat PLA	MD	700 ± 200	21 ± 10	26 ± 15	35 ± 5	5.7 ± 2.9
	TD	510 ± 170	11 ± 4	15 ± 5	18 ± 6	1.5 ± 0.9
Blend 1.25	MD	560 ± 240	60 ± 35	24 ± 5	34 ± 8	17 ± 11
	TD	470 ± 210	23 ± 7	17 ± 5	23 ± 4	4.1 ± 1.8
Blend 2.5	MD	800 ± 240	120 ± 50	22 ± 5	34 ± 6	29 ± 13
	TD	740 ± 300	45 ± 23	28 ± 5	26 ± 7	9.4 ± 6.9

All measurements represent the average with standard deviations of at least five runs.

topic worthy of further exploration, but is speculated to be associated with the processing conditions. Encouragingly, ϵ_b and toughness increase as the diblock content increases. Between films of the neat PDLLA and Blend 2.5, ϵ_b and toughness increase 5× in both MD and TD. This is a very promising result given that neither the E, σ_b, nor σ_{yield} are sacrificed. The same basic trends observed by Li and coworkers from injection molded samples[138] hold true for blown film extrusion.

7.6.3 Tear-propagation resistance testing: blown film samples

The tear-propagation resistances of the films were assessed with the trouser tear test. Representative data for a specimen undergoing tear testing are shown in Figure 7.10 from which the tear-propagation force is taken as the average force in the plateau region. The results for the three samples in MD and TD are depicted in Figure 7.11. Although the standard deviations of the data are large, the basic trend is that the tear-propagation resistance decreases as the diblock content increases, and there is no appreciable difference between MD and TD for a given sample. This is consistent with the qualitative observation that the blends tore more easily in the melt state; however, there is not necessarily any correlation to the solid state and melt state mechanical behavior. It is important to note that trouser tear test only measures the force needed to *propagate* a tear, and that creation of a tear is a fundamentally different phenomenon.

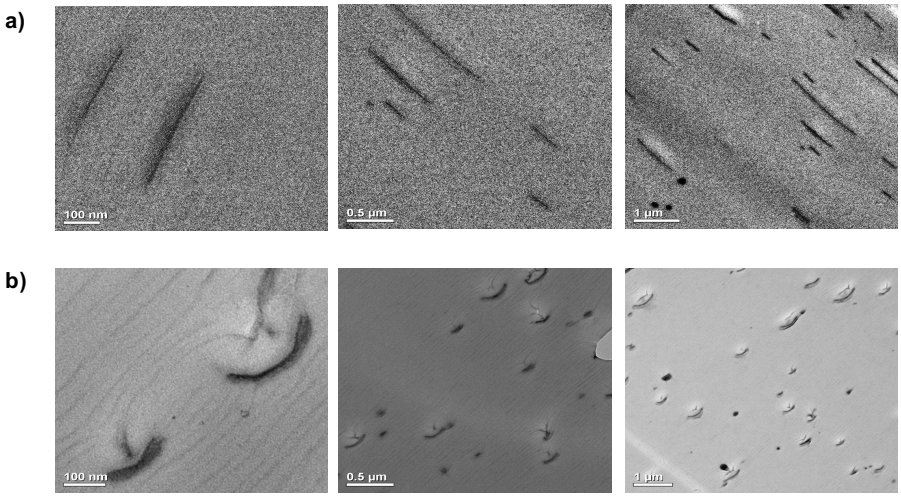

Figure 7.9: TEM images of a) blown films of Blend-2.5 showing anisotropy and stretching of the micelles in the MD, and b) compression molded films of PLLA Blend-2.5 in which the micelles are not stretched. Images taken by Tuoqi Li.

7.7 Branching PLA for blown film extrusion: preliminary results

As stressed earlier in this chapter, extensional rheology plays a pivotal role in bubble stability in blown film extrusion. Although it is possible to blow films out of PDLLA 4060D, bubble stability can only be attained under certain processing conditions due to the poor melt strength and lack of strain hardening. Additionally, because of the propensity for the PDLLA/diblock blends to tear, the processing window is even smaller for these materials. Thus, it is of particular interest to modulate the extensional behavior in order to expand the window of processability.

To the best knowledge of the author, only very recently have some looked at improving the processability of PLA specifically for blown film extrusion, the first publication coming in 2014.[261] In this work, the authors used Joncryl, a commercial copolymer with multiple epoxy functional groups, to branch commercial PLA via reactive extrusion. The

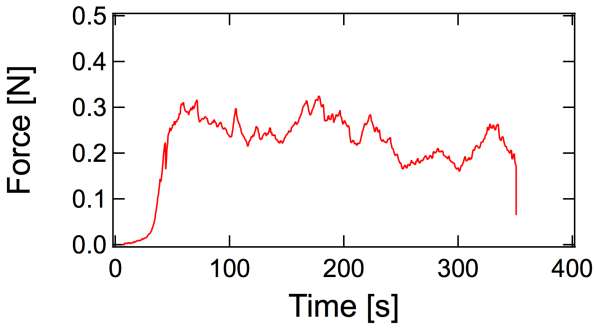

Figure 7.10: Representative data of a trouser tear test (Blend-1.25, MD).

resulting branched structure could achieve BURs almost double that of the neat PLA, and this was attributed to both an increase in melt strength and the onset of strain hardening. Plasticizers were also incorporated to increase the crystallization kinetics of PLA, as factor which widened the processing window further. The bulk of the remaining literature also use Joncryl or similar multifunctional epoxy coupling agents and have seen comparable results.[150,262] Although an attractive approach, epoxide functional groups have relatively slow reaction kinetics until temperatures are attained in which degradation occurs simultaneously,[263] making the resulting material difficult to control. Another approach that has been adopted is to polymerize branched structures via ring-opening polymerization from multifunctional initiators in which some of the materials were poly(L-lactide) and some were poly(D-lactide).[264] The varying stereoisomers created stereocomplexes with a T_m = 230 °C, and when combined with the branched structures, lead to more dramatic extensional hardening. Although bubble stability was improved, the economics of such an approach are not too attractive as the "D" isomer is more expensive than than the "L" isomer due to preferred stereochemistry during production.[265]

Due to these limitations, a simple, economic, and controlled approach has been investigated at the University of Minnesota that utilizes multifunctional aziridines rather than epoxides.[266] The aziridine functional groups can react with carboxylic acids at near 100% conversion in air with no side reactions within minutes[267] By first modifying the hydroxyl

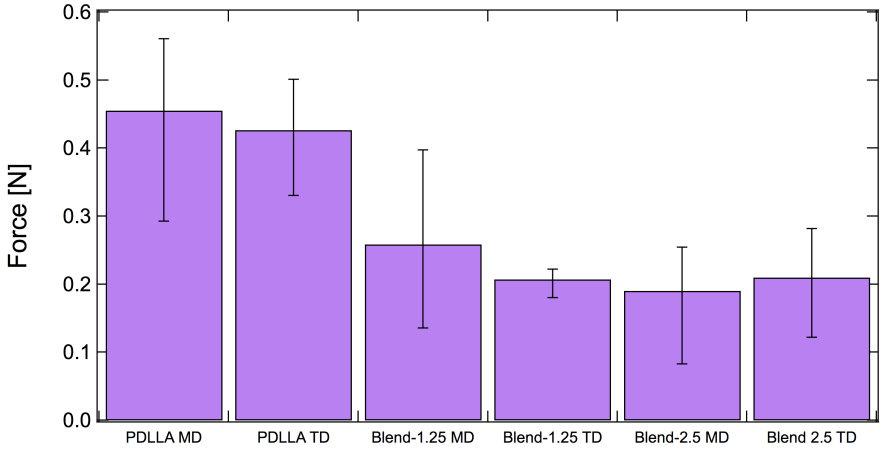

Figure 7.11: Trouser tear results for neat PDLLA 4060D, Blend-1.25, and Blend 2.5 in both the machine direction (MD) and transverse direction (TD). Shown is average tear-propagation resistance measured in Newtons of at least five specimens. Error bars are standard deviations.

end groups of PLA with dianhydrides, subsequent reactions with the multifunctional aziridine leads to structures with long chain branching.[266] This approach has been completed in batch mixers, but had not been attempted yet in a continuous process or scaled to quantities amenable to blown film extrusion.

Before adopting this two-step strategy, first the reaction between PLA and the multifunctional aziridine was adopted to ensure the reaction worked similarly as previous reports with the batch mixers. After considerable troubleshooting, the liquid feed port equipped with the angled port adapter provided the most successful feed location. This feed method allowed for the reactant solution to be fed directly into the polymer melt, ensuring effective dispersion and adoption into the melt. The results of these preliminary reactions are highlighted in Table 7.3. Increases in the molecular weight from SEC provides strong evidence that the multifunctional aziridine coupled the commercial PLA. The highest molecular weight was achieved by adding 1 stoichiometric equivalent of the multifunctional aziridine. As the multifunctional aziridine has a functionality ∼3, one stoichiometric equivalent refers

to one mole of the multifunctional aziridine to three moles of PLA. Adding more or less stoichiometric equivalents lead to less coupling, as would be expected from theory, lending the impression that the reaction is working as anticipated.

Table 7.3: Summary of SEC results from the reaction of PDLLA 4060D with a multifunctional aziridine

Sample	[a]Multifunctional aziridine added [Stoich. equiv.]	[b]$M_{n,PS}$ [kg mol^{-1}]	[b]$Đ$
Neat PDLLA	–	106	2.0
PLA-tAz-0.5	0.5	142	1.9
PLA-tAz-1.0	1.0	160	1.7
PLA-tAz-2.0	2.0	138	1.7

[a]Amount of the multifunctional aziridine is measured in terms of stoichiometric equivalents relative to the reactive end groups. For example, 1 mole of tri-aziridine corresponds with 3 moles of PLA. [b]Measured with SEC with an RI detector in THF at room temperature.

7.8 Conclusions and future work

This chapter has explored an approach to produce commercially viable films out of polylactide via blown film extrusion. Low molecular weight PEO-PBO diblocks were melt blended with commercial amorphous PDLLA at 1.25, 2.5 and 5 wt.% loadings. The resulting thermal properties, shear rheology, and extensional rheology were nearly identical for the blends with the neat PDLLA. These blends were then blown into films. It was found that the blends had slightly worse processability than the neat PDLLA, although processability of all materials was poor, attributed to the low melt strength. The mechanical properties of the films were measured with tensile and Trouser tear tests. The films had significant anisotropy from processing, yet the blends produced films that were up to 4× tougher than the neat PLA with no significant decrease in modulus. Tear propagation resistance for the

films made from the blends, though, was slightly worse. Very preliminary results demonstrate the feasibility of using multifunctional aziridine to branch PLA via reactive extrusion in a twin screw extruder.

There is a great deal of opportunity on this project. Further characterization of the mechanical properties of the films would be of interest. Drop-dart impact testing is a standard in the industry,[150] yet the small size of the lab-scale blown film extrusion has prevented the use of ASTM standard testing.[268] Other relevant industrial tests worthy of consideration include Elmendorf tear (tear-propagation resistance)[269] Graves tear (tear-initiation resistance)[270] and slow rate penetration resistance tests.[271] More fundamental tests such as the essential work of ductile fracture[272] could help bring insight to how the micelles toughen the thin films.

Finally, successfully integrating long-chain branching into the PDLLA is key. This would greatly expanded the processing window and allow for a more detailed investigation on the relationships between processing conditions and the final blend mechanical properties. As the TEM images in Figure 7.9 indicate, the extensional rates and FR surely affect the configuration of the micelles in the resulting films. The branched nature of the polymer itself could have beneficial on the mechanical properties, and the lack of crystallization in PDLLA make it a great candidate for this type of study – the literature on polyethylene films typically ignores polymer architecture due to the confounding effects of crystallization and crystallite orientation.

Chapter 8

Summary

This thesis looked at the rheological design of sustainable block copolymers, with a particular focus on polylactide-based materials for specific commodity applications in which extensional flows play a major role. Brief summaries of the chapters are presented here.

Chapter 2: The Rheology of Chewing Gum

Commercial chewing and bubble gum were subjected to the full gamut of rheological tests, exploring the linear and nonlinear rheological behavior in both shear and extension. Their unique rheological fingerprint was identified – chewing and bubbles gums are *critical-gel* fluids with *high extensibility*. One key distinction between chewing and bubble gums is that the latter consistently had higher stresses at break during extension, attributed to their need to be blown into large bubbles during use. These findings allow for the development of next-generation chewing gums that can incorporate alternate materials while maintaining the same sensory feel.

Chapter 3: Block Copolymer Blends for Chewing Gum Applications

Building off chapter 2, blends of block copolymers were designed for use in chewing gum applications. Using poly(D,L-lactide) (L) and poly(ϵ-decalactone) (D), elastomeric low molecular weight DL dibocks, moderate molecular weight DL diblocks, high molecular weight LDL triblocks, and high molecular weight $(LDL)_n$ multiblocks were synthesized using ring opening transesterfication polymerization (ROTEP). A series of blends consisting of 80 wt.% diblock and 20 wt.% triblock were made to study the effect of molecular weight and polymer composition on the resulting linear and nonlinear rheology in shear and extension. These blends were fit to models from chapter 2 to assess their viability as chewing gum bases. Preliminary results for blends of DL diblocks and $(LDL)_n$ multiblocks show how manipulating the polymer architecture can lead to remarkable elongations and break while simultaneously improving processability.

Chapter 4: Branched Multiblock Polymers from Coupling 4-arm Star Diblocks

To improve the toughness and processability of poly(lactic acid) (PLA), a branched multiblock polymer was prepared from D,L-lactide and ϵ-decalactone. A hydroxy telechelic four-arm star poly(ϵ-decalactone-*b*-D,L–lactide) diblock was synthesized using sequential ring opening transesterfication polymerization (ROTEP) and coupled using a substoichiometric amount of sebacoyl chloride to obtain a segmented multiblock with a comb-like architecture. Small angle x-ray scattering (SAXS) and transmission electron microscopy (TEM) revealed that this branched multiblock was microphase separated, but lacked long-range order. Unlike a linear multiblock of similar mass, the branched material demonstrated significant extensional hardening in the disordered state, suggesting much improved processability in polymer processing methods that require fast elongational flows. Additionally, the branched multiblock material exhibited remarkable tensile toughness. This simple synthetic approach allows for simultaneous control of mechanical and rheological properties using a single macromolecular architecture to address key practical issues with PLA.

Chapter 5: Branched Polyesters from Coupling Diols

This chapter continues the work from chapter 4 to explore an alternate and potentially more versatile route to create branched multiblock polymers via coupling. Theory dictates that coupling A_2 diols with a substoichiometric amount of mixtures of B_2 and B_3 coupling agents can lead to multiblocks with greater connectivity before the onset of gelation. Two different molecular weight PLA diols were used as model systems, and each was coupled with itself using varying ratios of B_2 and B_3 molecules. Results suggest that given sufficient entanglements, high coupling efficiency is more important than the starting molecular weight of the diol in dictating the extent of extensional hardening. Sustainable triblocks were synthesized and shown to be viable candidates for this coupling strategy.

Chapter 6: Pressure-Sensitive Adhesives Based on a Poly(lactide-*b*-β-methyl-δ-valerolactone-*b*-lactide) Triblock Copolymer

A poly(lactide-*b*-β-methyl-δ-valerolactone-*b*-lactide) (LVL) triblock copolmyer was used to create fully sustainable pressure-sensitive adhesives (PSAs) that have promising commercial viability due to the low cost of both monomers. A tackifier which preferentially solubilized the midblock was used to lower the modulus of the LVL triblock to satisfy the Dahlquist criterion. In addition to oscillatory shear, nonlinear shear creep and uniaxial extensional tests were run and correlated to tack, 180° peel, and shear resistance adhesion results. The resulting PSAs were shown to be potential candidates for general-use PSAs like post-it notes.

Chapter 7: Blown Film Extrusion of PLA-based Materials

This chapter explored an approach to produce commercially viable films out of polylactide via blown film extrusion. Low molecular weight PEO-PBO diblocks, known to toughen PLA, were melt blended with commercial amorphous PDLLA. The thermal properties, shear rheology, and extensional rheology were nearly identical between the blends and the

neat PDLLA, yet it was found that the blends had slightly worse processability. Films produced from the blends were up to 4× tougher in tensile testing than the neat PLA in both machine and transverse directions with no significant decrease in modulus. However, tear-propagation resistance for the films made from the blends was slightly worse. Very preliminary results demonstrate the feasibility of using multifunctional aziridine to branch PLA via reactive extrusion in a twin screw extruder in an effort to improve processability.

References

[1] Macosko, C.; Larson, R. *Rheology: Principles, Measurements, and Applications*; Wiley-VCH: New York, 1994; pp 1–4.

[2] Larson, R. G. *The Structure and Rheology of Complex Fluids*; Oxford University Press: New York, 1999; pp 1–21, 629.

[3] Laba, D., Ed. *Rheological Properties of Cosmetics and Toiletries*; CRC Press, 1993.

[4] Flatt, R. J.; Martys, N.; Bergström, L. The Rheology of Cementitious Materials. *MRS Bulletin* **2004**, *29*, 314–318.

[5] Spitael, P.; Macosko, C. W. Strain Hardening in Polypropylenes and its Role in Extrusion Foaming. *Polymer Engineering & Science* **2004**, *44*, 2090–2100.

[6] Francis, L. *Materials Processing: A Unified Approach to Processing of Metals, Ceramics, and Polymers*, 1st ed.; Elsevier, 2016.

[7] Duperrier, S.; Bernard, S.; Calin, A.; Sigala, C.; Chiriac, R.; Miele, P.; Balan, C. Design of a Series of Preceramic B-Tri(methylamino)borazine-Based Polymers as Fiber Precursors: Shear Rheology Investigations. *Macromolecules* **2007**, *40*, 1028–1034.

[8] Alarcón, T.; Byrne, H. M.; Maini, P. K. A Design Principle for Vascular Beds: The Effects of Complex Blood Rheology. *Microvascular Research* **2005**, *69*, 156–172.

[9] Vega, C.; Ubbink, J. Molecular Gastronomy: A Food Fad or Science Supporting Innovative Cuisine? *Trends in Food Science & Technology* **2008**, *19*, 372–382.

[10] Lade, R. K.; Musliner, A. D.; Macosko, C. W.; Francis, L. F. Evaluating Sag Resistance with a Multinotched Applicator: Correlation with Surface Flow Measurements and Practical Recommendations. *Journal of Coatings Technology and Research* **2015**, *12*, 809–817.

[11] Ewoldt, R. H.; Clasen, C.; Hosoi, A.; McKinley, G. H. Rheological Fingerprinting of Gastropod Pedal Mucus and Synthetic Complex Fluids for Biomimicking Adhesive Locomotion. *Soft Matter* **2007**, *3*, 634–643.

[12] Franck, A. The ARES-EVF: Option for Measuring Extensional Viscosity of Polymer Melts. TA Instruments, 2011.

[13] Xu, Y.; Thurber, C. M.; Lodge, T. P.; Hillmyer, M. A. Synthesis and Remarkable Efficacy of Model Polyethylene-*graft*-Poly(methyl methacrylate) Copolymers as Compatibilizers in Polyethylene/Poly(methyl methacrylate) Blends. *Macromolecules* **2012**, *45*, 9604–9610.

[14] Sasaki, M.; Adachi, M.; Kato, Y.; Fujii, S.; Nakamura, Y.; Urahama, Y.; Sakurai, S. Adhesion Property and Morphology of Styrene Triblock/Diblock Copolymer Blends. *Journal of Applied Polymer Science* **2010**, *118*, 1766–1773.

[15] Shin, J.; Martello, M. T.; Shrestha, M.; Wissinger, J. E.; Tolman, W. B.; Hillmyer, M. A. Pressure-Sensitive Adhesives from Renewable Triblock Copolymers. *Macromolecules* **2010**, *44*, 87–94.

[16] Adedeji, A.; Grünfelder, T.; Bates, F.; Macosko, C.; Stroup-Gardiner, M.; Newcomb, D. Asphalt Modified by SBS Triblock Copolymer: Structures and Properties. *Polymer Engineering & Science* **1996**, *36*, 1707–1723.

[17] Bates, F. S.; Hillmyer, M. A.; Lodge, T. P.; Bates, C. M.; Delaney, K. T.; Fredrickson, G. H. Multiblock Polymers: Panacea or Pandora's Box? *Science* **2012**, *336*, 434–440.

[18] Lee, I.; Bates, F. S. Synthesis, Structure, and Properties of Alternating and Random Poly(styrene-*b*-butadiene) Multiblock Copolymers. *Macromolecules* **2013**, *46*, 4529–4539.

[19] Meuler, A. J.; Hillmyer, M. A.; Bates, F. S. Ordered Network Mesostructures in Block Polymer Materials. *Macromolecules* **2009**, *42*, 7221–7250.

[20] Bates, C. M.; Maher, M. J.; Janes, D. W.; Ellison, C. J.; Willson, C. G. Block Copolymer Lithography. *Macromolecules* **2014**, *47*, 2–12.

[21] Lynd, N. A.; Meuler, A. J.; Hillmyer, M. A. Polydispersity and Block Copolymer Self-Assembly. *Progress in Polymer Science* **2008**, *33*, 875–893.

[22] Dalsin, S. J. Bottlebrush Polymers: Synthesis, Rheology, and Self-Assembly. Ph.D. Dissertation, University of Minnesota, 2016.

[23] Hopewell, J.; Dvorak, R.; Kosior, E. Plastics Recycling: Challenges and Opportunities. *Philosophical Transactions of the Royal Society B: Biological Sciences* **2009**, *364*, 2115–2126.

[24] Thompson, R. C.; Swan, S. H.; Moore, C. J.; Vom Saal, F. S. Our Plastic Age. *Philosophical Transactions of the Royal Society B: Biological Sciences* **2009**, *364*, 1973–1976.

[25] World Economic Forum, Ellen MacArthur Foundation, and McKinsey & Company. The New Plastics Economy – Rethinking the Future of Plastics. 2016, http://www.ellenmacarthurfoundation.org/publications.

[26] Barnes, D. K.; Galgani, F.; Thompson, R. C.; Barlaz, M. Accumulation and Fragmentation of Plastic Debris in Global Environments. *Philosophical Transactions of the Royal Society B: Biological Sciences* **2009**, *364*, 1985–1998.

[27] Gregory, M. R. Environmental Implications of Plastic Debris in Marine Settings—Entanglement, Ingestion, Smothering, Hangers-on, Hitch-hiking and Alien Invasions. *Philosophical Transactions of the Royal Society of London B: Biological Sciences* **2009**, *364*, 2013–2025.

[28] North, E. J.; Halden, R. U. Plastics and Environmental Health: The Road Ahead. *Reviews on Environmental Health* **2013**, *28*, 1–8.

[29] Hernández, N.; Williams, R. C.; Cochran, E. W. The Battle for the "Green" Polymer. Different Approaches for Biopolymer Synthesis: Bioadvantaged vs. Bioreplacement. *Organic & Biomolecular Chemistry* **2014**, *12*, 2834–2849.

[30] Williams, C. K.; Hillmyer, M. A. Polymers from Renewable Resources: A Perspective for a Special Issue of Polymer Reviews. *Polymer Reviews* **2008**, *48*, 1–10.

[31] Anastas, P.; Eghbali, N. Green Chemistry: Principles and Practice. *Chemical Society Reviews* **2010**, *39*, 301–312.

[32] Tang, S. L.; Smith, R. L.; Poliakoff, M. Principles of Green Chemistry: Productively. *Green Chemistry* **2005**, *7*, 761–762.

[33] Tsui, A.; Wright, Z. C.; Frank, C. W. Biodegradable Polyesters from Renewable Resources. *Annual Review of Chemical and Biomolecular Engineering* **2013**, *4*, 143–170.

[34] Garlotta, D. A Literature Review of Poly(lactic acid). *Journal of Polymers and the Environment* **2001**, *9*, 63–84.

[35] Drumright, R. E.; Gruber, P. R.; Henton, D. E. Polylactic Acid Technology. *Advanced Materials* **2000**, *12*, 1841–1846.

[36] Wang, S.; Cui, W.; Bei, J. Bulk and Surface Modifications of Polylactide. *Analytical and Bioanalytical Chemistry* **2005**, *381*, 547–556.

[37] Ikada, Y.; Tsuji, H. Biodegradable Polyesters for Medical and Ecological Applications. *Macromolecular Rapid Communications* **2000**, *21*, 117–132.

[38] Gupta, A.; Kumar, V. New Emerging Trends in Synthetic Biodegradable Polymers–Polylactide: A Critique. *European Polymer Journal* **2007**, *43*, 4053–4074.

[39] Jamshidian, M.; Tehrany, E. A.; Imran, M.; Jacquot, M.; Desobry, S. Poly-Lactic Acid: Production, Applications, Nanocomposites, and Release Studies. *Comprehensive Reviews in Food Science and Food Safety* **2010**, *9*, 552–571.

[40] Liu, H.; Zhang, J. Research Progress in Toughening Modification of Poly(lactic acid). *Journal of Polymer Science Part B: Polymer Physics* **2011**, *49*, 1051–1083.

[41] Miller, S. A. Sustainable Polymers: Opportunities for the Next Decade. *ACS Macro Letters* **2013**, *2*, 550–554.

[42] Lim, L.-T.; Auras, R.; Rubino, M. Processing Technologies for Poly(lactic acid). *Progress in Polymer Science* **2008**, *33*, 820–852.

[43] Martinetti, L.; Mannion, A. M.; Voje Jr, W. E.; Xie, R.; Ewoldt, R. H.; Morgret, L. D.; Bates, F. S.; Macosko, C. W. A Critical Gel Fluid with High Extensibility: The Rheology of Chewing Gum. *Journal of Rheology* **2014**, *58*, 821–838.

[44] Doublier, J.; Launay, B. Rheology of Galactomannan Solutions: Comparative Study of Guar Gum and Locust Bean Gum. *Journal of Texture Studies* **1981**, *12*, 151–172.

[45] Sanchez, C.; Renard, D.; Robert, P.; Schmitt, C.; Lefebvre, J. Structure and Rheological Properties of Acacia Gum Dispersions. *Food Hydrocolloids* **2002**, *16*, 257–267.

[46] Yaseen, E.; Herald, T.; Aramouni, F.; Alavi, S. Rheological Properties of Selected Gum Solutions. *Food Research International* **2005**, *38*, 111–119.

[47] Whitcomb, P.; Macosko, C. Rheology of Xanthan Gum. *Journal of Rheology* **1978**, *22*, 493–505.

[48] Andersen, L.; Wittorff, H.; Storey, R.; Isaksen, A. Biodegradable Elastomers for Chewing Gum Base. U.S. Patent 20040142066 A1, 2002.

[49] Morgret, L.; Haas, M.; Xia, X.; Hillmyer, M.; Martello, M.; Macosko, C.; Martinetti, L.; Bates, F.; Lee, S.; Bunczek, M. Chewing Gum Compositions. U.S. Patent 20130052301 A1, 2010.

[50] Phillips, D.; Morgret, L.; Xia, X.; Shen, C. Chewing Gums Having Improved Removability Based on Linear Viscoelastic Shear Rheology. U.S. Patent 20120269924 A1, 2010.

[51] Mestres, J. In *Formulation and Production of Chewing and Bubble Gum*; Fritz, D., Ed.; Kennedy's Books: Loughton, Essex, 2006; pp 47–74.

[52] Fritz, D. In *Formulation and Production of Chewing and Bubble Gum*; Fritz, D., Ed.; Kennedy's Books: Loughton, Essex, 2006; pp 239–252.

[53] Estruch, R. In *Formulation and Production of Chewing and Bubble Gum*; Fritz, D., Ed.; Kennedy's Books: Loughton, Essex, 2006; pp 93–118.

[54] Ewoldt, R.; Winter, P.; McKinley, G. MITlaos version 2.1 Beta for MATLAB. Self-published, 2007.

[55] Ewoldt, R. H.; Hosoi, A.; McKinley, G. H. New Measures for Characterizing Nonlinear Viscoelasticity in Large Amplitude Oscillatory Shear. *Journal of Rheology* **2008**, *52*, 1427–1458.

[56] Rohm, H.; Weidinger, K.-H. Rheological Behaviour of Butter at Small Deformations. *Journal of Texture Studies* **1993**, *24*, 157–172.

[57] Aranguren, M. I.; Mora, E.; DeGroot Jr, J. V.; Macosko, C. W. Effect of Reinforcing Fillers on the Rheology of Polymer Melts. *Journal of Rheology* **1992**, *36*, 1165–1182.

[58] Phan-Thien, N.; Safari-Ardi, M. Linear Viscoelastic Properties of Flour–Water Doughs at Different Water Concentrations. *Journal of Non-Newtonian Fluid Mechanics* **1998**, *74*, 137–150.

[59] Chambon, F.; Winter, H. H. Linear Viscoelasticity at the Gel Point of a Crosslinking PDMS with Imbalanced Stoichiometry. *Journal of Rheology* **1987**, *31*, 683–697.

[60] Rouse Jr, P. E. A Theory of the Linear Viscoelastic Properties of Dilute Solutions of Coiling Polymers. *The Journal of Chemical Physics* **1953**, *21*, 1272–1280.

[61] Doi, M.; Edwards, S. F. *The Theory of Polymer Dynamics*; Oxford University Press, 1988; Vol. 73.

[62] Leibler, L.; Rubinstein, M.; Colby, R. H. Dynamics of Reversible Networks. *Macromolecules* **1991**, *24*, 4701–4707.

[63] Ferry, J. D. *Viscoelastic Properties of Polymers*; John Wiley & Sons, 1980.

[64] Ng, T. S.; McKinley, G. H. Power Law Gels at Finite Strains: The Nonlinear Rheology of Gluten Gels. *Journal of Rheology* **2008**, *52*, 417–449.

[65] Ng, T. S.; McKinley, G. H.; Ewoldt, R. H. Large Amplitude Oscillatory Shear Flow of Gluten Dough: A Model Power-Law Gel. *Journal of Rheology* **2011**, *55*, 627–654.

[66] Winter, H. H.; Mours, M. *Neutron Spin Echo Spectroscopy Viscoelasticity Rheology*; Springer, 1997; pp 165–234.

[67] Dealy, J. M.; Larson, R. G. *Structure and Rheology of Molten Polymers*; Hanser Publishers: Munich, 2006; pp 283, 352–356, 377–378, 389.

[68] Lefebvre, J.; Pruska-Kedzior, A.; Kedzior, Z.; Lavenant, L. A Phenomenological Analysis of Wheat Gluten Viscoelastic Response in Retardation and in Dynamic Experiments over a Large Time Scale. *Journal of Cereal Science* **2003**, *38*, 257–267.

[69] Tschoegl, N. W. *The Phenomenological Theory of Linear Viscoelastic Behavior: An Introduction*; Springer-Verlag: Berlin, 1989; Chapter 3.

[70] Hyun, K.; Wilhelm, M.; Klein, C. O.; Cho, K. S.; Nam, J. G.; Ahn, K. H.; Lee, S. J.; Ewoldt, R. H.; McKinley, G. H. A Review of Nonlinear Oscillatory Shear Tests: Analysis and Application of Large Amplitude Oscillatory Shear (LAOS). *Progress in Polymer Science* **2011**, *36*, 1697–1753.

[71] Hyun, K.; Kim, S. H.; Ahn, K. H.; Lee, S. J. Large Amplitude Oscillatory Shear as a Way to Classify the Complex Fluids. *Journal of Non-Newtonian Fluid Mechanics* **2002**, *107*, 51–65.

[72] Ewoldt, R. H.; Bharadwaj, N. A. Low-Dimensional Intrinsic Material Functions for Nonlinear Viscoelasticity. *Rheologica Acta* **2013**, *52*, 201–219.

[73] Cho, K. S.; Hyun, K.; Ahn, K. H.; Lee, S. J. A Geometrical Interpretation of Large Amplitude Oscillatory Shear Response. *Journal of Rheology* **2005**, *49*, 747–758.

[74] Bach, A.; Almdal, K.; Rasmussen, H. K.; Hassager, O. Elongational Viscosity of Narrow Molar Mass Distribution Polystyrene. *Macromolecules* **2003**, *36*, 5174–5179.

[75] Bhattacharjee, P.; Oberhauser, J.; McKinley, G.; Leal, L.; Sridhar, T. Extensional Rheometry of Entangled Solutions. *Macromolecules* **2002**, *35*, 10131–10148.

[76] Sentmanat, M.; Wang, B. N.; McKinley, G. H. Measuring the Transient Extensional

Rheology of Polyethylene Melts Using the SER Universal Testing Platform. *Journal of Rheology* **2005**, *49*, 585–606.

[77] Clasen, C.; Plog, J.; Kulicke, W.-M.; Owens, M.; Macosko, C.; Scriven, L.; Verani, M.; McKinley, G. H. How Dilute are Dilute Solutions in Extensional Flows? *Journal of Rheology* **2006**, *50*, 849–881.

[78] McKinley, G. H.; Sridhar, T. Filament-Stretching Rheometry of Complex Fluids. *Annual Review of Fluid Mechanics* **2002**, *34*, 375–415.

[79] Spiegelberg, S. H.; McKinley, G. H. Stress Relaxation and Elastic Decohesion of Viscoelastic Polymer Solutions in Extensional Flow. *Journal of Non-Newtonian Fluid Mechanics* **1996**, *67*, 49–76.

[80] Matsumiya, Y.; Watanabe, H.; Takano, A.; Takahashi, Y. Uniaxial Extensional Behavior of $(SIS)_p$-type Multiblock Copolymer Systems: Structural Origin of High Extensibility. *Macromolecules* **2013**, *46*, 2681–2695.

[81] Morgret, L. Science-Based Design of High-Performance Bubblegum. Ph.D. Dissertation, Northwestern University, 2005.

[82] Treloar, L. R. G. *The Physics of Rubber Elasticity*; Oxford University Press, USA, 1975.

[83] Mark, J. E. The Effect of Strain-Induced Crystallization on the Ultimate Properties of an Elastomeric Polymer Network. *Polymer Engineering & Science* **1979**, *19*, 409–413.

[84] Gisler, T.; Ball, R. C.; Weitz, D. A. Strain Hardening of Fractal Colloidal Gels. *Physical Review Letters* **1999**, *82*, 1064.

[85] Fleissner, M. Elongational Flow of HDPE Samples and Bubble Instability in Film Blowing. *International Polymer Processing* **1988**, *2*, 229–233.

[86] Field, G. J.; Micic, P.; Bhattacharya, S. N. Melt Strength and Film Bubble Instability of LLDPE/LDPE Blends. *Polymer International* **1999**, *48*, 461–466.

[87] Cassagnau, P. Melt Rheology of Organoclay and Fumed Silica Nanocomposites. *Polymer* **2008**, *49*, 2183–2196.

[88] Watanabe, H.; Sato, T.; Osaki, K.; Aoki, Y.; Li, L.; Kakiuchi, M.; Yao, M.-L. Rheological Images of Poly(vinyl chloride) Gels. 4. Nonlinear Behavior in a Critical Gel State. *Macromolecules* **1998**, *31*, 4198–4204.

[89] Cussler, E. L.; Moggridge, G. D. *Chemical Product Design*; Cambridge University Press, 2011.

[90] Olson, G. B. Designing a New Material World. *Science* **2000**, *288*, 993–998.

[91] Drobny, J. G. *Handbook of Thermoplastic Elastomers*; William Andrew Publishing/Plastics Design Library, 2007; p 9.

[92] Holden, G. *Understanding Thermoplastic Elastomers*; Hanser Publishers, 2000; pp 97–104.

[93] Weidisch, R.; Gido, S.; Uhrig, D.; Iatrou, H.; Mays, J.; Hadjichristidis, N. Tetrafunctional Multigraft Copolymers as Novel Thermoplastic Elastomers. *Macromolecules* **2001**, *34*, 6333–6337.

[94] Zhu, Y.; Burgaz, E.; Gido, S. P.; Staudinger, U.; Weidisch, R.; Uhrig, D.; Mays, J. W. Morphology and Tensile Properties of Multigraft Copolymers with Regularly Spaced Tri-, Tetra-, and Hexafunctional Junction Points. *Macromolecules* **2006**, *39*, 4428–4436.

[95] Daniel, W. F.; Burdyńska, J.; Vatankhah-Varnoosfaderani, M.; Matyjaszewski, K.; Paturej, J.; Rubinstein, M.; Dobrynin, A. V.; Sheiko, S. S. Solvent-free, Supersoft

and Superelastic Bottlebrush Melts and Networks. *Nature Materials* **2016**, *15*, 183–189.

[96] Shi, W.; Lynd, N. A.; Montarnal, D.; Luo, Y.; Fredrickson, G. H.; Kramer, E. J.; Ntaras, C.; Avgeropoulos, A.; Hexemer, A. Toward Strong Thermoplastic Elastomers with Asymmetric Miktoarm Block Copolymer Architectures. *Macromolecules* **2014**, *47*, 2037–2043.

[97] Kautz, H.; Van Beek, D.; Sijbesma, R. P.; Meijer, E. Cooperative End-to-End and Lateral Hydrogen-Bonding Motifs in Supramolecular Thermoplastic Elastomers. *Macromolecules* **2006**, *39*, 4265–4267.

[98] Schmatloch, S.; van den Berg, A. M. J.; Alexeev, A. S.; Hofmeier, H.; Schubert, U. S. Soluble High-Molecular-Mass Poly(ethylene oxide)s via Self-Organization. *Macromolecules* **2003**, *36*, 9943–9949.

[99] McKay, K. W.; Gros, W. A.; Diehl, C. F. The Influence of Styrene–Butadiene Diblock Copolymer on Styrene–Butadiene–Styrene Triblock Copolymer Viscoelastic Properties and Product Performance. *Journal of Applied Polymer Science* **1995**, *56*, 947–958.

[100] Gibert, F.; Marin, G.; Derail, C.; Allal, A.; Lechat, J. Rheological Properties of Hot Melt Pressure-Sensitive Adhesives Based on Styrene–Isoprene Copolymers. Part 1: A Rheological Model for [SIS-SI] Formulations. *The Journal of Adhesion* **2003**, *79*, 825–852.

[101] Roos, A.; Creton, C. Effect of the Presence of Diblock Copolymer on the Nonlinear Elastic and Viscoelastic Properties of Elastomeric Triblock Copolymers. *Macromolecules* **2005**, *38*, 7807–7818.

[102] Creton, C.; Hu, G.; Deplace, F.; Morgret, L.; Shull, K. R. Large-Strain Mechanical Behavior of Model Block Copolymer Adhesives. *Macromolecules* **2009**, *42*, 7605–7615.

[103] Lee, S. Structure and Dynamics of Block Copolymer Based Soft Materials. Ph.D. Dissertation, University of Minnesota, 2011.

[104] Frick, E. M.; Zalusky, A. S.; ; Hillmyer, M. A. Characterization of Polylactide-*b*-Polyisoprene-*b*-Polylactide Thermoplastic Elastomers. *Biomacromolecules* **2003**, *4*, 216–223.

[105] Martello, M. T.; Hillmyer, M. A. Polylactide–Poly(6-methyl-ε-caprolactone)–Polylactide Thermoplastic Elastomers. *Macromolecules* **2011**, *44*, 8537–8545.

[106] Yu, J. M.; Dubois, P.; Teyssié, P.; ; Jérôme, R. Syndiotactic Poly(methyl methacrylate)(sPMMA)–Polybutadiene(PBD)–sPMMA Triblock Copolymers: Synthesis, Morphology, and Mechanical Properties. *Macromolecules* **1996**, *29*, 6090–6099.

[107] Tong, J.; Jerôme, R. Synthesis of Poly(methyl methacrylate)-*b*-Poly(*n*-butyl acrylate)-*b*-Poly(methyl methacrylate) Triblocks and Their Potential as Thermoplastic Elastomers. *Polymer* **2000**, *41*, 2499 – 2510.

[108] Sasaki, M.; Adachi, M.; Kato, Y.; Fujii, S.; Nakamura, Y.; Urahama, Y.; Sakurai, S. Adhesion Property and Morphology of Styrene Triblock/Diblock Copolymer Blends. *Journal of Applied Polymer Science* **2010**, *118*, 1766–1773.

[109] Martello, M. T.; Schneiderman, D. K.; Hillmyer, M. A. Synthesis and Melt Processing of Sustainable Poly(ε–decalactone)–*block*–Poly(lactide) Multiblock Thermoplastic Elastomers. *ACS Sustainable Chemistry & Engineering* **2014**, *2*, 2519–2526.

[110] Hiemenz, P.; Lodge, T. *Polymer Chemistry, Second Edition*; Taylor & Francis, 2007; pp 59, 483–485.

[111] Lomellini, P. Effect of Chain Length on the Network Modulus and Entanglement. *Polymer* **1992**, *33*, 1255–1260.

[112] Liu, C.; He, J.; Van Ruymbeke, E.; Keunings, R.; Bailly, C. Evaluation of Different Methods for the Determination of the Plateau Modulus and the Entanglement Molecular Weight. *Polymer* **2006**, *47*, 4461–4479.

[113] Larson, R.; Sridhar, T.; Leal, L.; McKinley, G.; Likhtman, A.; McLeish, T. Definitions of Entanglement Spacing and Time Constants in the Tube Model. *Journal of Rheology* **2003**, *47*, 809–818.

[114] Fox Jr, T. G.; Flory, P. J. Second-Order Transition Temperatures and Related Properties of Polystyrene. I. Influence of Molecular Weight. *Journal of Applied Physics* **1950**, *21*, 581–591.

[115] Jamshidi, K.; Hyon, S.-H.; Ikada, Y. Thermal Characterization of Polylactides. *Polymer* **1988**, *29*, 2229–2234.

[116] Sentmanat, M. L. Miniature Universal Testing Platform: From Extensional Melt Rheology to Solid-State Deformation Behavior. *Rheologica Acta* **2004**, *43*, 657–669.

[117] Mori, Y.; Lim, L. S.; ; Bates, F. S. Consequences of Molecular Bridging in Lamellae-Forming Triblock/Pentablock Copolymer Blends. *Macromolecules* **2003**, *36*, 9879–9888.

[118] Watanabe, H.; Matsumiya, Y.; Sawada, T.; ; Iwamoto, T. Rheological and Dielectric Behavior of Dipole-Inverted $(SIS)_p$-Type Multiblock Copolymers: Estimates of Bridge/Loop Fractions for Respective I Blocks and Effect of Loops on High Extensibility of Bridges. *Macromolecules* **2007**, *40*, 6885–6897.

[119] Holden, G.; Bishop, E. T.; Legge, N. R. Thermoplastic Elastomers. *Journal of Polymer Science Part C: Polymer Symposia* **1969**, *26*, 37–57.

[120] Martinetti, L. Uniaxial Extensional Behavior of A-B-A Thermoplastic Elastomers:

Structure-Properties Relationships and Modeling. Ph.D. Dissertation, University of Minnesota, 2015.

[121] Callister, W. D. *Materials Science and Engineering: An Introduction*; Wiley: New York, 1997; pp 120–121.

[122] Zhu, X.; Wang, S.-Q. Mechanisms for Different Failure Modes in Startup Uniaxial Extension: Tensile (Rupture-like) Failure and Necking. *Journal of Rheology* **2013**, *57*, 223–248.

[123] Hashimoto, T.; Yamasaki, K.; Koizumi, S.; Hasegawa, H. Ordered Structure in Blends of Block Copolymers. 1. Miscibility Criterion for Lamellar Block Copolymers. *Macromolecules* **1993**, *26*, 2895–2904.

[124] Hashimoto, T.; Koizumi, S.; Hasegawa, H. Ordered Structure in Blends of Block Copolymers. 2. Self-Assembly for Immiscible Lamella-Forming Copolymers. *Macromolecules* **1994**, *27*, 1562–1570.

[125] Koizumi, S.; Hasegawa, H.; Hashimoto, T. Ordered Structure in Blends of Block Copolymers. 3. Self-Assembly in Blends of Sphere-or Cylinder-Forming Copolymers. *Macromolecules* **1994**, *27*, 4371–4381.

[126] Lee, S.; Bluemle, M. J.; Bates, F. S. Discovery of a Frank-Kasper σ Phase in Sphere-Forming Block Copolymer Melts. *Science* **2010**, *330*, 349–353.

[127] Chanpuriya, S.; Kim, K.; Zhang, J.; Lee, S.; Arora, A.; Dorfman, K. D.; Delaney, K. T.; Fredrickson, G. H.; Bates, F. S. Cornucopia of Nanoscale Ordered Phases in Sphere-Forming Tetrablock Terpolymers. *ACS Nano* **2016**, *10*, 4961–4972.

[128] Mannion, A. M.; Bates, F. S.; Macosko, C. W. Synthesis and Rheology of Branched Multiblock Polymers Based on Polylactide. *Macromolecules* **2016**, *49*, 4587–4598.

[129] Anderson, K. S.; Schreck, K. M.; Hillmyer, M. A. Toughening Polylactide. *Polymer Reviews* **2008**, *48*, 85–108.

[130] Jacobsen, S.; Fritz, H.-G. Plasticizing Polylactide—The Effect of Different Plasticizers on the Mechanical Properties. *Polymer Engineering & Science* **1999**, *39*, 1303–1310.

[131] Lee, I.; Panthani, T. R.; Bates, F. S. Sustainable Poly(lactide–*b*–butadiene) Multiblock Copolymers with Enhanced Mechanical Properties. *Macromolecules* **2013**, *46*, 7387–7398.

[132] Gramlich, W. M. Toughening Polylactide with Phase-Separating Complex Copolymer Architectures. *Macromolecular Chemistry and Physics* **2015**, *216*, 145–155.

[133] Zhang, J.; Li, T.; Mannion, A. M.; Schneiderman, D. K.; Hillmyer, M. A.; Bates, F. S. Tough and Sustainable Graft Block Copolymer Thermoplastics. *ACS Macro Letters* **2016**, *5*, 407–412.

[134] Anderson, K. S.; Lim, S. H.; Hillmyer, M. A. Toughening of Polylactide by Melt Blending with Linear Low-Density Polyethylene. *Journal of Applied Polymer Science* **2003**, *89*, 3757–3768.

[135] Li, Y.; Shimizu, H. Improvement in Toughness of Poly(L-lactide) (PLLA) through Reactive Blending with Acrylonitrile–Butadiene–Styrene Copolymer (ABS): Morphology and Properties. *European Polymer Journal* **2009**, *45*, 738–746.

[136] Xu, Y.; Loi, J.; Delgado, P.; Topolkaraev, V.; McEneany, R. J.; Macosko, C. W.; Hillmyer, M. A. Reactive Compatibilization of Polylactide/Polypropylene Blends. *Industrial & Engineering Chemistry Research* **2015**, *54*, 6108–6114.

[137] Thurber, C. M.; Xu, Y.; Myers, J. C.; Lodge, T. P.; Macosko, C. W. Accelerating Reactive Compatibilization of PE/PLA Blends by an Interfacially Localized Catalyst. *ACS Macro Letters* **2014**, *4*, 30–33.

[138] Li, T.; Zhang, J.; Schneiderman, D. K.; Francis, L. F.; Bates, F. S. Toughening Glassy Poly(lactide) with Block Copolymer Micelles. *ACS Macro Letters* **2016**, *5*, 359–364.

[139] Stoclet, G.; Seguela, R.; Lefebvre, J.; Elkoun, S.; Vanmansart, C. Strain-Induced Molecular Ordering in Polylactide upon Uniaxial Stretching. *Macromolecules* **2010**, *43*, 1488–1498.

[140] Wu, L.; Cochran, E. W.; Lodge, T. P.; Bates, F. S. Consequences of Block Number on the Order-Disorder Transition and Viscoelastic Properties of Linear $(AB)_n$ Multiblock Copolymers. *Macromolecules* **2004**, *37*, 3360–3368.

[141] Xiong, M.; Schneiderman, D. K.; Bates, F. S.; Hillmyer, M. A.; Zhang, K. Scalable Production of Mechanically Tunable Block Polymers from Sugar. *Proceedings of the National Academy of Sciences* **2014**, *111*, 8357–8362.

[142] Jiao, M.; Yang, K.; Cao, J.; Liu, H.; Pan, W.; Gao, P. Designing and Characterization of Poly(L-Lactide)/Poly(ε-Caprolactone) Multiblock Copolymers. *Journal of Macromolecular Science, Part B* **2014**, *53*, 191–204.

[143] Makiguchi, K.; Ogasawara, Y.; Kikuchi, S.; Satoh, T.; Kakuchi, T. Diphenyl Phosphate as an Efficient Acidic Organocatalyst for Controlled/Living Ring-Opening Polymerization of Trimethylene Carbonates Leading to Block, End-Functionalized, and Macrocyclic Polycarbonates. *Macromolecules* **2013**, *46*, 1772–1782.

[144] Sawai, D.; Takahashi, K.; Sasashige, A.; Kanamoto, T.; Hyon, S.-H. Preparation of Oriented β-form Poly(L-lactic acid) by Solid-State Coextrusion: Effect of Extrusion Variables. *Macromolecules* **2003**, *36*, 3601–3605.

[145] Nouri, S.; Dubois, C.; Lafleur, P. G. Effect of Chemical and Physical Branching on Rheological Behavior of Polylactide. *Journal of Rheology* **2015**, *59*, 1045–1063.

[146] Wolf, F. K.; Frey, H. Inimer-Promoted Synthesis of Branched and Hyperbranched Polylactide Copolymers. *Macromolecules* **2009**, *42*, 9443–9456.

[147] Pitet, L. M.; Hait, S. B.; Lanyk, T. J.; Knauss, D. M. Linear and Branched Architectures from the Polymerization of Lactide with Glycidol. *Macromolecules* **2007**, *40*, 2327–2334.

[148] Liu, J.; Zhang, S.; Zhang, L.; Bai, Y. Preparation and Rheological Characterization of Long Chain Branching Polylactide. *Polymer* **2014**, *55*, 2472–2480.

[149] Corre, Y.-M.; Duchet, J.; Reignier, J.; Maazouz, A. Melt Strengthening of Poly(lactic acid) Through Reactive Extrusion with Epoxy-Functionalized Chains. *Rheologica Acta* **2011**, *50*, 613–629.

[150] Schneider, J.; Shi, X.; Manjure, S.; Gravier, D.; Narayan, R. Epoxy Functionalized Poly(lactide) Reactive Modifier for Blown Film Applications. *Journal of Applied Polymer Science* **2015**, *132*.

[151] Najafi, N.; Heuzey, M.-C.; Carreau, P. J.; Therriault, D.; Park, C. B. Rheological and Foaming Behavior of Linear and Branched Polylactides. *Rheologica Acta* **2014**, *53*, 779–790.

[152] You, J.; Lou, L.; Yu, W.; Zhou, C. The Preparation and Crystallization of Long Chain Branching Polylactide Made by Melt Radicals Reaction. *Journal of Applied Polymer Science* **2013**, *129*, 1959–1970.

[153] Xu, H.; Fang, H.; Bai, J.; Zhang, Y.; Wang, Z. Preparation and Characterization of High-Melt-Strength Polylactide with Long-Chain Branched Structure through γ-Radiation-Induced Chemical Reactions. *Industrial & Engineering Chemistry Research* **2014**, *53*, 1150–1159.

[154] Wang, L.; Jing, X.; Cheng, H.; Hu, X.; Yang, L.; Huang, Y. Rheology and Crystallization of Long-Chain Branched Poly(L-lactide)s with Controlled Branch Length. *Industrial & Engineering Chemistry Research* **2012**, *51*, 10731–10741.

[155] Han, J.; Zhu, D.; Gao, C. Fast Bulk Click Polymerization Approach to Linear and Hyperbranched Alternating Multiblock Copolymers. *Polymer Chemistry* **2013**, *4*, 542–549.

[156] Jikei, M.; Suzuki, M.; Itoh, K.; Matsumoto, K.; Saito, Y.; Kawaguchi, S. Synthesis of Hyperbranched Poly(L-lactide)s by Self-Polycondensation of AB_2 Macromonomers and their Structural Characterization by Light Scattering Measurements. *Macromolecules* **2012**, *45*, 8237–8244.

[157] Liu, M.-J.; Chen, S.-C.; Yang, K.-K.; Wang, Y.-Z. Biodegradable Polylactide Based Materials with Improved Crystallinity, Mechanical Properties and Rheological Behaviour by Introducing a Long-Chain Branched Copolymer. *RSC Advances* **2015**, *5*, 42162–42173.

[158] Olsén, P.; Borke, T.; Odelius, K.; Albertsson, A.-C. ε-Decalactone: A Thermoresilient and Toughening Comonomer to Poly(L-lactide). *Biomacromolecules* **2013**, *14*, 2883–2890.

[159] Schneiderman, D. K.; Hill, E. M.; Martello, M. T.; Hillmyer, M. A. Poly(lactide)-*block*-Poly(ε-caprolactone-co-ε-decalactone)-*block*-Poly(lactide) Copolymer Elastomers. *Polymer Chemistry* **2015**, *6*, 3641–3651.

[160] Anderson, K. S.; Hillmyer, M. A. Melt Chain Dimensions of Polylactide. *Macromolecules* **2004**, *37*, 1857–1862.

[161] Henton, D. E.; Gruber, P.; Lunt, J.; Randall, J. Polylactic Acid Technology. *Natural fibers, Biopolymers, and Biocomposites* **2005**, *16*, 527–577.

[162] McKee, M. G.; Unal, S.; Wilkes, G. L.; Long, T. E. Branched Polyesters: Recent Advances in Synthesis and Performance. *Progress in Polymer Science* **2005**, *30*, 507–539.

[163] Fredrickson, G. H.; Helfand, E. Fluctuation Effects in the Theory of Microphase Separation in Block Copolymers. *The Journal of Chemical Physics* **1987**, *87*, 697–705.

[164] Roe, R.-J.; Fishkis, M.; Chang, J. Small-Angle X-ray Diffraction Study of Thermal Transition in Styrene-Butadiene Block Copolymers. *Macromolecules* **1981**, *14*, 1091–1103.

[165] Hashimoto, T.; Ijichi, Y.; Fetters, L. J. Order–Disorder Transition of Starblock Copolymers. *The Journal of Chemical Physics* **1988**, *89*, 2463–2472.

[166] Owens, J. N.; Gancarz, I. S.; Koberstein, J. T.; Russell, T. P. Investigation of the Microphase Separation Transition in Low-Molecular-Weight Diblock Copolymers. *Macromolecules* **1989**, *22*, 3380–3387.

[167] Bates, F. S.; Rosedale, J. H.; Fredrickson, G. H. Fluctuation Effects in a Symmetric Diblock Copolymer Near the Order–Disorder Transition. *The Journal of Chemical Physics* **1990**, *92*, 6255–6270.

[168] Rosedale, J. H.; Bates, F. S.; Almdal, K.; Mortensen, K.; Wignall, G. D. Order and Disorder in Symmetric Diblock Copolymer Melts. *Macromolecules* **1995**, *28*, 1429–1443.

[169] Kennemur, J. G.; Hillmyer, M. A.; Bates, F. S. Rheological Evidence of Composition Fluctuations in an Unentangled Diblock Copolymer Melt Near the Order–Disorder Transition. *ACS Macro Letters* **2013**, *2*, 496–500.

[170] Krause, S. Microphase Separation in Block Copolymers. Zeroth Approximation Including Surface Free Energies. *Macromolecules* **1970**, *3*, 84–86.

[171] Ryan, A. J.; Macosko, C. W.; Bras, W. Order-Disorder Transition in a Block Copolyurethane. *Macromolecules* **1992**, *25*, 6277–6283.

[172] Velankar, S.; Cooper, S. L. Microphase Separation and Rheological Properties of Polyurethane Melts. 2. Effect of Block Incompatibility on the Microstructure. *Macromolecules* **2000**, *33*, 382–394.

[173] Beyer, F. L.; Gido, S. P.; Büschl, C.; Iatrou, H.; Uhrig, D.; Mays, J. W.; Chang, M. Y.; Garetz, B. A.; Balsara, N. P.; Tan, N. B. Graft Copolymers with Regularly Spaced, Tetrafunctional Branch Points: Morphology and Grain Structure. *Macromolecules* **2000**, *33*, 2039–2048.

[174] Duan, Y.; Thunga, M.; Schlegel, R.; Schneider, K.; Rettler, E.; Weidisch, R.; Siesler, H. W.; Stamm, M.; Mays, J. W.; Hadjichristidis, N. Morphology and Deformation Mechanisms and Tensile Properties of Tetrafunctional Multigraft Copolymers. *Macromolecules* **2009**, *42*, 4155–4164.

[175] Hutchings, L. R.; Dodds, J. M.; Rees, D.; Kimani, S. M.; Wu, J. J.; Smith, E. HyperMacs to Hyperblocks: A Novel Class of Branched Thermoplastic Elastomer. *Macromolecules* **2009**, *42*, 8675–8687.

[176] Hutchings, L. R.; Agostini, S.; Hamley, I. W.; Hermida-Merino, D. Chain Architecture as an Orthogonal Parameter To Influence Block Copolymer Morphology. Synthesis and Characterization of Hyperbranched Block Copolymers: HyperBlocks. *Macromolecules* **2015**, *48*, 8806–8822.

[177] Fredrickson, G. H.; Bates, F. S. Dynamics of Block Copolymers: Theory and Experiment. *Annual Review of Materials Science* **1996**, *26*, 501–550.

[178] Keßner, U.; Münstedt, H. Thermorheology as a Method to Analyze Long-Chain Branched Polyethylenes. *Polymer* **2010**, *51*, 507–513.

[179] Carella, J.; Gotro, J.; Graessley, W. Thermorheological Effects of Long-Chain Branching in Entangled Polymer Melts. *Macromolecules* **1986**, *19*, 659–667.

[180] Fetters, L. J.; Kiss, A. D.; Pearson, D. S.; Quack, G. F.; Vitus, F. J. Rheological Behavior of Star-Shaped Polymers. *Macromolecules* **1993**, *26*, 647–654.

[181] Dorgan, J. R.; Janzen, J.; Clayton, M. P.; Hait, S. B.; Knauss, D. M. Melt Rheology of Variable L-content Poly(lactic acid). *Journal of Rheology* **2005**, *49*, 607–619.

[182] Adams, C.; Hutchings, L.; Klein, P.; McLeish, T.; Richards, R. Synthesis and Dynamic Rheological Behavior of Polybutadiene Star Polymers. *Macromolecules* **1996**, *29*, 5717–5722.

[183] Kirkwood, K. M.; Leal, L. G.; Vlassopoulos, D.; Driva, P.; Hadjichristidis, N. Stress Relaxation of Comb Polymers with Short Branches. *Macromolecules* **2009**, *42*, 9592–9608.

[184] Kasehagen, L. J.; Macosko, C. W.; Trowbridge, D.; Magnus, F. Rheology of Long-Chain Randomly Branched Polybutadiene. *Journal of Rheology* **1996**, *40*, 689–709.

[185] Dalsin, S. J.; Hillmyer, M. A.; Bates, F. S. Linear Rheology of Polyolefin-Based Bottlebrush Polymers. *Macromolecules* **2015**, *48*, 4680–4691.

[186] Carvalho, M.; Padmanabhan, M.; Macosko, C. Single-Point Correction for Parallel Disks Rheometry. *Journal of Rheology* **1994**, *38*, 1925–1936.

[187] Lehermeier, H. J.; Dorgan, J. R. Melt Rheology of Poly(lactic acid): Consequences of Blending Chain Architectures. *Polymer Engineering & Science* **2001**, *41*, 2172–2184.

[188] Lentzakis, H.; Vlassopoulos, D.; Read, D.; Lee, H.; Chang, T.; Driva, P.; Hadjichristidis, N. Uniaxial Extensional Rheology of Well-Characterized Comb Polymers. *Journal of Rheology* **2013**, *57*, 605–625.

[189] Kotaka, T.; Okamoto, M.; Kojima, A.; Kwon, Y.; Nojima, S. Elongational Flow-Induced Morphology Change of Block Copolymers Part 1. A Polystyrene-*block*-Poly(ethylene butylene)-*block*-Polystyrene-*block*-Poly(ethylene butylene) Tetrablock Copolymer with Polystyrene Spherical Microdomains. *Polymer* **2001**, *42*, 1207–1217.

[190] Mao, R.; McCready, E. M.; Burghardt, W. R. Structural Response of an Ordered Block Copolymer Melt to Uniaxial Extensional Flow. *Soft Matter* **2014**, *10*, 6198–6207.

[191] Park, H. E.; Dealy, J. M.; Marchand, G. R.; Wang, J.; Li, S.; Register, R. A. Rheology and Structure of Molten, Olefin Multiblock Copolymers. *Macromolecules* **2010**, *43*, 6789–6799.

[192] Münstedt, H. Dependence of the Elongational Behavior of Polystyrene Melts on Molecular Weight and Molecular Weight Distribution. *Journal of Rheology* **1980**, *24*, 847–867.

[193] Münstedt, H.; Schwarzl, F. R. *Deformation and Flow of Polymeric Materials*; Springer, 2014; pp 442–445.

[194] Hepperle, J.; Münstedt, H. Rheological Properties of Branched Polystyrenes: Nonlinear Shear and Extensional Behavior. *Rheologica Acta* **2006**, *45*, 717–727.

[195] Kempf, M.; Ahirwal, D.; Cziep, M.; Wilhelm, M. Synthesis and Linear and Nonlinear Melt Rheology of Well-Defined Comb Architectures of PS and PpMS with a Low and Controlled Degree of Long-Chain Branching. *Macromolecules* **2013**, *46*, 4978–4994.

[196] Grijpma, D.; Van Hofslot, R.; Super, H.; Nijenhuis, A.; Pennings, A. Rubber Toughening of Poly(lactide) by Blending and Block Copolymerization. *Polymer Engineering & Science* **1994**, *34*, 1674–1684.

[197] Lebarbé, T.; Ibarboure, E.; Gadenne, B.; Alfos, C.; Cramail, H. Fully Bio-based Poly(L-lactide)-*b*-Poly(ricinoleic acid)-*b*-Poly(L–lactide) Triblock Copolyesters: Investigation of Solid-State Morphology and Thermo-Mechanical Properties. *Polymer Chemistry* **2013**, *4*, 3357–3369.

[198] Haynes, D.; Naskar, A. K.; Singh, A.; Yang, C.-C.; Burg, K. J.; Drews, M.; Harrison, G.; Smith, D. W. Poly(L-lactic acid) with Segmented Perfluoropolyether Enchainment. *Macromolecules* **2007**, *40*, 9354–9360.

[199] Koo, C. M.; Hillmyer, M. A.; Bates, F. S. Structure and Properties of Semicrystalline-Rubbery Multiblock Copolymers. *Macromolecules* **2006**, *39*, 667–677.

[200] Anderson, K. S.; Hillmyer, M. A. The Influence of Block Copolymer Microstructure on the Toughness of Compatibilized Polylactide/Polyethylene Blends. *Polymer* **2004**, *45*, 8809–8823.

[201] López-Rodríguez, N.; López-Arraiza, A.; Meaurio, E.; Sarasua, J. Crystallization, Morphology, and Mechanical Behavior of Polylactide/Poly(ε-caprolactone) Blends. *Polymer Engineering & Science* **2006**, *46*, 1299–1308.

[202] Meng, B.; Deng, J.; Liu, Q.; Wu, Z.; Yang, W. Transparent and Ductile Poly(lactic acid)/Poly(butyl acrylate) (PBA) Blends: Structure and Properties. *European Polymer Journal* **2012**, *48*, 127–135.

[203] Murariu, M.; Da Silva Ferreira, A.; Alexandre, M.; Dubois, P. Polylactide (PLA) Designed with Desired End-Use Properties: 1. PLA Compositions with Low Molecular Weight Ester-like Plasticizers and Related Performances. *Polymers for Advanced Technologies* **2008**, *19*, 636–646.

[204] Kfoury, G.; Raquez, J.-M.; Hassouna, F.; Odent, J.; Toniazzo, V.; Ruch, D.; Dubois, P. Recent Advances in High Performance Poly(lactide): from "Green" Plasticization to Super-Tough Materials via (Reactive) Compounding. *Frontiers in Chemistry* **2013**, *1*, 32.

[205] Flory, P. J. Molecular Size Distribution in Three Dimensional Polymers. I. Gelation. *Journal of the American Chemical Society* **1941**, *63*, 3083–3090.

[206] Flory, P. J. Molecular Size Distribution in Three Dimensional Polymers. II. Trifunctional Branching Units. *Journal of the American Chemical Society* **1941**, *63*, 3091–3096.

[207] Flory, P. J. Molecular Size Distribution in Three Dimensional Polymers. III. Tetrafunctional Branching Units. *Journal of the American Chemical Society* **1941**, *63*, 3096–3100.

[208] Macosko, C. W.; Miller, D. R. A New Derivation of Average Molecular Weights of Nonlinear Polymers. *Macromolecules* **1976**, *9*, 199–206.

[209] Schneiderman, D. K.; Vanderlaan, M. E.; Mannion, A. M.; Panthani, T. R.; Batiste, D. C.; Wang, J. Z.; Bates, F. S.; Macosko, C. W.; Hillmyer, M. A. Chemically Recyclable Biobased Polyurethanes. *ACS Macro Letters* **2016**, *5*, 515–518.

[210] Kohn, F.; Van Den Berg, J.; Van De Ridder, G.; Feijen, J. The Ring-Opening Polymerization of D,L-lactide in the Melt Initiated with Tetraphenyltin. *Journal of Applied Polymer Science* **1984**, *29*, 4265–4277.

[211] Walkenhorst, R.; Olivier, R. Determination of Polymer Structure by Gel Permeation Chromatography. *LC GC EUROPE* **2001**, *14*, 676–678.

[212] Brutman, J. P.; Delgado, P. A.; Hillmyer, M. A. Polylactide Vitrimers. *ACS Macro Letters* **2014**, *3*, 607–610.

[213] Sonntag, N. O. The Reactions of Aliphatic Acid Chlorides. *Chemical Reviews* **1953**, *52*, 237–416.

[214] Wang, Y.; Yang, L.; Niu, Y.; Wang, Z.; Zhang, J.; Yu, F.; Zhang, H. Rheological and Topological Characterizations of Electron Beam Irradiation Prepared Long-Chain Branched Polylactic Acid. *Journal of Applied Polymer Science* **2011**, *122*, 1857–1865.

[215] Yu, Y.; DesLauriers, P. J.; Rohlfing, D. C. SEC-MALS Method for the Determination of Long-Chain Branching and Long-Chain Branching Distribution in Polyethylene. *Polymer* **2005**, *46*, 5165–5182.

[216] Auhl, D.; Stange, J.; Münstedt, H.; Krause, B.; Voigt, D.; Lederer, A.; Lappan, U.; Lunkwitz, K. Long-Chain Branched Polypropylenes by Electron Beam Irradiation and Their Rheological Properties. *Macromolecules* **2004**, *37*, 9465–9472.

[217] McMurry, J. *Organic Chemistry*, 7th ed.; Brooks/Cole, New York, 2008; pp 802–803.

[218] Schneiderman, D. K.; Hillmyer, M. A. Aliphatic Polyester Block Polymer Design. *Macromolecules* **2016**, *49*, 2419–2428.

[219] Panthani, T. Structure-Property Relationships of Poly(lactide)-based Triblock and Multiblock Copolymers. Ph.D. Dissertation, University of Minnesota, 2016.

[220] Creton, C. Pressure-Sensitive Adhesives: An Introductory Course. *MRS Bulletin* **2003**, *28*, 434–439.

[221] Vendamme, R.; Schüwer, N.; Eevers, W. Recent Synthetic Approaches and Emerging Bio-inspired Strategies for the Development of Sustainable Pressure-Sensitive Adhesives Derived from Renewable Building Blocks. *Journal of Applied Polymer Science* **2014**, *131*.

[222] Ding, K.; John, A.; Shin, J.; Lee, Y.; Quinn, T.; Tolman, W. B.; Hillmyer, M. A.

High-Performance Pressure-Sensitive Adhesives from Renewable Triblock Copolymers. *Biomacromolecules* **2015**, *16*, 2537–2539.

[223] Lee, S.; Lee, K.; Kim, Y.-W.; Shin, J. Preparation and Characterization of a Renewable Pressure-Sensitive Adhesive System Derived from ε-decalactone, L-lactide, Epoxidized Soybean Oil, and Rosin Ester. *ACS Sustainable Chemistry & Engineering* **2015**, *3*, 2309–2320.

[224] Palkin, S.; Smith, W. A New Non-Crystallizing Gum Rosin. *Journal of the American Oil Chemists' Society* **1938**, *15*, 120–122.

[225] Fulzele, S.; Satturwar, P.; Dorle, A. Study of the Biodegradation and in Vivo Biocompatibility of Novel Biomaterials. *European Journal of Pharmaceutical Sciences* **2003**, *20*, 53 – 61.

[226] Emerson, W. S.; Longley, J. R. I.; Shafer, T. C. Lactone Preparation. U.S. Patent 2680118, 1954.

[227] Kraus, G.; Rollmann, K. The Entanglement Plateau in the Dynamic Modulus of Rubbery Styrene–diene Block Copolymers. Significance to Pressure-Sensitive Adhesive Formulations. *Journal of Applied Polymer Science* **1977**, *21*, 3311–3318.

[228] Fox, T. G. Influence of Diluent and of Copolymer Composition on the Glass Temperature of a Polymer System. *Bull. Am. Phys. Soc.* **1956**, *1*, 123–35.

[229] Dahlquist, C.; Patrick, R. *Treatise on Adhesion and Adhesives*; Marcel Dekker: New York, 1969; Vol. 2; p 219.

[230] Nakajima, N.; Babrowicz, R.; Harrell, E. Rheology, Composition, and Peel-Mechanism of Block Copolymer–Tackifier-Based Pressure Sensitive Adhesives. *Journal of Applied Polymer Science* **1992**, *44*, 1437–1456.

[231] Schneiderman, D. K.; Hillmyer, M. A. Aliphatic Polyester Block Polymer Design. *Macromolecules* **2016**, *49*, 2419–2428.

[232] ArizonaChemical, Product Data Sheet: SYLVALITE® RE 10L. `http://www.arizonachemical.com/wp-content/uploads/SYLVALITE%C2%AE-RE10L.pdf`.

[233] Deplace, F.; Carelli, C.; Mariot, S.; Retsos, H.; Chateauminois, A.; Ouzineb, K.; Creton, C. Fine Tuning the Adhesive Properties of a Soft Nanostructured Adhesive with Rheological Measurements. *The Journal of Adhesion* **2009**, *85*, 18–54.

[234] Yang, H. W.; Chang, E.-P. The Role of Viscoelastic Properties in the Design of Pressure-Sensitive Adhesives. *Trends in Polymer Science* **1997**, *5*, 380–384.

[235] Brown, K.; Hooker, J. C.; Creton, C. Micromechanisms of Tack of Soft Adhesives Based on Styrenic Block Copolymers. *Macromolecular Materials and Engineering* **2002**, *287*, 163–179.

[236] Zosel, A. The Effect of Fibrilation on the Tack of Pressure Sensitive Adhesives. *International Journal of Adhesion and Adhesives* **1998**, *18*, 265–271.

[237] Creton, C.; Hooker, J.; Shull, K. R. Bulk and Interfacial Contributions to the Debonding Mechanisms of Soft Adhesives: Extension to Large Strains. *Langmuir* **2001**, *17*, 4948–4954.

[238] Yang, H. W. Water-Based Polymers as Pressure-Sensitive Adhesives—Viscoelastic Guidelines. *Journal of Applied Polymer Science* **1995**, *55*, 645–652.

[239] Tse, M. F. Studies of Triblock Copolymer-Tackifying Resin Interactions by Viscoelasticity and Adhesive Performance. *Journal of Adhesion Science and Technology* **1989**, *3*, 551–570.

[240] ASTM Standard D2979: Standard Test Method for Pressure-Sensitive Tack of Adhesives Using an Inverted Probe Machine, ASTM International, West Conshohocken, PA, 2009. http://dx.doi.org.ezp1.lib.umn.edu/10.1520/D2979-01R09.

[241] Christensen, S. F.; Everland, H.; Hassager, O.; Almdal, K. Observations of Peeling of a Polyisobutylene-Based Pressure-Sensitive Adhesive. *International Journal of Adhesion and Adhesives* **1998**, *18*, 131–137.

[242] Gent, A. N.; Petrich, R. P. Adhesion of Viscoelastic Materials to Rigid Substrates. *Proceedings of the Royal Society of London A: Mathematical, Physical and Engineering Sciences* **1969**, *310*, 433–448.

[243] Kaelble, D. Theory and Analysis of Peel Adhesion: Rate-Temperature Dependence of Viscoelastic Interlayers. *Journal of Colloid Science* **1964**, *19*, 413–424.

[244] Chang, E. Viscoelastic Windows of Pressure-Sensitive Adhesives. *The Journal of Adhesion* **1991**, *34*, 189–200.

[245] IBISworld, Plastic Film, Sheet, & Bag Manufacturing. `http://clients1.ibisworld.com/reports/us/industry/ataglance.aspx?entid=509`.

[246] Kanai, T.; Campbell, G. A. In *Film Processing*; Kanai, T., Campbell, G. A., Eds.; Progress in Polymer Processing; Hanser Publishers: Munich, 2013; Chapter 1. Film Processing: Overview and Introductory Rheology, pp 1–12.

[247] `http://www.house.leg.state.mn.us/comm/minls86/H0403DE2.htm`.

[248] Briassoulis, D. An Overview on the Mechanical Behaviour of Biodegradable Agricultural Films. *Journal of Polymers and the Environment* **2004**, *12*, 65–81.

[249] BioBag, Agricultural Film: The Alternative to Traditional Plastic Mulch Film. `http://biobagusa.com/products/agricultural-film/`.

[250] Personal communication with Shilpa Manjure, Ph.D.; Product Development Manager at Natur-Tec.

[251] Carrasco, F.; Pagès, P.; Gámez-Pérez, J.; Santana, O.; Maspoch, M. Processing of Poly(lactic acid): Characterization of Chemical Structure, Thermal Stability and Mechanical Properties. *Polymer Degradation and Stability* **2010**, *95*, 116 – 125.

[252] Cantor, K. *Blown Film Extrusion: An Introduction*; Hanser Publishers, 2006; pp 9, 107, 126–128.

[253] Micic, P.; Bhattacharya, S. N.; Field, G. Transient Elongational Viscosity of LLDPE/LDPE Blends and its Relevance to Bubble Stability in the Film Blowing Process. *Polymer Engineering & Science* **1998**, *38*, 1685–1693.

[254] Micic, P.; Bhattacharya, S. N. Rheology of LLDPE, LDPE and LLDPE/LDPE blends and its Relevance to the Film Blowing Process. *Polymer International* **2000**, *49*, 1580–1589.

[255] Münstedt, H.; Steffl, T.; Malmberg, A. Correlation Between Rheological Behaviour in Uniaxial Elongation and Film Blowing Properties of Various Polyethylenes. *Rheologica Acta* **2005**, *45*, 14–22.

[256] Münstedt, H.; Kurzbeck, S.; Stange, J. Importance of Elongational Properties of Polymer Melts for Film Blowing and Thermoforming. *Polymer Engineering & Science* **2006**, *46*, 1190–1195.

[257] Francis, L. MATS 4301: Blown Film Extrusion Memo. Self-published, 2014.

[258] Witzke, D. R. Introduction to Properties, Engineering, and Prospects of Polylactide Polymers. Ph.D. Dissertation, Michigan State University, 1997, pp 122.

[259] Chang, A.; Inge, T.; Tau, L.; Hiltner, A.; Baer, E. Tear Strength of Ductile Polyolefin Films. *Polymer Engineering & Science* **2002**, *42*, 2202–2212.

[260] Jones, T. D. Modification of Polypropylene through Blending. Ph.D. Dissertation, University of Minnesota, 2000.

[261] Mallet, B.; Lamnawar, K.; Maazouz, A. Improvement of Blown Film Extrusion of Poly(lactic acid): Structure–Processing–Properties Relationships. *Polymer Engineering & Science* **2014**, *54*, 840–857.

[262] Al-Itry, R.; Lamnawar, K.; Maazouz, A. Biopolymer Blends Based on Poly(lactic acid): Shear and Elongation Rheology/Structure/Blowing Process Relationships. *Polymers* **2015**, *7*, 939–962.

[263] Orr, C.; Cernohous, J.; Guegan, P.; Hirao, A.; Jeon, H.; Macosko, C. Homogeneous Reactive Coupling of Terminally Functional Polymers. *Polymer* **2001**, *42*, 8171–8178.

[264] Nouri, S.; Lafleur, P.; Dubois, C. Enhanced Film Blowing of Polylactide by Incorporating Branched Chains and Stereocomplex Crystals. *International Polymer Processing* **2015**, *30*, 500–510.

[265] Schroeder, J. Overview of Natureworks. Oral Presentation, 2015.

[266] Gu, L.; Xu, Y.; Naredla, R.; Hoye, T.; Macosko, C. PLA Branching with Anhydrides and Tri-functional Aziridine. APS Meeting Abstracts. 2016.

[267] Martinez, H.; Hillmyer, M. A. Carboxy-Telechelic Polyolefins in Cross-Linked Elastomers. *Macromolecules* **2014**, *47*, 479–485.

[268] ASTM Standard D1709: Impact Resistance of Plastic Film by the Free-Falling Dart Method, ASTM International, West Conshohocken, PA, 2016. http://dx.doi.org.ezp1.lib.umn.edu/10.1520/D1709-16A.

[269] ASTM Standard D1922: Propagation Tear Resistance of Plastic Film and Thin Sheeting by Pendulum Method, ASTM International, West Conshohocken, PA, 2015. http://dx.doi.org.ezp1.lib.umn.edu/10.1520/D1922-15.

[270] ASTM Standard D1004: Tear Resistance (Graves Tear) of Plastic Film and Sheeting, ASTM International, West Conshohocken, PA, 2013. http://dx.doi.org.ezp1.lib.umn.edu/10.1520/D1004-13.

[271] ASTM Standard F1306: Standard Test Method for Slow Rate Penetration Resistance of Fleixble Barrier Films and Laminates, ASTM International, West Conshohocken, PA, 2016. http://dx.doi.org.ezp1.lib.umn.edu/10.1520/F1306-16.

[272] Mai, Y.-W.; Cotterell, B. On the Essential Work of Ductile Fracture in Polymers. *International Journal of Fracture* **1986**, *32*, 105–125.